DYNAMIC MODELLING FOR CONTROL OF HIGH RATE ANAEROBIC WASTEWATER TREATMENT PROCESSES

RICHARD M. JONES, B. Eng. Mgt.

A Thesis

Submitted in Partial Fulfilment of the Requirements

for the Degree

Doctor Of Philosophy

McMaster University

DYNAMIC MODELLING FOR CONTROL OF ANAEROBIC TREATMENT

DOCTOR OF PHILOSOPHY (1992) McMASTER UNIVERSITY

(Chemical Engineering) Hamilton, Ontario

TITLE: Dynamic Modelling for Control of High Rate Anaerobic Wastewater Treatment Processes

AUTHOR: Richard M. Jones, B. Eng. Mgt. (McMaster University)

SUPERVISORS: Dr. John F. MacGregor
Dr. Keith L. Murphy

NUMBER OF PAGES: xxii, 233

ABSTRACT

The overall goal of this research was to develop an improved understanding of the dynamic behaviour necessary to define monitoring and control requirements of high rate anaerobic biological wastewater treatment processes. This required generation of an extensive non-steady state data set.

Data were collected during dynamic experiments on a 77 L pilot scale anaerobic fluidized bed, operated at the Wastewater Technology Centre in Burlington, Ontario. Experiments consisted of 12 and 36 hour pulse inputs of substrates specific to the distinct groups of microorganisms present in the process, and ranged from 7 to 21 days in length. The methane and carbon dioxide production rates, biogas hydrogen content, pH, effluent concentrations of volatile acid intermediates and chemical oxygen demand (COD) were measured using on-line instrumentation or laboratory analysis of discrete samples.

Experimental results demonstrated the relative importance of substrate and product inhibition on various reaction steps in the process, and indicated that the short term dynamic response can change significantly over time. The gas phase hydrogen concentration, previously proposed as an indicator of process stability, was found to have limited utility as a monitoring variable. The loss in potential methane production and the increased chemical requirements for pH control were shown to represent a significant cost during an upset. This suggests that in addition to the environmental incentive, an economic incentive exists to maintain stable operation of the process.

A mechanistic, four-bacterial population dynamic model of the process was formulated. Due to the lack of suitable mechanistic models for bacterial concentrations, the model was only

able to predict the short term dynamic response. An extended Kalman filter was used to combine the four population model with stochastic models for the bacteria concentration states. A sensitivity analysis was required to select a subset of parameters and stochastic states for estimation.

The extended Kalman filter allowed the model to track the measured states, although in some cases this tracking could only be achieved through unrealistic adjustments of the bacterial concentration states. The time-variable behaviour of the estimated stochastic states indicated a number of potential model improvements.

ACKNOWLEDGEMENTS

Funding for this research was provided by Environment Canada, the Federal Panel on Energy R&D (PERD), and the ISTC Biotechnology Strategy. I would like to express my thanks and appreciation to the following:

My supervisory committee consisting of Dr. John MacGregor, Dr. Keith Murphy, Dr. Eric Hall and Dr. Gilles Patry, for their advice, support, and direction;

Dr. Bruce Jank, Dr. Henryk Melcer, Dr. Eric Hall, and Gordon Speirs for providing the working environment that allowed me to complete this work;

Todd Harvey and Stephen Way for operating the pilot plant;

Gerry Ward for installing and maintaining the on-line instrumentation;

Mark Yendt for providing advice and suggestions regarding the computer programs; and Evelyn Mercer for preparing the final manuscript.

Finally, I would like to thank my wife, Kathy, for her patience and support throughout.

TABLE OF CONTENTS

LIST OF FIGURES

LIST OF TABLES

LIST OF SYMBOLS

$(CO_2)_D$	Carbon dioxide dissolved in the liquid phase (mmole/L)
$\%CO2$	Measured gas phase carbon dioxide concentration
$\underline{\alpha}$	Vector of unmeasured disturbance states
ΔG°	Standard Gibbs free energy change (kJ)
ε_f	Porosity of fluidized bed
ε_s	Porosity of settled bed
∇	Backward difference operator
η_{AF}	Maximum acid formation yield factor
$\underline{\theta}$	Vector of unknown process parameters
θ_c	Biomass solids retention time (d)
θ_c^{min}	Minimum biomass solids retention time to prevent wash-out (d)
λ	Mass transfer overall effectiveness factor
λ_e	External mass transfer effectiveness factor
λ_i	Internal mass transfer effectiveness factor
μ	Specific growth rate (d^{-1})
μ_{AF}	Acid-former specific growth rate (d^{-1})
μ_{AM}	Acetoclastic methanogen specific growth rate (d^{-1})
μ_{BA}	Butyric acid utilizing acetogen specific growth rate (d^{-1})
μ_{max}	Maximum specific growth rate (d^{-1})
$\mu_{max,AF}$	Maximum specific growth rate - acid-formers (d^{-1})
$\mu_{max,AM}$	Maximum specific growth rate - acetoclastic methanogens (d^{-1})
$\mu_{max,BA}$	Maximum specific growth rate - butyric acetogens (d^{-1})
$\mu_{max,PA}$	Maximum specific growth rate - propionic acetogens (d^{-1})
μ_{PA}	Propionic acid utilizing acetogen specific growth rate(d^{-1})
$\nu_{A,AF}$	Stoichiometric coefficient for acid-former acetate production (mg/mg)

$\nu_{A,BA}$	Stoichiometric coefficient for acetogenic acetate production from butyrate (mg/mg)
$\nu_{A,PA}$	Stoichiometric coefficient for acetogenic acetate production from propionate (mg/mg)
$\nu_{B,AF}$	Stoichiometric coefficient for butyrate production (mg/mg)
$\nu_{CH4,AM}$	Stoichiometric coefficient for acetoclastic methanogenesis (mmole/mg)
$\nu_{CH4,HM}$	Stoichiometric coefficient for methane from hydrogen (mmole/mmole)
$\nu_{H,A,AF}$	Stoichiometric coefficient for hydrogen in acid-former acetate production reaction
$\nu_{H,BA}$	Stoichiometric coefficient for hydrogen in acetogenic consumption of butyrate (mmole/mg)
$\nu_{H,B,AF}$	Stoichiometric coefficient for hydrogen in butyrate production reaction (mmole/mg)
$\nu_{H,PA}$	Stoichiometric coefficient for hydrogen in acetogenic consumption of propionate (mmole/mg)
$\nu_{H,P,AF}$	Stoichiometric coefficient for hydrogen in propionate production reaction (mmole/mg)
$\nu_{P,AF}$	Stoichiometric coefficient for propionate production (mg/mg)
$\mathbf{Q}$	Normalized output sensitivity coefficient
ρ	Normalized state sensitivity coefficient
$\rho_{A,AF}$	Regulation function for the production of acetic acid by acid-formers
$\rho_{B,AF}$	Regulation function for the production of butyric acid by acid formers
$\rho_{P,AF}$	Regulation function for the production of propionic acid by acid-formers
ψ	Sensitivity coefficient of deterministic states with respect to stochastic states
φ	Output sensitivity coefficient
$\underline{A}$	Jacobian matrix of the state model equations
a_S	Total biofilm surface area (m^2)
BOD_5	Five day biochemical oxygen demand
B_V	Bacterial loss rate (mg/L•d)
C	Effluent tracer concentration (DPM/mL)
COD	Chemical oxygen demand
CSTR	Continuous stirred tank reactor
D_a	Damkohler number
d_p	Diameter of a reactor bed media particle
DPM	Disintegrations per minute
D_w	Diffusivity in water (m^2/d)

$FBOD_5$	Filtered five day biochemical oxygen demand
FCOD	Filtered chemical oxygen demand
f_P	Maximum fraction of propionic acid from acid-formers (mg/L)
FTKN	Filtered total Kjeldahl nitrogen
FTP	Filtered total phosphorus
$\underline{H}$	Jacobian matrix of the measurement equations
HRT	Hydraulic retention time
HRT_o	Observed hydraulic retention time
$\underline{K}$	Kalman gain
K_{AF}	Saturation coefficient - acid-formers (mg/L)
K_{AM}	Saturation coefficient - acetoclastic methanogens (mg/L)
K_{BA}	Saturation coefficient - butyric acetogens (mg/L)
K_{GP}	Saturation coefficient - acid-former propionate production (mg/L)
K_{H2CO3}	Bicarbonate equilibrium constant at 38 °C
KH_{CO2}	Henry's law coefficient for carbon dioxide at 38 °C (mmole/L•atm)
K_i	Inhibition coefficient (mg/L)
$K_{I,AM}$	Inhibition coefficient - acetoclastic methanogens (mg/L)
$K_{I,BA}$	Inhibition coefficient - butyric acetogens (mg/L)
$K_{I,GA}$	Inhibition coefficient - acid-former acetate production (mg/L)
$K_{I,PA}$	Inhibition coefficient - propionic acetogens (mg/L)
k_L	Mass transfer coefficient in the biofilm stagnant liquid layer (m/d)
K_La	Carbon dioxide mass transfer coefficient (d^{-1})
k_{max}	Maximum rate constant (mg/mg•d)
K_{PA}	Saturation coefficient - propionic acetogens (mg/L)
K_S	Saturation constant (mg/L)
L	Thickness of stagnant liquid layer surrounding a biofilm (m)
L_f	Biofilm thickness (m)
MW_A	Molecular weight of acetic acid (mg/mmole)
MW_B	Molecular weight of butyric acid (mg/mmole)
MW_G	Molecular weight of glucose (mg/mmole)
MW_P	Molecular weight of propionic acid (mg/mmole)
n	Number of states
n^d	Number of deterministic states
$NH4\text{-}N$	Ammonia nitrogen
n^s	Number of stochastic states
$\underline{P}$	State estimation error variance-covariance matrix

P_{pCO2}	Partial pressure of carbon dioxide in the gas phase (atm)
PRBS	Pseudo-random binary sequence
P_T	Total pressure (atm)
Q	Total feed flow rate (L/d)
Q_C	Caustic addition rate for pH control (L/d)
$Q_{G,CH4}$	Methane flow rate (L/d)
$Q_{G,CO2}$	Carbon dioxide flow rate (L/d)
$Q_{G,T}$	Total gas flow rate (L/d)
Re	Reynolds number
r_S	Rate of substrate consumption (mg/L•d)
RTD	Resistance temperature detector
$\underline{R}_v$	Covariance matrix of measurement error vector
$\underline{R}_w$	Covariance matrix of state error vector
r_X	Rate of production of viable bacteria (mg/L•d)
S	Substrate concentration (mg/L)
S_A	Acetic acid concentration (mg/L)
S_B	Butyric acid concentration (mg/L)
Sc	Schmidt number
S_{COD}	Measured chemical oxygen demand concentration (mg/L)
S_G	Biodegradable (non-volatile acid) soluble organics concentration(mg/L)
S_{H+}	Aqueous hydrogen ion concentration
S_{HCO3}	Bicarbonate concentration (mmole/L)
S_I	Concentration of non-biodegradable components (mg/L)
S_{IC}	Total inorganic carbon concentration (mmole/L)
S_P	Propionic acid concentration (mg/L)
S_Z	Net cation concentration (mmole/L)
t	Time (d)
t_G	Gas-liquid carbon dioxide gas transfer rate (mmole/L•d)
t_G	Carbon dioxide gas transfer rate (mmole/L•d)
TKN	Total Kjeldahl nitrogen
TOC	Total organic carbon
TP	Total phosphorus
$\underline{u}$	Vector of known process inputs
UFCOD	Insoluble (particulate) chemical oxygen demand
u_o	Empty bed upflow velocity (cm/s)
$\underline{v}$	Vector of measurement noise

V	Reactor liquid volume (L)
V_G	Reactor gas phase volume (L)
V_S	Volume of 1 mmole of ideal gas at 1 atm and 38 °C (L/mmole)
VSS	Volatile suspended solids
$\underline{w}$	State error vector
$\underline{w}^d$	Deterministic state error vector
$\underline{w}^s$	Stochastic state error vector
$\underline{x}$	State variable vector
X	Concentration of viable bacteria (mg/L)
X_{AF}	Acid-former concentration(mg/L)
X_{AM}	Acetoclastic methanogen concentration (mg/L)
X_{BA}	Butyric acid utilizing acetogen concentration (mg/L)
$\underline{x}^d$	Vector of deterministic states
$\underline{\hat{x}}^d$	Estimated deterministic state vector
X_f	Concentration of biomass in a biofilm (g/m^3)
X_{PA}	Propionic acid utilizing acetogen concentration (mg/L)
$\underline{\hat{x}}^s$	Estimated stochastic state vector
$\underline{x}^s$	Vector of stochastic states
$\underline{y}$	Vector of observed outputs
Y	Growth yield (mg/mg)
Y_{AF}	Acid-former yield coefficient (mg/mg)
Y_{AM}	Acetoclastic methanogens yield coefficient (mg/mg)
Y_{BA}	Butyric acid acetogens yield coefficient (mg/mg)
Y_c	Synthesis yield coefficient (mg/mg)
Y_p	Product yield coefficient (mg/mg)
Y_{PA}	Propionic acid acetogens yield coefficient (mg/mg)
Z_B	Concentration of caustic for pH control (mmole/L)

CHAPTER 1

INTRODUCTION

Anaerobic biological degradation has long been used in standard technologies for the stabilization of animal manures and municipal wastewater treatment plant sludges. Over the past two decades, an improvement in understanding of the complex mechanisms governing the behaviour of this process and the development of new high rate reactor designs have expanded the application of anaerobic degradation to the treatment of soluble wastewaters containing high concentrations of dissolved, biodegradable organic materials. Anaerobic treatment has a number of cost advantages which are becoming increasingly recognized by practitioners. Full scale anaerobic reactors have been installed for wastewater treatment in a wide range of applications including the treatment of food processing, pulp and paper manufacturing, pharmaceutical manufacturing, landfill leachate, and petrochemical manufacturing wastewaters (Iza, *et al.*, 1991).

As wastewater generators face increasingly stringent effluent quality regulations, and as the cost of operating and expanding treatment plants increases, there will be more pressure to optimize existing treatment facilities. In many industrial applications, treatment plants can be faced with wide variations in loading rates and in concentrations of inhibitory or toxic wastewater constituents. These dynamic disturbances can cause upset conditions in biological treatment processes resulting in reduced treatment efficiencies. The perceived potential for upset from dynamic disturbances may in some cases eliminate anaerobic treatment from consideration during the selection of alternate treatment technologies.

To ensure continuous, trouble-free and efficient operation, an anaerobic process must

be operated to minimize the negative effects of dynamic disturbances on the anaerobic microorganisms. However, the development of the necessary operational and process control strategies is hampered by a lack of understanding of dynamic process behaviour and by the limited availability of sensors for the on-line measurement of important process variables.

In an effort to improve understanding of dynamic behaviour, a number of researchers have formulated mathematical dynamic models of the anaerobic treatment process. Published models include those of Andrews and Graef (1971), Hill and Barth (1977), Rozzi *et al.* (1985b) and Costello *et al.* (1991a), among others. The structure and complexity of the models have generally followed developments in the level of understanding of anaerobic degradation at the microbiological level.

Few anaerobic dynamic modelling studies have gone beyond the model structure hypothesis stage. However, the evaluation of the model structure using actual operating process data is one of the most important steps in dynamic modelling. Not only are the initial hypotheses tested, but information on the practicality of calibrating and applying the model for the intended purpose is obtained. The difficulties in calibrating anaerobic process dynamic models due to time-variable disturbances and parameters have not previously been considered. There are few available data sets that are sufficiently detailed to be useful for calibration and verification of dynamic models.

In addition, there has been little effort made towards exploring the applications of dynamic models. The objective of most studies to date has been to extend engineering knowledge of the process. Dynamic modelling can also be used to investigate potential operational and control strategies, and can be used as a tool in the design of these strategies. Using state estimation techniques, dynamic models can use signals from existing sensors to provide on-line estimates of other process variables.

1.1 RESEARCH OBJECTIVES

The overall goal of this research was to develop an improved understanding of the dynamic behaviour necessary to define monitoring and control requirements of high rate anaerobic treatment processes in order to optimize existing processes and extend potential application to less typical applications. The key steps necessary in this research effort were:

i) to gather a data set on the response of a high rate anaerobic reactor which would be useful for dynamic model selection, calibration and verification;

ii) to compile a dynamic model describing the observed process responses;

iii) to explore the requirements for calibrating a dynamic model when faced with a high level of uncertainty in the model structure;

iv) to utilize the dynamic model and the data set to determine critical areas for further research on operation and control of anaerobic treatment systems.

1.2 RESEARCH APPROACH AND SUMMARY

The background on the microbiological mechanisms and kinetic factors affecting design and control of high rate anaerobic treatment processes was reviewed. Previous model development, calibration and application efforts were then explored. This review is summarized in Chapter 2.

Dynamic experimentation was conducted on a pilot scale anaerobic fluidized bed reactor. This process configuration was chosen to reduce the likelihood that non-ideal hydraulic characteristics and diffusion limitations in the reactor would confound the dynamic biological response of the system. The mixing and mass transfer characteristics of the system were confirmed through a liquid tracer test and an analysis of the mass transfer kinetics.

Dynamic experiments on the anaerobic fluidized bed were designed to perturb the various reaction steps in the anaerobic degradation process. This was achieved by introducing feed pulses of glucose, propionic acid, butyric acid and acetic acid substrates into the system.

The response of a number of conventional monitoring parameters were recorded in addition to trace concentrations of gas phase hydrogen. The pilot plant and the experimental procedures and design are summarized in Chapter 3. Experimental results are summarized in Chapter 4.

A mathematical model was formulated based on a four population conceptual model and the experimental results from the pilot plant. The steps in formulating the model and initial model testing are described in Chapter 5.

Model calibration involved the use of the extended Kalman filter non-linear state estimator which allowed simultaneous estimation of the model parameters and the time-variable disturbances affecting the model. Due to the large number of parameters in the model, a sensitivity analysis was required to select the subset of parameters which were the most important to estimate. The observability of the estimated states and parameters was tested using a simulated data set. The calibration methodology, the sensitivity analysis and the initial testing using simulated data are summarized in Chapter 6. Estimation of the states and parameters using experimental data from the pilot plant is described in Chapter 7. This analysis was also used to indicate potential model improvements.

In Chapter 8, the experimental results are discussed in terms of their impact on operation and design of high rate anaerobic treatment processes. An effort was made to analyse the environmental and economic impact of a process upset in order to provide some direction for future research requirements. The dynamic model was used to demonstrate one possible operating strategy to reduce these costs. Finally, further potential model applications and model development requirements are discussed.

CHAPTER 2

BACKGROUND

2.1 MICROBIOLOGY

2.1.1 Biochemical Stages

The anaerobic degradation of organic matter consists of a complex series of reactions which result from the metabolic processes of several different groups of bacteria living in a symbiotic association. The net result of these reactions is the conversion of a wide variety of organic substrate materials into methane and carbon dioxide.

The present state of knowledge of the anaerobic decomposition of organic matter is illustrated in Figure 2.1 (McInerney *et al.*, 1979; Price, 1985; Harper and Pohland, 1986). The first step in the process is the hydrolysis of large organic molecules by extracellular enzymes. Carbohydrates are hydrolysed to monosaccharides; fats are hydrolysed to glycerol and fatty acids; proteins are hydrolysed to amino acids. The next stage in the sequence is the degradation of the products of the hydrolysis stage predominantly into hydrogen, carbon dioxide, and short chain (volatile) fatty acids consisting primarily of acetic acid, propionic acid and butyric acid.

Depending on the specific substrates and species of organisms present, different pathways could be involved at the acid production stage. The degradation of monosaccharides typically occurs by glycolysis via the Embden Meyerhof pathway. Long chain fatty acids are degraded by beta-oxidation. Weng and Jeris (1976) presented a pathway for deamination of amino acids. Many different species of acid-forming bacteria have been isolated in anaerobic

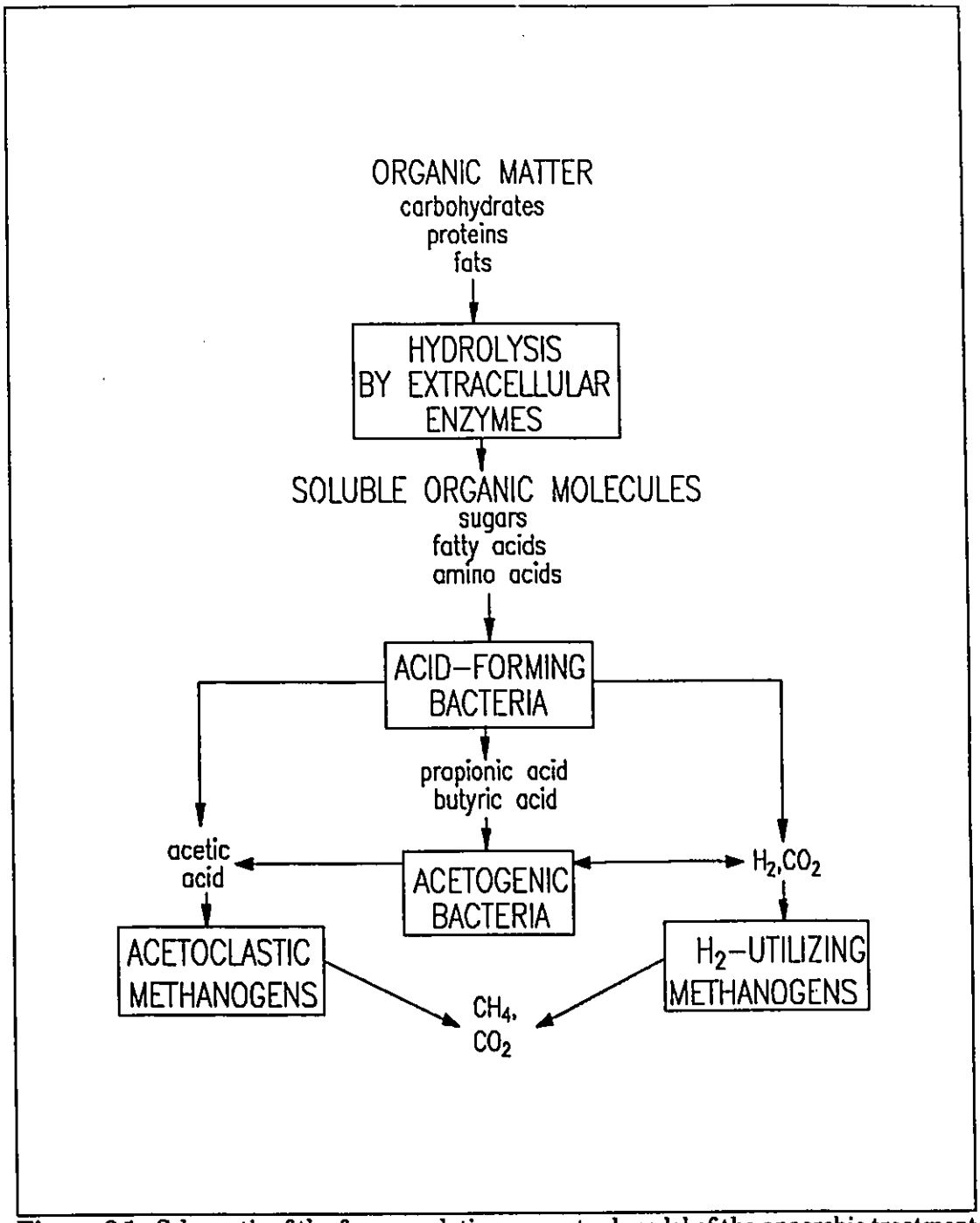

Figure 2.1: Schematic of the four population conceptual model of the anaerobic treatment process.

digestors (Price, 1985).

Propionic and longer chain fatty acids produced in the acid-forming stage are degraded to acetic acid, carbon dioxide and hydrogen by obligate hydrogen-producing acetogenic (OHPA) bacteria (McInerney *et al.*, 1979). An isolated culture of *Syntrophomonas wolfei* was observed to metabolize butyric through octanoic acids via beta-oxidation to acetate and hydrogen, or acetate, propionate and hydrogen (McInerney *et al.*, 1981). Another OHPA species, *Syntrophobacter wolinii*, degrades propionate to acetate, hydrogen and carbon dioxide (Boone and Bryant, 1980). A group of bacteria referred to as the homoacetogens metabolize carbon dioxide and hydrogen and produce acetic acid. However, in the anaerobic digestion process, the homoacetogens probably cannot compete with other hydrogen-utilizing species for substrate (Zeikus, 1979).

In the final stages of the reaction sequence, acetoclastic methanogens produce methane and carbon dioxide from acetic acid. This reaction is thought to produce 65-70% of the methane from the process (McInerney *et al.*, 1979). Methane is also produced from hydrogen and carbon dioxide by hydrogen-utilizing methanogens. The specific substrates utilized vary between methanogens. For example, *Methanothrix* degrades acetic acid only, *Methanosarcina* degrades acetic acid as well as hydrogen and carbon dioxide, and *Methanobacterium* utilizes hydrogen and carbon dioxide only (Harper and Pohland, 1986).

Sulphur-reducing bacteria such as *Desulfovibrio vulgaris* can also exist in the anaerobic digestion process (Price, 1985). These bacteria utilize sulphate (SO_4^{2-}) as a terminal electron acceptor, utilize organic compounds as a carbon and energy source, and can utilize hydrogen as an energy source. Sulphur-reducing bacteria may decrease methane production by competing for methanogenic substrates or by producing sulphides which are known to inhibit methanogenesis (Hilton and Oleszkiewicz, 1988).

The need to maintain a balance between all bacterial populations in the anaerobic digestion process in order to maximize waste stabilization has long been recognized

(McCarty, 1964). Methanogenesis has normally been thought to be the overall rate-limiting step in the treatment of soluble wastewaters and many studies have been conducted in which volatile fatty acid accumulations have been observed during overloading or process stress (Barnes *et al.*, 1984; Guiot and van den Berg, 1984; Stover *et al.*, 1985; Kennedy *et al.*, 1985; Eng *et al.*, 1986; Jones and Hall, 1989).

2.1.2 Interspecies Hydrogen Transfer and Regulation of the Biochemical Stages

There has been a major emphasis in recent years on the role that hydrogen plays in the accumulation of intermediate compounds in the anaerobic digestion process. Hydrogen is produced in the acid-forming stages of the anaerobic process and is removed by hydrogen-utilizing methanogens in reducing carbon dioxide to methane. Studies of specific anaerobic cultures and analysis of the thermodynamics of the various anaerobic conversions have shown the importance of this interspecies hydrogen transfer in the regulation of anaerobic processes.

The importance of interspecies hydrogen transfer was first discovered when studies revealed that *Methanobacillus omelianskii* is in fact a co-culture of a hydrogen-utilizing methanogen and an ethanol-oxidizing organism (Bryant, *et al.*, 1967). The products of the ethanol oxidation are acetate and hydrogen;

$$CH_3CH_2OH + H_2O \rightarrow CH_3COO^- + H^+ + 2H_2 \qquad \Delta G^\circ = +9.6\ kJ \qquad (2.1)$$

The positive standard free energy change (ΔG°) indicates that the above reaction will only proceed towards completion if the products are continuously removed from the reaction environment. In the ethanol degrading co-culture discovered by Bryant and coworkers, this is achieved by the oxidation of the hydrogen by a hydrogen-utilizing methanogen;

$$4H_2 + CO_2 \rightarrow CH_4 + 2H_2O \qquad \Delta G^\circ = -135.6\ kJ \qquad (2.2)$$

The butyrate and propionate degrading OHPA organisms, *Syntrophomonas wolfei* and *Syntrophobacter wolinii* would only grow in co-culture with hydrogen-utilizing methanogens when studied by Boone and Bryant (1980). The respective acetogenic reactions by which these compounds are degraded are as follows:

$$CH_3CH_2CH_2COO^- + 2H_2O \rightarrow 2CH_3COO^- + H^+ + 2H_2 \qquad \Delta G^\circ = +48.1 \text{ kJ} \qquad (2.3)$$

and,

$$CH_3CH_2COO^- + 3H_2O \rightarrow CH_2COO^- + HCO_3^- + H^+ + 3H_2 \qquad \Delta G^\circ = +76.1 \text{ kJ} \qquad (2.4)$$

The ΔG° for each of these reactions again shows the necessity of maintaining low product concentrations. Hydrogen-utilizing methanogens maintain a low hydrogen concentration through the reaction in Equation (2.2) while acetoclastic methanogens remove acetate according to Equation (2.5).

$$CH_3COO^- + H_2O \rightarrow CH_4 + HCO_3^- \qquad \Delta G^\circ = -31.0 \qquad (2.5)$$

Hydrogen is thought to play an important role in the degradation of carbohydrates via the Embden-Meyerhof pathway, as illustrated in Figure 2.2. The concentration of hydrogen in the reaction environment can influence the concentration of products formed by affecting reactions at several points in the pathway. Reactions at points A and B proceed with a transfer of electrons (hydrogen) to the oxidized form of the nicotinamide-adenine dinucleotide carrier molecule (NAD^+). For these reactions to proceed continuously, the reduced (NADH) form of the carrier molecule must be re-oxidized to NAD^+. This occurs through the reduction of protons to form hydrogen gas, as shown in Equation (2.6).

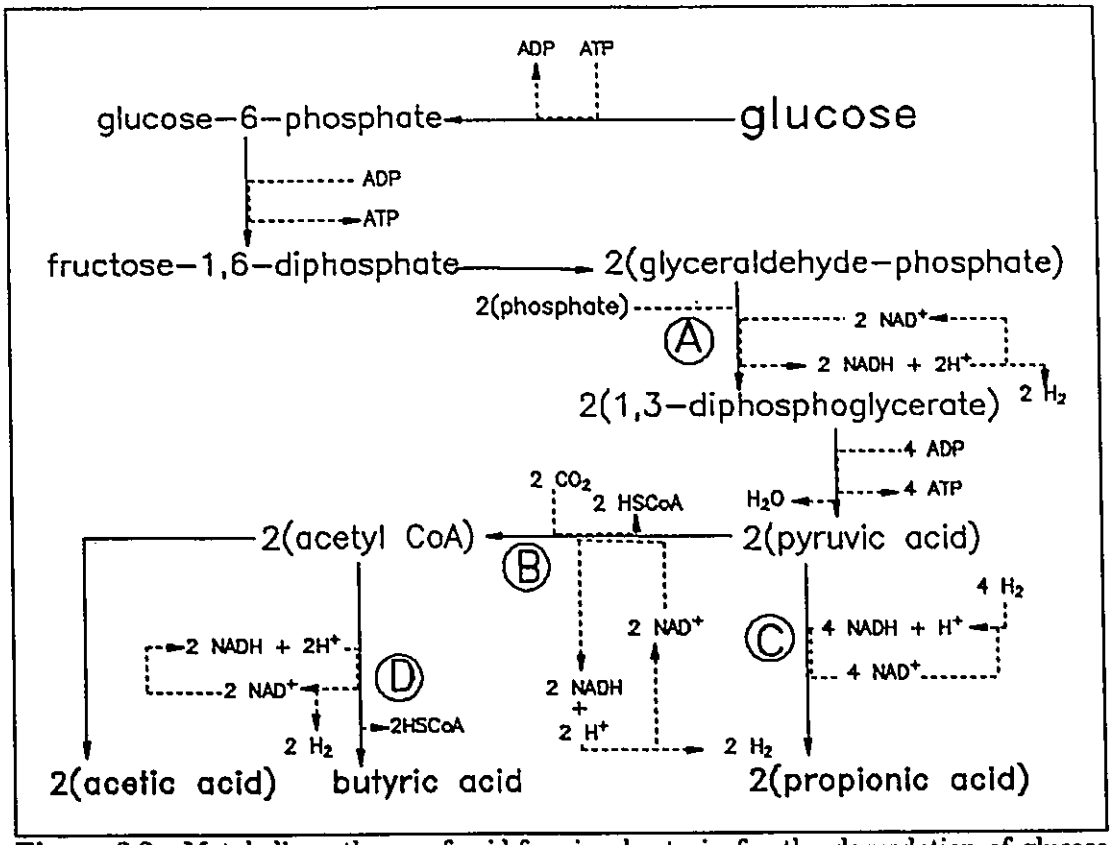

Figure 2.2: Metabolic pathway of acid-forming bacteria for the degradation of glucose (after Mosey, 1983).

$$H^+ + NADH \rightarrow NAD^+ + H_2 \qquad \Delta G^\circ = +123.4 \text{ kJ} \quad (2.6)$$

The terminal hydrogen (electron) acceptors in an anaerobic process are normally carbon dioxide or oxidized forms of sulphur. However, if hydrogen-utilizing methanogens or sulphur-reducing bacteria do not remove the hydrogen to sufficiently low levels to allow the above reaction to proceed, it has been postulated that the acid-forming bacteria will utilize the excess hydrogen to reduce pyruvic acid or acetyl coenzyme A at points C and D to produce propionic acid and butyric acid, respectively (Mosey, 1983).

A number of studies using suspended growth cultures have demonstrated hydrogen effects experimentally. Chung (1976) studied pure cultures of various acid-forming rumen

bacteria. It was shown that during a glucose fermentation, increasing the hydrogen concentration in the culture would result in an increase in the production of formate, lactate, ethanol and butyrate and a decrease in the production of acetate. Kaspar and Wuhrmann (1978) observed inhibition of propionate degradation in municipal anaerobic digestor sludge when the gas phase hydrogen concentration was raised to 5000 ppm (0.5%). Lower concentrations of hydrogen had no measurable effect on propionate degradation. Fukuzaki *et al.* (1990) also observed inhibition of propionate degradation when the gas phase hydrogen concentration in a batch suspended culture was varied between 1% and 91% by injecting hydrogen into the headspace. A hydrogen-utilizing methanogen reversed the inhibition when added to a culture inhibited by 91% hydrogen.

2.1.3 Volatile Acid and pH Inhibition

Inhibition effects of other intermediate compounds have also been demonstrated experimentally. Kaspar and Wuhrmann (1978) observed complete inhibition of propionate degradation when 4800 mg/L of acetate was added to a suspended growth culture. Denac *et al.* (1988b) observed accumulations of propionic acid as reactor loading increased. Fukuzaki *et al.* (1990) observed inhibition of propionate degradation by addition of propionate and acetate. Batch experimentation by Mawson *et al.* (1991) indicated substrate and product inhibition of both propionate and acetate degradation.

The requirement to maintain the proper pH in anaerobic processes has long been recognized (McCarty, 1964). Studies have been conducted to examine the pH effects on various stages of the process. Van den Berg *et al.* (1976) found the optimum pH range for methane production from acetic acid in an enriched methanogenic culture was 6.5 to 7.1. Beyond this range, methane production dropped rapidly. Heyes and Hall (1983) investigated the pH inhibition of propionate oxidation in a mixed culture digester. Kinetics of two distinct groups of propionate-utilizing acetogens were identified. The slower growing group was completely

inhibited by a pH shock from 7.0 to 6.0 while the faster growing group was less sensitive to pH shock.

One mechanism hypothesized for pH inhibition in microorganisms is related to the higher permeability of the cell membrane to un-ionized (neutral) compounds. When un-ionized volatile acid substrates diffuse into a cell from a low pH environment, the acids dissociate inside the cell at the higher pH. This causes inhibition either through acidification of the cell cytoplasm, or through a decrease in net ATP production due to the energy required to remove excess protons from the cell (Attal *et al.*, 1988).

2.2 KINETICS

In a fixed-film biochemical system, the reaction rates may be controlled by either the diffusional resistance of substrates in the biofilm, or by the reaction rate kinetics in the biomass. In this section, the reaction rate equations used for anaerobic systems will be reviewed. Models which can be used to assess the significance of mass transfer resistance in a fixed film system will also be presented.

2.2.1 Reaction Rate Kinetics

The rate of bacterial growth in biological processes is usually expressed by the first order equation:

$$r_X = \mu X \tag{2.7}$$

where, r_X = the rate of production of viable bacteria (mg/L•d); μ = the specific growth rate (d^{-1}); and X = the concentration of viable bacteria (mg/L).

The consumption of substrates is related to the rate of bacterial growth through the yield:

$$Y = \frac{r_X}{-r_S} \tag{2.8}$$

where, Y = the growth yield (mg bacteria/mg substrate); and, r_S = the rate of substrate consumption (mg/L•d).

The rate of substrate utilization can therefore be expressed as a first order equation with respect to the concentration of viable cells:

$$-r_S = \frac{\mu}{Y} X \tag{2.9}$$

The effect of the concentration of the growth limiting substrate on μ has most frequently been expressed by the empirical Monod expression which is similar in structure to the autocatalytic Michealis-Menten kinetic equation for a single substrate, single enzyme reaction:

$$\mu = \frac{\mu_{max} S}{K_s + S} \tag{2.10}$$

where, K_s = the saturation constant (mg/L); μ_{max} = the maximum specific growth rate (d^{-1}); and, S = the substrate concentration (mg/L).

In some cases, μ_{max} and Y are combined so that,

$$-r_S = \frac{K_{max} S}{K_S + S} X \tag{2.11}$$

where, $K_{max} = \mu_{max} / Y$ = the maximum rate constant (mg substrate /mg bacteria•d).

Many pure and mixed culture studies have been conducted to determine values for μ_{max}, K_s, and Y for the microorganisms that exist in anaerobic processes. Pavlostathis and

Giraldo-Gomez (1991) have compiled results from a number of these studies. The range of kinetic data reported in this review is shown in Table 2.1.

Table 2.1: Range of kinetic data reported in literature (Pavlostathis and Giraldo-Gomez, 1991)

Reaction step	μ_{max} (d^{-1})	K_s (mg COD/L)	Y (mgVSS/mgCOD)
Acid-former fermentation of glucose	7.2 to 30	22 to 530	0.14 to 0.17
Acetogenic oxidation of propionic acid	0.13 to 1.2	17 to 500	0.025 to 0.051
Acetogenic oxidation of butyric acid	0.35 to 0.86	12 to 300	0.03 to 0.047
Acetoclastic methanogenesis	0.08 to 1.4	15 to 420	0.01 to 0.054
Methanogenesis from hydrogen and carbon dioxide	0.05 to 4.07	4.8×10^{-5} to 0.145	0.017 to 0.045

The Monod kinetic expression has been modified by many researchers to quantify the inhibition effects observed in biological processes (Luong, 1987). In a dynamic model of the anaerobic process, Andrews (1969) used the following kinetics to describe acetoclastic methanogenesis:

$$\mu = \frac{\mu_{max}}{1 + \frac{K_s}{S} + \frac{S}{K_i}} \qquad (2.12)$$

where, K_i = an inhibition constant (mg/L); and, S = the concentration of (un-ionized) acetic acid (mg/L). Similar equations were utilized in later dynamic models of the anaerobic process (Andrews and Graef, 1971; Hill and Barth, 1977; Moletta *et al.*, 1986).

Mosey (1983) proposed kinetic expressions for the acid-forming and acetogenic stages

which incorporated the regulation effects of hydrogen. The unregulated substrate uptake rates of the acid-formers and the acetogenic bacteria was postulated to occur according to Monod kinetics. The regulated production rates of acetic, propionic and butyric acid and the consumption rates of propionic and butyric acid were calculated by modifying the Monod kinetics through regulation functions based on the relative concentrations of NADH and NAD^+. The Nernst equation was used to derive a relationship between the concentration of gas phase hydrogen and the ratio of NADH and NAD^+ within the acid-forming bacteria. Similar kinetic expressions were utilized in the dynamic models published by Ide (1988) and Costello *et al.* (1991a). The major assumption incorporated into these kinetic expressions is that there exists a common hydrogen pool such that the hydrogen concentrations within all bacteria in the system, in the bulk liquid phase, and in the gas phase are in equilibrium.

2.2.2 Mass Transfer Kinetics

For a substrate to react in a fixed microbial film of thickness, L_f, it must first be transported by molecular diffusion across a stagnant liquid layer of thickness, L, resulting in a substrate concentration gradient across the liquid layer. A substrate concentration gradient in the biofilm can also occur as molecular diffusion and reaction of the substrate occur simultaneously.

The rate of substrate removal (r_s) in a fixed film system is the product of the substrate flux into the biofilm (J) in units of mass of substrate per unit of biofilm surface area per unit time, and the biofilm surface area (A):

$$-r_S = JA \tag{2.13}$$

If Monod kinetics can be assumed to apply in the biofilm, the equation for the substrate flux into the biofilm can be written as follows (Rittmann and McCarty; 1981):

$$J = \lambda k_{max} X_f L_f \frac{S}{K_S + S} \tag{2.14}$$

where, k_{max} = the maximum specific rate of substrate utilization (mass of substrate per unit mass of biomass per unit time); X_f = the concentration of biomass in the biofilm (mass of biomass per unit volume); L_f = the biofilm thickness; S = the substrate concentration in the bulk phase of the reactor (mass of substrate per unit volume); and, K_s = the saturation constant (mass per unit volume). The effectiveness factor, λ, is the ratio of the actual reaction rate to the theoretical reaction rate that would occur in the absence of mass transfer resistance. In other words, as the effectiveness factor approaches unity, mass transfer effects become less important in the overall rate of reaction.

The mass transfer resistance occurring in a fixed film reactor can be divided into the external resistance through the stagnant liquid layer, and the internal resistance in the biofilm. Correlations have been developed for the calculation of effectiveness factors for both internal (λ_i) and external (λ_e) mass transfer resistances.

a) External mass transfer resistance

The diffusion of a soluble substrate across the stagnant liquid layer surrounding a biofilm can be expressed by Fick's first law as follows:

$$J = -D_w \frac{dS}{dz} = \frac{D_w}{L}(S - S_s) \tag{2.15}$$

where, S_s is the concentration of substrate at the surface of the biofilm (mass of substrate per unit volume); L is the thickness of the stagnant liquid layer surrounding the biofilm (length); and, D_w is the diffusivity of the substrate in water (area per unit time). The mass transfer coefficient, k_L in units of length per unit time, is expressed as follows:

$$k_L = \frac{D_w}{L} \tag{2.16}$$

Empirical correlations for k_L have been developed for different flow situations. Kissel (1986) expressed the correlation for k_L in liquid-fluidized beds as follows:

$$k_L = \frac{(0.81/\epsilon_f)\, D_w (Re)^{1/2} (Sc)^{1/3}}{d_p} \tag{2.17}$$

where, ε_f is the porosity of the fluidized bed; Re is the Reynolds number; Sc is the Schmidt number; and, d_p is the diameter of a media particle (length).

For Monod kinetics at the biofilm, Grady and Lim (1980) have derived the equation for the effectiveness factor for external mass transfer resistance, λ_e:

$$\lambda_e = \frac{(K^*+1)\{1-K^*-D_a+[(1-K^*-D_a)^2+4K^*]^{0.5}\}}{(1+K^*-D_a)+[(1-K^*-D_a)^2+4K^*]^{0.5}} \tag{2.18}$$

in which,

$$K^* = \frac{K_s}{S} \tag{2.19}$$

and

$$D_a = \frac{k_{max} X_f V_f / a_s}{k_L S} \tag{2.20}$$

where, V_f = the total biofilm volume; and, a_s = the total biofilm surface area. The

dimensionless term, D_a, is often referred to as the Damkohler number.

As λ_e approaches unity, the effect of external mass transfer resistance is negligible and the substrate concentration at the surface of the biofilm can be assumed equal to the bulk substrate concentration.

b) Internal mass transfer resistance

Atkinson and Davies (1974), obtained the following equations for the effectiveness factor, λ_i, for mass transfer resistance within the biofilm:

$$\lambda_i = \begin{cases} 1 - \dfrac{\tanh(L_f^*)}{L_f^*}\left[\dfrac{\phi}{\tanh\phi} - 1\right] & \phi \le 1 \\ \dfrac{1}{\phi} - \dfrac{\tanh(L_f^*)}{L_f^*}\left[\dfrac{1}{\tanh(\phi)} - 1\right] & \phi \ge 1 \end{cases} \tag{2.21}$$

in which,

$$L_f^* = \frac{L_f}{\sqrt{(K_s D_f)/(kX_f)}} \tag{2.22}$$

$$\phi = \frac{L_f^*}{\sqrt{(1+2S^*)}} \tag{2.23}$$

where, D_f = the mass diffusivity of the substrate in the biofilm (area per unit time), and $S^* = S/K^*$ (dimensionless). As the value of λ_i approaches unity, diffusional resistances can be considered negligible and the concentration of substrates and products can be assumed to be uniform throughout the depth of the biofilm.

2.3 PROCESS DESIGN

The biomass solids retention time (θ_c) in an anaerobic treatment process must be sufficient to prevent the wash-out of the slowest growing microorganism necessary for the degradation of the wastewater constituents. If the loss of biomass through decay is neglected, it can be shown that the following relationship exists between the bacterial specific growth rate (μ) and θ_c at steady state (Parkin and Owen, 1986):

$$\frac{1}{\theta_c} = \mu \qquad (2.24)$$

The minimum solids retention time required to prevent wash-out (θ_c^{min}) is thus given as follows:

$$\theta_c^{min} = \frac{1}{\mu_{max}} \qquad (2.25)$$

The kinetic data summarized in Table 2.1 indicate that for the treatment of soluble wastewaters, the growth rates of the methanogenic or the acetogenic bacteria typically determine θ_c^{min}. Design practice must incorporate an adequate margin of safety in the solids retention time to allow an anaerobic reactor to withstand variable loads of toxic or inhibitory compounds without washing out the affected microorganisms.

In a continuous stirred tank reactor (CSTR) such as a conventional sludge digester, θ_c is equal to the hydraulic retention time (HRT). Although a number of different high rate anaerobic reactor configurations have emerged (Iza *et al.*, 1991), the common feature found in the high rate designs is the ability to decouple the HRT and θ_c. This allows high concentrations of biomass to accumulate while operating the process at relatively low hydraulic retention times. The result is that long solids retention times are achieved at high volumetric

organic loading rates. Biomass solids retention times in high rate anaerobic reactors have been estimated in excess of 100 days (Mueller and Mancini, 1975). Volumetric organic loading rates greater than 30 kg COD/m^3•d have been achieved at full scale (Hickey *et al.*, 1991), although the typical range is between 3 and 20 kg COD/m^3•d (Totzke, 1990). This has lead to the application of anaerobic processes to the treatment of a wide variety of industrial wastewaters.

The use of biomass retention mechanisms has enabled systems to operate at high loading rates with increased stability due to the high concentrations of biomass which accumulate in the reactor. However, shorter retention times also result in more rapid changes in the operational state of the process. Maintenance of process stability under highly dynamic operating conditions will thus require new developments in monitoring and control strategies, particularly as anaerobic processes are applied to more inhibitory industrial wastewaters.

2.4 PROCESS CONTROL

Although the revolution in the design of anaerobic treatment processes has lead to greatly improved reliability and enabled systems to operate at high organic loading rates, anaerobic systems applied to many industrial wastewaters can still be faced with dynamic conditions which can reduce the performance of the treatment process. For example, Wheatley *et al.* (1988) operated a 25 m^3 anaerobic filter pilot plant at a sugar confectionary factory and found that due to upsets caused by large fluctuations in the wastewater strength, stable operation could only be achieved at loading rates below 3 kg COD/m^3•d. Saslawsky *et al.* (1988), reported difficulties in restarting a full scale anaerobic filter during treatment of sulphite pulp mill evaporator condensates. Following short interruptions in wastewater flow, stable plant operation could not be obtained above loading rates of 1.5 kg COD/m^3•d without reseeding and the addition of cosubstrates. During a laboratory study of sequential anaerobic-aerobic treatment of a thermomechanical pulp mill effluent, Rintala and Vuoriranta (1988)

found that loading increases to an upflow anaerobic sludge blanket (UASB) pretreatment process could result in accumulations of volatile acids and subsequent reductions in chemical oxygen demand (COD) removal efficiencies from greater than 75% to less than 40%. The upsets lasted from a day to several weeks and caused increased aeration requirements in the downstream activated sludge unit.

The overall objective of a process control system for an anaerobic treatment process is the maintenance of an environment within the process which will allow the microorganims to achieve the maximum conversion of the biodegradable wastewater components to methane. The specification of some low level control loops which support this objective is relatively straightforward. For example, pH and temperature must be maintained within specific ranges to maintain maximum waste conversion rates. Controllers for these parameters can be designed with a minimal knowledge of the actual physical, chemical and biological phenomena affecting the dynamic behaviour of process pH or temperature, and the parameters are readily measurable on-line. Although it has been suggested that pH measurement is too problematic to allow the use of pH as a feedback variable in anaerobic processes (Rozzi, *et al.*, 1985a; Weiland and Rozzi, 1991), pH measurement and control appear to be standard practice in full scale anaerobic systems (Henry and Varaldo, 1988; Saslawsky *et al.*, 1988; Schlott *et al.*, 1988; Lettinga and Hulshoff Pol, 1991). The alternatives to pH measurement and control, such as on-line determination of bicarbonate concentrations (Pauss *et al.*, 1990b), are significantly more complex and do not completely eliminate the requirement for pH measurement.

Less straightforward is the design of controllers which will prevent process upsets due to organic or toxic overloading. The first requirement of such a control system is the prediction or earliest possible detection of such an upset. Assuming that pH and temperature control in the system are adequate, prediction of an upset requires the ability to monitor and determine the impact of variations in the concentrations of biodegradable and inhibitory components of the influent wastewater. Early detection of process upsets requires a choice of

monitoring variables which will respond quickly to upsets.

Conventional monitoring variables for anaerobic processes include volatile acids, alkalinity, COD removal, gas production rates and methane and carbon dioxide content of the biogas. After formulating kinetic expressions for hydrogen effects in the anaerobic process, Mosey (1983) proposed the use of hydrogen as an indicator of process stability. Several subsequent studies have demonstrated a gas phase hydrogen response to increases in organic loading (Barnes *et al.*, 1984; Mosey and Fernandes, 1989; Smith and McCarty, 1990). Hickey and Switzenbaum (1991) investigated the use of trace levels of hydrogen and carbon monoxide in the biogas as indicators of the status of specific metabolic pathways within the process. In any case, the ability to interpret the response of process monitoring variables requires a knowledge of the interactions of the measured variables and the internal process states.

Once a process upset has been detected, control actions must be implemented to correct the conditions causing the upset. The action required will depend on the type of upset. For example, overloads of biodegradable and inhibitory compounds may be diverted or equalized. Determination of the type and degree of control action required will again require an understanding of the dynamic interactions occurring within the process. Simplified models of the anaerobic digestion process have been utilized to design adaptive controllers to maintain effluent substrate concentration levels at a given setpoint through manipulation of the feedrate (Renard *et al.*, 1988; Dochain and Bastin, 1985). Although these designs were successful in meeting the control objectives, the practical limitations of using feedrate control were not addressed in these studies. A similar approach has been used in the design of an adaptive controller for the hydrogen concentration (Dochain *et al.*, 1991).

The preceding discussion indicates that in order to protect and maximize conversion in an anaerobic wastewater treatment process, it is important to understand the dynamic interactions which affect process performance. A significant amount of research has been conducted over the last two decades developing mechanistic dynamic models which would lead

to an improved understanding of process behaviour. The following section provides an historical overview of the major developments in mechanistic models of anaerobic processes.

2.4.1 Dynamic Modelling

The evolution of dynamic models of the anaerobic treatment process has followed the development of understanding of the microbiological interactions within the process. As understanding improved, another level of complexity was added to published anaerobic process models.

Andrews (1969) published the first dynamic mathematical model for a continuous flow, completely-mixed anaerobic digestion process. Under the assumption that acetoclastic methanogenesis is the rate limiting step in the process, the single-bacterial population model was comprised of dynamic mass balances for the effluent concentrations of acetic acid and bacterial solids. The kinetics for bacterial growth and substrate utilization were described by equation (2.11). The original model was subsequently extended by Andrews and Graef (1971) by incorporating interactions between volatile acids, pH, alkalinity, gas production rate and gas composition. The structure of the model which defined these interactions formed the basis for many later models of the process.

In an effort to model the degradation of more complex wastes, Hill and Barth (1977) developed a two-bacterial population model which included the reactions of the acid-forming bacteria and the methane-forming bacteria. This model was similar in structure to the model of Andrews and Graef in that the interactions between the gas, liquid and biological phases of the reactor were considered. The state variables included were insoluble organic matter, soluble organics, volatile acids, acid-forming bacteria, methanogenic bacteria, dissolved carbon dioxide, gas phase carbon dioxide, cation concentration and ammonium concentration. Methane production and pH were predicted in the same way as the Andrews and Graef model. A number of models similar to the Hill and Barth model have been published, including those

of Rozzi (1984) and Moletta *et al.* (1986), among others.

As the conceptual structure for the anaerobic degradation process shown in Figure 2.1 emerged, dynamic models were formulated which incorporated the reactions of the acid-formers, the acetogens, the acetoclastic methanogens and the hydrogen-utilizing methanogens. Rozzi *et al.* (1985b) incorporated the kinetic equations developed by Mosey (1983) into a comprehensive model which considered the interactions between the gas, liquid and biological phases of the reactor in a manner similar to earlier one and two-bacterial population models. State variables estimated by the model included reactor concentrations of glucose, acetic acid, propionic acid, butyric acid, cations and dissolved CO_2, and the gas phase concentration of hydrogen. Ide (1988) applied a similar model structure to simulate anaerobic filters. More recently, Costello *et al.* (1991a) extended the four-bacterial population model to include reactions resulting in the possible accumulation of lactic acid in the system. Labib *et al.* (1988) studied the dynamics of butyric acid degradation in an anaerobic fluidized bed reactor. A model was formulated which incorporated the inhibition effects of acetate and hydrogen on butyrate degradation as observed during short term influent pulses of acetate and formate.

2.4.2 Model Calibration

The time-variable behaviour of a process can in general be expressed by the following lumped parameter representation:

$$\frac{d\underline{x}(t)}{dt} = f(\underline{x}(t), \underline{u}(t), \underline{\theta}, \underline{\alpha}(t)) \tag{2.26}$$

$$\underline{y}(t) = h(\underline{x}(t), \underline{u}(t), \underline{\theta}, \underline{\nu}(t)) \tag{2.27}$$

where, $\underline{x}(t)$ is a vector of state variables characterizing the system dynamic behaviour; $\underline{u}(t)$

is a vector of known process inputs; $\underline{\theta}$ is a vector of unknown process parameters; and, $\underline{\alpha}\ (t)$ is a vector of unmeasured disturbance states which represent both unmeasured inputs and unknown internal mechanisms. The observed outputs, $\underline{y}\ (t)$, are corrupted by some amount of measurement noise, as represented by $\underline{v}\ (t)$.

Model calibration has generally been considered to be the procedure required to estimate the values of the unknown parameters, $\underline{\theta}$, from the observations $\underline{y}\ (t)$ and $\underline{u}\ (t)$. To achieve this, a criterion is used to give a measure of how well a model fits the observations. The most commonly used criterion is to minimize a squared-error cost function (*SSQ*):

$$SSQ = \sum_{i=1}^{N} e_i^2 \tag{2.28}$$

where,

$$e_i = y(t_i) - \hat{y}(t_i) \tag{2.29}$$

and $\hat{y}\ (t_i)$ is the model estimate of $y\ (t_i)$.

Anaerobic dynamic process models have typically been calibrated using kinetic data from previous batch culture experiments. Few examples of the direct calibration of anaerobic process models exist in the literature. Carr and O'Donnell (1977) compared responses predicted by the single bacterial Andrews and Graef (1971) model to experimental step test data from laboratory scale, continuous flow, complete-mixed digestors fed with an acetic acid substrate. Kinetic parameters in the model were adjusted to give the best visual fit of model predictions to the experimental data collected during step changes in the influent acetic acid concentration. Chalon *et al.* (1982) used a squared-error cost function based on the difference between actual and predicted daily gas production rates from a laboratory scale digester to calibrate a two population model similar in form to the model developed by Hill and Barth

(1977). Furumai *et al.* (1991) used data from batch experiments on an anaerobic fluidized bed reactor to determine kinetic parameters for the degradation of propionic acid, butyric acid and acetic acid through a least squares regression. The same experimental method was used by Denac *et al.* (1988b) to estimate kinetic parameters of acid degradation for use in a four population model. Costello *et al.* (1991b) estimated the maximum substrate uptake rate coefficients for butyrate-utilizing acetogens, acetoclastic methanogens and hydrogen-utilizing methanogens, and the influent concentration of bicarbonate by minimizing the sum of the squared errors for volatile acid concentrations, biogas flowrate and the methane content of the biogas using data from previously published experiments in which the process response to step changes in influent loading were recorded (Denac, *et al.*, 1988a; Eng, *et al.*, 1986; Grauer, 1986).

The difficulty in considering model calibration as only the estimation of the unknown parameters, $\underline{\theta}$, is that process behaviour is also affected by the disturbance states, $\underline{\alpha}\ (t)$. Failure to consider the effects of $\underline{\alpha}\ (t)$ while estimating $\underline{\theta}$ will lead to significant time-dependent biases in the parameters (Beck and Young, 1976). This problem has been addressed in polymerization systems by simultaneously estimating $\underline{\theta}$ and $\underline{\alpha}\ (t)$ by an extended Kalman filter (Kozub and MacGregor, 1992). Time dependent variations in the parameter states have been used to assist in improving the model structure (Beck and Young, 1976; Beck, 1989)

There are a number of examples of the application of the extended Kalman filter for parameter estimation in biological systems. Stephanopoulos and San (1984) investigated the use of an extended Kalman filter for the on-line estimation of the specific growth rate, μ, and the growth yield, Y, in pure culture suspended growth systems. Both parameters were considered to be completely empirical with no substrate dependent model assumed for μ. A similar approach was used by Bastin and Dochain (1986) for the on-line estimation of μ. The difficulty with this approach is that the lack of structure in the bacterial kinetic term results in a model which is of limited use for simulation and forecasting. The use of an extended

Kalman filter to assist in operational control of a biological wastewater treatment plant was first investigated by Beck (1981). The filter incorporated a model for the activated sludge process and was found to give reasonable estimates of the concentrations of the two nitrifying bacterial species from measurements of the influent flow-rate and ammonium-N concentration, and the effluent concentrations of ammonium-N, nitrite-N, and nitrate-N. Holmberg and Olsson (1985) used an extended Kalman filter to estimate the oxygen transfer rate and respiration rate in a simulation study of an activated sludge process. A non-linear oxygen mass balance equation was used in the filter. The Kalman filter was shown to converge to the true parameter values. Preliminary investigations have been conducted on the use of a Kalman filter for the on-line estimation of total volatile acids in anaerobic processes using a simple model of the acid-base system (Jones *et al.*, 1988). In a simulation study, an extended Kalman filter incorporating a two-population model of the anaerobic process was used to estimate the concentrations of acid-forming bacteria, methane-forming bacteria, and volatile acids (Jones *et al.*, 1989).

2.5 JUSTIFICATION FOR THE PRESENT RESEARCH

Although a number of comprehensive dynamic models have been proposed for anaerobic treatment processes, there are a limited number of studies in which these models have been calibrated and tested using actual process data. In high rate anaerobic processes, the large difference between the magnitude of the hydraulic retention time and the solids retention time is expected to result in large differences in the time constants of important dynamic phenomena in the process. Experimental design and data collection must reflect the fact that a response in substrate and product states may be essentially complete within a few hours of the initiation of a disturbance whereas the response may change dramatically within days or weeks due to more gradual changes in biomass characteristics. As a result, the magnitude of a disturbance must be sufficiently large and the monitoring frequency must be

sufficiently high to obtain information on the short term response of the system, while experiments must be of sufficient duration to assess the longer term responses of the system. There are no previously published dynamic studies on high rate anaerobic processes which satisfy all of these criteria. Model calibration and testing must be conducted with such a data set to adequately evaluate the model structure. In addition, calibration difficulties caused by the large number of parameters in anaerobic process models and the possible time-variable nature of these parameters have not previously been addressed.

A major objective of this study was to design and conduct experiments which would result in a data set suitable for dynamic modelling. Whereas previous researchers have compiled dynamic models based on a conceptual understanding of the interactions in the process such as shown in Figure 2.1, an objective of this study was to only include those phenomena which appeared significant during dynamic experimentation. The intention was to compile a model which would be practical to calibrate. Another objective of the study was to explore the requirements for calibrating the model when faced with uncertainty in the long term response of a system.

CHAPTER 3

EXPERIMENTAL EQUIPMENT AND PROCEDURES

Experimentation was conducted on a pilot scale high rate anaerobic fluidized bed reactor operated at Environment Canada's Wastewater Technology Centre (WTC) in Burlington, Ontario. The objective of the experimental program was to generate data characterizing the dynamic response of the process to dynamic inputs of organic substrates. This chapter describes the pilot plant hardware, summarizes the characteristics of the pilot plant wastewater feed, describes the pilot plant start-up and operating procedures utilized prior to dynamic experimentation, and summarizes the dynamic experimental design. The dynamic experiments were designed iteratively. Initial dynamic experimentation provided information which was used to set the magnitude and duration of dynamic forcing functions in the final design.

3.1 PILOT PLANT FACILITIES

The anaerobic fluidized bed reactor had an empty bed liquid volume of 77 L. The reaction zone in the system consisted of an acrylic cylinder 0.15 m in diameter and 3 m high. An upper settling zone was also constructed from an acrylic cylinder, 0.23 m in diameter and 1 m high. An inverted PVC cone suspended from the top of the reactor functioned as a gas-liquid-solid separator. Sample ports were installed along the length of the reactor.

The pilot plant was equipped with two Watson-Marlow Model 501U variable speed peristaltic feed pumps. The recycle pump was a Robbins and Meyers rotary positive displacement pump with a variable speed SECO DC drive. A sand trap was installed in the

recycle line on the suction side of the recycle pump. For pH control, NaOH was added to the reactor recycle by a Cole-Palmer peristaltic pump.

Heat was supplied to the system through a heat tape wrapped around a 1.5 m length of galvanized steel recycle line. A feed preheater installed between the feed pumps and the reactor inlet consisted of a 20 L insulated glass reservoir filled with water and a 600 W immersion heater. The feed flowed through a copper coil immersed in the preheater.

The initial media in the reactor was a silica sand with the size distribution shown in Figure 3.1. The dp_{10} of the media was approximately 120 μm with a uniformity coefficient of 2.3. The initial settled bed height was 1.85 m. The expanded bed height was controlled by pumping sand from the top of the bed at 2.95 m, through a centrifugal pump to shear excess biomass from the media. The pump discharged into the reaction zone above the expanded bed, allowing the returned sand to settle and the biomass to wash out in the effluent.

Sensors installed on the pilot plant allowed for the on-line measurement of several process variables. A wet test meter equipped with a digital shaft encoder was used for biogas flow measurement. Infrared analysers measured the biogas methane and carbon dioxide content. Trace levels of hydrogen in the biogas were measured with a gas chromatograph equipped with an automatic injection valve. The five minute sampling cycle consisted of one minute of sample elution and a four minute column backflush. The detector in the hydrogen analysis system employed a heated bed of mercuric oxide which reacts with reducing gases such as hydrogen to form mercury vapour. The resulting concentration of mercury vapour is directly proportional to the hydrogen inlet concentration, and is detected by an ultraviolet photometer (Trace Analytical, 1985). The reactor pH was measured in the effluent recycle stream using a potentiometric probe. A resistance temperature detector (RTD) was also installed in the recycle stream. Recycle flowrate was measured with a magnetic flowmeter. Further details on the on-line instrumentation are summarized in Table 3.1.

The pilot plant on-line sensors were interfaced to a Control Microsystems SAFE 8000

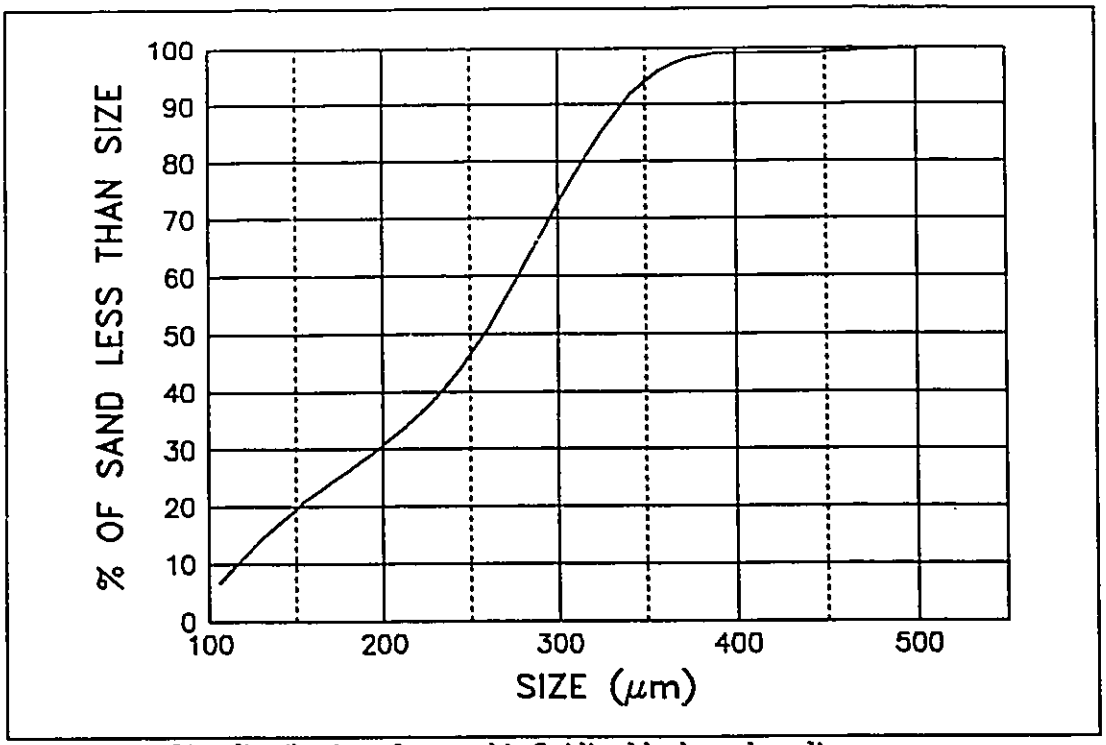

Figure 3.1: Size distribution of anaerobic fluidized bed sand media.

Table 3.1: List of on-line instrumentation

On-line variable	Instrument	Model
Biogas flowrate	Wet test meter equipped with digital shaft encoder	• GCA/Precision Scientific wet test meter • ModTronic 717S digital encoder
Biogas CH_4 content	Infrared analyser	Astro Infrared Analyzer 5000
Biogas CO_2 content	Infrared analyser	Beckman Model 864
Biogas H_2 content	• Gas chromatograph • Reduction gas detector	• Trace Analytical RGA2 Chromatograph Module • Trace Analytical RGD2 Reduction Gas Detector • Spectra-Physics SP4270 Integrator
Reactor pH	Potentiometric pH probe	• Beckman Series 3 pH Amplifier • Beckman Model 940 pH Analyser
Reactor temperature	Resistance Temperature Detector	
Recycle flowrate	Magnetic flowmeter	0.5 in. bore Brooks-MAG

data acquisition and control system. The SAFE 8000 contained digital input-output (I/O) cards, analog I/O cards, and a microprocessor card which was programmable in BASIC. A Texas Instruments (TI) Portable Professional computer provided for operator interface to the SAFE 8000 front end, long term data storage, and daily plotting. Measurements made on-line were stored to disc on the TI computer at 5 minute intervals. Proportional-integral-derivative (PID) controllers were configured for the on-line feedback control of pH, temperature and recycle rate. Experimental forcing functions were automated through the open-loop control of the variable speed feed pumps. A schematic of the pilot plant is shown in Figure 3.2, including the sensors and control elements interfaced to the microcomputer.

For pH and temperature control, control action was achieved by varying the length of time that the final control element would remain on during the 5 minute control interval. After several dynamic experiments, it was found that the NaOH addition rate was a non-linear function of the pump "time-on". To obtain an estimate of the instantaneous addition rate, the NaOH addition pump flowrate was measured over a range of pump "time-on's", and a calibration curve was generated through a linear regression fit of an equation to the calibration data. The results of the NaOH addition pump calibration are shown in Figure 3.3. Because the calibration curve was not generated until after dynamic experimentation, there is considerable uncertainty in the pH control action during dynamic experiments.

3.2 WASTEWATER CHARACTERISTICS, COLLECTION AND STORAGE

Wastewater used in this study was molasses and brandy stillage from Reider Distillery in Grimsby, Ontario. The wastewater was shipped by tanker truck to the WTC, where it was held in a 60 000 L outdoor storage tank equipped with a mixer. Five loads were received over the duration of the project. The stillage characteristics, based on grab samples from the incoming tanker trucks, are summarized in Table 3.2. Raw wastewater was pumped as needed from the outdoor tank to an indoor, mixed and refrigerated 5000 L feed storage tank

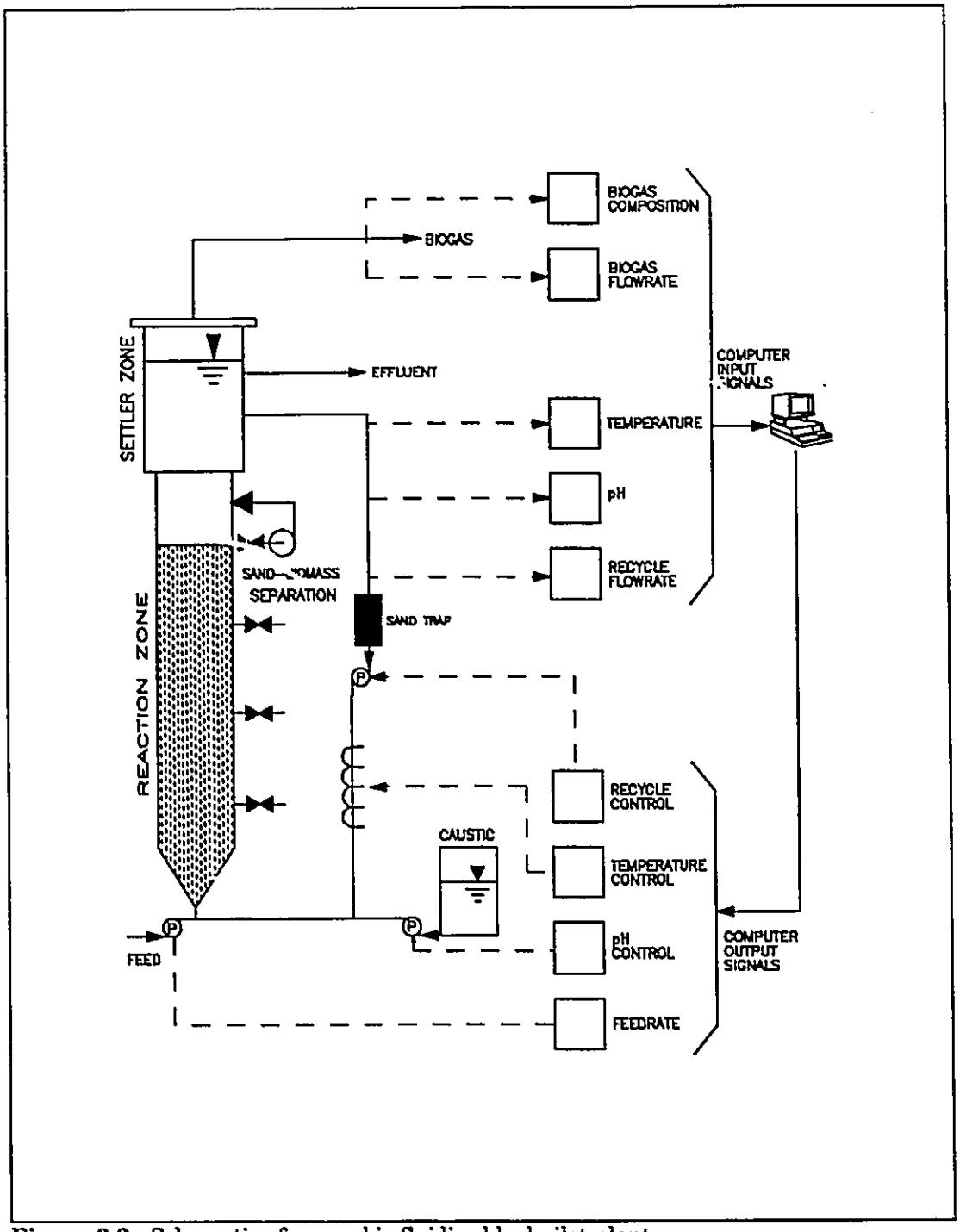

Figure 3.2: Schematic of anaerobic fluidized bed pilot plant.

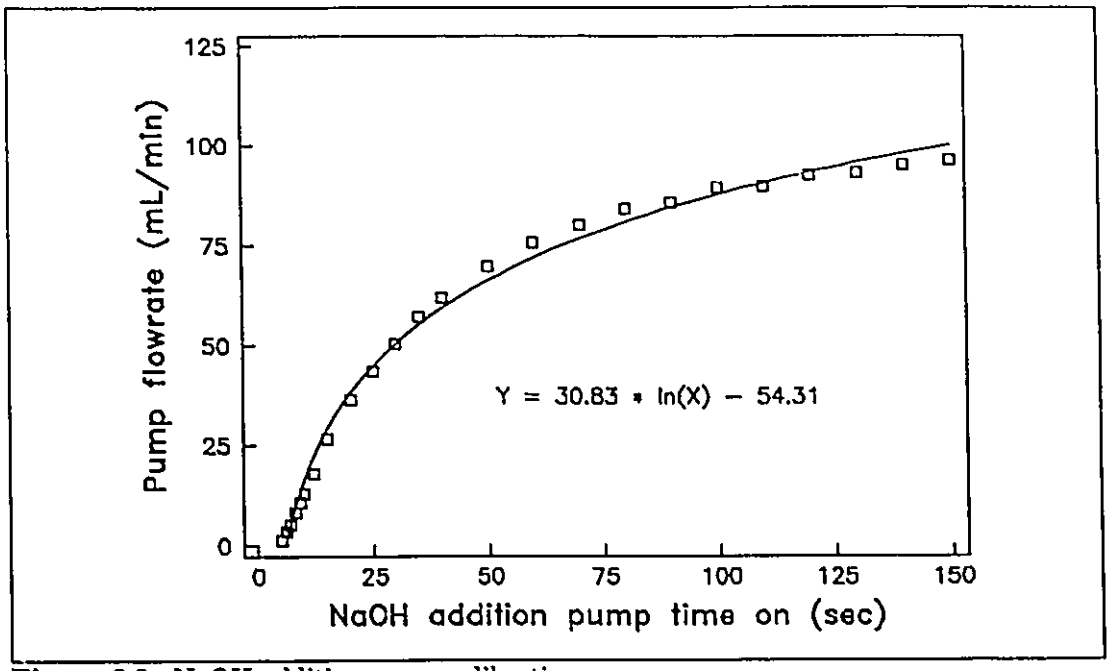

Figure 3.3: NaOH addition pump calibration curve.

Table 3.2: Raw wastewater characteristics

Parameter (mg/L)	Load 1	2	3	4	5	Mean
COD	38950	42650	22100	59000	68300	46200
Filtered COD	33450	27000	20600	54700	19500	39500
BOD_5	19500	16500	4665	-	20700	15300
Filtered BOD_5	18900	12300	2415	-	20400	13500
TOC	12847	9095	9503	-	11500	10700
TKN	665	887	186	-	1860	900
Filtered TKN	382	282	183	-	515	340
NH4-N	55	44	31	-	28	40
Total P	143	132	24	-	109	102
Filtered Total P	89	77	17	-	51	58

Notes: 1) Operating day on which load received:
1 - Before 1
2 - 90
3 - 442
4 - 569
5 - 832
2) Mean concentrations rounded to three significant figures.
3) "-" signifies missing data

where it was diluted to the desired concentration by the addition of tap water.

3.3 REACTOR START-UP AND OPERATION

Before feeding was initiated, the anaerobic fluidized bed reactor was filled with a 15% dilution of stillage wastewater, and 6 L of biomass seed stripped from a previously used sand medium. The volatile suspended solids (VSS) concentration of the seed was 17 000 mg/L. The initial feed to the reactor was also a 15% dilution of stillage and the hydraulic retention time based on the empty bed volume was maintained at approximately 3 days. For the first 7 days of operation, the reactor was continuously seeded by feeding 4 L/d of biomass from an operating pilot scale anaerobic hybrid reactor. The VSS concentration of this seed was 24 000 mg/L. The setpoints for pH and temperature were 6.6 and 35 °C, respectively. The recycle rate was maintained between 1 and 2 L/min, resulting in an upflow velocity between 0.056 and 0.112 $m^3/min \cdot m^2$. After 130 days of operation, the recycle rate was increased to operate within the range of 3 to 4 L/min due to poor fluidization in the lower regions of the bed. The resulting range in the upflow velocity was 0.17 to 0.23 $m^3/min \cdot m^2$.

The reactor loading was increased to a target volumetric organic loading rate of 10 kg $COD/m^3 \cdot d$ by increasing the feedrate when the effluent total volatile acid concentration was less than 1000 mg/L and when the trend in the biogas production rate was upwards. Subsequent steady state loading rates were adjusted through adjustments in the dilution and feedrate of the stillage wastewater, and through addition of synthetic spike solutions consisting of combinations of glucose, acetic acid, propionic acid, and butyric acid. Nutrient levels in the combined feed were maintained at a maximum COD:N:P ratio of approximately 600:5:1 by supplementing the spike solutions with NH_4OH and K_2HPO_4.

3.4 TRACER TEST

A tracer test was conducted on the fluidized bed reactor to determine the reactor

mixing characteristics and effective volume. Tritium-enriched water with a total activity of 1.92×10^8 disintegrations/minute (DPM) was injected into the reactor as a tracer. Effluent samples were initially collected at 5 minute intervals, with the sampling interval increasing to 10 minutes, 15 minutes, 1 hour, and 4 hours as the test progressed. The first sample was collected at the time of the tracer injection. The final sample was collected 50.5 hours after injection of the tracer.

3.5 EXPERIMENTAL DESIGN

3.5.1 Preliminary Experimentation

Initial experimentation was conducted on the fluidized bed reactor to collect information for the design of subsequent dynamic experiments. A glucose spike solution with a COD concentration of 270 000 mg/L was automatically added to the reactor feed in a pseudo-random binary sequence (PRBS) of pulses under direct control of the data acquisition and control system. The spike solution was prepared in 10 L batches and during a pulse was pumped into the reactor feed at a nominal rate of 3.5 mL/min (5 L/d). The actual pumping rates were calculated by monitoring the volumes of spike solution used. The PRBS sequence was composed of an 8 day sequence of random on-off switches of the spike pump, with a planned minimum switching time of 6 hours. The designed sequence of loading rate increments for the preliminary glucose run is shown in Figure 3.4. The concentration and feedrate of the stillage wastewater was maintained at a constant level during the run to achieve an approximate average organic loading of 10 kg COD/m^3•d.

3.5.2 Final Experimental Design

Final experiments consisted of a series of 7 day runs in which loading pulses were implemented by adding spike solutions of either glucose, acetic acid, propionic acid or butyric acid. Each spike solution consisted of 270 000 mg COD/L of the appropriate substrate. The

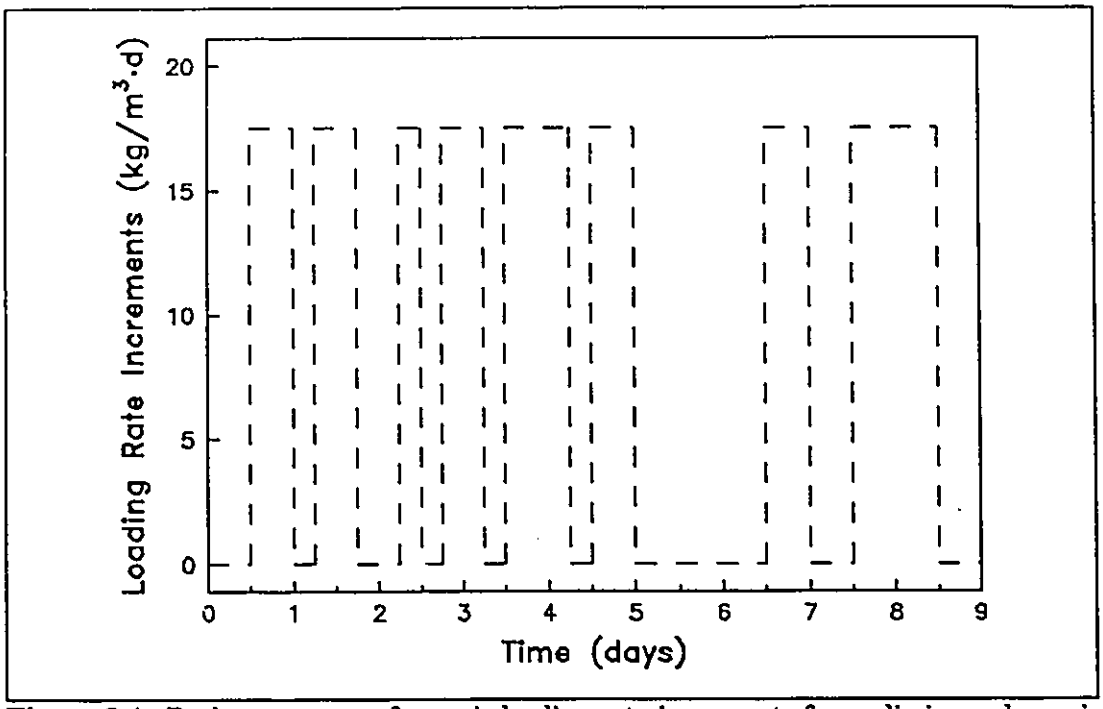

Figure 3.4: Design sequence of organic loading rate increments for preliminary dynamic experiment.

spike solution was prepared in 10 L batches and during a pulse was added to the reactor feed at a nominal rate of 7.2 mL/min. The actual volumes of spike solution used were monitored to confirm the addition rate. The mass addition rate of NaOH for pH control was also monitored during dynamic experiments by measuring the volume of NaOH solution used on a daily basis and by titrating a sample of each new 40 L batch of NaOH solution with hydrochloric acid.

The designed sequence of loading rate increments for the acetic acid, propionic acid, and butyric acid runs is shown in Figure 3.5. The sequence consisted of a 36 hour pulse followed by a resting period of 36 hours at the baseline loading rate, followed by a final 12 hour pulse. Each experiment was 7 days long.

The planned implementation of the glucose runs was for three consecutive 7 day periods, with each 7 day period using the same sequence of loading rate increments as the volatile acid runs. A midpoint loading period was included between the first and second week

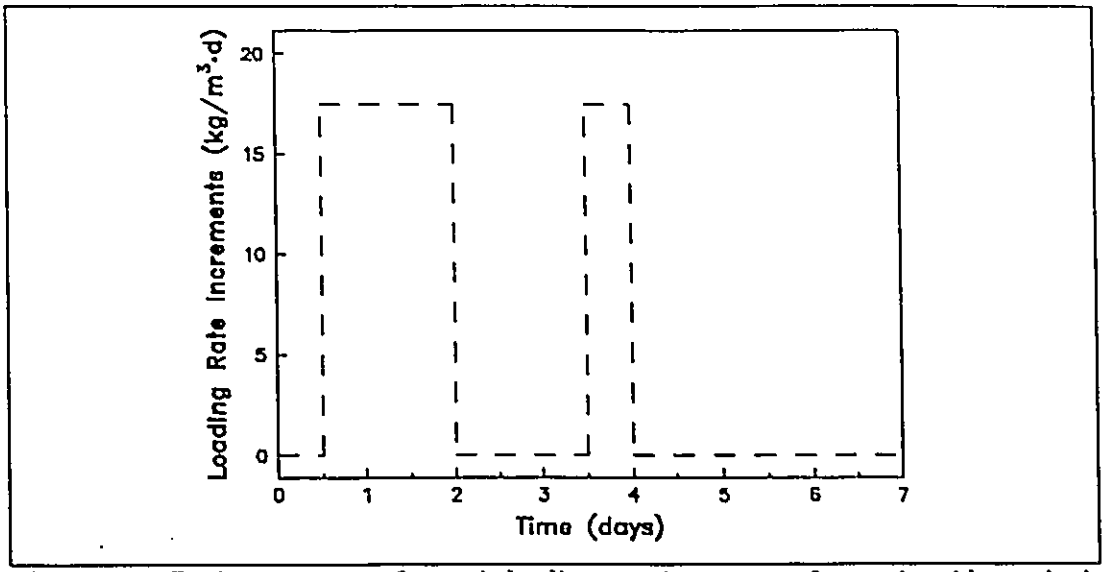

Figure 3.5: Design sequence of organic loading rate increments for acetic acid, propionic acid, and butyric acid experiments.

of the run to allow the process response following different initial conditions to be compared. The final week of the glucose run allowed a comparison to the process response during the first week in order to determine whether the process had returned to the same initial state as before the run. The planned sequence of loading rate increments for the glucose runs is shown in Figure 3.6.

3.6 SAMPLING, ANALYSIS AND INSTRUMENTATION MAINTENANCE

As a check for data collected and stored on-line, local instrument readings of temperature, pH, biogas carbon dioxide content, biogas methane content and biogas production were recorded on a daily basis. In the operating periods before dynamic experimentation and between dynamic experiments, grab samples of the stillage feed and the reactor effluent were collected 5 days per week for analysis of the parameters listed in Table 3.3. Total volatile solids concentrations in the reactor were determined periodically from samples collected at ports 0.72 m, 1.34 m, 2.29 m, and 2.65 m from the bottom of the reactor.

Pilot plant instrumentation calibration was checked routinely and re-calibration or

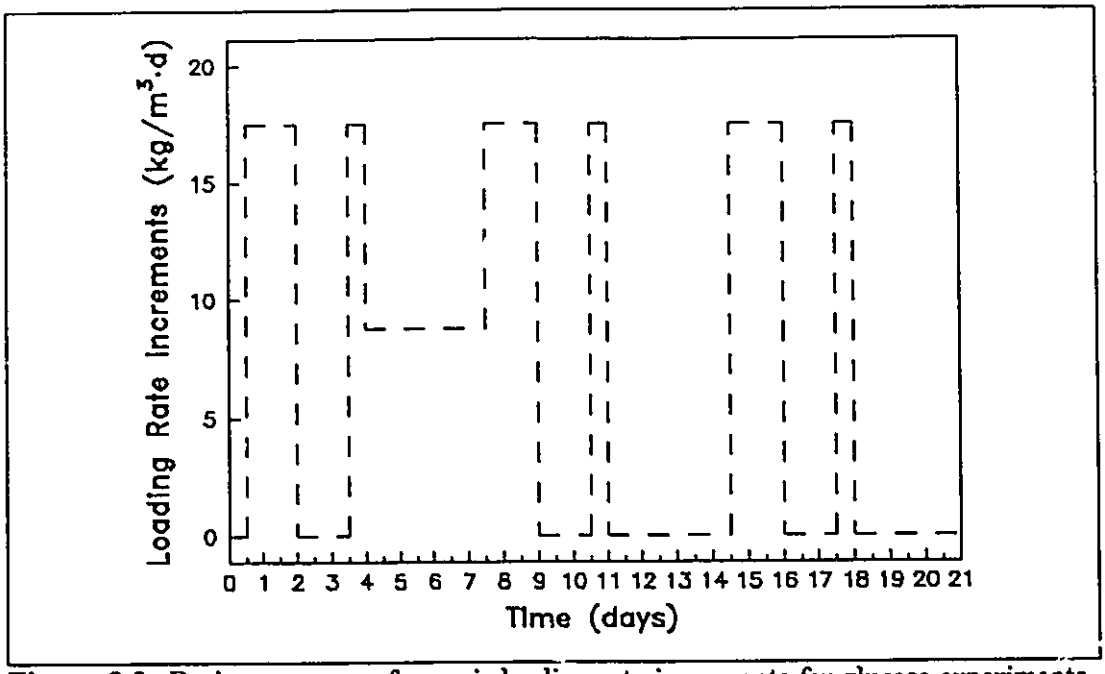

Figure 3.6: Design sequence of organic loading rate increments for glucose experiments.

Table 3.3: Pilot plant routine off-line analysis schedule

Parameter	Frequency of analysis (analyses/week)	
	Feed	Effluent
COD	3	3
Filtered COD	3	3
BOD_5 *	1	1
Filtered BOD_5 *	1	1
TOC *	1	1
TKN *	1	1
Filtered TKN *	1	1
NH_4 *	1	1
Total P *	1	1
Filtered Total P *	1	1
Volatile Acids	5	5

* Analyses conducted during pilot plant operating days 1 - 400

repairs were made as necessary. The RTD was removed from the recycle line and cleaned with distilled water every two weeks. The pH probe was removed, cleaned and checked for calibration using standard buffer solutions every two weeks. Reference and measuring electrodes in the pH probe required replacement every 2 to 4 months. Calibration of the on-line infrared analysers was checked weekly through an off-line gas chromatographic analysis of biogas samples. During the experimental period, the infrared analysers were re-calibrated monthly. The hydrogen analyser calibration was checked daily using gas standards when it was operating for dynamic experiments. The analyser was recalibrated if any of the gas standard analyses were more than 10% in error. Re-calibration was generally required at least once per week.

An automatic sampler was used to collect grab samples of effluent for off-line analysis of COD and volatile acids during dynamic experiments. Samples were collected at 1 hour intervals during the preliminary PRBS experiment and at 2 hour intervals during the final acetic acid, propionic acid, butyric acid and glucose pulse experiments. Samples were collected every 8 hours in the periods between pulse experiments.

Sample preparation and analyses were performed according to standard WTC methods described in Appendix A.

CHAPTER 4

EXPERIMENTAL RESULTS AND DISCUSSION

The pilot scale anaerobic fluidized bed reactor was operated for 697 days prior to dynamic experimentation. Cumulative operating data from this period are presented to establish a baseline for performance of the system. In addition, the results and analysis of the tracer test are presented. Finally, results from dynamic experiments consisting of pulse inputs of acetic acid, propionic acid, butyric acid and glucose are presented and discussed. Detailed data from each dynamic experiment have been included in Appendix C. Daily operating data for the pilot plant for the entire experimental period have been included in Appendix D.

4.1 PRE-EXPERIMENT REACTOR OPERATION

In the period of reactor operation prior to dynamic experimentation, problems in maintaining the sand inventory in the reactor were encountered. During preliminary load increase experiments conducted in this period, the low inventory of sand and the resultant low biomass concentrations in the reactor resulted in poor chemical oxygen demand (COD) removal efficiencies. To alleviate these problems, the sand medium was gradually replaced with sand sized between 210 and 354 μm.

The concentrations of volatile solids retained in the reactor during the pre-experiment operating period are plotted in Figure 4.1. The concentrations were measured in samples collected along the length of the bed, and averaged over the reaction zone volume (47 L). Variations in the volatile solids concentrations reflect the changes in the operating conditions

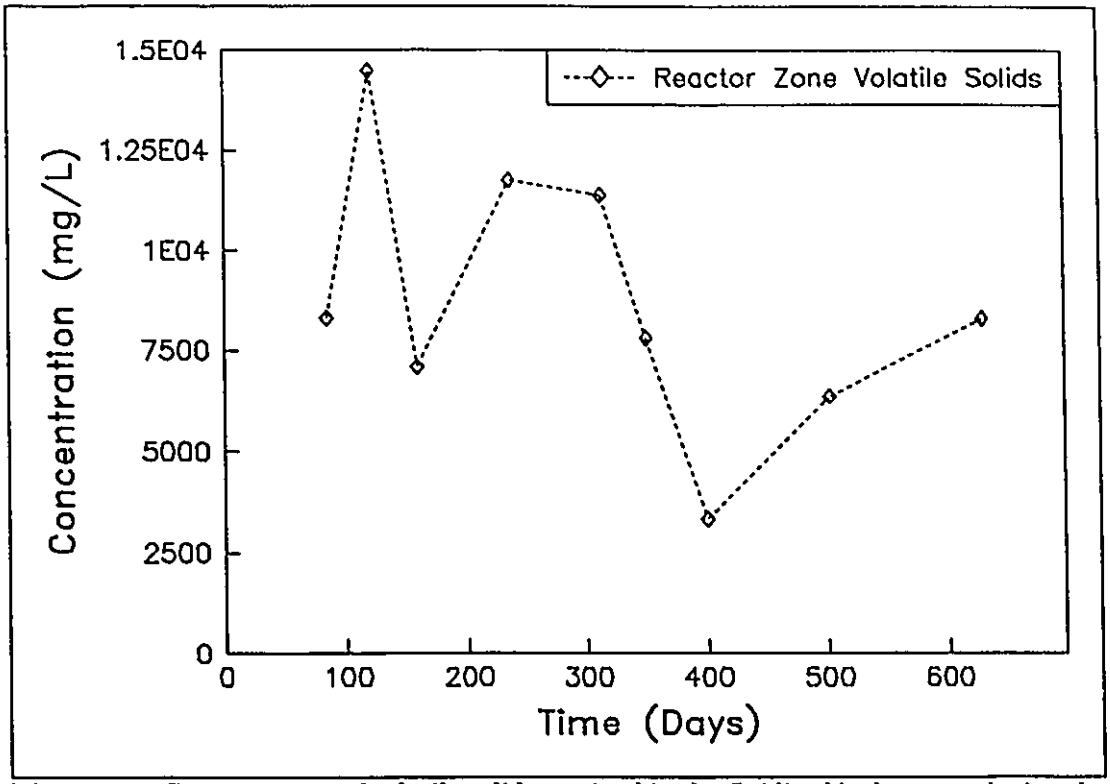

Figure 4.1: Concentration of volatile solids retained in the fluidized bed reactor during the pre-experimental period.

during the pre-experimentation operating period. For the first 130 days of operation, the recycle rate was maintained between 1 and 2 L/min. During this period, the mass of volatile solids retained in the reactor increased rapidly. Due to poor fluidization in the lower regions of the bed, the recycle rate was increased after day 130 to operate within the range of 3 to 4 L/min. This resulted in an initial decrease in the retained volatile solids concentration. However, by operating day 200, the volatile solids had increased to a steady state concentration in the reactor zone of approximately 12 g/L. A number of reactor shut downs due to mechanical problems resulted in a decrease in the concentration of volatile solids retained in the reactor between operating days 300 and 400. From day 400 until the end of the pre-experimentation period, a relatively stable period of operation resulted in a gradual increase in the retained volatile solids concentration.

Cumulative operating data for the start-up and pilot plant operation prior to dynamic experimentation are summarized in Table 4.1. The presentation of the data has been divided into the entire pre-experimentation operating period, and the last 197 days of operation prior to dynamic experiments. The latter operating period represents a relatively stable operation.

The composition of the wastewater feed was quantified by calculating the various fractions contributing to the total COD load. The total COD load was calculated from the total COD concentrations measured in the pilot plant feed. The soluble COD load was calculated from measurements of COD in filtered feed samples (FCOD). The particulate COD load was calculated as the difference between the total COD load and the soluble COD load. The volatile acid COD load was calculated from the concentrations of acetic, propionic and butyric acid measured in the feed.

The results shown in Table 4.1 indicate that the feed COD was predominantly soluble. During Period B, 47% of the soluble COD in the feed was comprised of volatile acids indicating that acidification of the feed was occurring during storage and that a portion of the particulate COD in the feed was comprised of acid-forming bacteria.

The removal efficiencies of total COD and soluble COD during Period B were 72% and 74%, respectively. Although the removal of particulate COD appeared to be significant during Period B (67%), the particulate COD removal efficiency over the entire operating period was 20%. A low removal efficiency of insoluble material is expected in a fluidized bed due to the low hydraulic retention time. The higher removal efficiency observed during Period B may have been due to the difficulty in obtaining a representative sample of insoluble material leaving the reactor. Solid material accumulated in recycle lines, effluent lines and the sand trap and periodic cleaning of the lines was required by flushing with clean water. Solids may also have been removed from the system when the bed was re-fluidized after power failures and maintenance shutdowns.

Less than 20% of the effluent soluble COD was comprised of volatile acids during

Table 4.1: Cumulative operating data for anaerobic fluidized bed for operating periods prior to dynamic experimentation

Parameter	Period A	Period B
Total COD load (kg/m^3)	5710	1020
Hydraulic load (m^3/m^3)	669	186
Effluent total COD (kg/m^3)	2320	280
Total COD removed (kg/m^3)	3390	740
% Total COD removal	59	72
Soluble COD load (kg/m^3)	5000	794
% of total COD load	87	77
Effluent soluble COD (kg/m^3)	1750	209
Soluble COD removed (kg/m^3)	3250	585
% Soluble COD removal	65	74
Particulate COD load (kg/m^3)	713	231
% of total COD load	13	23
Effluent particulate COD (kg/m^3)	571	76
Particulate COD removed (kg/m^3)	142	155
% Particulate COD removal	20	67
Volatile acid COD load (kg/m^3)	1900	372
% of soluble COD load	38	47
Effluent volatile acid COD (kg/m^3)	822	40
% of effluent soluble COD	47	19
Non-acid effluent soluble COD (kg/m^3)	924	169
% of soluble COD load	19	21
Biogas Production (m^3/m^3)	1570	262
Methane Production (m^3/m^3)	1050	201
% Methane	68	77
Methane Yield (m^3/kg total COD removed)	0.31	0.27
% Total COD removed recovered as CH_4 (m^3/kg COD removed * 2.54 kg COD/m^3 CH_4*100%)	78	69
Methane Yield (m^3/kg soluble COD removed)	0.32	0.34
% Soluble COD removed recovered as CH_4 (m^3/kg COD removed * 2.54 kg COD/m^3 CH_4*100%)	81	86
NaOH added (g NaOH/L feed)		0.21

Notes:
1) All loading calculations based on empty bed reactor volume of 77 L.
2) All loading calculations rounded to three significant figures.

Period A: Reactor operating days 1-697
Period B: Reactor operating days 500-697

Period B. The remaining effluent soluble COD was approximately 20% of the soluble COD load, indicating that this proportion of the feed soluble COD could be considered non-biodegradable.

The closure of the reactor COD balance was examined by calculating the observed methane yield as a percent of the theoretical methane yield. Separate methane yield calculations were based on total COD removal and soluble COD removal. Only 69% of the total COD removed was recovered as measured methane production during Period B. This reinforces the hypothesis that some of the particulate COD removal observed was not due to biodegradation but was in fact due to the accumulation of insoluble material in the reactor system, with intermittent removal through cleaning and flushing of the system. When calculated on the basis of soluble COD removal, the actual methane yield was 86% of the theoretical methane yield.

Methane dissolved in the effluent can have a significant effect on the COD balance at low loadings. The dissolved methane concentration in the effluent was estimated assuming gas-liquid equilibrium and using a Henry's law coefficient of 1.13×10^{-3} mol/L•atm (Pauss *et al.*, 1990a). During period B, the addition of the estimated dissolved methane to the measured methane production increases the cumulative methane production shown in Table 4.1 by approximately 4 m^3/m^3. The methane yield based on soluble COD removal then increases to 89% of the theoretical methane yield. COD removal can also occur through sulphate reduction. Although the sulphate content of the wastewater was not measured during Period B, previous studies have indicated that sulphate can be present in molasses stillage (Hilton and Archer, 1988; Souza, *et al.*, 1991). With the relative standard deviation of the COD analysis expected to be approximately 10% (*Standard Methods*, 1985), the addition of estimated dissolved methane to the total methane production and the assumption that some sulphate reduction occurred results in a complete COD balance.

4.2 TRACER TEST RESULTS AND ANALYSIS

The fluidized bed reactor operating conditions during the tracer test are shown in Table 4.2. Results from the test are summarized in Table 4.3. The observed hydraulic retention time (HRT_o) was calculated from the following expression from Levenspiel (1972):

$$HRT_o = \frac{\sum t_i \; C_i \; \Delta t_i}{\sum \; C_i \; \Delta t_i} \tag{4.1}$$

where, C_i is the measured effluent concentration of the tracer (DPM/mL); t_i is the discrete time value at which C_i was measured (hr); and, Δt_i is the time interval between effluent concentration measurements (hr).

When a pulse of inert tracer is introduced to the influent at time, $t = 0$, the effluent concentration, $C(t)$, from a continuous stirred tank reactor (CSTR) can be represented by:

$$C(t) = C_o e^{\left(-\frac{t}{HRT_o}\right)} \tag{4.2}$$

where, C_o is the effluent tracer concentration at time, $t = 0$, assuming complete and instantaneous mixing. C_o is equal to the mass of tracer injected divided by the effective volume of the reactor.

At a feed flowrate of 5.0 L/hr, the HRT_o was calculated to be 14.3 hours. This result indicates an effective reactor volume of 71.7 L. The effective reactor volume is expected to be less than the empty bed reactor volume due to the volume occupied by the bed medium and the biomass. The effective volume also includes the recycle lines and the sand trap. The measured effluent tracer concentration is compared to the expected response from a CSTR with an HRT_o equal to 14.3 hours in Figure 4.2. The total tracer recovered from the test based on the area under the effluent tracer concentration response curve was 84.6% of the mass of tracer injected. Incomplete tracer recoveries can be due to errors in the chemical analysis of the tracer or in the assumed reactor feedrate (Hall, 1985). In Figure 4.2, the measured

effluent concentrations were adjusted by a constant factor to result in 98% tracer recovery over 4 nominal hydraulic retention times. The results show that the mixing characteristics of the fluidized bed reactor can be adequately described by an ideal CSTR model.

Table 4.2: Fluidized bed reactor operating conditions during tracer test	
Parameter	Value
Feed flowrate (L/hr)	5.0
Empty bed volume (L)	77.0
Nominal HRT (hr)	15.4
Recycle/Feed (L/L)	48.0
Mass of tracer injected (DPM)	1.92×10^8

Table 4.3: Tracer test results	
Parameter	Value
Observed HRT (hr)	14.3
Effective reactor volume (L)	71.7
% tracer recovered	84.6

4.3 DYNAMIC EXPERIMENTAL RESULTS

The total COD loading rates on the fluidized bed reactor are plotted for the dynamic experimentation period in Figure 4.3. The preliminary glucose spike experiment (glucose run #1) was implemented from day 1 to day 10 of the experimental period. From day 43 to day 77, an acetic acid run, a propionic acid run and a glucose run (glucose run #2) were implemented in sequence. Control problems were encountered immediately following glucose run #2. The pilot plant was shut down from day 97 to day 106 while a faulty temperature compensation circuit in the pH analyser was repaired and blockages caused by biomass growth in the recycle

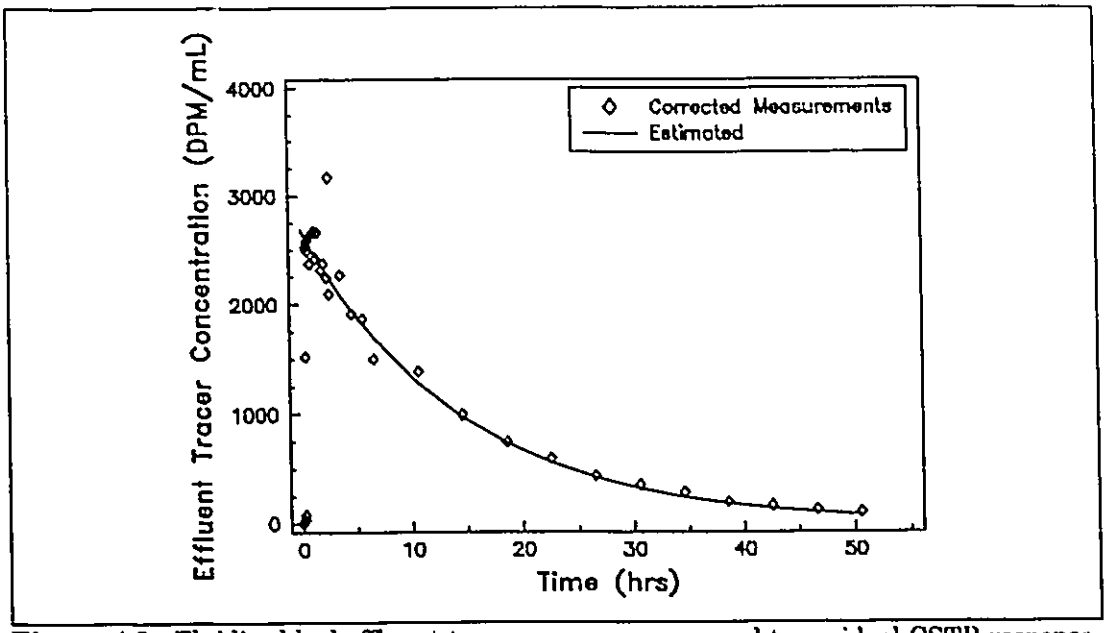

Figure 4.2: Fluidized bed effluent tracer response compared to an ideal CSTR response.

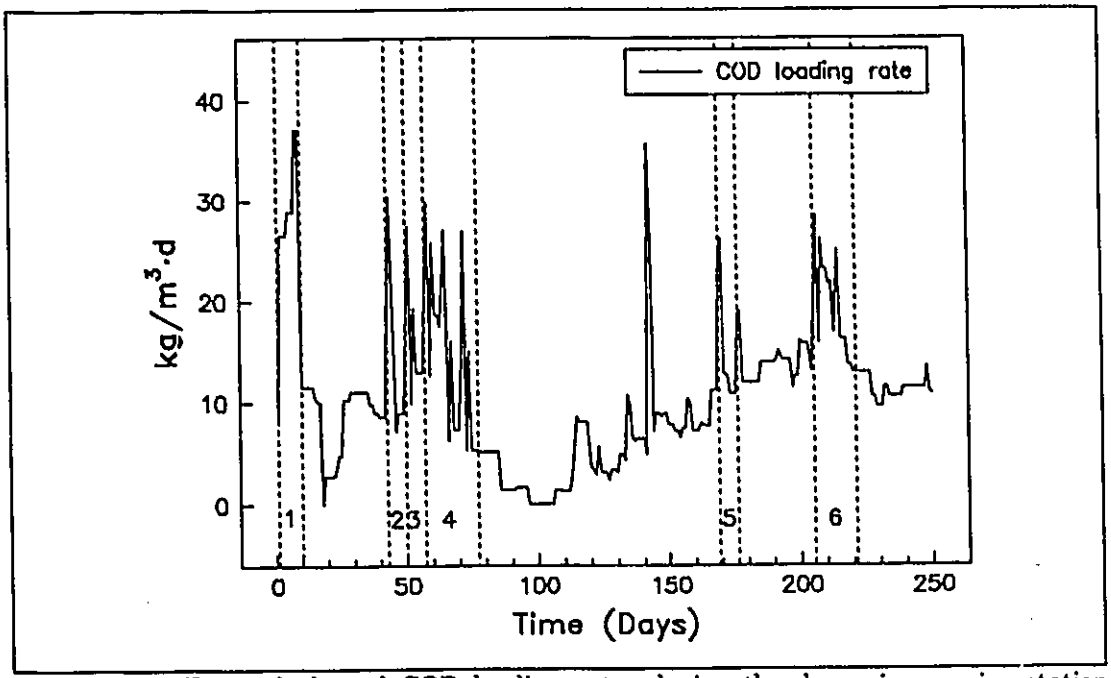

Figure 4.3: Empty bed total COD loading rates during the dynamic experimentation period. (1) glucose run #1 (preliminary experiment); (2) acetic acid run; (3) propionic acid run; (4) glucose run #2; (5) butyric acid run; (6) glucose run #3.

lines were cleared. A glucose run initiated on day 142 was aborted when it was found that the spike addition pump calibration was in error and the actual volume of glucose spike solution added to the reactor feed could not be calculated. A butyric acid run was implemented from day 169 to day 175 and a final glucose run (glucose run #3) was conducted from day 205 to day 220. The third week of glucose run #3 was cancelled due to a line blockage in the system caused by biomass growth.

Total volatile solids concentrations measured in the reactor over the dynamic experimentation period are plotted in Figure 4.4. Concentrations were calculated based on the reaction zone volume (47 L). Although sample collections for reactor total volatile solids concentrations were planned to immediately precede and immediately follow any set of experimental runs, operating problems at times prevented representative samples from being collected. The overall trend in the volatile solids concentration appeared to be upwards, indicating a growth in biomass over the course of the dynamic experimental period. The increase over any one experimental run was always less than 10%.

In the following subsections, the results from all of the completed dynamic experiments are presented and discussed. For all of the experiments, the influent concentration forcing functions, the observed process response, and the behaviour of the control variables are shown. For the final experiments, the calculated conversion efficiency of the pulsed substrates are shown. The influent filtered COD (FCOD) concentration forcing functions represent the combined concentration of the diluted distillery wastewater and the pulse addition of the synthetic spike solution. Effluent FCOD concentrations were calculated by subtracting the COD equivalents of the effluent volatile acids from the measured effluent FCOD. An oxygen demand balance is presented for each of the final experiments in order to assess the fate of the pulsed substrate.

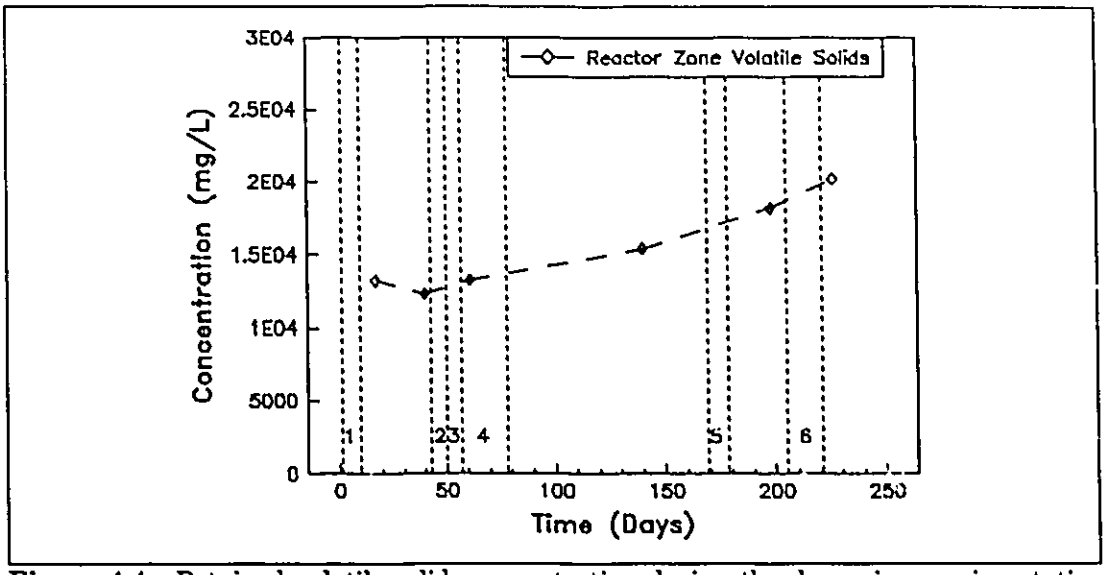

Figure 4.4: Retained volatile solids concentration during the dynamic experimentation period. (1) glucose run #1 (preliminary experiment); (2) acetic acid run; (3) propionic acid run; (4) glucose run #2; (5) butyric acid run; (6) glucose run #3.

4.3.1 Preliminary Experiment

The influent forcing function and the observed process response during the preliminary glucose experiment (glucose run #1) are plotted in Figure 4.5. The effluent FCOD, gas production and gas phase hydrogen concentration were observed to respond to each individual pulse. With the exception of a significant response during the first day of the run, the volatile acids concentration gradually increased throughout the first 5 days of the run. After day 5 of the experiment, the pulse frequency was decreased while the amplitude was increased. This input pattern resulted in an increased signal-to-noise ratio in the volatile acid response.

The behaviour of the controlled variables, reactor temperature and pH, is shown in Figure 4.6. Temperature control was poor throughout the run as the temperature of the reactor appeared to be correlated to the ambient temperature in the pilot plant area. Reasonable pH control was achieved throughout the run, although the controller had some difficulty in maintaining the pH during the larger pulses in the latter part of the experiment.

The results from this run were used to design the subsequent dynamic experiments

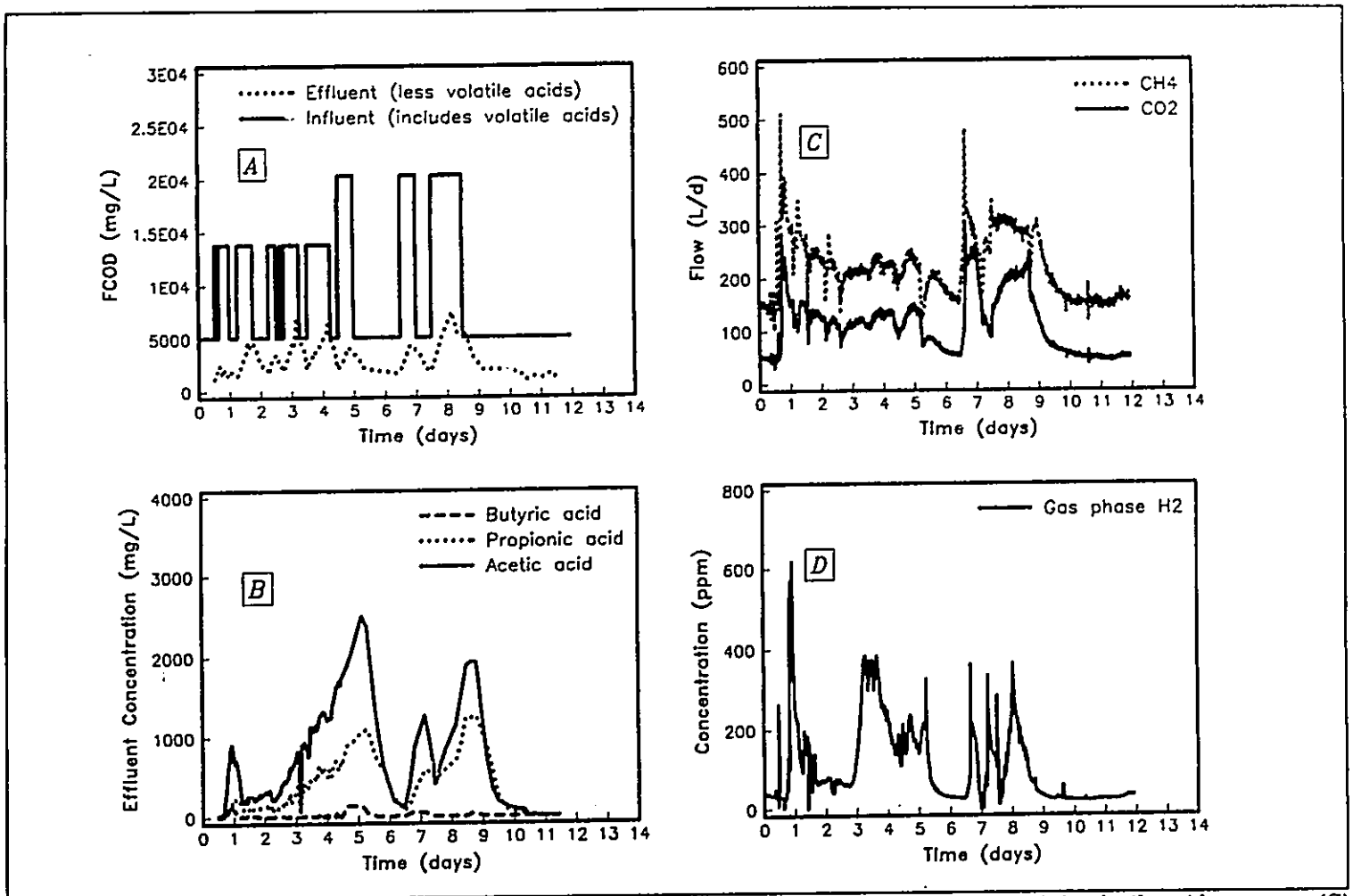

Figure 4.5: Glucose run #1 results - (A) influent forcing function and effluent FCOD response; (B) volatile acid response; (C) gas production rate response; (D) gas phase hydrogen concentration response.

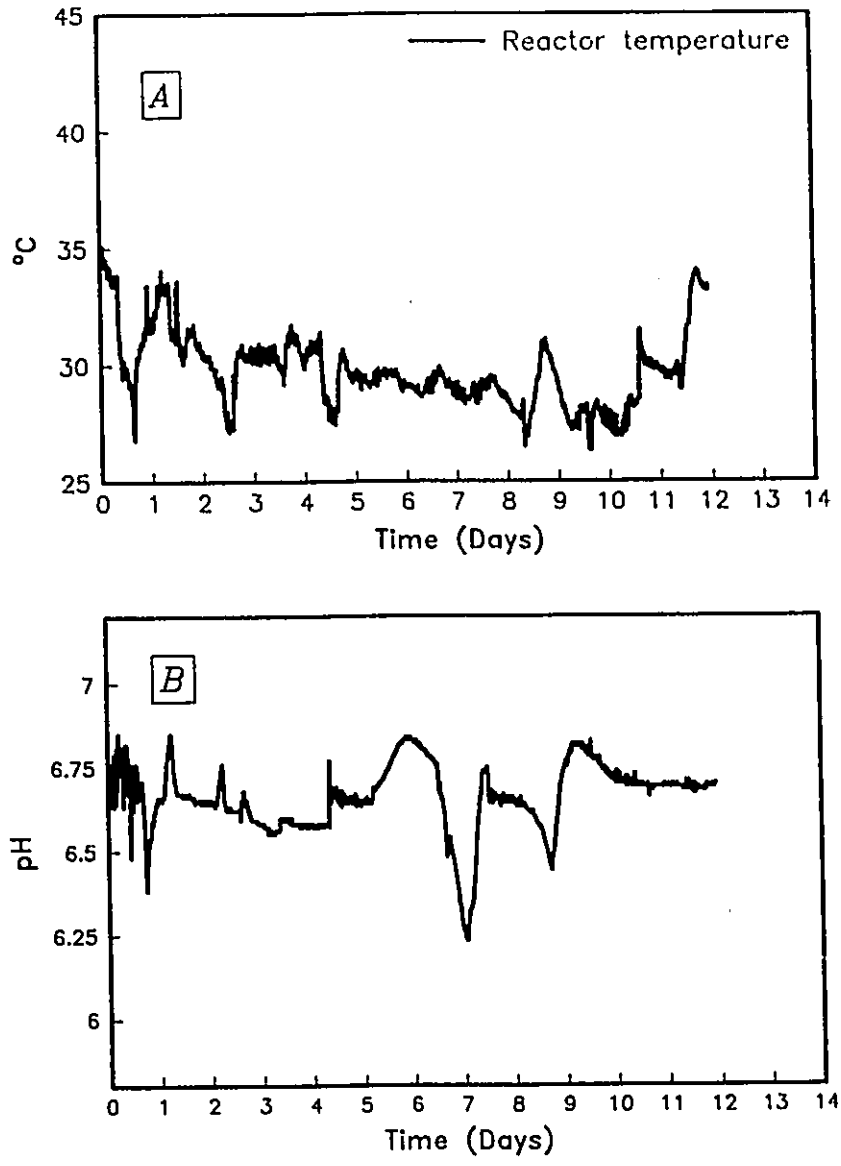

Figure 4.6: Behaviour of controlled variables during glucose run #1 - (A) temperature; (B) pH.

on the pilot plant. Later experiments were designed with a similar pulse frequency as was used after the fifth day of the run. The amplitude of the pulses was reduced by approximately twenty percent as it was anticipated that higher effluent volatile acid levels could occur during the pulse addition of volatile acid substrates and pH control difficulties could result. Temperature control was improved by insulating the reactor and preheating the reactor feed.

4.3.2 Final Experiments

The influent forcing function and the observed process response during the acetic acid, propionic acid and glucose run #2 are shown in Figures 4.7 and 4.8. The results for the acetic acid run, the propionic acid run, and glucose run #2 are enlarged in Figures 4.9 to 4.11, 4.12 to 4.14, and 4.15 to 4.17, respectively. The results of the butyric acid run are plotted in Figures 4.19 to 4.22. The results from glucose run #3 are shown in Figures 4.23 to 4.26.

In the acetic acid run, the decrease in the calculated non-acid effluent FCOD concentration to negative levels during the first pulse of the run (Figure 4.9(A)), indicated a possible analytical bias in either the FCOD or volatile acid concentrations. Subsequent analyses on samples of known concentration indicated that some acetic acid may volatilize from COD samples before analysis.

The capacity of the process to degrade the incoming acetic acid appeared to increase during the first pulse, as shown by the decreasing trend in the effluent acetic acid concentration (Figure 4.9(B)) and the gradual increase in the methane production rate (Figure 4.9(C)) after an initial rapid transient. The increase in capacity was apparent through the second pulse, where the breakthrough of acetic acid in the effluent was significantly reduced relative to the first pulse. The increase in methane production rate within the first 2 hours after the start of the second pulse was approximately 2.5 times greater than the initial transient which occurred within the same period of time after the start of the first pulse.

The conversion efficiency of the acetic acid pulse is shown in Figure 4.10.

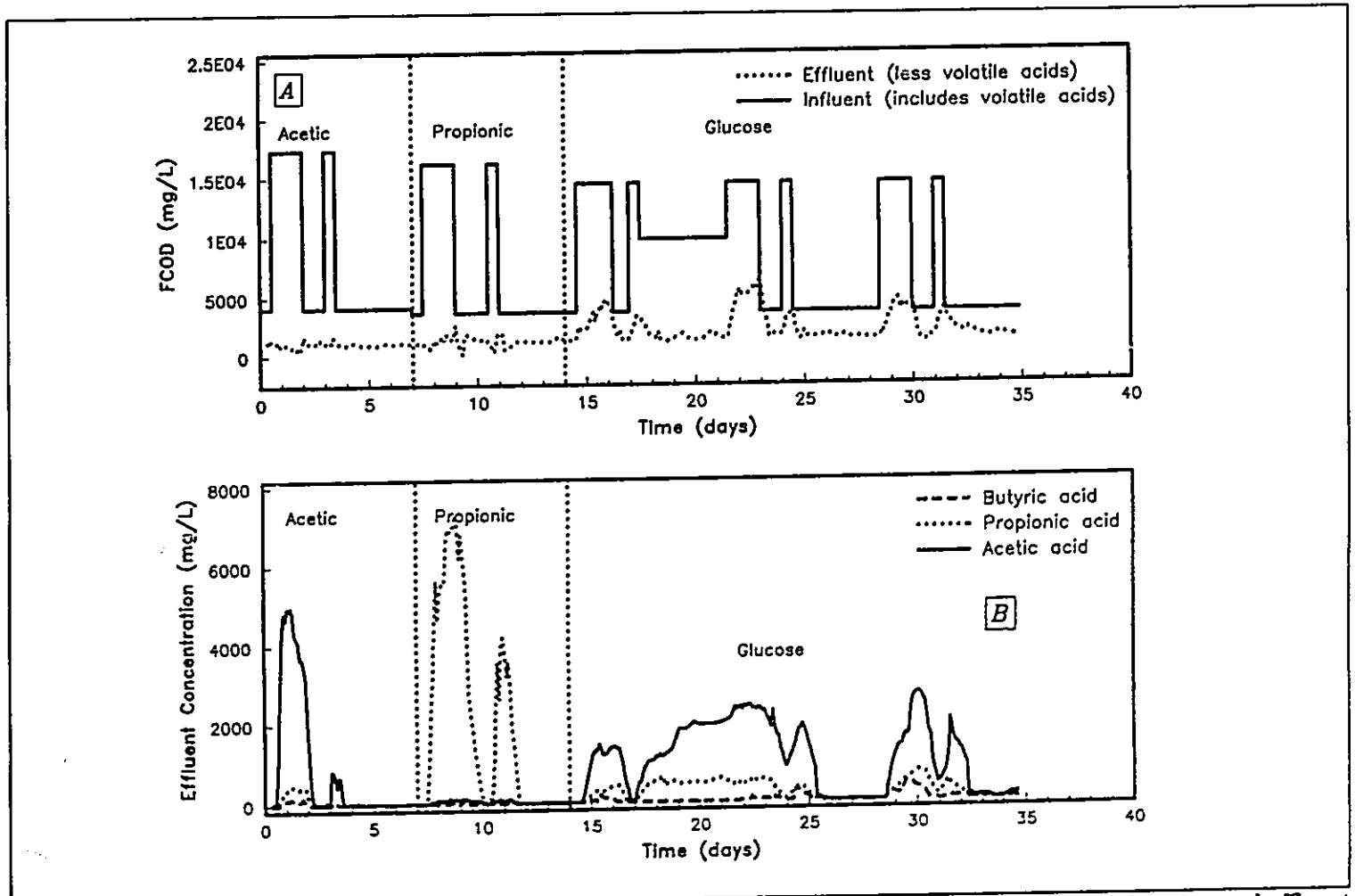

Figure 4.7: Results from acetic acid run, propionic acid run and glucose run #2 - (A) influent forcing function and effluent FCOD response; (B) volatile acid response.

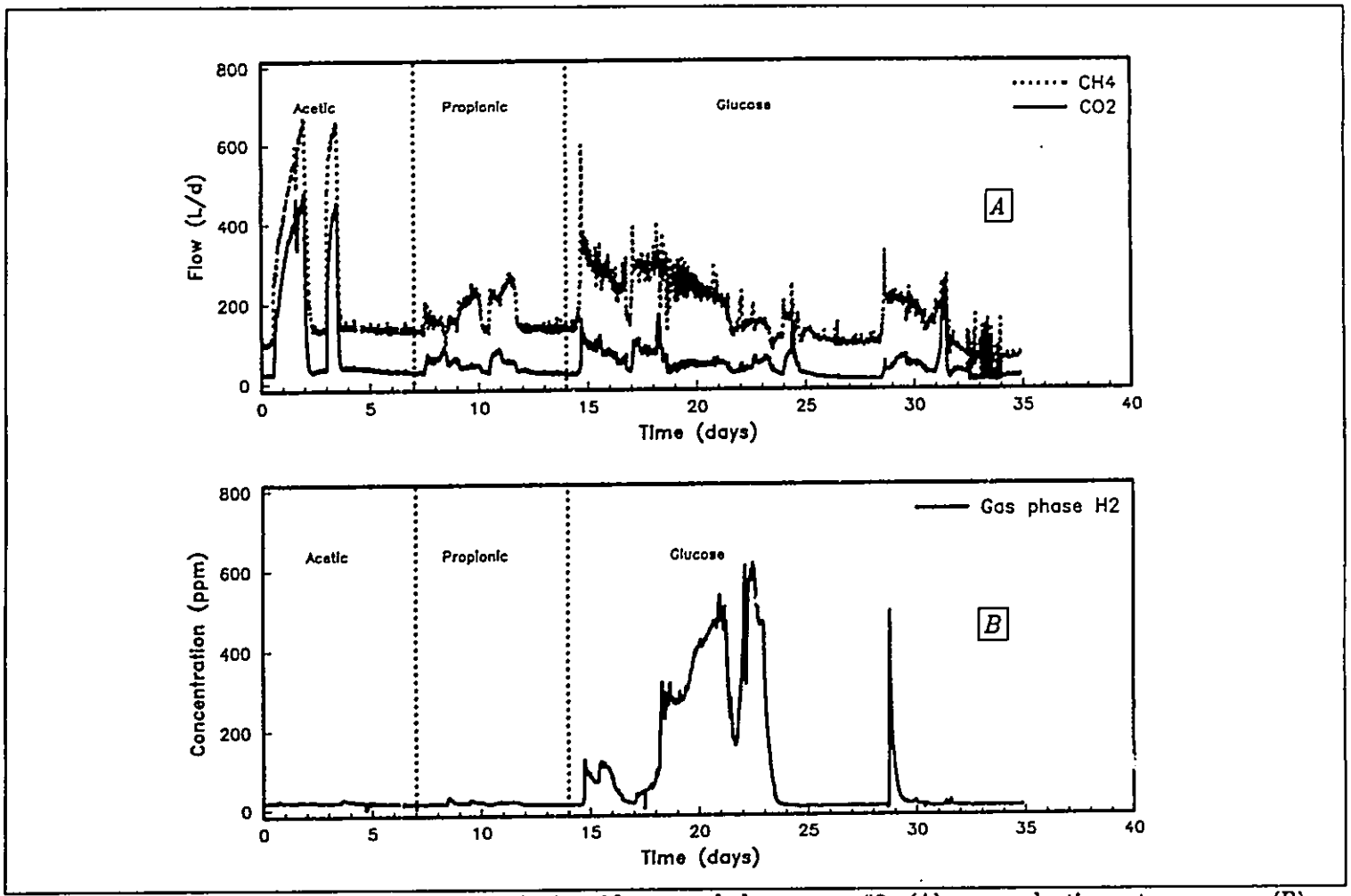

Figure 4.8: Results from acetic acid run, propionic acid run, and glucose run #2 - (A) gas production rate response; (B) gas phase hydrogen concentration response.

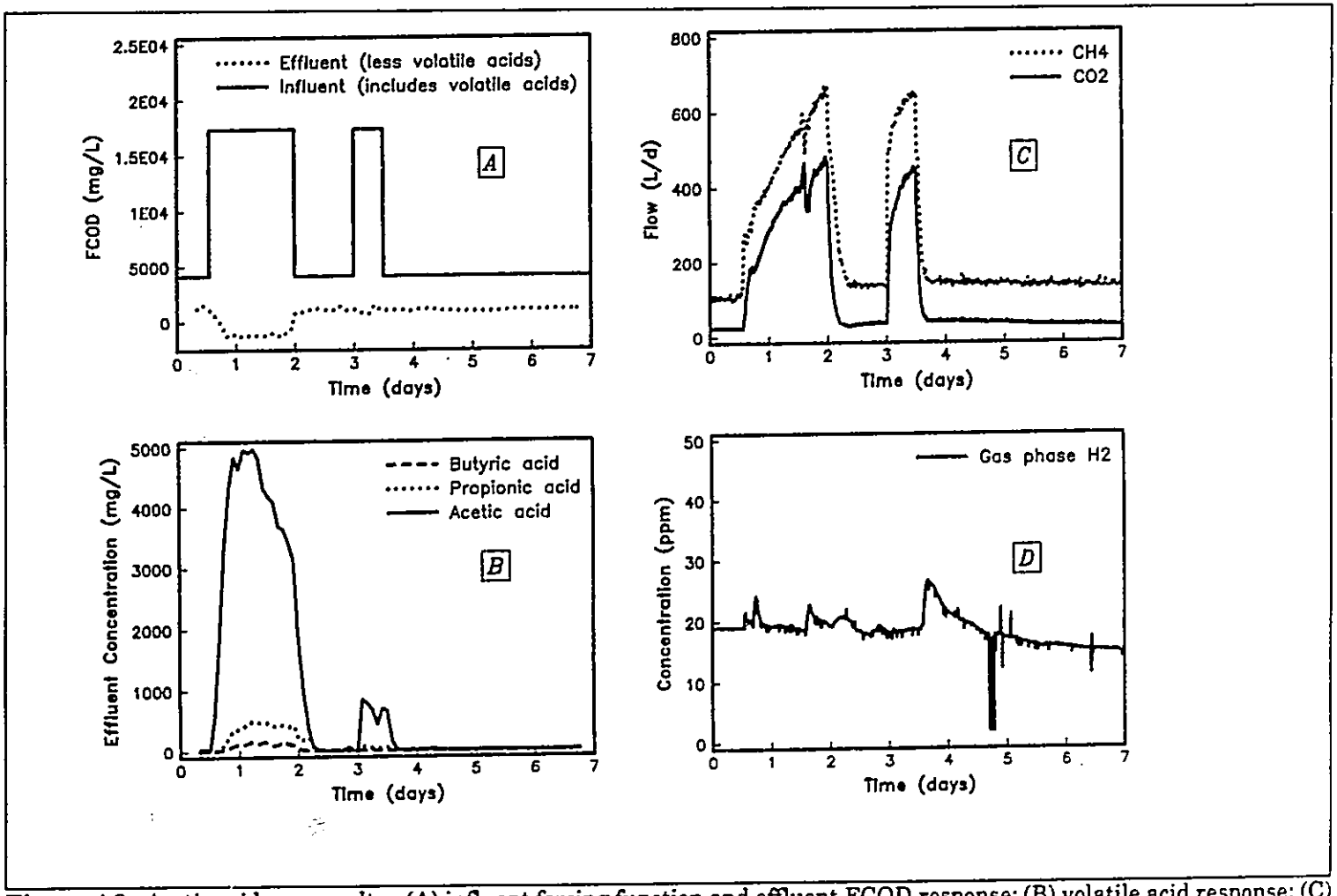

Figure 4.9: Acetic acid run results - (A) influent forcing function and effluent FCOD response; (B) volatile acid response; (C) gas production rate response; (D) gas phase hydrogen concentration response.

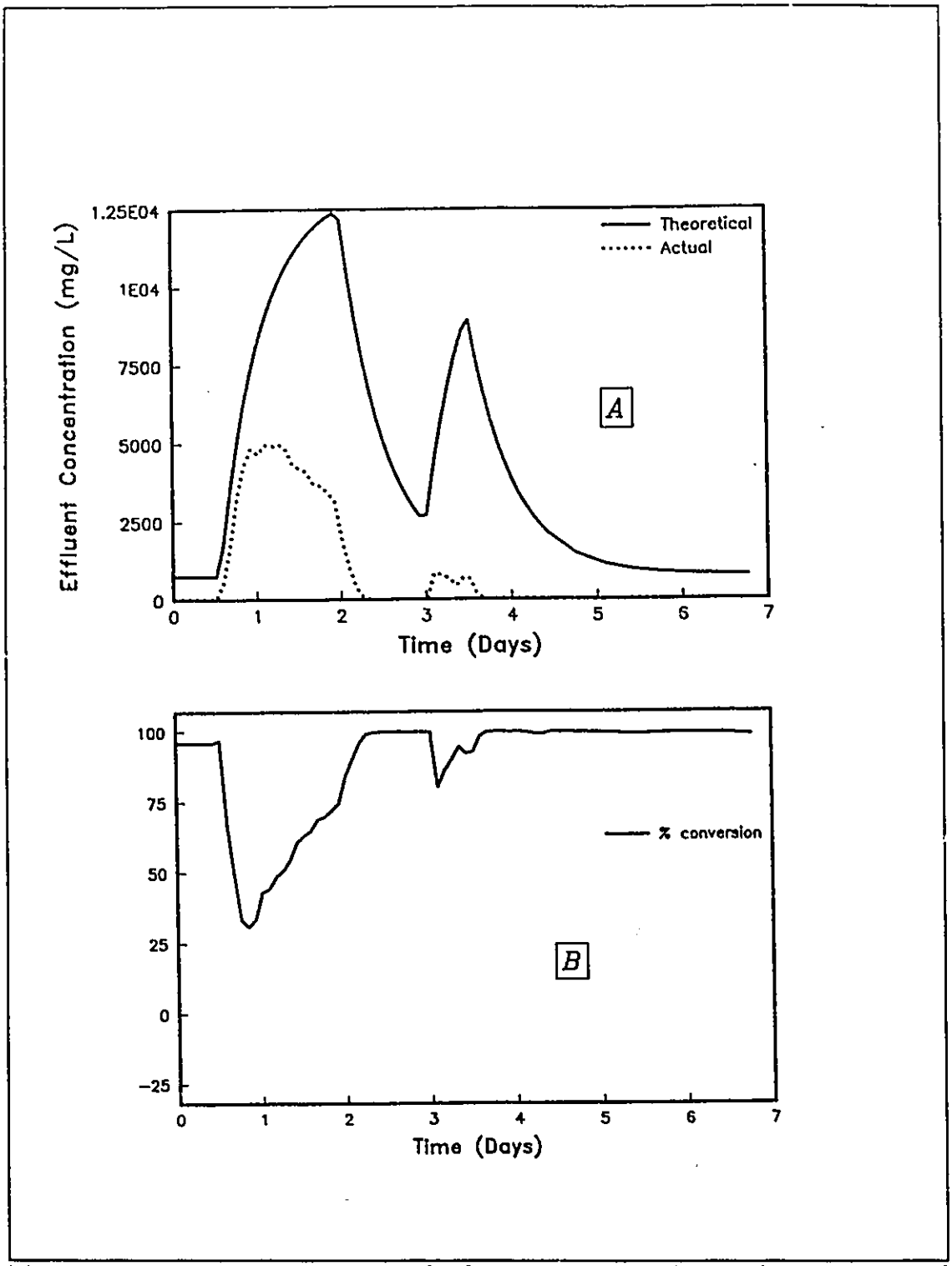

Figure 4.10: Conversion of the acetic acid pulse - (A) response of the actual process compared to a CSTR response with no conversion; (B) conversion efficiency.

Figure 4.10(A) shows the actual effluent concentration of acetic acid and the theoretical response of an ideal CSTR in which there is no conversion of the influent acetic acid. The conversion efficiency presented in Figure 4.10(B) is calculated from the difference between the theoretical and the actual concentrations in the upper plot. The increase in the capacity of the reactor to degrade the acetic acid is readily apparent in these plots. The acetic acid conversion efficiency initially decreases to approximately 30% during the first pulse, but begins to increase within 3 hours after the start of the transient. The initial conversion efficiency is significantly higher during the second pulse.

The appearance of propionic and butyric acid in the reactor effluent during the acetic acid run (Figure 4.9(B)) indicated a possible inhibition of the conversion of these compounds to acetic acid by the acetogenic bacteria or an increase in the rate of production of these acids from the degradation of organic substrates in the distillery wastewater. The concentration of hydrogen in the gas phase (Figure 4.9(D)) did not change significantly during the experiment. Temperature and pH control (Figure 4.11) were adequate throughout the run, although an increase in the pH controller gain was required during the first few hours of the first pulse when the pH initially decreased to approximately 6.3. The NaOH consumption during the acetic acid experiment was 1.8 g NaOH/L feed (Table 4.4).

An oxygen demand balance (Table 4.5) was calculated over the 7 days of the acetic acid run by integrating the mass flow rates of the influent FCOD, the effluent volatile acid COD equivalents, the effluent non-volatile acid FCOD, and the COD equivalent of the biogas methane. Only FCOD concentrations were considered in the balance under the assumption that the production of biomass during an experiment would be negligible and would thus contribute little to the output COD. Although the effluent non-volatile acid FCOD is probably low due to the loss of acetic acid from COD samples, the total measured output FCOD was more than 90% of the input FCOD.

An increase in the capacity of the system to degrade the incoming volatile acid pulse

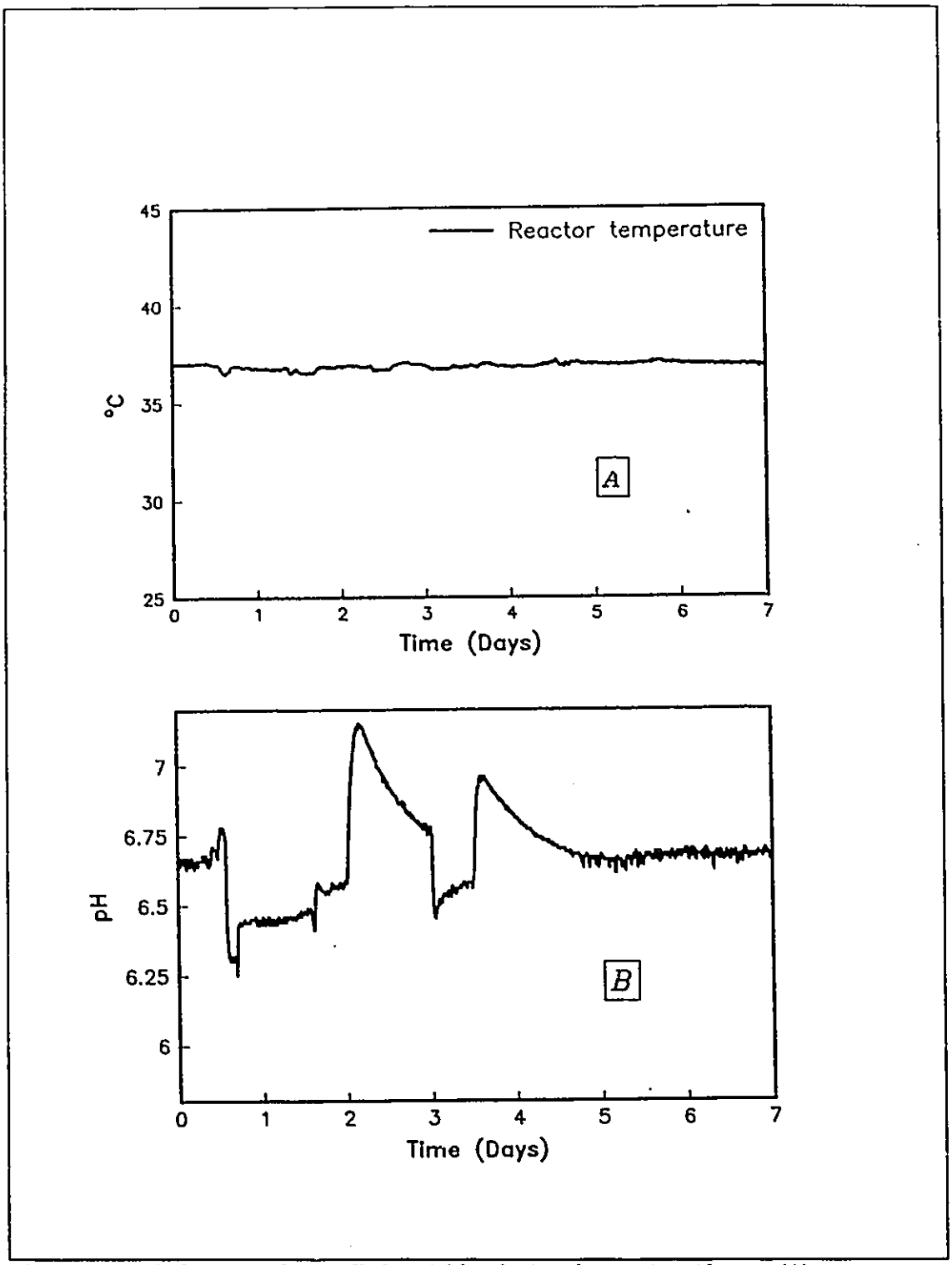

Figure 4.11: Behaviour of controlled variables during the acetic acid run - (A) temperature; (B) pH.

Table 4.4: NaOH consumption for pH control during dynamic experiments	
Experiment	NaOH added (g NaOH/L feed)*
Acetic acid run	1.8
Propionic acid run	1.8
Butyric acid run	1.0
Glucose run #2	1.4
Glucose run #3	1.6
*NaOH added calculated from measurement of volume of NaOH consumed and titration measurement of NaOH concentration	

Table 4.5: Acetic acid run oxygen demand balance		
Parameter	Mass COD (g)	% of input FCOD
Input FCOD *	6393	100
Effluent Acetic Acid	773	12.1
Effluent Propionic Acid	110	1.7
Effluent Butyric Acid	40	0.6
Effluent Non-Volatile Acid FCOD	505	7.9
Total Effluent FCOD	1428	22.3
FCOD Removed	4965	77.8
Biogas Methane	4374	68.4
Total Output FCOD	5802	90.7
* Includes measured FCOD of distillery wastewater feed and calculated COD equivalent of acetic acid pulses		

was not apparent during the propionic acid run (Figure 4.12 and Figure 4.13). The effluent propionic acid concentration did not exhibit a downward trend before the end of an influent pulse. Acetoclastic methane production appeared to be inhibited by the elevated levels of propionic acid, as shown by the declining rate after an initial peak (Figure 4.12(C)). The low

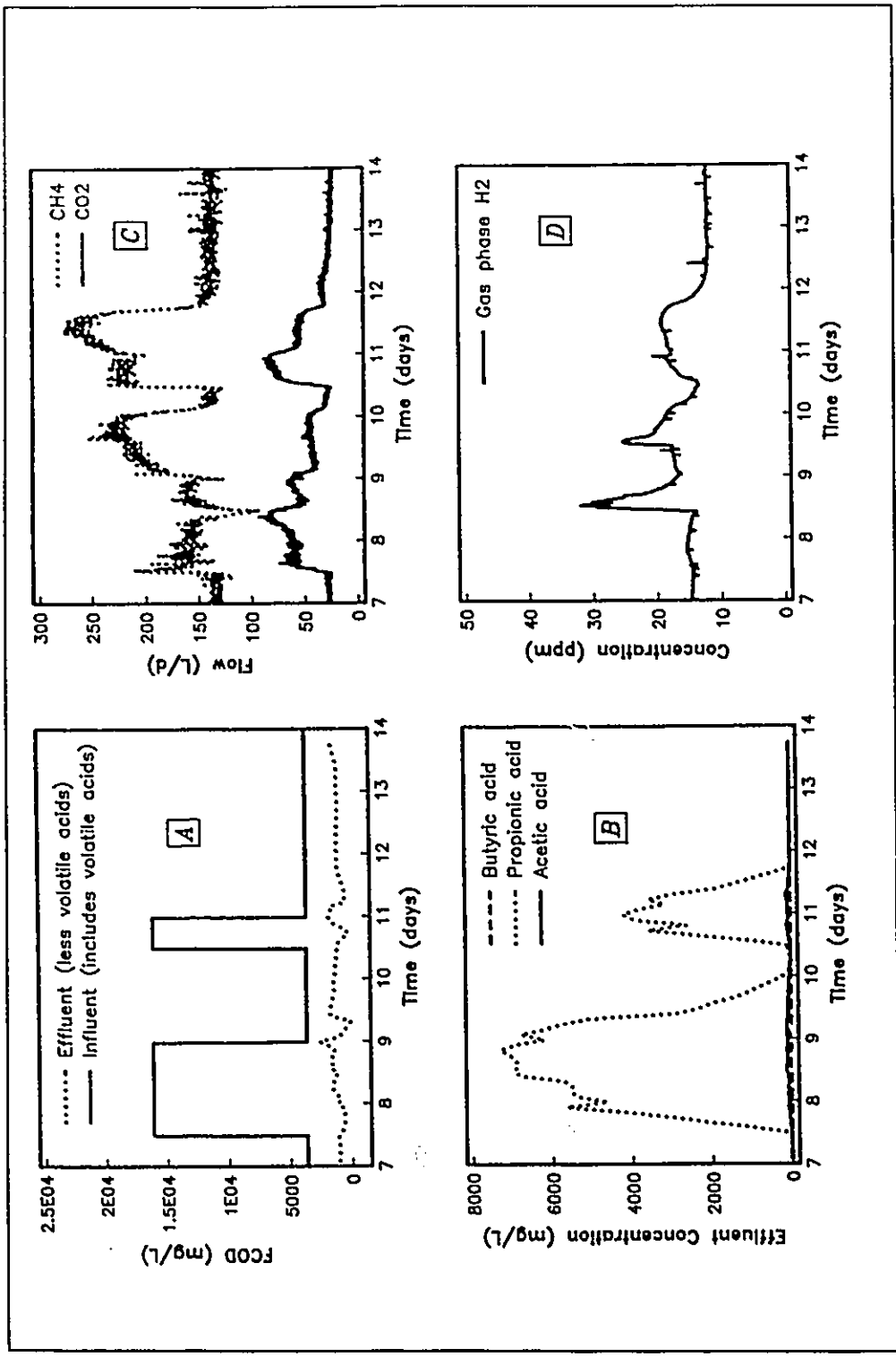

Figure 4.12: Propionic acid run results - (A) influent forcing function and effluent FCOD response; (B) volatile acid response; (C) gas production rate response; (D) gas phase hydrogen concentration response.

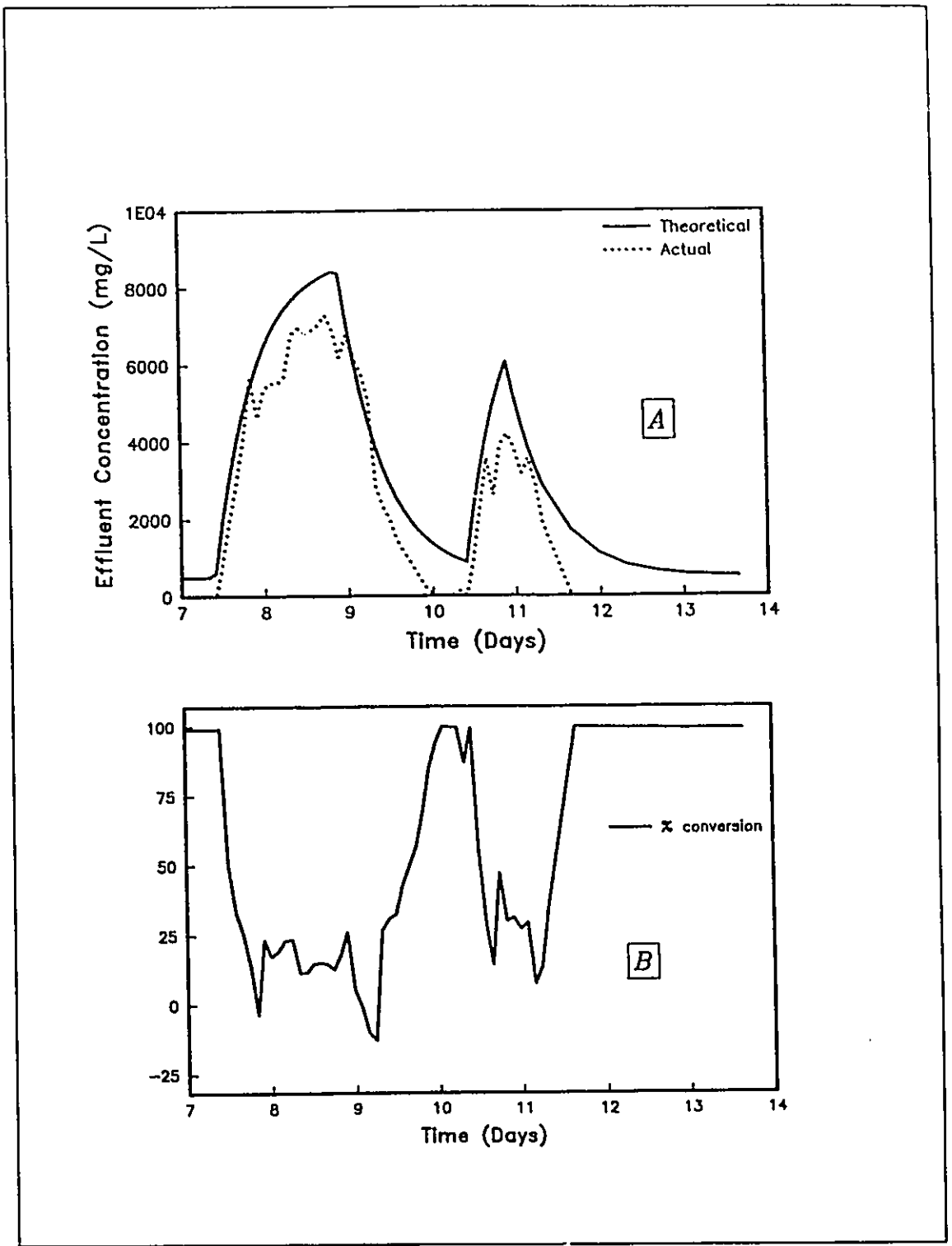

Figure 4.13: Conversion of the propionic acid pulse - (A) response of the actual process compared to a CSTR response with no conversion; (B) conversion efficiency.

conversion of the propionic acid spike can also be seen from the relatively high proportion of the effluent FCOD comprised of propionic acid (Table 4.6). The closure of the propionic acid run oxygen demand balance was within 5%.

The sudden decrease in methane production between day 8 and day 9 was in response to a 6 hour loss in pH control caused by a blockage in the caustic addition line, resulting in a drop in pH to 5.9 (Figure 4.14(B)). The pH upset also resulted in a sudden increase in the gas phase hydrogen concentration (Figure 4.12(D)), indicating a possible inhibition of the hydrogen-utilizing methanogens. The NaOH consumption during the run was 1.8 g NaOH/L feed (Table 4.4). The change in the hydrogen concentration throughout the run was relatively small, indicating essentially complete conversion of hydrogen to methane.

Table 4.6: Propionic acid run oxygen demand balance

Parameter	Mass COD (g)	% of input FCOD
Input FCOD *	6319	100
Effluent Acetic Acid	42	0.7
Effluent Propionic Acid	2613	41.3
Effluent Butyric Acid	13	0.2
Effluent Non-Volatile Acid FCOD	1004	15.9
Total Effluent FCOD	3672	58.1
FCOD Removed	2647	41.9
Biogas Methane	2966	46.9
Total Output FCOD	6638	105.0

* Includes measured FCOD of distillery wastewater feed and calculated COD equivalent of propionic acid pulses

The performance of the process deteriorated during the three week glucose experiment (glucose run #2), as shown by the increasing accumulation of volatile acids during pulses and during the midpoint feed period (Figure 4.15(B)). A decreasing trend in the methane

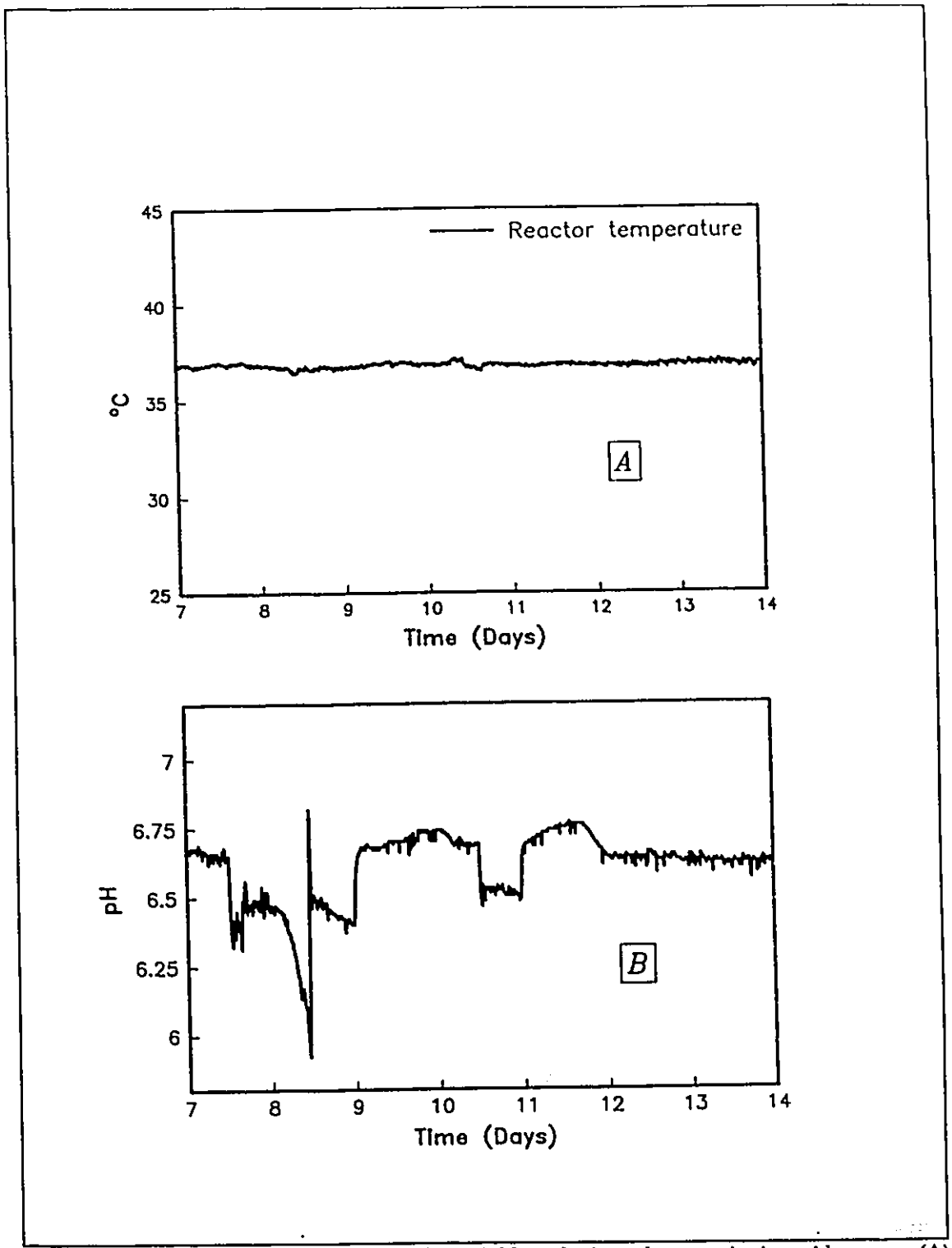

Figure 4.14: Behaviour of controlled variables during the propionic acid run - (A) temperature; (B) pH.

production rate was also observed (Figure 4.15(C)). The accumulation of volatile acids was accompanied by an increase in the gas phase hydrogen concentration (Figure 4.15(D)) during the first and second weeks of the run. The methane transient during the first few days of the glucose experiment was similar in shape to the methane response during the first two days of the propionic acid run, indicating a similar form of inhibition may have been occurring. During the last week of the glucose run, although the capacity of the process to degrade accumulated volatile acids remained at a reduced level, the hydrogen concentration quickly returned to pre-experiment levels following an initial transient. The low conversion efficiency of non-volatile acid COD during baseline loading periods (Figure 4.16) can be attributed to non-biodegradable material in the distillery wastewater feed (Table 4.1).

Problems in pH control were experienced throughout the run and temperature control deteriorated during the last few days of the run (Figure 4.17). The control problems were caused by blockages forming in the recycle lines affecting the on-line measurements from the pH and temperature sensors. The NaOH consumption during the run was 1.4 g NaOH/L feed (Table 4.4).

An increase in suspended solids was observed during the glucose run, as is evident in the plot of the reactor effluent particulate COD concentration (Figure 4.18). The particulate COD concentration was calculated as the difference between total COD and FCOD measurements. Increases in the effluent particulate COD concentration were significantly greater during the glucose run in comparison to the acetic and propionic acid runs. This indicates that acid-forming bacteria were likely growing in the suspended phase of the reactor during the glucose experiment. On day 21, the recycle lines were flushed with clean water in an attempt to reduce flow blockages. The decrease in the hydrogen concentration (Figure 4.15(D)) which coincided with this event is further evidence that some of the acid-former activity was present in the suspended phase of the reactor. In addition, the COD balance (Table 4.7) indicated that the total effluent FCOD and methane COD only accounted for

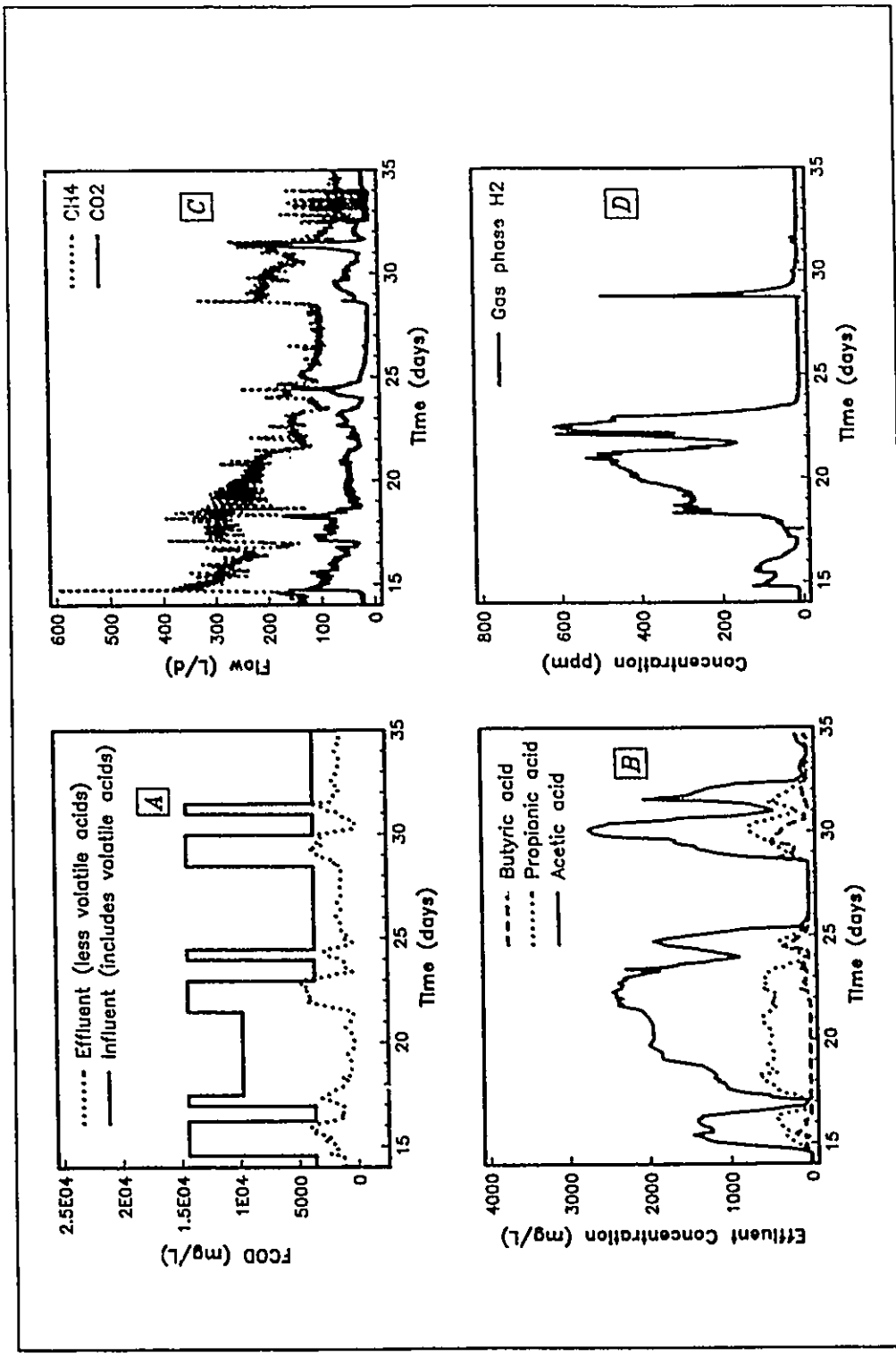

Figure 4.15: Glucose run #2 results - (A) influent forcing function and effluent FCOD response; (B) volatile acid response; (C) gas production rate response; (D) gas phase hydrogen concentration response.

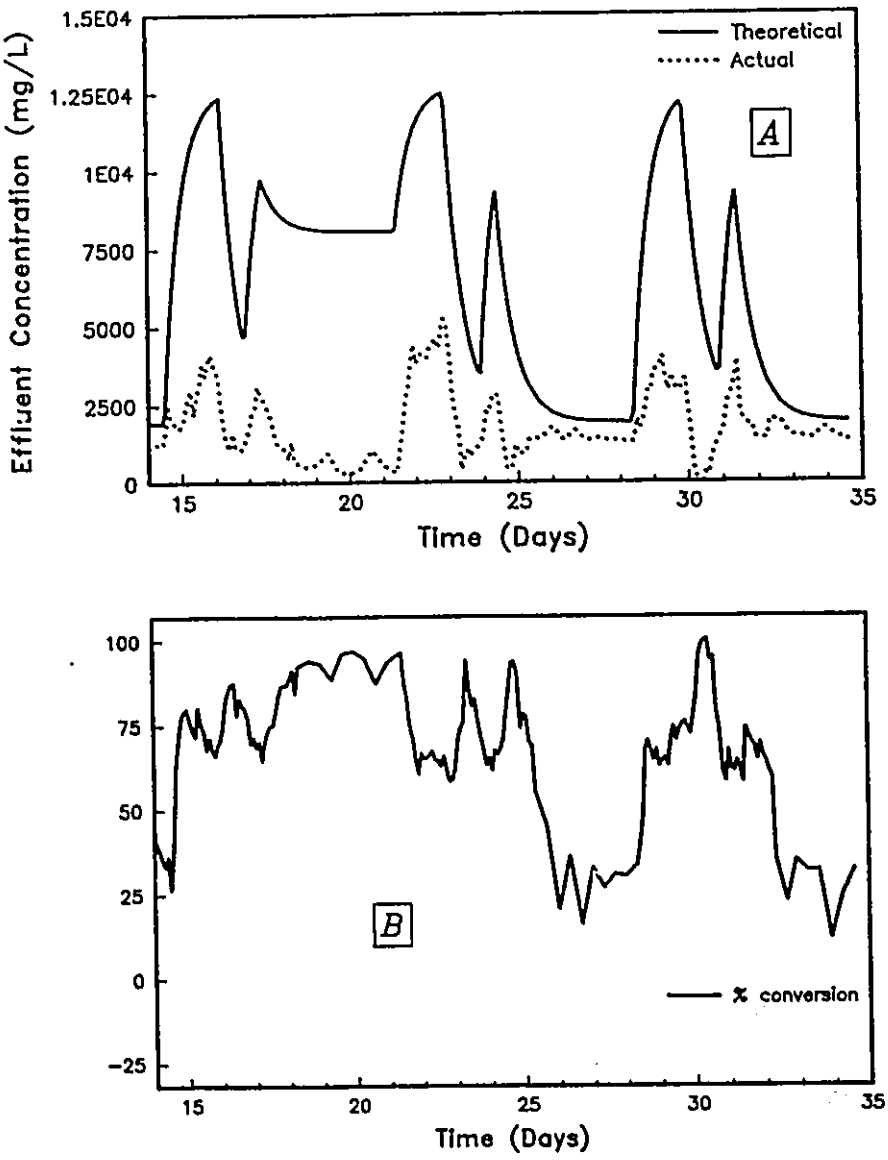

Figure 4.16: Conversion of the glucose pulse during glucose run #2 - (A) response of the actual process compared to a CSTR response with no conversion; (B) conversion efficiency.

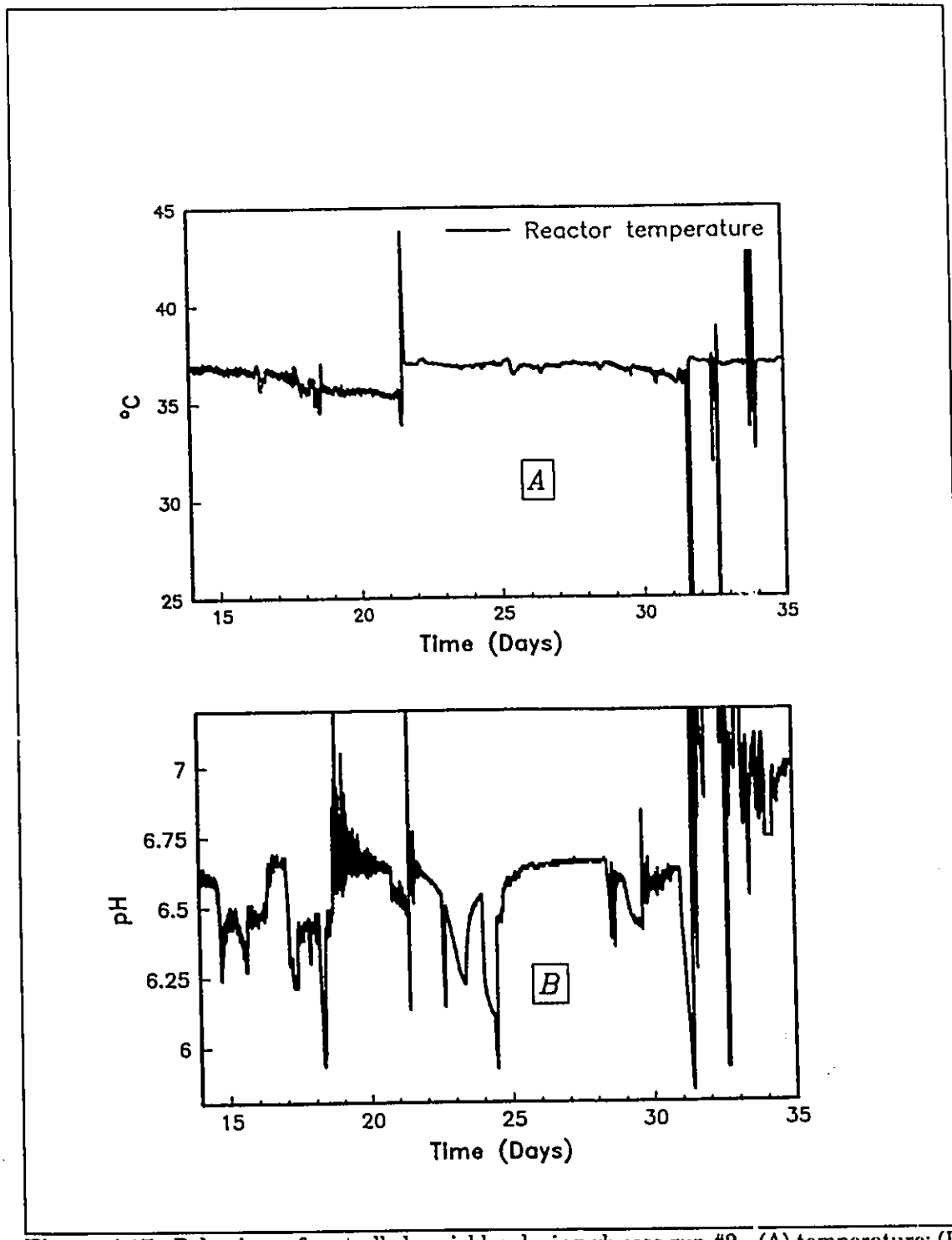

Figure 4.17: Behaviour of controlled variables during glucose run #2 - (A) temperature; (B) pH.

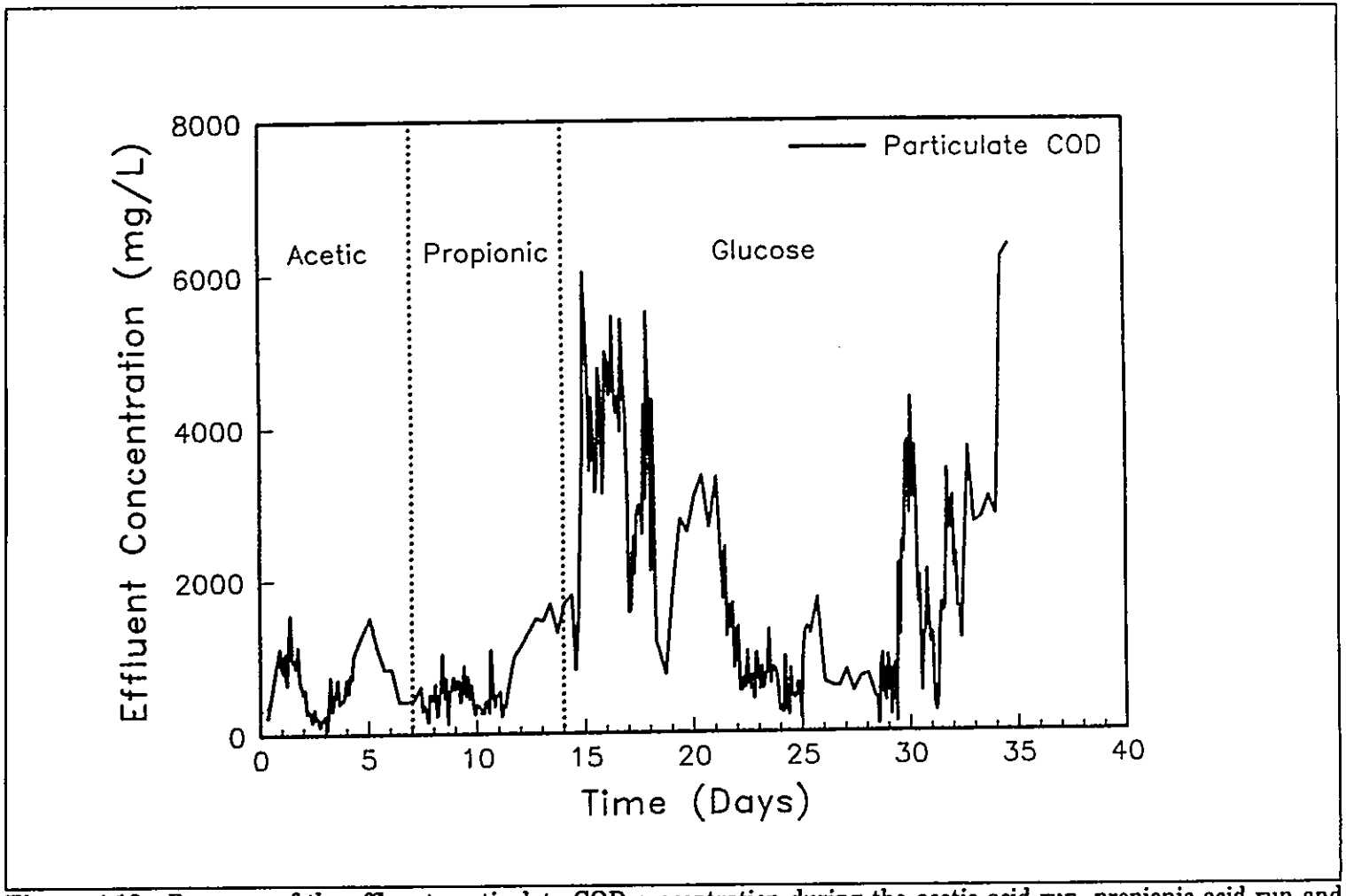

Figure 4.18: Response of the effluent particulate COD concentration during the acetic acid run, propionic acid run and glucose run #2.

Table 4.7: Glucose run #2 oxygen demand balance

Parameter	Mass COD (g)	% of input FCOD
Input FCOD *	20427	100
Effluent Acetic Acid	2872	14.1
Effluent Propionic Acid	1029	5.0
Effluent Butyric Acid	273	1.3
Effluent Non-Volatile Acid FCOD	4643	22.7
Total Effluent FCOD	8817	43.1
FCOD Removed	11610	57.0
Biogas Methane	8850	43.3
Total Output FCOD	17667	86.4

* Includes measured FCOD of distillery wastewater feed and calculated COD equivalent of glucose pulses.

86% of the input FCOD during the glucose run.

There were not sufficient measurements taken to conduct an adequate solids balance to test the hypothesis that the poor closure in the COD balance was due to the growth of acid-forming bacteria. However, if the assumption is made that all of the missing COD is due to biomass growth, a yield can be calculated and compared to typical values reported in the literature. This calculation is summarized in Table 4.8. The COD of bacterial cells was estimated from the stoichiometry of endogenous respiration given by Hoover and Porges (1952). The biomass yield calculated in this way is within the range reported in the review by Pavlostathis and Giraldo-Gomez (1991) for acid-former fermentation of glucose.

The influent forcing function and observed process response during the butyric acid run is shown in Figure 4.19. Temperature and pH control were very good throughout the run (Figure 4.20). NaOH consumption was 1.0 g NaOH/L feed (Table 4.4). During the first pulse, the effluent butyric acid concentration reached levels greater than those expected from an ideal

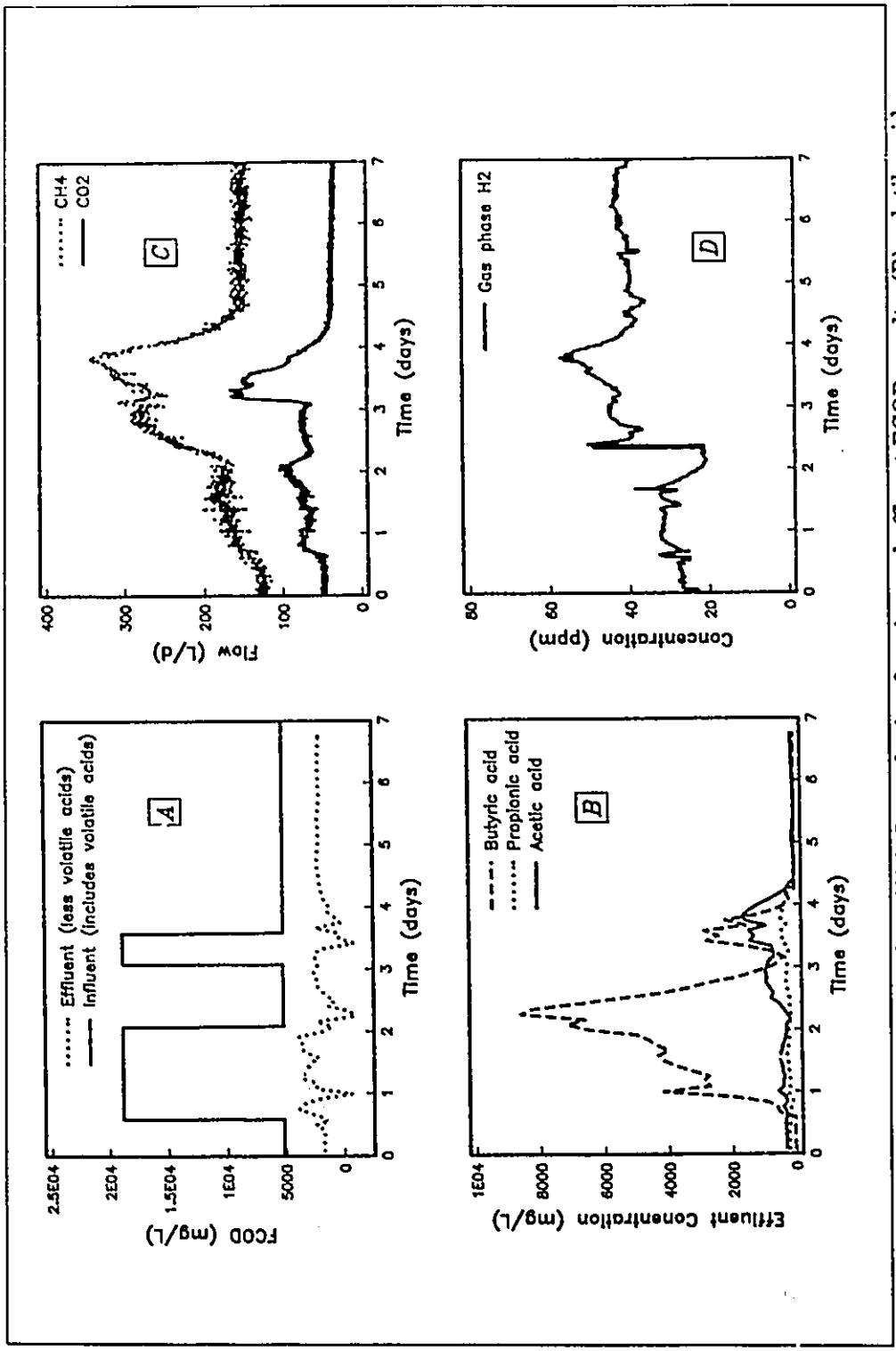

Figure 4.19: Butyric acid run results - (A) influent forcing function and effluent FCOD results; (B) volatile acid response; (C) gas production rate response; (D) gas phase hydrogen concentration response.

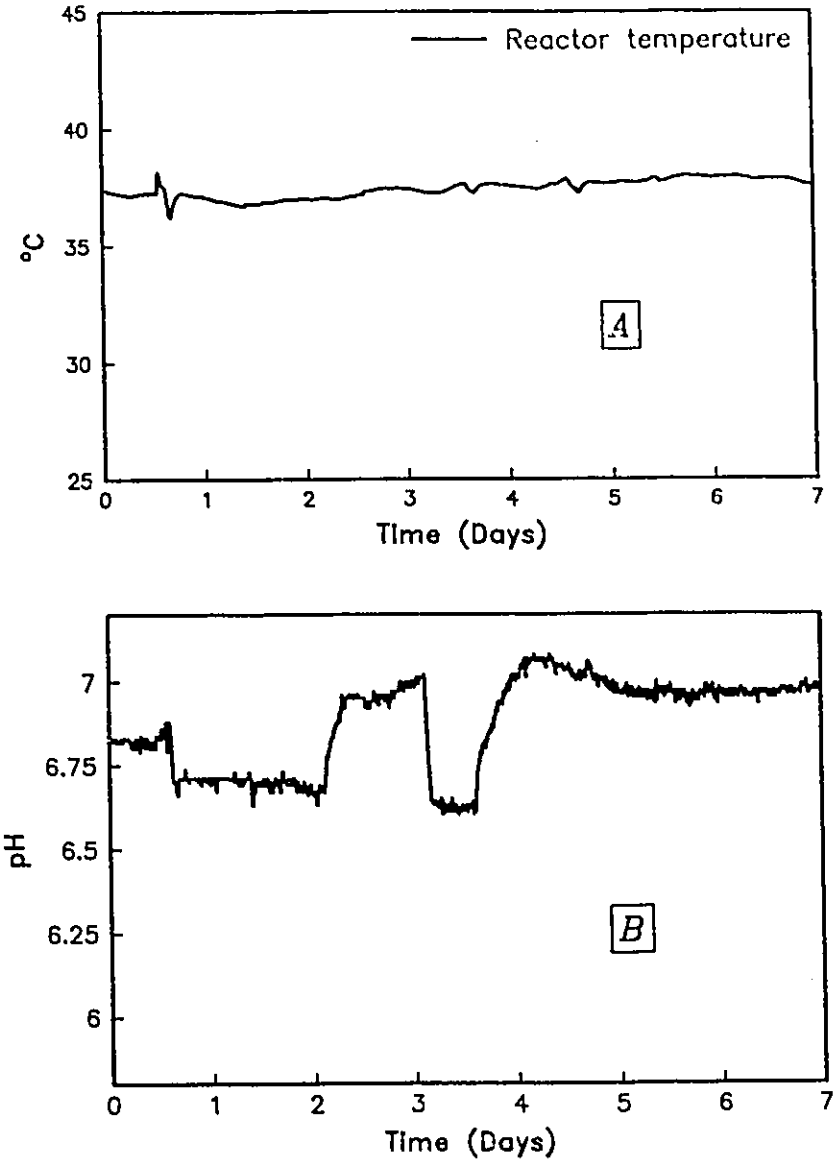

Figure 4.20: Behaviour of controlled variables during the butyric acid run - (A) temperature; (B) pH.

Table 4.8: Estimated biomass yield coefficient during glucose run #2.	
Parameter	Value
(1) Filtered COD Removed	11610 g
(2) Assumed Biomass COD (Input FCOD - Total Output FCOD)	2760 g
(3) COD of cells	1.42 g COD/g VSS
(4) Biomass Yield ((4) = (2)/((1)*(3)))	0.17 g VSS/g COD removed

CSTR in which there is no conversion of the incoming butyric acid (Figure 4.21(A)). This response indicates that butyrate-utilizing acetogenic bacteria may be substrate inhibited and that part of the accumulating butyric acid originated from the distillery wastewater feed. Methane production (Figure 4.19(C)) did not appear to be inhibited by the high concentrations of butyric acid, although a significant increase was observed as butyric acid concentrations (Figure 4.19(B)) began to decrease at the end of the first pulse. The increasing acetic acid concentration at this point indicates that the lower methane production rate during high butyric acid concentrations may have been due to a lack of available methanogenic substrate (acetate). There was no significant response in the gas phase hydrogen concentration (Figure 4.19(D)). The sudden change in hydrogen concentration between day 2 and 3 was due to instrument recalibration.

The closure of the butyric acid run oxygen demand balance (Table 4.9) was within 3%. The relatively high effluent particulate COD concentration (Figure 4.22) prior to the first pulse was due to a power failure necessitating a re-fluidization of the reactor bed two days before the start of the run.

The results from glucose run #3 are plotted in Figures 4.23 to 4.26. The run was started with elevated levels of effluent volatile acid and particulate COD concentrations as shown in Figure 4.23(B) and Figure 4.26, respectively. This was likely due to cleaning of the reactor recycle and effluent lines the week before the experiment. The process response during

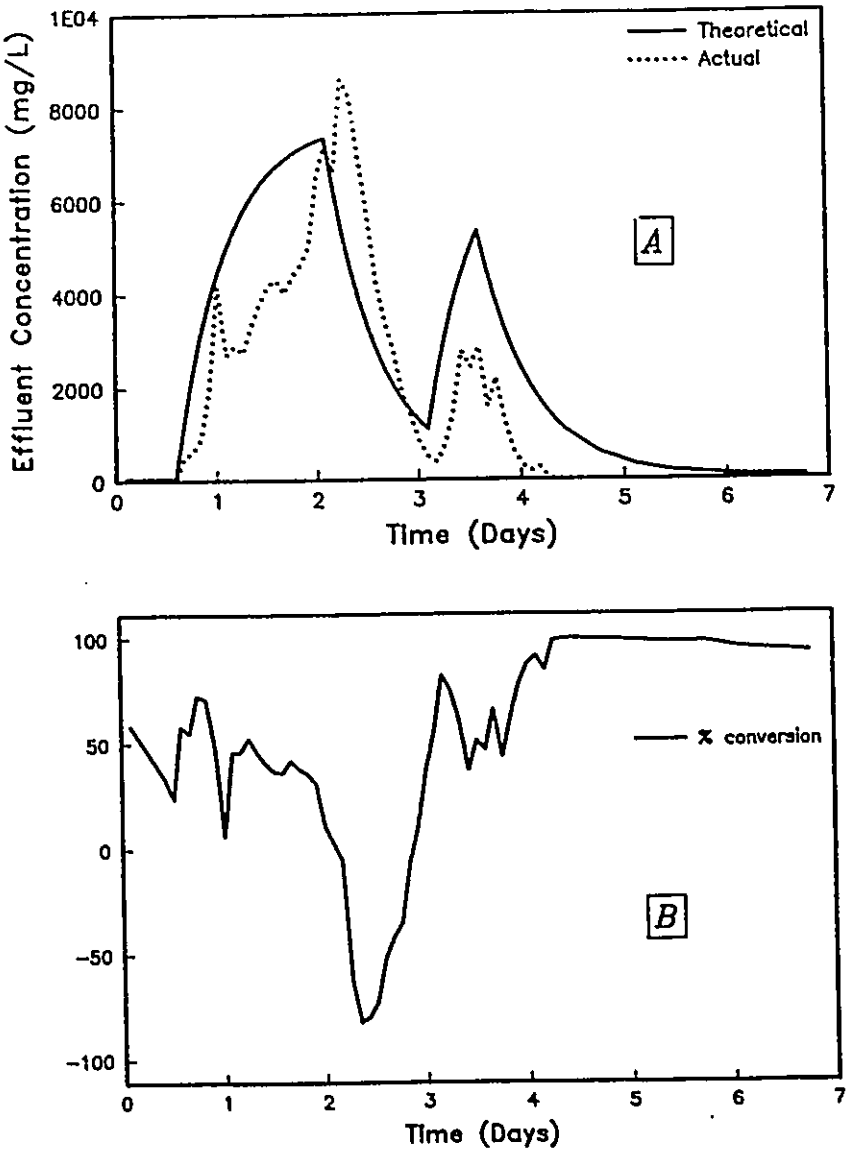

Figure 4.21: Conversion of the butyric acid pulse - (A) response of the actual process compared to a CSTR response with no conversion; (B) conversion efficiency.

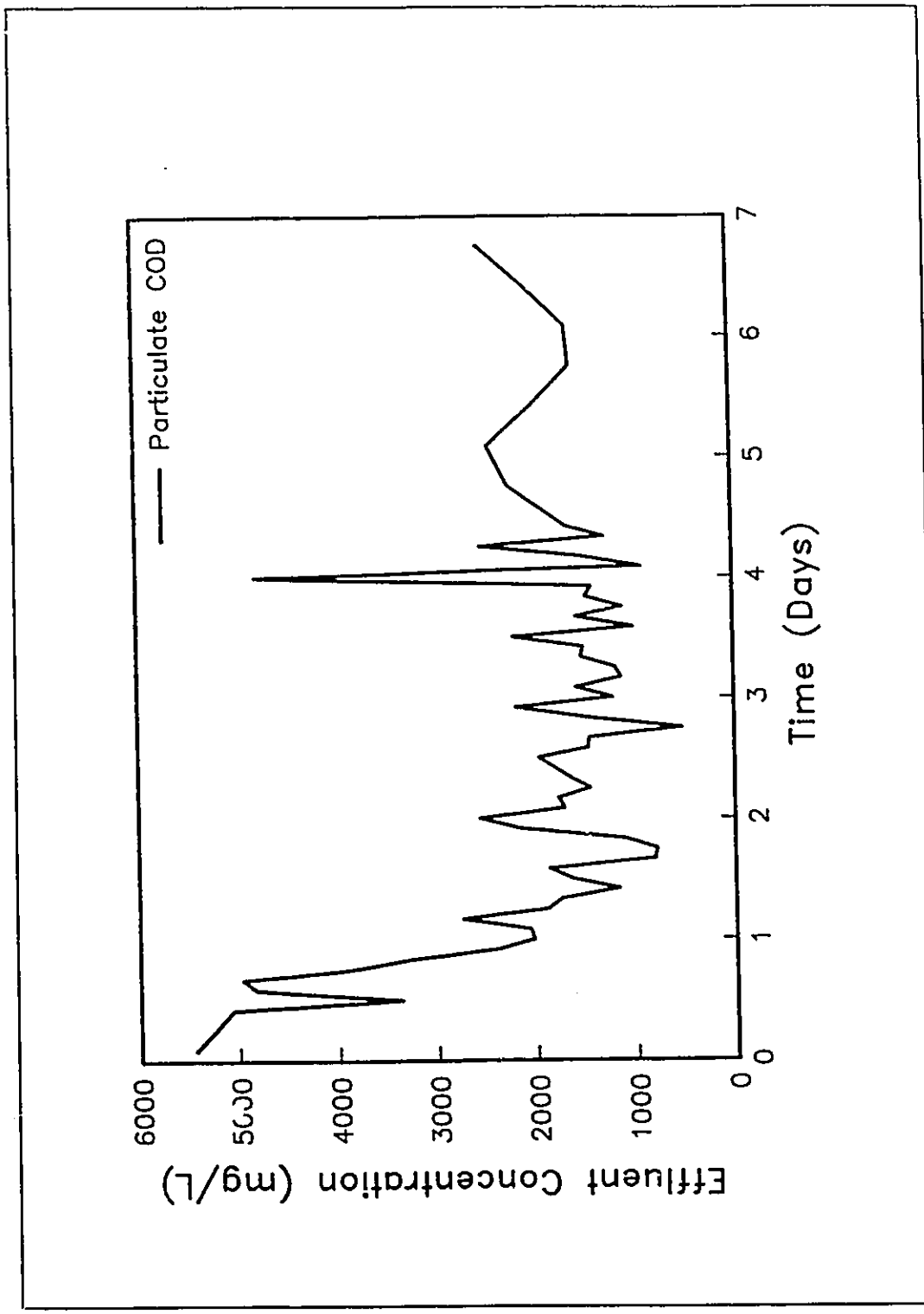

Figure 4.22: Response of the effluent particulate COD concentration during the butyric acid run.

Table 4.9: Butyric acid run oxygen demand balance

Parameter	Mass COD (g)	% of input FCOD
Input FCOD *	7659	100
Effluent Acetic Acid	358	4.7
Effluent Propionic Acid	195	2.5
Effluent Butyric Acid	2373	31.0
Effluent Non-Volatile Acid FCOD	1635	21.3
Total Effluent FCOD	4561	59.5
FCOD Removed	3098	40.0
Biogas Methane	3308	43.2
Total Output FCOD	7869	102.7

* Includes measured FCOD of distillery wastewater feed and calculated COD equivalent of butyric acid pulses

this run differed from glucose run #2 in that the performance of the process appeared to improve during the first 7 days of the run. This was indicated by an increasing methane production rate (Figure 4.23(C)) during the second pulse and throughout the midpoint feed period, and the maintenance of a relatively low and stable effluent volatile acid concentration during the midpoint feed period. A significant response in the gas phase hydrogen concentration (Figure 4.23(D)) was observed during the first 7 days of the run with measurements exceeding 2000 ppm during the first pulse. During the final 6 days of the run, the acetic acid response continued to decrease in magnitude while the propionic acid concentration remained at elevated levels. The hydrogen concentration decreased suddenly between day 6 and 7 and stayed at low levels throughout the remainder of the experiment. The reactor feed line was partially plugged after day 11. Temperature and pH control were adequate throughout the run (Figure 4.24). NaOH addition for pH control was 1.6 g NaOH/L feed (Table 4.4).

As with the glucose run #2, the oxygen demand balance (Table 4.10) closure was poor.

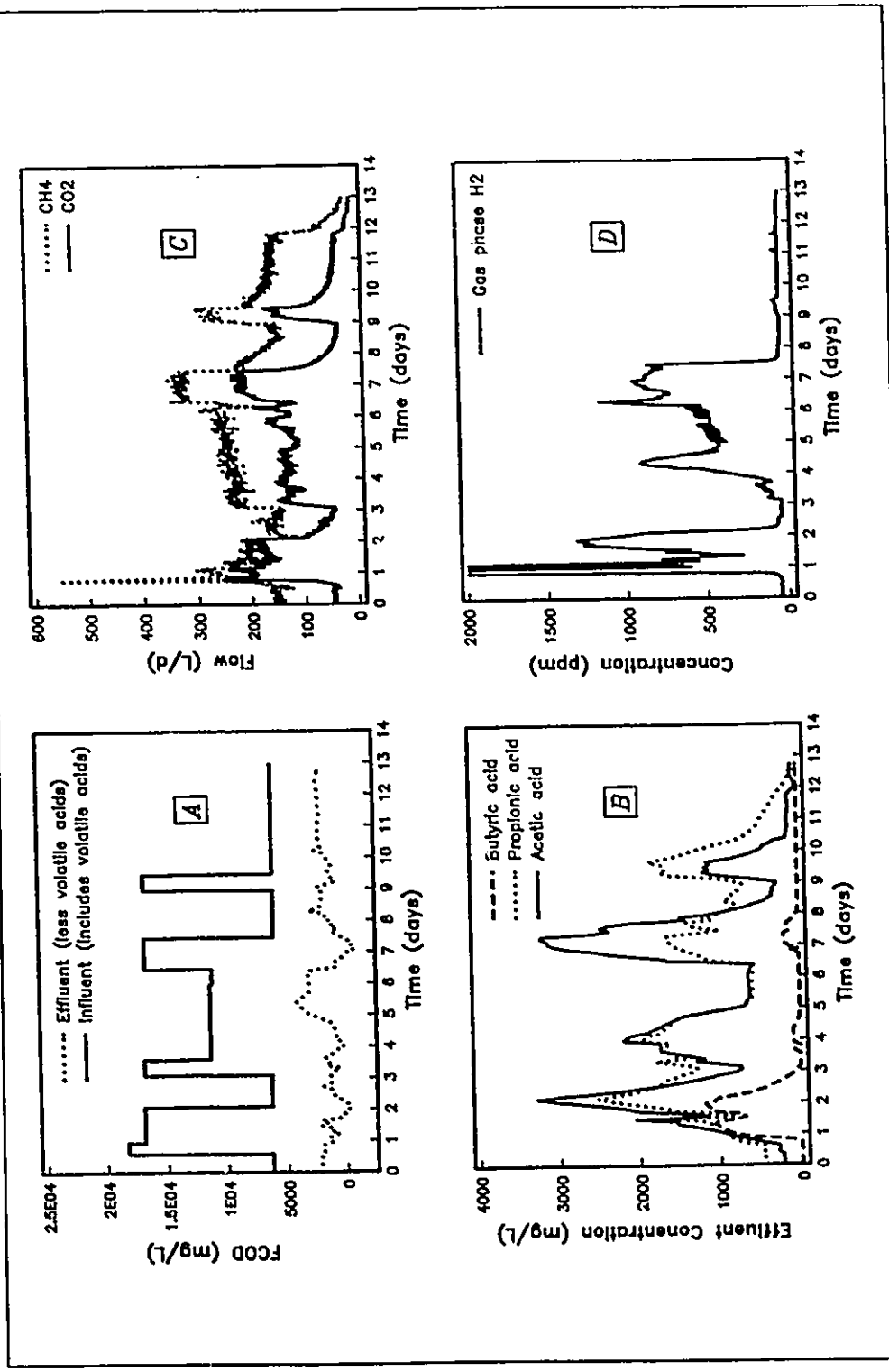

Figure 4.23: Glucose run #3 results - (A) influent forcing function and effluent FCOD response; (B) volatile acid response; (C) gas production rate response; (D) gas phase hydrogen concentration response.

Table 4.10: Glucose run #3 oxygen demand balance		
Parameter	Mass COD (g)	% of input FCOD
Input FCOD *	15640	100
Effluent Acetic Acid	1724	11.0
Effluent Propionic Acid	2396	15.3
Effluent Butyric Acid	414	2.6
Effluent Non-Volatile Acid FCOD	2289	14.7
Total Effluent FCOD	6823	43.6
FCOD Removed	8817	56.4
Biogas Methane	6428	41.1
Total Output FCOD	13251	84.7

* Includes measured FCOD of distillery wastewater feed and calculated COD equivalent of glucose pulses.

The calculation shown in Table 4.11 again indicates that the assumption that the missing COD can be attributed to biomass growth results in a reasonable value for the biomass yield coefficient.

Table 4.11: Estimated biomass yield coefficient during glucose run #3	
Parameter	Value
(1) FCOD Removed	8817 g
(2) Assumed Biomass COD (Total Input FCOD - Total FCOD)	2389 g
(3) COD of cells	1.42 g COD/g VSS
(4) Biomass yield ((4) = (2)/((1)*(3)))	0.19 g VSS/g COD removed

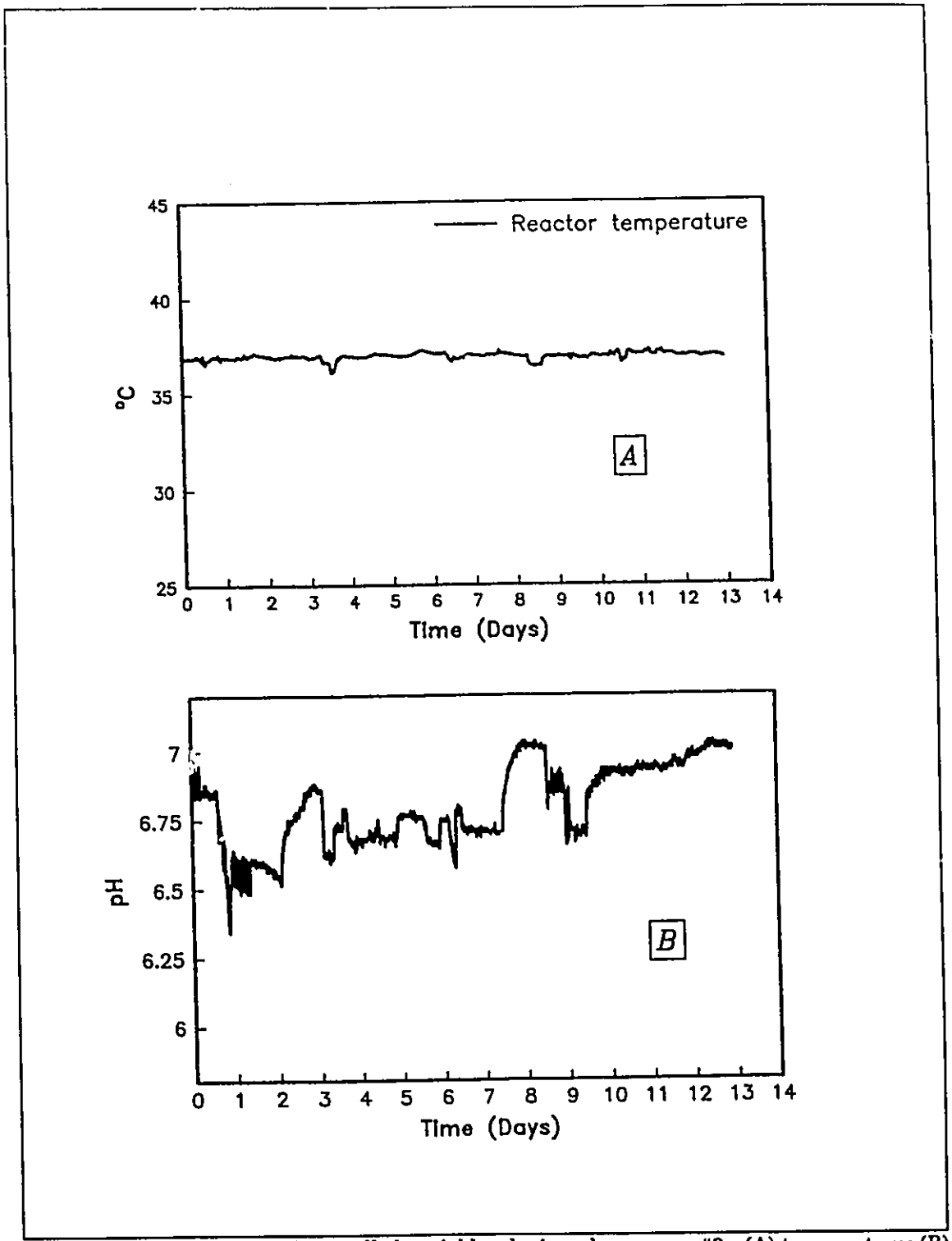

Figure 4.24: Behaviour of controlled variables during glucose run #3 - (A) temperature; (B) pH.

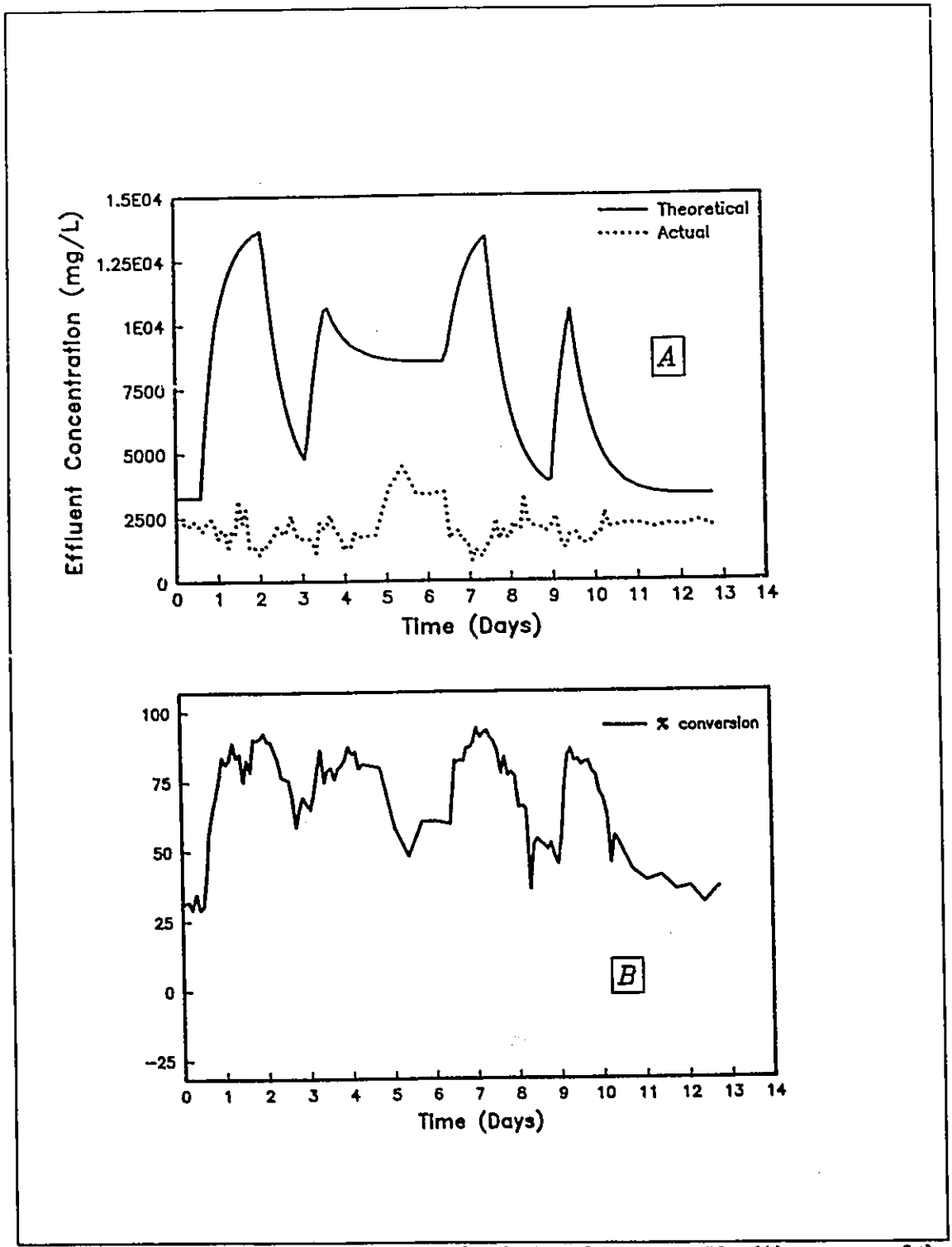

Figure 4.25: Conversion of the glucose pulse during glucose run #3 - (A) response of the actual process compared to a CSTR response with no conversion; (B) conversion efficiency.

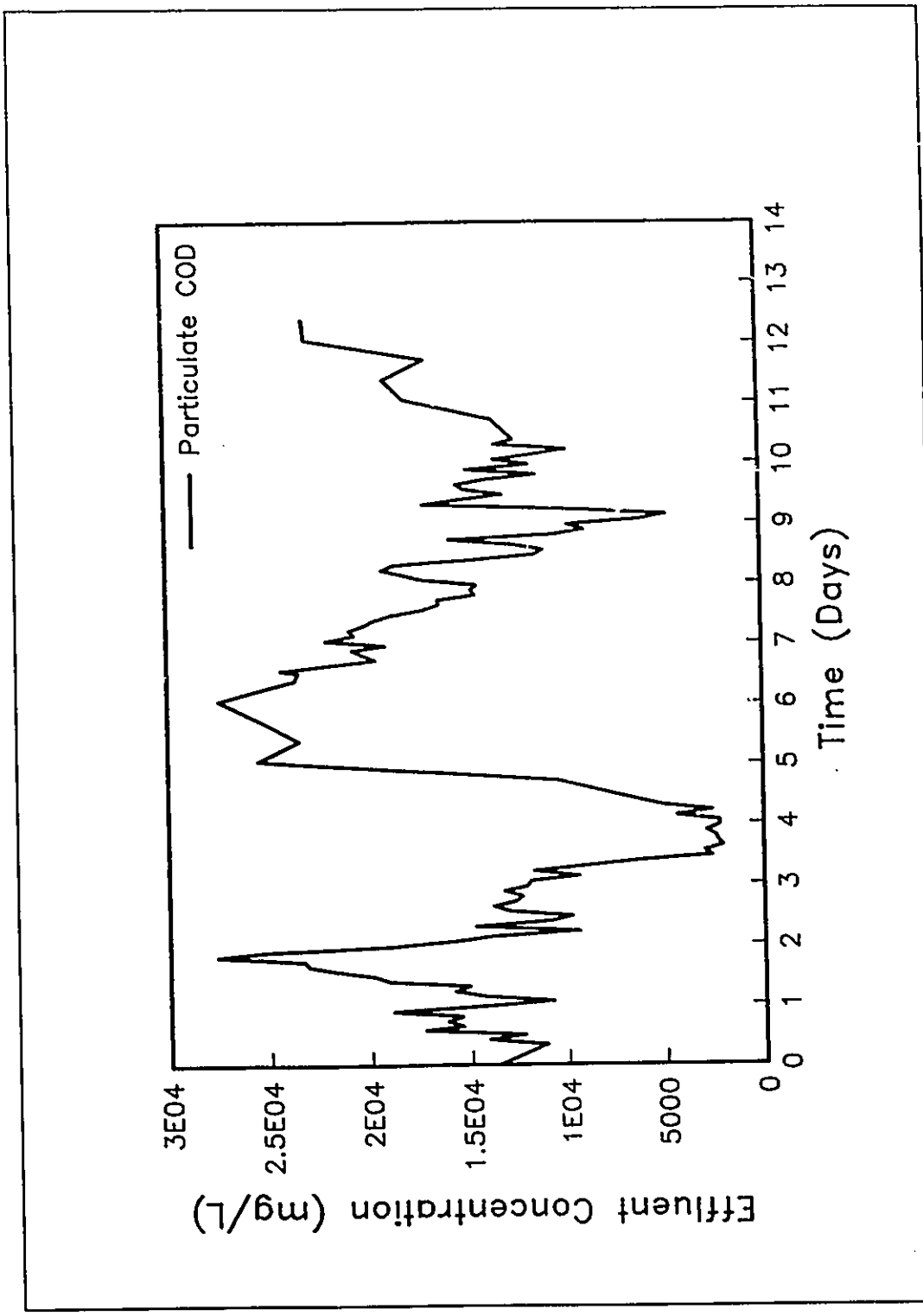

Figure 4.26: Response of the effluent particulate COD concentration during glucose run #3.

4.4 SUMMARY AND DISCUSSION OF SIGNIFICANT EXPERIMENTAL RESULTS

The dynamic experiments on the fluidized bed reactor demonstrated the relative importance of substrate and product inhibition on the various reaction steps in the process. The results also indicated that the short term dynamic response of a high rate anaerobic process can change significantly over time. The most significant findings of the experimental program and the possible implications on modelling, monitoring and process control are summarized in this section.

During the acetic acid experiment, acetoclastic methanogenesis was not significantly inhibited by elevated concentrations of acetic acid. Many previous dynamic models of the anaerobic process (Andrews and Graef, 1971; Hill and Barth, 1977; Ide, 1988; among others) have utilized a substrate inhibition term in the kinetic expression for acetoclastic methanogenesis. These results indicate that this kinetic expression is not appropriate.

High acetic acid concentrations during the acetic acid experiment resulted in increases in reactor concentrations of propionic and butyric acids. Inhibition of propionic and butyric acid degradation by acetate has previously been demonstrated in laboratory-scale batch cultures (Fukuzaki *et al.*, 1990; Mawson *et al.*, 1991) and in suspended-growth, completely-mixed cultures (Kaspar and Wuhrmann, 1978). Labib *et al.* (1988) provided strong evidence for acetate inhibition of butyrate degradation in a laboratory-scale anaerobic fluidized bed reactor. These results provide a further demonstration of the significance of acetate inhibition on butyrate degradation and also indicate that acetate inhibition of the net degradation rate of propionate is significant in a continuous-flow, high rate anaerobic system. There was not sufficient information from the experiments to differentiate between the effects of acetate on the production rate of propionate and butyrate and the effects of acetate on the degradation rate of propionate and butyrate.

The capacity of the anaerobic fluidized bed reactor to convert acetic acid to methane increased rapidly during the acetic acid experiments. For example, during the first pulse of

the acetic acid experiment, the volumetric organic loading rate was increased by approximately 20 kg COD/m^3•d for a 36 hour period through the addition of acetic acid to the reactor feed. The COD removal efficiency of the incoming acetic acid pulse increased from approximately 25% to 75% over the 36 hours. The acetogenic conversion rate of propionic acid and butyric acid did not increase during similar pulse experiments over the same time period. McCarty and Mosey (1991) suggested that the population of propionate degrading organisms (*Syntrophobacter wolinii*) will be very low during operation at modest loading rates because of low substrate levels. If the level of propionic acid in the reactor increases, the initial growth response of the organisms will be slow due to a low initial population.

In addition, elevated levels of propionic acid were observed to inhibit acetoclastic methanogenesis in these experiments. These results demonstrate the importance of maintaining operating conditions which will support the growth of acetogenic bacteria. For example, the first stage of a two stage treatment system could be operated to produce significant effluent concentrations of propionate and butyrate. This would ensure the maintenance of a population of acetogenic organisms in the second stage of the system. Ensuring favourable conditions for acetogenic growth may be a more critical factor for process stability than the growth of methanogens. As long as acetoclastic methanogenesis is not inhibited by high levels of propionic acid, it appears that a process can increase its capacity to convert acetic acid to methane relatively quickly.

The gas phase hydrogen concentration did not respond during volatile acid pulse experiments and the response was inconsistent during glucose pulse experiments. Hydrogen is not a product of acetate degradation and therefore a response during the acetic acid experiment was not expected. The lack of a hydrogen response during the propionic and butyric acid experiments may have been due to the low conversion of these substrates. The response during the first half of glucose run #2 and glucose run #3 was significant and appeared to exhibit some correlation to the accumulation of volatile acids in the process.

During the latter portions of each run, the hydrogen response was minimal or quickly returned to baseline levels in spite of continued accumulations of volatile acids. These results indicate that any difference between hydrogen production and consumption rates may change rapidly, possibly due to changes in the relative concentrations of active acid-forming bacteria and hydrogen-utilizing methanogenic bacteria. The values reported by Pavlostathis and Giraldo-Gomez (1991) for the maximum specific growth rate (μ_{max}) of hydrogen-utilizing methanogens indicate that these bacteria may grow relatively rapidly in response to increased substrate availability.

The observations of the hydrogen response indicate that the gas phase hydrogen concentration alone has limited utility as a monitoring variable. Interpretation of the hydrogen response requires a knowledge of the changes in the relative activity of the various organisms producing or consuming hydrogen. In addition, the lack of a consistent correlation between the accumulation of volatile acids and the gas phase hydrogen concentration indicates that inhibition of propionate and butyrate degradation by hydrogen is not the most important factor affecting the response of volatile acid intermediates during organic overloads. Previous studies demonstrating inhibition of propionate degradation by hydrogen (Kaspar and Wuhrmann, 1978; Fukuzaki *et al.*, 1990) were conducted at significantly higher gas phase hydrogen concentrations than observed in the present set of experiments. At the highest concentration reported (91% hydrogen in the gas phase) by Fukuzuki *et al.* (1990), addition of a hydrogen-utilizing methanogen to the culture reversed the inhibition.

Hickey and Switzenbaum (1991) also found that gas phase hydrogen concentrations did not remain at elevated levels during an organic overload to a laboratory scale sludge digestor while effluent concentrations of acetic and higher molecular weight acid concentrations did increase. Pauss *et al.* (1990a) have argued that hydrogen concentrations must be measured in the liquid phase because liquid-to-gas mass transfer limitations may result in liquid phase hydrogen concentrations much higher than would be expected if the gas

and liquid phases were in equilibrium. The experimental evidence of this phenomenon is contradictory. While Pauss *et al.* (1990a) provided convincing evidence of hydrogen mass transfer limitations in a CSTR reactor, Labib *et al.* (1988) found that the gas and liquid phase hydrogen concentrations were at equilibrium in an anaerobic fluidized bed reactor.

The addition of a glucose substrate pulse to the reactor resulted in the rapid growth of suspended solids which caused a number of mechanical and control problems. Although the pilot plant reactor was operated at a relatively low HRT of approximately 12 hours, there was probably sufficient time for a significant level of acid-former growth in the suspended phase of the reactor. Using the minimum value for the acid-former maximum specific growth rate (μ_{max}) reported by Pavlostathis and Giraldo-Gomez (1991), the minimum solids retention time required to prevent wash-out of the acid-formers is calculated from Equation (2.25):

$$\theta_c^{min} = \frac{1}{\mu_{max}} = \frac{1}{7.2\ d^{-1}} = 3.3\ hours$$

Because θ_c^{min} is significantly less than the HRT, it appears likely that acid-former growth was occurring in the suspended phase of the reactor. Any high rate anaerobic process application in which large dynamic increases in highly biodegradable carbohydrate substrates are expected should therefore consider the growth in suspended solids expected and if necessary provide for the efficient removal of these solids. Failure to consider the solids growth possible under dynamic conditions could result in problems such as plugging of piping, plugging of reactor media, and fouling of measurement sensors.

CHAPTER 5

DYNAMIC MODEL FORMULATION

In this chapter, the formulation of a dynamic mathematical model of the anaerobic fluidized bed pilot plant is presented. The philosophy used in developing the model was to minimize model complexity so that application and calibration would be practical. Although the simplest form of mathematical model for the process would be an empirical input-output model, such a model would not explicitly relate measurable process behaviour to internal mechanisms occurring in the system and would thus provide little information to be extrapolated to future operating scenarios for a plant. At the other extreme, a highly structured model based on all of the theoretical relationships thought to exist in anaerobic systems could be compiled. However, such models typically contain many unobservable states and are difficult to calibrate owing to the large number of model parameters.

In this research, a lumped parameter model was formulated based on the four population conceptual model previously shown in Figure 2.1. Although several four population models have been published previously, little attention has been given to the practical difficulties in calibrating such models. During formulation of the model presented here, simplifications were made at several points in an effort to simplify calibration.

Andrews (1989) has outlined the following steps in a general approach to the development of models of wastewater treatment processes:

1) identify the significant reactions;

2) establish the stoichiometry;

3) determine the kinetics;

4) characterize the reactor;

5) apply material balances; and,

6) test the model.

These steps were used as an outline for this chapter.

5.1 SIGNIFICANT REACTIONS

Table 5.1 summarizes the overall stoichiometry for the energy-producing reactions for the anaerobic degradation of glucose as mediated by the micro-organisms present in the process. The degradation of carbohydrate substrates such as glucose was assumed to be mediated by a single generic group of bacteria referred to as the acid-formers. The stoichiometry for a glucose substrate is shown in section A of the table. Propionate, butyrate and acetate were assumed to be the only significant volatile acid products from the acid-forming stage. Propionate and butyrate were assumed to be degraded to acetate, carbon dioxide and hydrogen by separate groups of acetogenic bacteria, as shown in section B of the table. Section C of the table shows the stoichiometry for acetoclastic and hydrogenotrophic methanogenesis.

Table 5.2 summarizes the chemical equilibria considered important in the process. A number of reactions were neglected for the particular system studied. Sulphate reduction was not included, and sulphur compounds and ammonia were not considered in the acid-base system.

5.2 STOICHIOMETRY

As previously shown, the rate of substrate utilization for synthesis and energy, $-r_s$ (mg/L•d), can be expressed through the following equation:

Table 5.1: Stoichiometry for anaerobic degradation of glucose

A. Energy producing reactions of the acid-forming bacteria

$C_6H_{12}O_6$ (glucose) + $2H_2$ → $2CH_3CH_2COOH$ (propionic) + $2H_2O$

$C_6H_{12}O_6$ → $CH_3CH_2CH_2COOH$ (butyric) + $2CO_2$ + $2H_2$

$C_6H_{12}O_6$ + $2H_2O$ → $2CH_3COOH$ (acetic) + $2CO_2$ + $4H_2$

B. Energy producing reactions of the acetogenic bacteria

CH_3CH_2COOH + $2H_2O$ → CH_3COOH + CO_2 + $3H_2$

$CH_3CH_2CH_2COOH$ + $2H_2O$ → $2CH_3COOH$ + $2H_2$

C. Energy producing reactions of the methanogenic bacteria

CH_3COOH → CH_4 + CO_2

$4H_2$ + CO_2 → CH_4 + $2H_2O$

Table 5.2: Physical-chemical equilibria in the anaerobic process model

$$CO_2(g) \leftrightharpoons CO_2(aq)$$

$$CO_2(aq) + H_2O \leftrightharpoons H^+ + HCO_3^-$$

$$-r_S = \frac{\mu}{Y} X \qquad (2.9)$$

where, μ is the bacterial specific growth rate (d^{-1}), Y is the growth yield (mg biomass formed/mg substrate utilized), and X is the concentration of viable bacteria (mg/L).

If the concentrations of the substrate and metabolic products are written in consistent units such as chemical oxygen demand (COD), the rate of product formation, r_p (mg/L•d), is equal to the rate of substrate utilization less the uptake of substrate as a carbon source:

$$r_p = \frac{\mu}{Y} X - Y_c \mu X \\ = Y_p \mu X \tag{5.1}$$

where, Y_c is a synthesis yield coefficient (mg of substrate utilized as a carbon source per mg of biomass formed), and Y_p is a product yield coefficient (mg of product formed per mg of biomass formed). From equation (5.1), it can be seen that Y_p can be expressed as follows:

$$Y_p = (\frac{1}{Y} - Y_c) \tag{5.2}$$

In the present model, it was assumed that for low energy yielding reactions such as the acetogenic conversion of propionate and butyrate and acetic acid conversion to methane, Y_c would be much less than $1/Y$, therefore:

$$Y_p \approx \frac{1}{Y} \tag{5.3}$$

In the case of carbohydrate degradation, the experiments in this study showed that the growth of acid-forming bacteria could be significant, and equation (5.3) may not be a reasonable approximation. Therefore, a maximum acid-formation yield factor, η_{AF} was introduced, and the rate of uptake of a carbohydrate substrate, r_G, is expressed as follows:

$$-r_G = \frac{1}{\eta_{AF}} (\frac{\mu_{AF}}{Y_{AF}}) X_{AF} \tag{5.4}$$

where, μ_{AF}, Y_{AF}, and X_{AF} are respectively, the specific growth rate, the yield coefficient, and the concentration of the acid-forming bacteria.

The model formulated in this study is written in terms of the mass concentrations of the specific substrates and products. Therefore, a stoichiometric coefficient based on the reactions shown in Table 5.1 is included. For the acid-former reactions, regulation functions

were used to determine the relative proportions of the volatile acid products. The rate of product formation for the acid-forming bacteria is written as follows:

$$r_{j,AF} = \nu_{j,AF}\rho_{j,AF}\frac{\mu_{AF}}{Y_{AF}}X_{AF} \tag{5.5}$$

where, $r_{j,AF}$ is the rate of formation of product j from the acid-forming reactions; $\nu_{j,AF}$ is the stoichiometric coefficient for product j in the energy-producing reactions of the acid-formers; and, $\rho_{j,AF}$ is the regulation function for the production of product j by the acid-formers.

For other biochemical reactions represented, the rate of product formation, $r_{j,k}$ is written as follows:

$$r_{j,k} = \nu_{j,k}\left(\frac{\mu_k}{Y_k}\right)X_k \tag{5.6}$$

where, $\nu_{j,k}$ is the stoichiometric coefficient of product j in the energy yielding reactions of bacterial group k.

5.3 KINETICS

The reaction rates can be controlled by the kinetics of molecular diffusion into the biofilm or by the reaction rate kinetics within the biofilm. The relative significance of each mechanism was examined by calculating effectiveness factors for an appropriate range of operating parameters. Appropriate structures for the reaction rate kinetics were chosen based on the qualitative analysis of the experimental results summarized in Chapter 4.

5.3.1 Mass Transfer Kinetics

Table 5.3 summarizes the parameters used in the mass transfer calculations. Table 5.4 summarizes results from the calculation of the external mass transfer resistance effectiveness

factor, λ_e, for acetate, glucose, and hydrogen for the range of operating conditions specified. The effectiveness factors given in the Table 5.4 are the minimum values for the given ranges of parameters. For acetate and glucose there is no indication of significant external mass transfer resistance. For hydrogen, there is evidence of a slight external mass transfer resistance. This indicates that the rate of hydrogen utilization by the methanogens may be greater than the rate of hydrogen diffusion across the stagnant liquid layer surrounding the biofilm. It should be noted that all of the studies referenced by Pavlostathis and Giraldo-Gomez (1991) utilized an externally supplied hydrogen gas substrate when estimating the kinetic parameters. Mass transfer limitations in these experiments would result in apparently high K_S values. It can be shown that decreasing the K_S value results in a lower value of λ_e. The significance of external mass transfer on the kinetics of hydrogen utilization may therefore be higher than indicated in Table 5.4.

Calculated values of λ_i for the range of operating conditions and kinetic parameters given in Table 5.4 are shown in Table 5.5. The calculations show that mass transfer resistance within the biofilm can be considered negligible for acetate and glucose. A slight mass transfer resistance is evident for hydrogen.

The existence of mass transfer limitations on hydrogen utilization could result in hydrogen concentration gradients in both the biofilm and the stagnant liquid layer surrounding the biofilm. This could reduce the magnitude of a hydrogen response in both the gas and liquid phase of a reactor when hydrogen is both produced and consumed within the biofilm, as the hydrogen consumption rate may be higher than the rate of diffusion from the biofilm. When acid-forming bacteria were growing in the suspended phase of the reactor during the glucose experiment, external mass transfer resistances may have reduced the availability to the biofilm of hydrogen produced in acid-forming reactions, resulting in an increase in the magnitude of the response of the hydrogen concentration in the gas phase.

Table 5.3: Summary of parameters used in mass transfer calculations

Parameter	Value
Assumed porosity of settled bed; ε_s (1)	0.5
Porosity of fluidized bed; ε_f (2)	0.65
Media diameter; dp_{10} (cm)	120×10^{-4}
Assumed biofilm thickness; L_f (cm) (3)	50×10^{-4}
Calculated number of media particles; N (2)	1.8×10^{10}
Calculated total surface area of biofilm; a_s (cm^2) (2)	1.6×10^{7}
Calculated total volume of biofilm; V_f (m^3) (2)	0.03
Diffusivity of acetate in water; $D_{w,a}$ (cm^2/d)	1.37
Diffusivity of glucose in water; $D_{w,g}$ (cm^2/d)	0.69
Diffusivity of hydrogen in water; $D_{w,H2}$ (cm^2/d)	5.85
Dynamic viscosity of water at 35 °C; ν (cm^2/s)	0.724
Schmidt number for acetate; $Sc_{w,a} = \nu/D_{w,a}$	4.6×10^{4}
Schmidt number for glucose; $Sc_{w,g} = \nu/D_{w,g}$	9.1×10^{4}
Schmidt number for hydrogen; $Sc_{w,a} = \nu/D_{w,H2}$	1.1×10^{4}
Empty bed upflow velocity; u_o (cm/s)	0.33
Reynolds number; $Re = (dp_{10} + L_f)u_o/\nu$	7.75×10^{-3}

Notes:
(1) From Wang *et al.* (1986)
(2) Calculations summarized in Appendix B
(3) Conservative estimate based on a qualitative microscopic examination of a sample of the reactor medium

Table 5.4: Calculation of external effectiveness factors

Parameter	Substrate		
	Acetic acid	Glucose	Hydrogen
Substrate removal; $k_{max}X_fV_f$ (g COD/d)	7.0×10^2 (1)	7.5×10^2 (1)	60 to 3×10^3 (2)
Mass transfer coefficient; k_L (cm/d) (6)	4.2×10^2	2.6×10^2	1.1×10^3
Bulk phase substrate concentration; S (g COD/m^3)	10	10	10^{-9} (3)
Saturation constant; K_s (g COD/m^3)	10 to 10^4 (4)	20 to 2.0×10^4 (5)	0.016 to 0.6 (4)
Damkohler number; $D_a = k_{max} X_f V_f/(a_e k_L S)$	10^{-6}	10^{-6}	10^2 to 10^8
$K^* = K_s/S$	1.0 to 10^3	2.0 to 2.0×10^3	10^7 to 10^9
Minimum external effectiveness factor; λ_e (7)	1.0	1.0	0.95

Notes:
(1) Substrate removal calculated from present experiments
(2) k_{max} obtained from Pavlostathis and Giraldo-Gomez (1991); X_f assumed equal to 1000 g/m^3
(3) Assuming gas-liquid equilibrium is equivalent to a gas phase H_2 concentration of 100 ppm
(4) Pavlostathis and Giraldo-Gomez (1991)
(5) Henze and Harremoes (1983)
(6) From Equation (2.17)
(7) From Equation (2.18)

Table 5.5: Calculation of internal effectiveness factors

Parameter	Substrate		
	Acetic Acid	Glucose	Hydrogen
Specific substrate removal; $k_{max} X_f$ (g COD/m^3•d)	2.3×10^4	2.5×10^4	2.0×10^3 to 9.0×10^4
$L_f^* = L_f / (2K_s D_f / (k_{max} X_f)^{0.5}$ (1),(2)	10^{-4} to 10^{-3}	10^{-4} to 10^{-3}	10^{-3} to 10^{-2}
$S^* = S/K_s$ (1)	1.0 to 1.0×10^{-3}	0.5 to 5×10^{-4}	6×10^{-8} to 2×10^{-9}
Minimum internal effectiveness factor; λ_i (3)	1.0	1.0	0.99

Notes:
(1) Saturation constant and substrate concentration ranges as in Table 5.4
(2) Assumed $D_f = 0.8 * D_w$ (Williamson and McCarty, 1976)
(3) From Equation (2.21)

5.3.2 Reaction Rate Kinetics

The calculations summarized in the previous section show that diffusional limitations have a relatively unimportant effect on the reaction rates of glucose and volatile acids. Therefore, the substrate uptake kinetics of the acid-formers, acetogens and the acetoclastic methanogens were assumed to be reaction rate controlled. The experimental results also indicated that product inhibition of the acetogens and the acetoclastic methanogens was significant. Due to the low levels of gas phase hydrogen observed during the experiments, it was assumed that there were no significant reaction rate limitations for the consumption of hydrogen by methanogenic bacteria, and the regulation of bacterial reaction rates by the hydrogen concentration was assumed to be unimportant in this system.

The process rate equations used in this model are summarized in Table 5.6. The

Table 5.6: Anaerobic model process rate equations

$$\mu_{AF} = \mu_{max,AF} \frac{S_G}{K_{AF} + S_G} \tag{5.7}$$

$$\rho_{P,AF} = \frac{S_A}{K_{GP} + S_A} f_P \tag{5.8}$$

$$\rho_{A,AF} = \frac{1}{1 + \frac{S_A}{K_{I,GA}}} \tag{5.9}$$

$$\rho_{B,AF} = 1 - \rho_{A,AF} - \rho_{P,AF} \tag{5.10}$$

$$\mu_{PA} = \mu_{max,PA} \frac{S_P}{(K_{PA} + S_P)(1 + \frac{S_A}{K_{I,PA}})} \tag{5.11}$$

$$\mu_{BA} = \mu_{max,BA} \frac{S_B}{(K_{BA} + S_B)(1 + \frac{S_A}{K_{I,BA}})} \tag{5.12}$$

$$\mu_{AM} = \mu_{max,AM} \frac{S_A}{(K_{AM} + S_A)(1 + \frac{S_P}{K_{I,AM}})} \tag{5.13}$$

nomenclature for the model variables and the model parameters is shown in Tables 5.7 to 5.9. The rate equations are based on conventional Monod kinetics. In this model, the distribution of products at the acid-forming stage is regulated by the acetic acid concentration. Although other researchers (Mosey, 1983; Rozzi *et al.*, 1985b; Ide, 1988; Costello *et al.*, 1991a) have written the kinetic equations for acid production rates based on the hydrogen partial pressure, in this study there was no evidence that hydrogen regulation functions based on gas phase hydrogen partial pressure would be appropriate. Product inhibition of the growth rates of propionate- degrading acetogens and butyrate-degrading acetogens is modelled by non-competitive inhibition functions. Inhibition of the growth rate of acetoclastic methanogens by propionate is also modelled through a non-competitive inhibition function.

5.4 REACTOR HYDRAULIC CHARACTERISTICS

The reactor tracer test conducted on the fluidized bed reactor indicated that the reactor hydraulics could be represented as an ideal CSTR. The effluent substrate concentrations are therefore used in the kinetic equations of the model. For modelling purposes, it was assumed that there was no biological activity in the suspended phase of the reactor. The biomass concentrations represented in the process kinetics are therefore the retained fixed film biomass concentrations.

5.5 MATERIAL BALANCES

The basic equation for each material balance across a defined system boundary is

$$Accumulation = Input - Output + Reaction \tag{5.14}$$

For liquid phase and biomass phase components, the system boundary is the reactor liquid volume. Input terms for each balance consist of the mass flow rate of the component of interest in the reactor influent. Output terms consist of the mass flow rate in the liquid

Table 5.7: Anaerobic dynamic model variables

Variable	Description
S_G	Biodegradable (non-volatile acid) soluble organics concentration(mg/L)
S_P	Propionic acid concentration (mg/L)
S_B	Butyric acid concentration (mg/L)
S_A	Acetic acid concentration (mg/L)
S_Z	Net cation concentration (mmole/L)
S_{IC}	Total inorganic carbon concentration (mmole/L)
S_{HCO3}	Bicarbonate concentration (mmole/L)
P_{gCO2}	Partial pressure of carbon dioxide in the gas phase (atm)
S_I	Concentration of non-biodegradable components (mg/L)
X_{AF}	Acid-former concentration(mg/L)
X_{PA}	Propionic acid utilizing acetogen concentration (mg/L)
X_{BA}	Butyric acid utilizing acetogen concentration (mg/L)
X_{AM}	Acetoclastic methanogen concentration (mg/L)
μ_{AF}	Acid-former specific growth rate (d^{-1})
$\rho_{P,AF}$	Regulation function for the production of propionic acid by acid-formers
$\rho_{A,AF}$	Regulation function for the production of acetic acid by acid-formers
$\rho_{B,AF}$	Regulation function for the production of butyric acid by acid formers
μ_{PA}	Propionic acid utilizing acetogen specific growth rate(d^{-1})
μ_{BA}	Butyric acid utilizing acetogen specific growth rate (d^{-1})
μ_{AM}	Acetoclastic methanogen specific growth rate (d^{-1})
t_G	Carbon dioxide gas transfer rate (mmole/L•d)
Z_B	Concentration of caustic for pH control (mmole/L)
Q	Total feed flow rate (L/d)
Q_C	Caustic addition rate for pH control (L/d)
$Q_{G,CH4}$	Methane flow rate (L/d)
$Q_{G,CO2}$	Carbon dioxide flow rate (L/d)
$Q_{G,T}$	Total gas flow rate (L/d)
t	Time (d)

Table 5.8: Anaerobic dynamic model constants (kinetics and stoichiometry)

Constant	Description	Value
Y_{AF}	Acid-former yield coefficient (mg/mg)	0.15
Y_{PA}	Propionic acid acetogens yield coefficient (mg/mg)	0.04
Y_{BA}	Butyric acid acetogens yield coefficient (mg/mg)	0.04
Y_{AM}	Acetoclastic methanogens yield coefficient (mg/mg)	0.055
MW_G	Molecular weight of glucose (mg/mmole)	180
MW_P	Molecular weight of propionic acid (mg/mmole)	74
MW_B	Molecular weight of butyric acid (mg/mmole)	88
MW_A	Molecular weight of acetic acid (mg/mmole)	60
$\nu_{P,AF}$	Stoichiometric coefficient for propionate production (mg/mg)	$2(MW_P)/(MW_G)$
$\nu_{B,AF}$	Stoichiometric coefficient for butyrate production (mg/mg)	$1(MW_B)/(MW_G)$
$\nu_{A,AF}$	Stoichiometric coefficient for acid-former acetate production (mg/mg)	$2(MW_A)/(MW_G)$
$\nu_{A,PA}$	Stoichiometric coefficient for acetogenic acetate production from propionate (mg/mg)	$MW_A/(MW_P)$
$\nu_{A,BA}$	Stoichiometric coefficient for acetogenic acetate production from butyrate (mg/mg)	$2(MW_A)/(MW_B)$
$\nu_{CH4,AM}$	Stoichiometric coefficient for acetoclastic methanogenesis (mmole/mg)	$1/(MW_A)$
$\nu_{CH4,HM}$	Stoichiometric coefficient for methane from hydrogen (mmole/mmole)	1/4
$\nu_{H,P,AF}$	Stoichiometric coefficient for hydrogen in propionate production reaction (mmole/mg)	$-2/MW_G$
$\nu_{H,B,AF}$	Stoichiometric coefficient for hydrogen in butyrate production reaction (mmole/mg)	$2/MW_G$
$\nu_{H,A,AF}$	Stoichiometric coefficient for hydrogen in acid-former acetate production reaction (mmole/mg)	$4/MW_G$
$\nu_{H,PA}$	Stoichiometric coefficient for hydrogen in acetogenic consumption of propionate (mmole/mg)	$3/(MW_P)$
$\nu_{H,BA}$	Stoichiometric coefficient for hydrogen in acetogenic consumption of butyrate (mmole/mg)	$2/(MW_B)$
$\mu_{max,AF}$	Maximum specific growth rate - acid-formers (d^{-1})	13.0
$\mu_{max,PA}$	Maximum specific growth rate - propionic acetogens (d^{-1})	0.4
$\mu_{max,BA}$	Maximum specific growth rate - butyric acetogens (d^{-1})	0.4
$\mu_{max,AM}$	Maximum specific growth rate - acetoclastic methanogens (d^{-1})	0.3

Table 5.9: Anaerobic dynamic model constants (physical-chemical)		
Constant	Description	Value
V	Reactor liquid volume (L)	73
V_G	Reactor gas phase volume (L)	30
K_La	Carbon dioxide mass transfer coefficient (d^{-1})	100
KH_{CO2}	Henry's law coefficient for carbon dioxide at 38 °C (mmole/L•atm)	26.6
P_T	Total pressure (atm)	1
K_{H2CO3}	Bicarbonate equilibrium constant at 38 °C	4.73×10^{-7}
V_S	Volume of 1 mmole of ideal gas at 1 atm and 38 °C (L/mmole)	0.0255

Table 5.10: Anaerobic dynamic model parameters	
Parameter	Description
η_{AF}	Maximum acid formation yield factor
$K_{I,AM}$	Inhibition coefficient - acetoclastic methanogens
K_{AF}	Saturation coefficient - acid-formers
K_{PA}	Saturation coefficient - propionic acetogens
K_{BA}	Saturation coefficient - butyric acetogens
K_{AM}	Saturation coefficient - acetoclastic methanogens
$K_{I,PA}$	Inhibition coefficient - propionic acetogens
$K_{I,BA}$	Inhibition coefficient - butyric acetogens
$K_{I,GA}$	Inhibition coefficient - acid-former acetate production
f_P	Maximum fraction of propionic acid from acid-formers
K_{GP}	Saturation coefficient - acid-former propionate production

effluent, and transfer to the reactor gas phase. For gas phase components, the system boundary is the reactor gas phase volume. Input terms consist of the transfer of gas phase components from the liquid phase to the gas phase. Output terms consist of the flow of the gas phase components in the biogas leaving the system.

Material balances for soluble liquid phase components and gas phase components are shown in Table 5.11. In these balances, the subscript "0" refers to influent concentrations, and the subscript "1" refers to effluent concentrations. Substrates for which material balances are included are biodegradable (non-volatile acid) soluble organics (such as glucose), propionic acid, butyric acid and acetic acid. A balance for soluble non-biodegradable components is also included.

Table 5.11: Dynamic model material balances for liquid and gas phase components

$$\frac{dS_{G,1}}{dt} = \frac{Q}{V}(S_{G,0}-S_{G,1}) - \frac{1}{\eta_{AF}}\frac{1}{Y_{AF}}\mu_{AF}X_{AF} \tag{5.15}$$

$$\frac{dS_{P,1}}{dt} = \frac{Q}{V}(S_{P,0}-S_{P,1}) + \frac{\nu_{P,AF}}{Y_{AF}}\rho_{P,AF}\mu_{AF}X_{AF} - \frac{1}{Y_{PA}}\mu_{PA}X_{PA} \tag{5.16}$$

$$\frac{dS_{B,1}}{dt} = \frac{Q}{V}(S_{B,0}-S_{B,1}) + \frac{\nu_{B,AF}}{Y_{AF}}\rho_{B,AF}\mu_{AF}X_{AF} - \frac{1}{Y_{BA}}\mu_{BA}X_{BA} \tag{5.17}$$

$$\frac{dS_{A,1}}{dt} = \frac{Q}{V}(S_{A,0}-S_{A,1}) + \frac{\nu_{A,AF}}{Y_{AF}}\rho_{A,AF}\mu_{AF} + \frac{\nu_{A,PA}}{Y_{PA}}\mu_{PA}X_{PA} + \frac{\nu_{A,BA}}{Y_{BA}}\mu_{BA}X_{BA} - \frac{1}{Y_{AM}}\mu_{AM}X_{AM} \tag{5.18}$$

$$\frac{dS_{Z,1}}{dt} = \frac{Q}{V}(S_{Z,0}-S_{Z,1}) + \frac{Z_B}{V}Q_C \tag{5.19}$$

Table 5.11 continued on next page ...

Table 5.11: Dynamic model material balances for liquid and gas phase components

$$\frac{dS_{IC,1}}{dt} = \frac{Q}{V}(S_{IC,0}-S_{IC,1}) + \frac{\nu_{CO2,A,AF}}{Y_{AF}}\rho_{A,AF}\mu_{AF}X_{AF} + \frac{\nu_{CO2,B,AF}}{Y_{AF}}\rho_{B,AF}\mu_{AF}X_{AF} + \frac{\nu_{CO2,PA}}{Y_{PA}}\mu_{PA}X_{PA} + \frac{\nu_{CO2,AM}}{Y_{AM}}\mu_{AM}X_{AM} - \nu_{CO2,HM}\left(\left(\nu_{H,P,AF}\rho_{P,AF} + \nu_{H,A,AF}\rho_{A,AF} + \nu_{H,B,AF}\rho_{B,AF}\right)\frac{\mu_{AF}}{Y_{AF}}X_{AF} + \frac{\nu_{H,PA}}{Y_{PA}}\nu_{PA}X_{PA} + \frac{\nu_{H,BA}}{Y_{BA}}\nu_{BA}X_{BA}\right)\nu_{CO2,HM} + t_G \quad (5.20)$$

$$\frac{dS_{I,1}}{dt} = \frac{Q}{V}(S_{I,0}-S_{I,1}) \quad (5.21)$$

$$\frac{dP_{pCO2}}{dt} = -P_T V_S t_G \frac{V}{V_G} - \frac{Q_{G,T}P_{pCO2}}{V_G} \quad (5.22)$$

Inclusion of a material balance for liquid phase inorganic carbon and gas phase carbon dioxide allows for the calculation of reactor pH. To complete the inorganic carbon balance, relationships describing the interaction between the gas and liquid phase carbon dioxide concentrations and the bicarbonate-carbonic acid equilibrium are required. Andrews and Graef (1971) were the first researchers to include this system in a dynamic model, and the same approach was used here. For the transfer of carbon dioxide between the gas phase and the liquid phase, the following mass transfer expression is included in the model:

$$t_G = K_L a\,(KH_{CO2}P_{pCO2} - (CO_2)_{D,1}) \quad (5.23)$$

where, t_G is the carbon dioxide gas transfer rate (mmole/L•d), $K_L a$ is the carbon dioxide liquid-

gas mass transfer coefficient (d^{-1}), KH_{CO2} is Henry's law coefficient for carbon dioxide (mmole/L•atm), P_{pCO2} is the partial pressure of carbon dioxide in the gas phase (atm), and $(CO_2)_{D,1}$ is the concentration of carbon dioxide dissolved in the liquid phase (mmole/L). $(CO_2)_{D,1}$ can be expressed in terms of the model variables as follows:

$$(CO_2)_{D,1} = S_{IC,1} - S_{HCO3,1} \tag{5.24}$$

where, $S_{IC,1}$ is the total inorganic carbon concentration (mmole/L), and $S_{HCO3,1}$ is the bicarbonate concentration (mmole/L).

The gas phase carbon dioxide balance requires the calculation of the total biogas flowrate. The total methane flowrate is comprised of acetoclastic methane production and hydrogenotrophic methane production. Because it was assumed that no rate limitations exist for the utilization of hydrogen by the methanogenic bacteria, the hydrogenotrophic methane production was assumed to occur in constant stoichiometric proportion to the net hydrogen production from the acid-formers and acetogens. The total volumetric methane production rate, $Q_{G,CH4}$ (L/d), is therefore expressed as follows:

$$\begin{aligned} Q_{G,CH4} = V_S V \Big(& \Big(\nu_{CH4,AM} \frac{\mu_{AM}}{Y_{AM}} X_{AF} + \nu_{CH4,HM} \Big(\big(\nu_{H,PAF} \rho_{P,AF} \\ & + \nu_{H,BAF} \rho_{B,AF} + \nu_{H,AAF} \rho_{A,AF} \big) \frac{\mu_{AF}}{Y_{AF}} X_{AF} \\ & + \nu_{H,PA} \frac{\mu_{PA}}{Y_{PA}} X_{PA} + \nu_{H,BA} \frac{\mu_{BA}}{Y_{BA}} X_{BA} \Big) \Big) \end{aligned} \tag{5.25}$$

where, V is the reactor liquid volume (L), V_S is the volume of 1 mmole of ideal gas at the reactor temperature and pressure (L/mmole), $\nu_{i,j,k}$ are stoichiometric coefficients as defined in Table 5.8, $\rho_{j,AF}$ are the regulation functions defined in Tables 5.6 and 5.7 for the production of product j by the acid-formers, μ_k is the specific growth rate of bacterial group k as defined in Tables 5.6 and 5.7, Y_k is the biomass yield coefficient for bacterial group k as defined in Table 5.8, and X_k is the concentration of bacterial group k as defined in Table 5.7.

The volumetric carbon dioxide flow rate, $Q_{G,CO2}$ (L/d), is expressed as follows:

$$Q_{G,CO2} = -VV_S t_G \tag{5.26}$$

The total biogas flowrate, $Q_{G,T}$ (L/d), is comprised of the methane and carbon dioxide flowrates:

$$Q_{G,T} = Q_{G,CH4} + Q_{G,CO2} \tag{5.27}$$

The reactor bicarbonate concentration, $S_{HCO3,1}$, is calculated through an electroneutrality balance. The expression formulated by Andrews and Graef (1971) for the pH range between 6 and 8 was modified for the three individual volatile acid concentrations considered in this model as follows:

$$S_{HCO3,1} = S_{Z,1} - \frac{S_{A,1}}{MW_A} - \frac{S_{P,1}}{MW_P} - \frac{S_{B,1}}{MW_B} \tag{5.28}$$

where, $S_{Z,1}$ is the net cation concentration (mmole/L), $S_{A,1}$, $S_{P,1}$, and $S_{B,1}$ are the respective concentrations of acetic acid, propionic acid and butyric acid (mg/L), and MW_A, MW_P, and MW_B are the respective molecular weights of acetic acid, propionic acid, and butyric acid (mg/mmole). The material balance for S_Z used by Andrews and Graef (1971) was modified by including an input term for the addition of a strong base for pH control (Table 5.11). Finally, the pH is calculated from the bicarbonate equilibrium relationship:

$$10^{-pH} = \frac{K_{H2CO3}(S_{IC,1} - S_{HCO3,1})}{S_{HCO3,1}} \tag{5.29}$$

where K_{H2CO3} is the bicarbonate equilibrium constant.

A general material balance for bacterial group k (X_k) in the reactor can be written as follows:

$$\frac{dX_k}{dt} = \mu_k X_k - B_{V,k} \tag{5.30}$$

To complete this material balance, an expression for the bacterial loss rate, $B_{V,k}$ is required. In a high rate anaerobic reactor, this term depends on complex mechanisms such as biofilm sloughing and solid-gas-liquid separation. Due to the operation of the fluidized bed reactor with a constant expanded bed height, it was assumed that the bacterial loss rates, $B_{V,k}$, were equal to the respective growth rates, $\mu_k X_k$, in each balance. Therefore, the bacterial mass balances for the fluidized bed are written as follows:

$$\frac{dX_k}{dt} = 0 \tag{5.31}$$

5.6 MODEL SOLUTION

The model was programmed in FORTRAN-77 on an HP-1000 minicomputer using the RTE-A operating system. Differential equations were solved using Gear's method for stiff sets of equations (Gear, 1971). The model was later programmed using the Advanced Continuous Simulation Language (ACSL), a continuous simulation language developed by Mitchell and Gauthier Associates (1987). This allowed parameter estimation on a SUN-3 UNIX workstation, using the SIMUSOLV computer program (Steiner *et al.*, 1986).

5.7 INITIAL MODEL TESTING

For initial model testing, saturation coefficients listed in Table 5.10 were set to the average of the values from the experimental studies summarized in Pavlostathis and Giraldo-Gomez (1991). The values of the additional parameters listed in Table 5.10 were adjusted to give the best visual fit to experimental results. The resulting parameter values are shown in Table 5.12. Influent concentrations, initial conditions, and feedrates required for the mass

Table 5.12: Anaerobic dynamic model parameter values for initial testing

Parameter	Value
η_{AF}	0.80
$K_{I,AM}$	1000 mg/L
K_{AF}	300 mg/L
K_{PA}	130 mg/L
K_{BA}	10 mg/L
K_{AM}	75 mg/L
$K_{I,PA}$	500 mg/L
$K_{I,BA}$	1000 mg/L
$K_{I,GA}$	250 mg/L
f_P	0.80
K_{GP}	1000 mg/L production

balances in Table 5.11 were set to the actual conditions in glucose run #2 (Appendix C). The concentrations of acid-formers (X_{AF}), propionic acid utilizing acetogens (X_{PA}), and the acetoclastic methanogens (X_{AM}) were obtained through the method of maximum likelihood using the SIMUSOLV computer program to provide the best fit of the model estimates to the measured values of $S_{COD,I}$, $S_{P,I}$, $S_{A,I}$, and $Q_{G,CH4}$ during glucose run #2. Two test cases were considered for fitting the model. In "Test Case 1", the data from day 14 to day 21 were used for model fitting. "Test Case 2" utilized data from day 28 to day 35. The resulting bacterial concentration estimates are shown in Table 5.13.

As discussed in Chapter 4, examination of the experimental results indicated that some acetic acid may volatilize from COD samples before analysis, thereby causing a bias in the measured effluent COD at high effluent acetic acid concentrations. When the non-volatile acid portion of the soluble effluent COD ($S_{COD,I}$) is calculated, there would appear to be a reduction in the value of this variable during periods of high acetic acid concentrations as observed

Table 5.13: Fitted bacterial concentrations in initial model testing		
Variable	Test Case 1	Test Case 2
X_{AF}	185 mg/L	160 mg/L
X_{PA}	2800 mg/L	2400 mg/L
X_{BA}	750 mg/L	750 mg/L
X_{AM}	2100 mg/L	1200 mg/L

during the acetic acid experiment. The correction required on measurements of $S_{COD,1}$ to account for the loss in COD from the sample due to acetic acid volatilization should therefore be proportional to the concentration of acetic acid ($S_{A,1}$):

$$Corrected S_{COD,1} = Correction factor * S_{A,1} + S_{COD,1} \quad (5.32)$$

A correction factor was derived from the acetic acid run by rearranging Equation (5.32) and solving for the correction factor. The average value of $S_{COD,1}$ measured during the baseline loading periods in the acetic acid run was assumed to be representative of the actual or corrected value. The correction factor was calculated from the difference between the mean $S_{COD,1}$ measured during baseline loading periods in the acetic acid run, and the mean $S_{COD,1}$ measured during the acetic acid pulses as follows:

$$Correction factor = \frac{Mean measured S_{COD,1}(baseline) - Mean measured S_{COD,1}(during pulse)}{Mean measured S_{A,1}(during pulse)} \quad (5.33)$$

Note that, in terms of the model variables,

$$S_{COD,1} = S_{G,1} + S_{I,1} \quad (5.34)$$

where, $S_{G,1}$ is the effluent biodegradable (non-volatile acid) soluble organics concentration, and $S_{I,1}$ is the effluent concentration of non-biodegradable COD. For the purposes of parameter estimation, $S_{COD,1}$ values were corrected according to equations 5.32 and 5.33.

Simulation results are compared to process measurements in Figures 5.1 and 5.2. The adequacy of pH and gas phase composition predictions were not assessed during initial model testing due to their dependence on accurate predictions of the substrate states and due to the difficulty in obtaining an accurate value for the caustic addition rate, Q_C, during the dynamic experiments. The results show that the given parameter set and bacterial concentrations provide a reasonable estimate of the process response to the first glucose spike. After day 19, the model predictions deviate significantly from the actual process response. "Test Case 2" shows that appropriate adjustments in the model bacterial concentrations (Table 5.13) will allow the model to fit later portions of the run (Figures 5.3 and 5.4).

These results indicate that states or parameters assumed to be time-invariant may in fact change significantly over time. The mechanistic dynamic model could be enhanced by attempting to develop equations which describe the time-variable behaviour of these states. However, in this case, there is insufficient knowledge of the true mechanisms affecting these states. An alternative approach is to use empirical stochastic models of the states for which there is insufficient information to formulate mechanistic models. An extended Kalman filter allows a multivariable process model to combine both mechanistic and stochastic models for the process states. The states which are described entirely by a stochastic model are recursively estimated based on the measured input-output behaviour of the process. The time-variable estimates of the stochastic states could provide information on significant disturbances affecting process behaviour which could lead to improved operation and control, or could lead to improvements in the mechanistic portion of the model. Non-recursive parameter estimation methods such as used by SIMUSOLV provide no information on the time-variable behaviour of these states and thus provide little of this additional information.

It was therefore concluded that the use of an extended Kalman filter to simultaneously estimate states in the fluidized bed process described by mechanistic and stochastic models would provide valuable insights into the dynamic behaviour of the process. The next chapter describes the formulation of the algorithm for the anaerobic fluidized bed process.

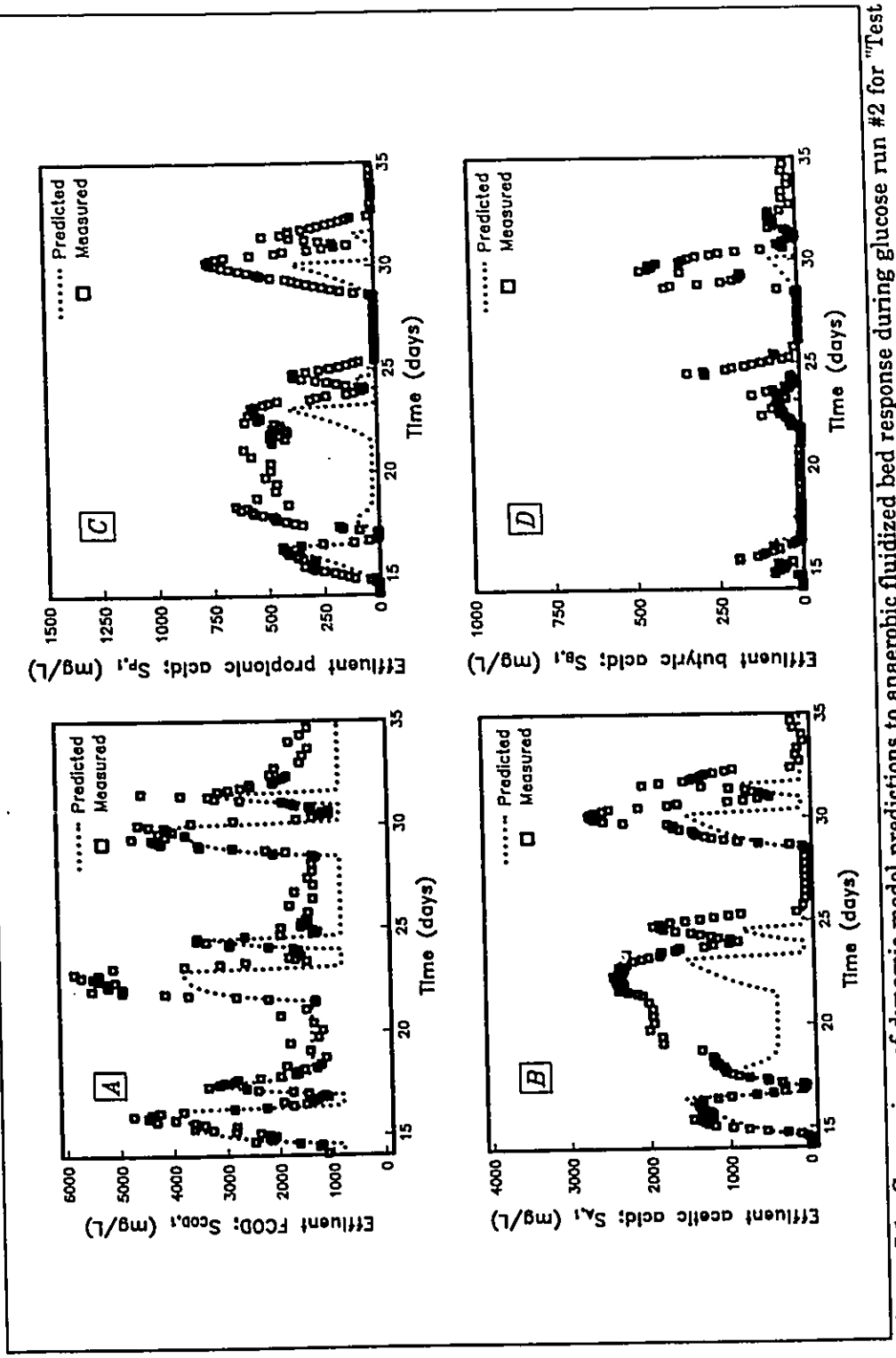

Figure 5.1: Comparison of dynamic model predictions to anaerobic fluidized bed response during glucose run #2 for "Test Case 1" - (A) FCOD; (B) acetic acid; (C) propionic acid; (D) butyric acid.

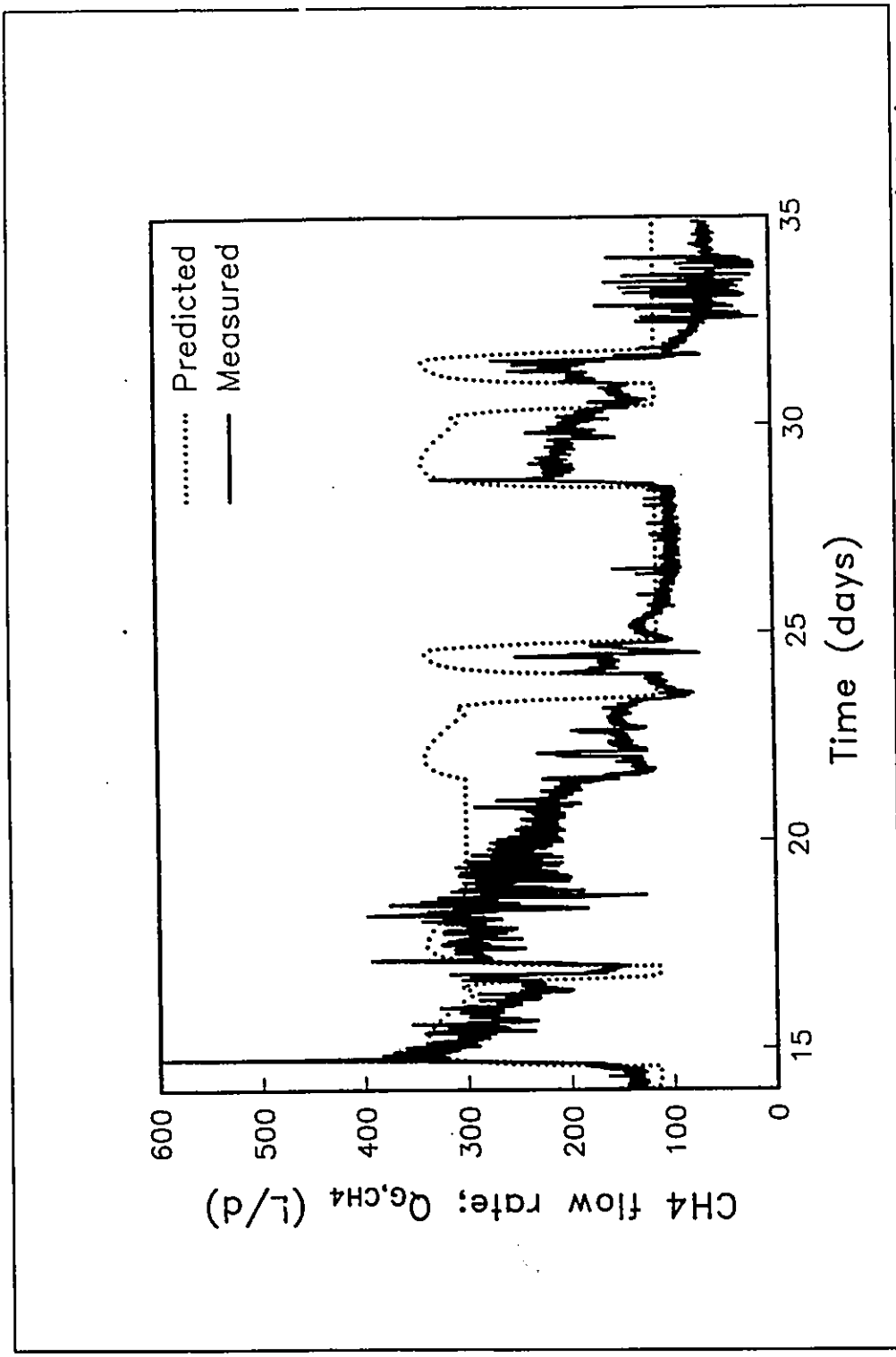

Figure 5.2: Comparison of dynamic model predictions to anaerobic fluidized bed methane production rate during glucose run #2 for "Test Case 1".

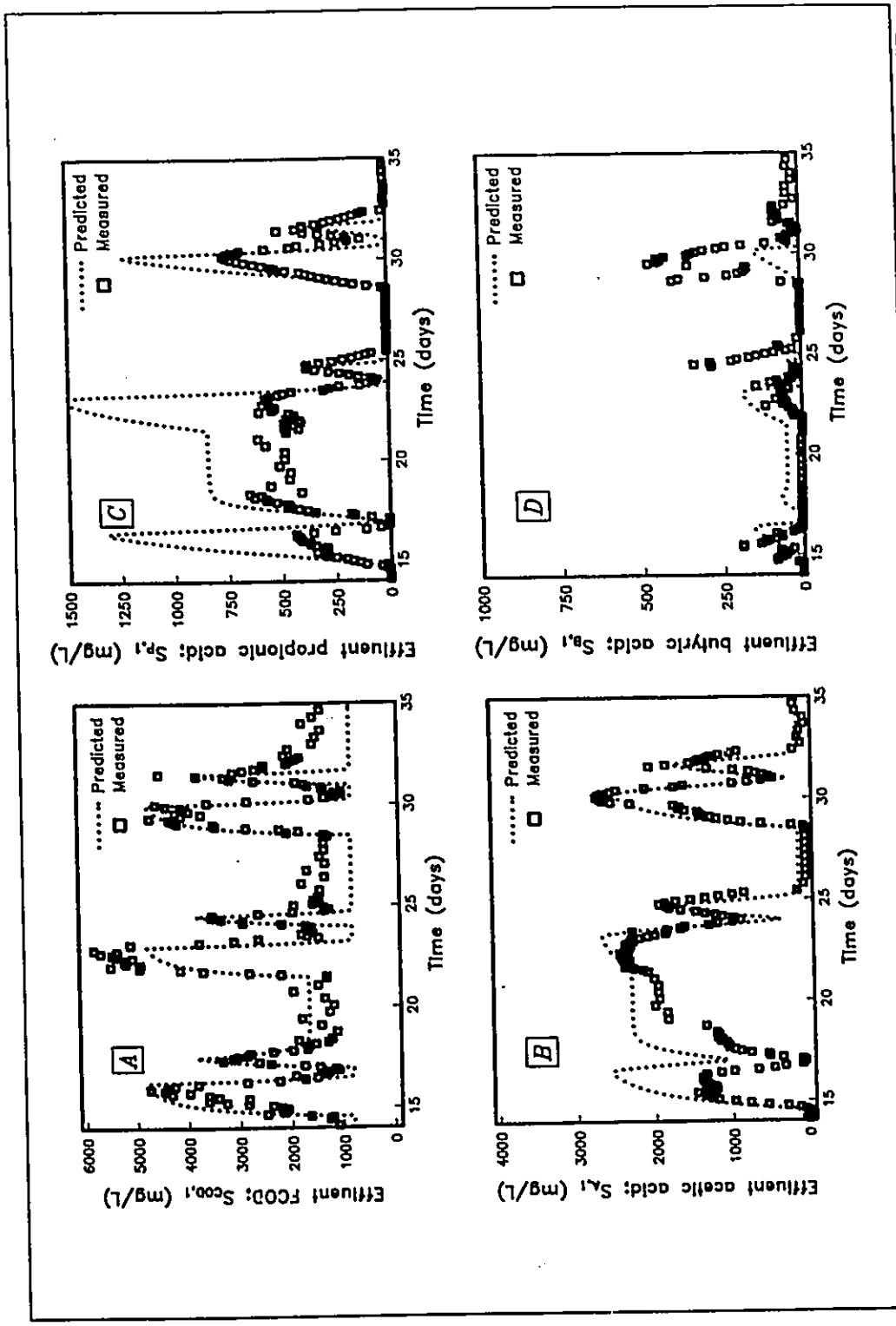

Figure 5.3: Comparison of dynamic model predictions to anaerobic fluidized bed response during glucose run #2 for "Test Case 2" - (A) FCOD; (B) acetic acid; (C) propionic acid; (D) butyric acid.

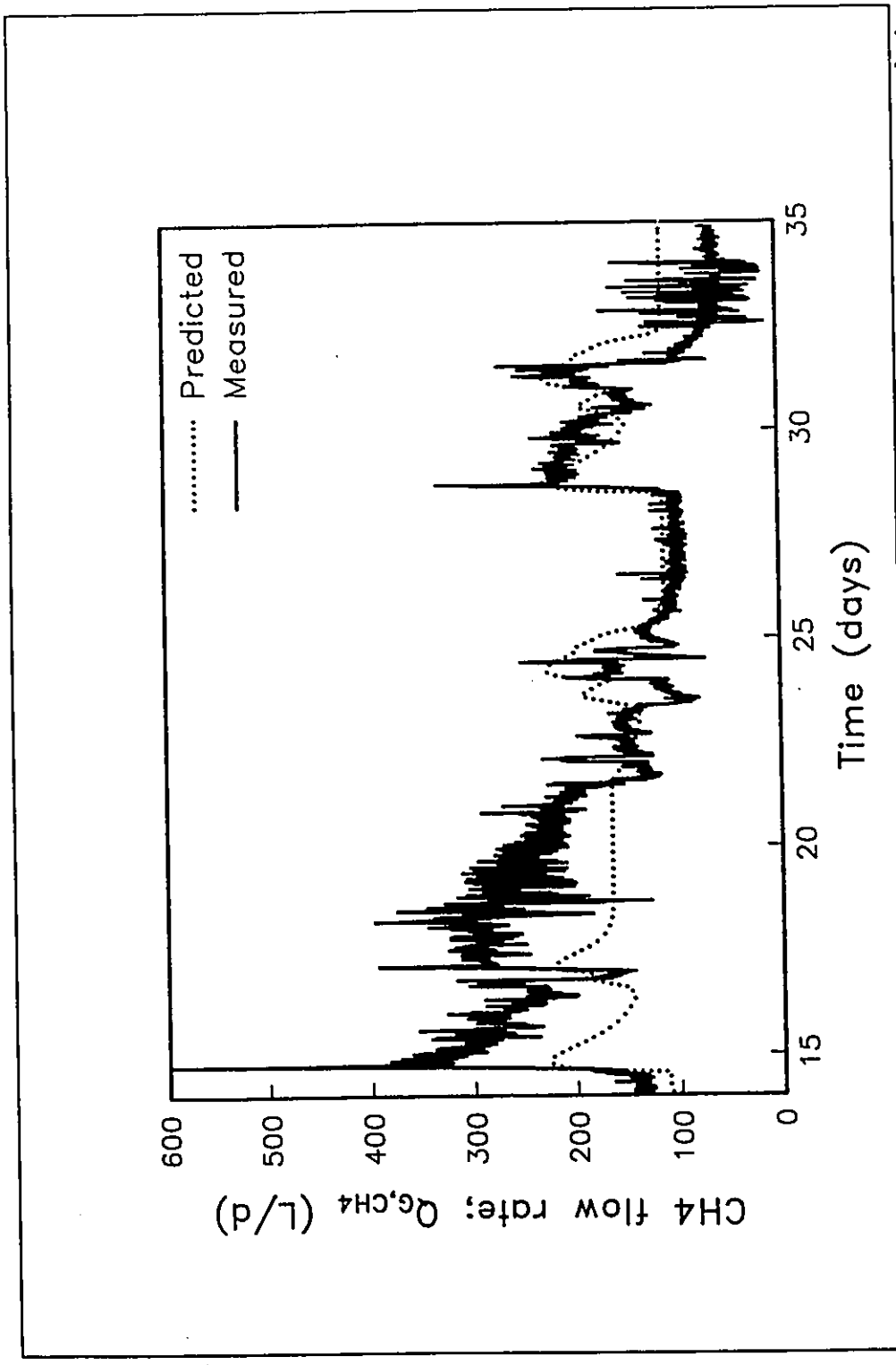

Figure 5.4: Comparison of dynamic model predictions of anaerobic fluidized bed methane production rate response during glucose run #2 for "Test Case 2".

CHAPTER 6

DYNAMIC MODEL CALIBRATION METHODOLOGY

6.1 EXTENDED KALMAN FILTER

In the context of dynamic modelling, the state of a process is defined as the set of dependent variables which describe the operation of the process at any point in time. The portion of a dynamic model derived from unsteady-state material and energy balances and expressed in the form of a set of continuous, first-order, non-linear differential equations is known as the mechanistic or deterministic portion of the model. In general,

$$\frac{d\underline{x}^d}{dt} = f^d(\underline{x}, \underline{u}, t) \tag{6.1}$$

where $\underline{x}$ is the n-dimensional vector of process states, $\underline{x}^d$ is the subset of $\underline{x}$ containing the n^d deterministic states and $\underline{u}$ is the r-dimensional vector of known inputs. The state vector also includes an n^s-dimensional vector of stochastic states, $\underline{x}^s$, which is comprised of model parameters and disturbance states. The incorporation of stochastic disturbance states in the model accounts for unmeasured factors that can cause a shift in process behaviour and cause the actual process behaviour to drift away from the deterministic model predictions. The choice of meaningful stochastic states is especially important in complex systems such as biological wastewater treatment processes where there is a limited knowledge of the true mechanisms affecting the dynamic behaviour of the process. For state estimation purposes, the dynamics of the stochastic states are represented as follows:

$$\frac{d\underline{x}^s}{dt} = 0 \tag{6.2}$$

Denoting the current state estimate at time t_k given input and process measurements up to time t_k as $\hat{\underline{x}}(t_k \mid t_k)$, the prediction of the state vector over the time interval t_k to t_{k+1} is obtained by integrating the Equation (6.1) and Equation (6.2) to give,

$$\hat{\underline{x}}^d(t_{k+1} \mid t_k) = \hat{\underline{x}}^d(t_k \mid t_k) + \int_{t_k}^{t_{k+1}} f^d(\underline{x}, \underline{u}, t)\, dt \tag{6.3}$$

$$\hat{\underline{x}}^s(t_{k+1} \mid t_k) = \hat{\underline{x}}^s(t_k \mid t_k) \tag{6.4}$$

Performing a local linearization and discretization of the state model given by equations (6.1) and (6.2) given a constant vector of known inputs ($\underline{u}(t_k) = 0$) and about the predicted conditions $\hat{\underline{x}}(t_{k+1} \mid t_k) = \hat{\underline{x}}_{k+1\mid k}$ (where the discrete sampling instants are designated as $k,k+1,\ldots$) gives,

$$\underline{x}_{k+1} = \underline{A}_k \underline{x}_k + \underline{w}_k \tag{6.5}$$

with

$$\underline{x}^d_{k+1} = \underline{A}^d_k \underline{x}^d_k + \underline{A}^s_k \underline{x}^s_k + \underline{w}^d_k \tag{6.6}$$

$$\underline{x}^s_{k+1} = \underline{x}^s_k + \underline{w}^s_k \tag{6.7}$$

$$\underline{x}_k = \begin{bmatrix} \underline{x}^d_k \\ \underline{x}^s_k \end{bmatrix} \tag{6.8}$$

$$\underline{A}_k = \begin{bmatrix} \underline{A}^d_k & \underline{A}^s_k \\ \underline{0} & \underline{I} \end{bmatrix} \tag{6.9}$$

In the above equations, $\underline{A}_k$ is the Jacobian matrix of $f(\underline{x}, \underline{u}, t)$ with respect to $\hat{\underline{x}}_{k+1|k}$. The ij^{th} elements of the submatrices $\underline{A}_k^d$ and $\underline{A}_k^s$ are given by,

$$A_{ij}^d\Big|_k = \left.\frac{\partial f_i^d}{\partial x_j^d}\right|_{k+1|k} \tag{6.10}$$

$$A_{ij}^s\Big|_k = \left.\frac{\partial f_i^d}{\partial x_j^s}\right|_{k+1|k} \tag{6.11}$$

The variable $\underline{w}_k$ is a vector of normally distributed random errors known as white noise. The white noise has zero mean and a covariance matrix $\underline{R}_w$. For the deterministic states, $\underline{w}_k^d$ accounts for errors in (6.6) arising from modelling errors, errors due to linearization, and errors in the model settings of $\underline{u}_k$. The disturbance and parameter states are shown by (6.7) to be represented by a nonstationary random walk model. The behaviour of states described by such a model is characterized by random fluctuations about a changing mean level. The white noise vector $\underline{w}_k^s$ represents the amount of change occurring over the sampling period t_k to t_{k+1}. For convenience and lack of information regarding individual covariances, $\underline{R}_w$ is usually taken to be diagonal with the diagonal elements (variances) corresponding to $\underline{w}_k^d$, chosen to reflect the magnitude of the error expected in the deterministic model over the integration interval. The diagonal elements in $\underline{R}_w$ corresponding to the variance of $\underline{w}_k^s$ are chosen to reflect disturbance magnitude or the change in parameter value expected over the sampling interval. The choice of variances of $\underline{w}_k^s$ is used to tune the Kalman filter to give good tracking behaviour.

The m-dimensional vector of process measurements is generally a non-linear function of the states and inputs, such as

$$\underline{y}_k = h(\underline{x}_k, \underline{u}_k, t_k) + \underline{v}_k \tag{6.12}$$

where, $\underline{v}_k$ is a zero mean white noise vector of measurement errors with covariance matrix $\underline{R}_v$. The diagonal (variance) elements of this matrix can be obtained from a knowledge of the precision of the measurement sensor or from replicated measurement data.

When a new set of observations, $\underline{y}_{k+1}$ becomes available at time, t_{k+1}, the state estimates obtained through equations (6.3) and (6.4) are updated using the linear Kalman filter equations with the locally linearized model. This updated estimate is given by

$$\hat{\underline{x}}_{k+1|k+1} = \hat{\underline{x}}_{k+1|k} + \underline{K}_k\{\underline{y}_{k+1} - h(\hat{\underline{x}}_{k+1|k}, \underline{u}_k, t_k)\} \tag{6.13}$$

where, $\underline{K}_k$ is the linear Kalman gain at t_k. For a linear system, Kalman (1960) derived the equations for $\underline{K}_k$ which would minimize the variance of the estimation error ($\underline{x}_k - \hat{\underline{x}}_{k|k}$). A linear approximation of the optimal solution can be obtained for non-linear systems from the following equations (Jazwinski, 1970):

$$\underline{P}_{k+1|k} = \underline{A}_k \underline{P}_{k|k} \underline{A}_K^T + \underline{R}_w \tag{6.14}$$

$$\underline{K}_k = \underline{P}_{k+1|k} \underline{H}_k^T (\underline{H}_k \underline{P}_{k+1|k} \underline{H}_k^T + \underline{R}_v)^{-1} \tag{6.15}$$

$$\underline{P}_{k+1|k+1} = \underline{P}_{k+1|k} - \underline{K}_k \underline{H}_{k+1} \underline{P}_{k+1|k} \tag{6.16}$$

where $\underline{P}_{k|k}$ is the covariance matrix of the state estimation error, and $\underline{H}_k$ is the Jacobian matrix of $h(\underline{x}, \underline{u}, t)$ with respect to $\underline{x}_{k+1|k}$, with the ij^{th} element given by,

$$H_{ij}|_k = \left.\frac{\partial h_i}{\partial x_j}\right|_{k+1|k} \tag{6.17}$$

Equations (6.3), (6.4), and (6.13) to (6.16) define the extended Kalman filter. The steps in implementing the algorithm are as follows:

1) At sample time t_k, with a given set of inputs ($\underline{u}(t_k)$) and the current state estimate

($\underline{x}(t_k \mid t_k)$) equations (6.3) and (6.4) are used calculate a one-step ahead prediction of the state vector, $\hat{\underline{x}}(t_{k+1} \mid t_k)$;

2) The linearized and discretized model matrices are calculated at the predicted states;

3) The covariance matrix of the one-step ahead prediction, $\underline{P}_{k+1|k}$, and the Kalman gain, $\underline{K}_k$, are calculated using the locally linearized model matrices in equations (6.14) and (6.15), respectively;

4) When measurements become available at t_{k+1}, the state estimates and the covariance matrix are updated using equations (6.13) and (6.16), respectively;

5) The time step is incremented and steps (1) to (4) are repeated.

A conceptual illustration of the algorithm is shown in Figure 6.1.

6.2 FORMULATION OF THE EXTENDED KALMAN FILTER FOR THE ANAEROBIC PROCESS

The non-linear model of the anaerobic treatment process described in Chapter 5 was incorporated into the extended Kalman filter algorithm as described in the following list.

1) The measured inputs are the reactor feed flow rate, the volumetric caustic addition rate, the caustic concentration, and the influent concentrations of the soluble wastewater components:

$$\underline{u} = (Q\ ,\ Q_c\ ,\ Z_B\ ,\ S_{G,0}\ ,\ S_{P,0}\ ,\ S_{B,0}\ ,\ S_{A,0}\ ,\ S_{Z,0}\ ,\ S_{IC,0}\ ,\ S_{I,0})^T$$

2) The deterministic states are those for which a mass balance can be written based on physical, chemical, and biological phenomena occurring in the process:

$$\underline{x}^d = (\ S_{G,1}\ ,\ S_{P,1}\ ,\ S_{B,1}\ ,\ S_{A,1}\ ,\ S_{Z,1}\ ,\ S_{IC,1}\ ,\ S_{I,1}\ ,\ P_{pCO2})^T$$

The material balances for the deterministic states are summarized in Table 5.11.

3) The process measurement vector is:

$$\underline{y} = (Q_{G,CH4}\ ,\ \%CO2,\ S_{H^+}\ ,\ S_{A,1}\ ,\ S_{P,1}\ ,\ S_{B,1}\ ,\ S_{COD})^T$$

where, $\%CO2 = (P_{pCO2}/P_T)*100$

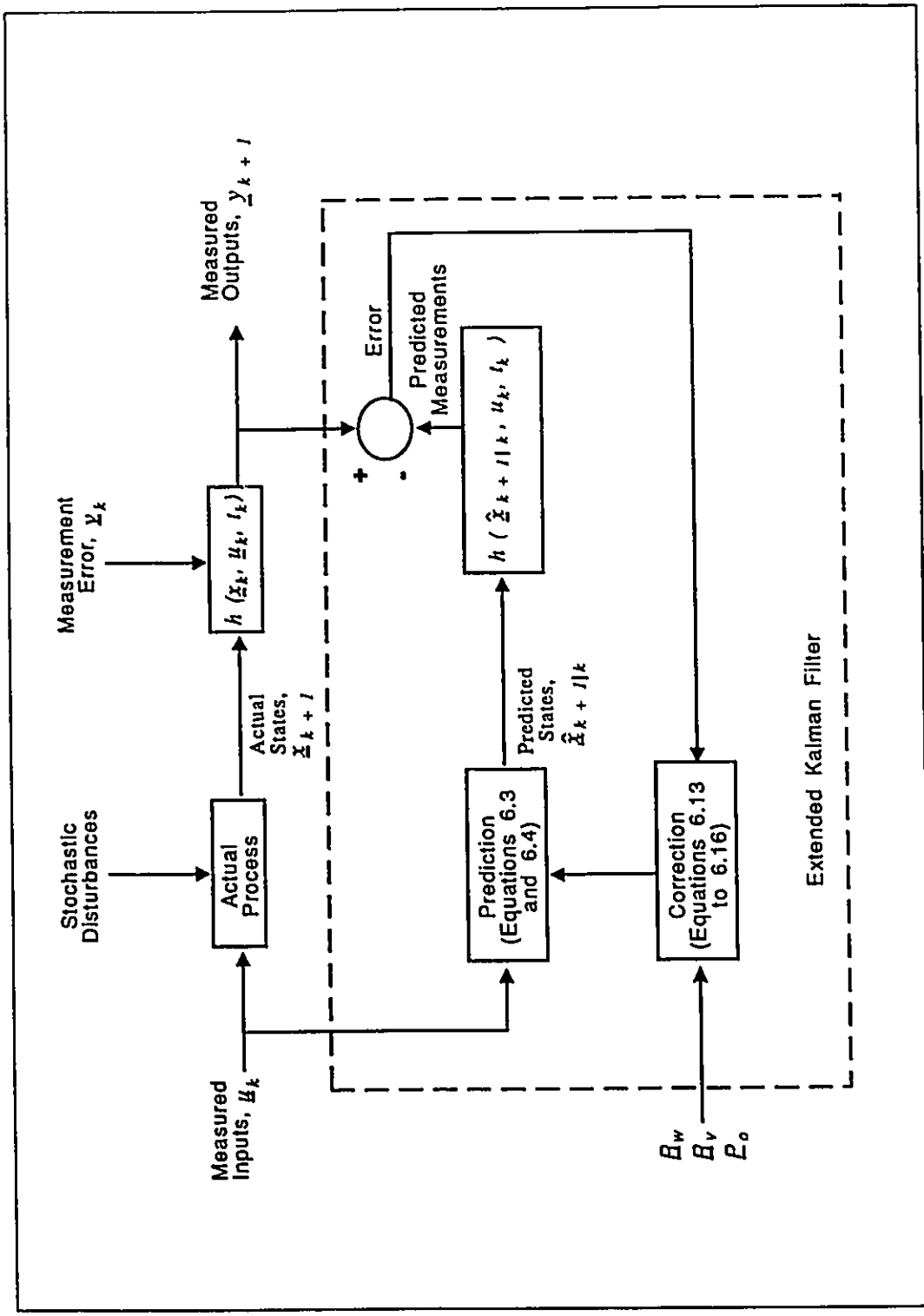

Figure 6.1: A conceptual illustration of the extended Kalman filter algorithm.

$$S_{H^+} = 10^{-pH} * 1000$$

$$S_{COD} = S_{G,1} + S_{I,1}$$

4) The stochastic states include unmeasured process disturbances, internal process states for which there is insufficient mechanistic knowledge to write a deterministic model, and time-invariant parameters for which the actual value is unknown. In this model, the possible stochastic states are:

$$\underline{x}^s = (X_{AF}, X_{PA}, X_{BA}, X_{AM}, \eta_{AF}, K_{AF}, K_{PA}, K_{BA}, K_{AM}, K_{GP}, K_{I,AM}, K_{I,PA}, K_{I,BA}, K_{I,BA}, K_{I,GA}, f_P)$$

The maximum number of stochastic states that can be estimated is equal to the number of process measurements ($\underline{y}$).

The set of deterministic model equations, as represented in this discussion by Equation (6.1), and as summarized in detail in Table 5.11, were solved to obtain the one-step ahead prediction of the state vector using Gear's method for stiff sets of differential equations (Gear, 1971). The linearized model matrices $\underline{A}^d$ and $\underline{A}^s$ were obtained analytically from the nonlinear model equations according to Equations (6.10) and (6.11). Discretization of the model matrices was conducted from the following equation (Astrom and Wittenmark, 1984):

$$A_k = e^{[A(t_k)\,T]} \tag{6.18}$$

where, T is the sampling interval, t_k - t_{k-1}. The exponent in equation 6.18 was calculated through a Taylor series expansion as follows:

$$e^{[A(t_k)T]} = I + A(t_k)T + \frac{1}{2!}A(t_k)^2T^2 + \frac{1}{3!}A(t_k)^3T^3 + \ldots \tag{6.19}$$

The linearized model matrix equations, the model discretization calculations and the Kalman filter algorithm were programmed in FORTRAN-77 on an HP-1000 minicomputer using the RTE-A operating system.

6.3 STATE AND PARAMETER OBSERVABILITY

For the entire state vector $\underline{x}$ to be estimated from the outputs, $\underline{y}$, the unmeasured system states must be uniquely related to the measurements. If this is the case, the system is completely observable. For the linear state space model with n states:

$$\underline{x}_{k+1} = \underline{A}\underline{x}_k + \underline{w}_k \tag{6.20}$$

$$\underline{y}_k = \underline{H}\underline{x}_k + \underline{v}_k \tag{6.21}$$

the observability condition is satisfied if,

$$Rank[\underline{H}^T \underline{A}^T\underline{H}^T (\underline{A}^T)^2\underline{H}^T \ldots (\underline{A}^T)^{n-1}\underline{H}^T] = n$$

If the rank is less than n, not all of the states can be inferred through the model and measurements given by equations (6.20) and (6.21).

Although a system may satisfy the observability condition, the test provides no indication of the quality of information contained in the measurements. In practice, the ability to observe the system states and parameters will depend on the degree to which errors in those states and parameters affect the system outputs. In this study, it was necessary to select a subset of the stochastic state vector which could be estimated from the available data. This was achieved through an analysis of the sensitivity of the outputs to changes in the stochastic states and parameters. A selected subset of stochastic states to be estimated from the actual experimental data was confirmed through simulations in which the extended Kalman filter was used to estimate the parameters from a simulated measurement vector. This analysis is described in the following sections.

6.3.1 Sensitivity Analysis

The effect of differential variations of the stochastic states on the predictions of the deterministic model states are quantifiable through a set of sensitivity coefficients expressed

as follows:

$$\psi_{ij} = \frac{\partial x_i^d}{\partial x_j^s} \tag{6.22}$$

where; $i = 1,2,..n^d$; and, $j = 1,2,..n^s$. The set of equations for the sensitivity coefficients are derived by differentiation of (6.1) with respect to the stochastic states, $\underline{x}^s$. Details of the derivation are given by Atherton *et al.* (1975) among others. Expressing the results in terms of the present linearized model matrices gives

$$\dot{\underline{\Psi}} = \underline{A}^d \underline{\Psi} + \underline{A}^s \tag{6.23}$$

where $\underline{\Psi}$ is the n^d x n^s matrix of sensitivity coefficients, and $\underline{A}^d$ and $\underline{A}^s$ are the linearized model matrices defined earlier. The j^{th} column of $\underline{\Psi}$ is the vector of sensitivity coefficients for the j^{th} stochastic state x_j^s. Equations (6.1) and (6.23) can be solved jointly in computer packages such as ODESSA (Leis and Kramer, 1988). However, the computations can be simplified by only calculating the sensitivity coefficients at steady state, so that

$$\dot{\underline{\Psi}} = \underline{0} \tag{6.24}$$

and,

$$\underline{A}^d \underline{\Psi} = -\underline{A}^s \tag{6.25}$$

A normalized sensitivity coefficient to show (% change in x_i^d)/(% change in x_i^s) is defined as follows:

$$\rho_{ij} = \psi_{ij} \frac{x_j^s}{x_i^d} \tag{6.26}$$

Similarly, a sensitivity coefficient for the outputs can be defined as follows:

$$\varphi_{qj} = \frac{\partial y_q}{\partial x_j^s} \tag{6.27}$$

where, $q = 1,2,...,m$.

Differentiation of (6.12) with respect to x_j^s yields,

$$\frac{\partial y_q}{\partial x_j^s} = \varphi_{qj} = \sum_{l=1}^{n^d} \frac{\partial h_q}{\partial x_l^d} \frac{\partial x_l^d}{\partial x_j^s} = \sum_{l=1}^{n^d} \frac{\partial h_q}{\partial x_l^d} \psi_{lj} \tag{6.28}$$

Expressing the results in matrix notation gives,

$$\underline{\Phi} = \underline{H}^d \underline{\Psi} \tag{6.29}$$

where, $\underline{H}^d$ is the m x n^d submatrix of $\underline{H}$ comprised of the first n^d columns of $\underline{H}$.

The normalized sensitivity coefficients of the outputs are given by,

$$\varrho_{qj} = \varphi_{qj} \frac{x_j^s}{y_q} \tag{6.30}$$

Normalized sensitivity coefficients for the present model were evaluated at four steady states. The steady states were simulated using the parameter set defined in Table 6.1. The simulated reactor feedrate was 120 L/d. The values of all other model constants were as shown in Tables 5.8 and 5.9. The four sets of simulated steady state influent and effluent substrate concentrations are shown in Figure 6.2.

The resulting sets of normalized sensitivity coefficients are shown in Tables 6.2 to 6.5. As an arbitrary indication of the parameters having the most significant affect on the process outputs, any normalized sensitivity coefficient with a value greater than 1 is printed in bold characters.

Table 6.1: Anaerobic dynamic model parameter states used in simulating the sensitivity analysis steady states

Parameter	Description	Value
X_{AF}	Acid-former concentration	450 mg/L
X_{PA}	Propionate-utilizing acetogen concentration	850 mg/L
X_{BA}	Butyrate-utilizing acetogen concentration	500 mg/L
X_{AM}	Acetoclastic methanogen concentration	1000 mg/L
η_{AF}	Maximum acid formation yield factor	0.67
$K_{I,AM}$	Inhibition coefficient - acetoclastic methanogens	500 mg/L
K_{AF}	Saturation coefficient - acid-formers	2200 mg/L
K_{PA}	Saturation coefficient - propionic acetogens	50 mg/L
K_{BA}	Saturation coefficient - butyric acetogens	7.3 mg/L
K_{AM}	Saturation coefficient - aceticlastic methanogens	25 mg/L
$K_{I,PA}$	Inhibition coefficient - propionic acetogens	600 mg/L
$K_{I,BA}$	Inhibition coefficient - butyric acetogens	5000 mg/L
$K_{I,GA}$	Inhibition coefficient - acid-former acetate production	250 mg/L
f_P	Maximum fraction of propionic acid from acid-formers	0.69
K_{GP}	Saturation coefficient - acid-former propionate production	1000 mg/L

Examination of Tables 6.2 to 6.5 indicates that there is a wide variation in the sensitivity of the output predictions to changes in any specific stochastic state over the four steady states. As a result, the ability to estimate a specific stochastic state will depend on the region of process operation. Table 6.6 lists the stochastic states for which a one percent change results in a one percent or greater change in the outputs $Q_{G,CH4}$, $S_{A,I}$, $S_{P,I}$, and $S_{COD,I}$ at each steady state. The effects on the outputs $\%CO_2$, and S_{IN} were not included in the classification because of the difficulty in evaluating the physical-chemical models in this study. At the steady states corresponding to lower COD loadings, the half saturation constants K_{PA}, K_{HA}, and K_{AM} have a significant effect on the model predictions. This is expected in the regions where

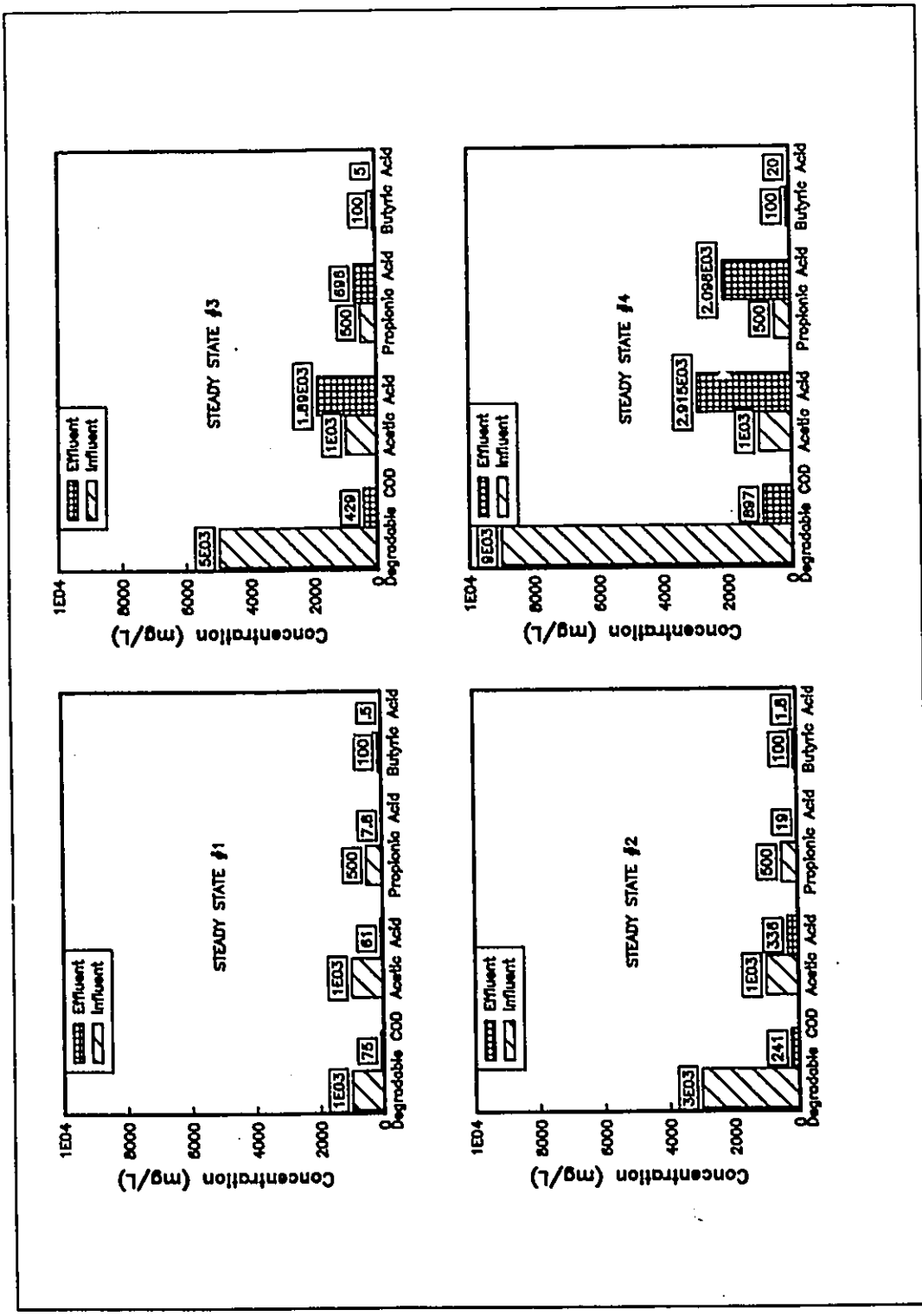

Figure 6.2: Simulated steady states used in the model sensitivity analysis.

Table 6.2: Normalized sensitivity coefficients for steady state #1

	Outputs (y)						
x^*	$Q_{G,CH4}$	$\%CO_2$	S_{H+}	$S_{A,I}$	$S_{P,I}$	$S_{B,I}$	S_{COD}
X_{AF}	-0.055	0.045	0.044	0.053	0.011	0.04	-0.067
X_{PA}	-0.12	-0.013	-0.018	-0.0427	-1.14	-0.011	0.0
X_{BA}	-0.020	-0.00024	-0.00037	0.0011	0.0016	-1.1	0.0
X_{AM}	-0.70	0.25	0.037	-3.1	-0.46	-0.82	0.0
η_{AF}	0.22	0.53	0.52	0.63	0.13	0.48	0.067
$K_{I,AM}$	-0.011	0.0039	0.00057	-0.048	-0.0071	-0.013	0.0
K_{AF}	0.053	-0.043	-0.042	-0.051	-0.011	-0.39	0.064
K_{PA}	0.11	0.011	0.016	0.0369	1.0	0.0097	0.0
K_{BA}	0.019	0.00022	0.00035	-0.00104	-0.00015	1.0	0.0
K_{AM}	0.20	-0.074	-0.011	1.0	0.13	0.24	0.0
$K_{I,PA}$	-0.011	-0.0012	-0.0017	-0.00395	-0.11	-0.001	0.0
$K_{I,BA}$	-0.00025	-0.000002	-0.000004	0.00001	0.000002	-0.013	0.0
$K_{I,GA}$	-0.0065	0.10	0.083	0.00094	0.00014	-0.53	0.0
f_P	0.032	0.00049	0.0007	0.0018	0.045	-0.086	0.0
K_{GP}	-0.000002	0.0	0.0	-0.000001	-0.00003	0.000054	0.0

Table 6.3: Normalized sensitivity coefficients for steady state #2

	Outputs ($\underline{y}$)						
$\underline{x}^T$	$Q_{G,CH4}^{\%}$	$\%CO_2$	S_{H^+}	$S_{A,I}$	$S_{P,I}$	$S_{B,I}$	S_{COD}
X_{AF}	-0.078	0.0075	0.13	0.253	0.25	0.16	-0.20
X_{PA}	-0.10	0.017	-0.12	-0.225	-1.5	-0.063	0.0
X_{BA}	-0.046	-0.0019	0.00014	0.0068	0.0057	-1.2	0.0
X_{AM}	-0.13	1.2	-1.7	-5.5	-4.6	-1.5	0.0
η_{AF}	0.22	0.077	1.3	2.6	2.6	1.6	0.20
$K_{I,AM}$	-0.0050	0.044	-0.065	-2.0	-0.17	-0.058	0.0
K_{AF}	0.070	-0.0067	-0.11	-0.227	-0.23	-0.14	0.18
K_{PA}	0.072	-0.013	0.083	0.162	1.1	0.045	0.0
K_{BA}	0.037	0.0016	-0.00012	-0.0054	-0.0046	1.0	0.0
K_{AM}	0.0093	-0.083	0.12	0.379	0.32	0.11	0.0
$K_{I,PA}$	-0.036	0.0063	-0.041	-0.807	-0.55	-0.022	0.0
$K_{I,BA}$	-0.0029	-0.00012	0.00001	0.00043	0.00036	-0.078	0.0
$K_{I,GA}$	-0.022	0.30	0.18	0.0264	0.022	-0.59	0.0
f_P	0.020	-0.0070	0.041	0.0827	0.54	-0.40	0.0
K_{GP}	-0.00001	0.000003	-0.00002	-0.00004	-0.0003	0.0002	0.0

Table 6.4: Normalized sensitivity coefficients for steady state #3

	Outputs (y)						
$\underline{x}^s$	$Q_{G,CH4}$	$\%CO_2$	S_{H+}	$S_{A,I}$	$S_{P,I}$	$S_{B,I}$	S_{COD}
X_{AF}	-0.17	0.71	-0.22	0.12	0.33	0.12	-0.32
X_{PA}	0.42	-2.2	0.37	-0.058	-1.3	0.10	0.0
X_{BA}	-0.13	0.017	-0.0065	0.0064	0.0093	-1.7	0.0
X_{AM}	0.47	-2.0	1.0	-0.63	-0.91	0.11	0.0
η_{AF}	-1.1	6.3	-1.9	1.1	2.9	1.1	0.32
$K_{I,AM}$	0.27	-1.2	0.60	-0.36	-0.53	0.065	0.0
K_{AF}	0.15	-0.59	0.18	-0.10	-0.28	-1.1	0.27
K_{PA}	-0.028	0.15	-0.025	0.0039	0.088	-0.00069	0.0
K_{BA}	0.075	-0.010	0.0039	-0.0038	-0.0055	0.99	0.0
K_{AM}	-0.0062	0.026	-0.013	0.0082	0.012	-0.0014	0.0
$K_{I,PA}$	0.31	-1.7	0.28	-0.044	-1.0	0.0079	0.0
$K_{I,BA}$	-0.035	0.0047	-0.0018	0.0018	0.0026	-0.46	0.0
$K_{I,GA}$	-0.027	0.41	0.052	0.11	0.17	-0.35	0.0
f_P	-0.62	2.67	-0.46	0.077	1.6	-1.5	0.0
K_{GP}	0.00014	-0.00062	0.00011	-0.00001	-0.0004	0.00035	0.0

Table 6.5: Normalized sensitivity coefficients for steady state #4

	Outputs ($\underline{y}$)						
$\underline{x}^*$	$Q_{G,CH4}$	$\%CO_2$	S_{H+}	$S_{A,I}$	$S_{P,I}$	$S_{B,I}$	S_{COD}
X_{AF}	-0.091	2.2	-0.019	0.080	0.19	0.41	-0.58
X_{PA}	0.019	-2.1	-0.1	0.12	-0.26	-0.055	0.0
X_{BA}	-0.29	0.14	-0.0058	0.027	0.015	-3.5	0.0
X_{AM}	0.095	-1.1	0.093	-0.14	-0.078	0.067	0.0
η_{AF}	-0.37	13.8	-0.12	0.51	1.2	2.6	0.58
$K_{I,AM}$	0.077	-0.85	0.075	-0.11	-0.063	0.054	0.0
K_{AF}	0.065	-1.5	0.013	-0.057	-0.13	-0.29	0.41
K_{PA}	-0.0004	0.048	0.0023	-0.0027	0.0062	0.0013	0.0
K_{BA}	0.076	-0.039	0.0015	-0.0071	0.0039	0.94	0.0
K_{AM}	-0.0008	0.0090	-0.00079	0.0012	0.00067	-0.00057	0.0
$K_{I,PA}$	0.015	-1.7	-0.082	0.097	-0.22	-0.046	0.0
$K_{I,BA}$	-0.11	0.055	-0.021	0.0099	0.0054	-1.3	0.0
$K_{I,GA}$	-0.048	0.94	0.060	0.071	0.39	-0.59	0.0
f_P	-0.40	7.0	0.32	-0.35	0.89	-4.0	0.0
K_{GP}	0.00007	-0.0012	-0.00005	0.00006	-0.00015	0.00068	0.0

Table 6.6: Stochastic states with the most significant effect on the outputs, $Q_{G,CH4}$, $S_{A,1}$, $S_{P,1}$, $S_{B,1}$, and $S_{COD,1}$

Steady State No.	Stochastic States
1	X_{PA}, X_{BA}, X_{AM}, K_{PA}, K_{BA}, K_{AM}
2	X_{PA}, X_{BA}, X_{AM}, η_{AF}, $K_{I,AM}$, K_{PA}
3	X_{PA}, X_{BA}, η_{AF}, $K_{I,PA}$, f_P
4	η_{AF}, f_P

the substrate concentrations are low and the substrate removal rates are essentially first order with respect to substrate concentration. There appear to be specific regions of operation where kinetic inhibition parameters significantly affect the model predictions, as shown by the classification $K_{I,AM}$ and $K_{I,PA}$ in steady states #2 and #3, respectively. The bacterial concentrations X_{PA}, X_{BA}, and X_{AM}, the maximum acid formation yield factor, η_{AF}, and the maximum fraction of propionate produced by the acid-formers, f_P, have a significant effect over the widest region of operation, with the latter two parameters being particularly significant at the highest biodegradable (non-volatile acid) soluble organic influent concentration (steady state #4).

6.3.2 Simulated State Estimation Runs

A preliminary subset of stochastic states for estimation by the extended Kalman filter algorithm was selected based on the sensitivity analysis and insight into the state variations which would be significant under various operating scenarios. Estimation of the following subset of stochastic states was initially tested:

$$\underline{x}' = (X_{AF} , X_{PA} , X_{BA} , X_{AM} , \eta_{AF} , f_P)$$

Although none of the sensitivity coefficients corresponding to X_{AF} were greater than 1.0, the experimental results indicated that significant changes in the acid-former concentration could occur during influent spikes of biodegradable (non-volatile acid) soluble

organics. The half saturation constants which showed significant effects in the sensitivity analysis were not included because it was assumed that the region of interest in process control applications would be during upset conditions when the effluent concentrations of volatile acids and soluble organics were at elevated levels. The inhibition parameters found to be significant were not included because of the narrow region of operation in which these parameters significantly affected process output predictions.

The estimation of the selected stochastic states was tested through a simulation study. Using the input forcing functions from the initial 7 days of glucose run #2, the model defined in Chapter 5 was used to generate the measurement vector, $\underline{y}$. As in the actual experiments, the on-line measurements ($Q_{G,CH4}$, $\%CO_2$, S_{IN}) were available at 10 minute intervals, and the off-line measurements ($S_{A,I}$, $S_{P,I}$, $S_{B,I}$, $S_{COD,I}$) were available at 2 hour intervals.

To simulate the actual measurement noise expected, the simulated process measurements were corrupted with additive Gaussian white noise. The variance of the white noise in the on-line measurements was estimated by pooling the variance of each measurement calculated during the steady state periods of operation at the beginning of each dynamic experiment. The volatile acid measurement noise was estimated from replicates of samples prepared with known volatile acid concentrations. The variance of volatile acid measurement noise was found to be dependent on the volatile acid concentration. The variances of the measurement noise are summarized in Table 6.7.

In the simulated actual process, variations in the stochastic states X_{AF}, X_{PA}, and X_{AM} were represented by a series of ramps. All other stochastic states were set to constant values as summarized in Table 6.8.

(a) Simulated state estimation run #1

In this run, the model was used without the extended Kalman filter to estimate the process states and measurements. The stochastic states were therefore constant in the model

Table 6.7: Variance of white noise added to simulated measurements		
Output	Measurement	Variance
y_1	$Q_{G,CH4}$	120 (L/d)^2
y_2	$\%CO_2$	5.0
y_3	S_{H+}	5.0 x 10^{-9} (mmole/L)^2
y_4	$S_{A,I}$	$0.004(S_{A,I})^2$ (mg/L)^2
y_5	$S_{P,I}$	$0.004(S_{P,I})^2$ (mg/L)^2
y_6	$S_{B,I}$	$2.0(S_{B,I})$ (mg/L)
y_7	$S_{COD,I}$	$100 + 0.004(S_{A,I})^2 + 0.004(S_{P,I})^2 + 2.0(S_{B,I})$

Table 6.8: Anaerobic dynamic model constant stochastic (parameter) states used in simulated "actual" process		
State	Description	Value
X_{BA}	Butyrate-utilizing acetogen concentration	400 mg/L
η_{AF}	Maximum acid formation yield factor	0.50
$K_{I,AM}$	Inhibition coefficient - acetoclastic methanogens	500 mg/L
K_{AF}	Saturation coefficient - acid-formers	2200 mg/L
K_{PA}	Saturation coefficient - propionic acetogens	50 mg/L
K_{BA}	Saturation coefficient - butyric acetogens	7.3 mg/L
K_{AM}	Saturation coefficient - acetoclastic methanogens	25 mg/L
$K_{I,PA}$	Inhibition coefficient - propionic acetogens	600 mg/L
$K_{I,BA}$	Inhibition coefficient - butyric acetogens	5000 mg/L
$K_{I,GA}$	Inhibition coefficient - acid-former acetate production	250 mg/L
f_P	Maximum fraction of propionic acid from acid-formers	0.77
K_{GP}	Saturation coefficient - acid-former propionate production	1000 mg/L

throughout the run. Figures 6.3 and 6.4 show these open loop (model only) estimates of the states $S_{COD,I}$, $S_{A,I}$, $S_{P,I}$ and $S_{B,I}$, and the measurements $Q_{G,CH4}$ and $\%CO_2$. Also in Figure 6.4,

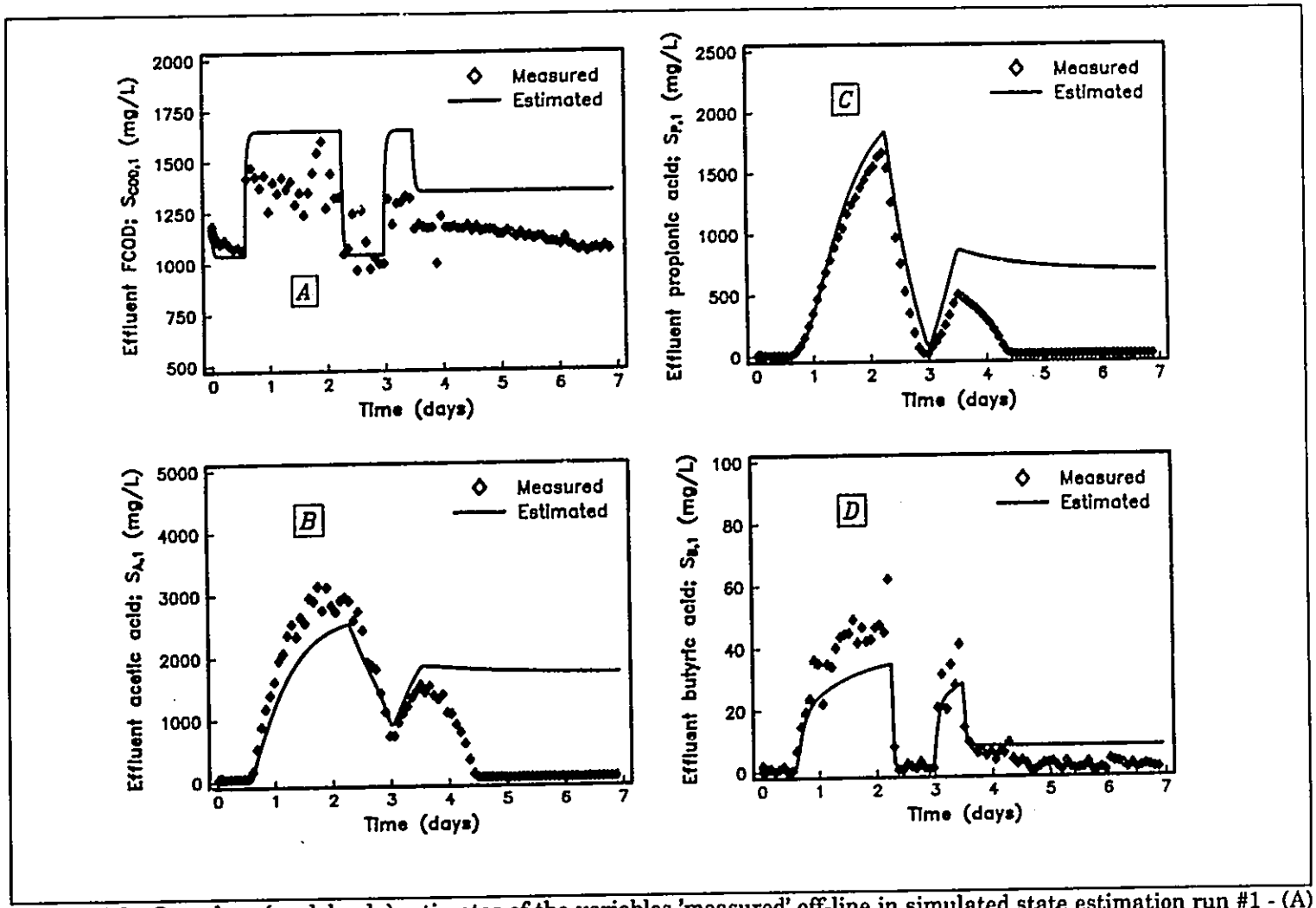

Figure 6.3: Open loop (model only) estimates of the variables 'measured' off-line in simulated state estimation run #1 - (A) $S_{COD,1}$; (B) $S_{A,1}$; (C) $S_{P,1}$; (D) $S_{B,1}$.

S_{H^+} has been converted to pH. Figure 6.5 shows the variations in the bacterial concentration stochastic states in comparison to the constant values assumed in generating the estimates. The plots show that significant biases develop between the model estimates and the measured outputs when the stochastic states are not estimated. The plots of $\%CO_2$ and pH in Figure 6.4 indicate the difficulty in predicting these outputs when large biases in the substrate states exist.

(b) Simulated state estimation run #2

In this case, the extended Kalman filter algorithm was used to simultaneously estimate the stochastic states and the deterministic states, and to filter the process measurement vector. The variance of the white noise added to the simulated measurements was also used to set the diagonal elements of $\underline{R}_v$. Off-diagonal elements in $\underline{R}_v$ were assumed equal to zero. The diagonal elements were set as follows:

$\underline{R}_v = Diag$ (120. , 5.0 , 5.0 x 10^{-9} , $0.004(S_{A,I})^2$, $.004(S_{P,I})^2$, $2.0(S_{B,I})$, $500 + 0.004(S_{A,I})^2 + 0.004(S_{P,I})^2 + 2.0(S_{B,I})$)

Settings for the diagonal elements of $\underline{R}_w$ were also required for the initialization of the extended Kalman filter. To estimate the order of magnitude of the variance of $\underline{w}^d_k$, a first order difference for the states, $\underline{x}^d$, over a specified period of operation is calculated as follows:

$$\nabla \underline{x}^d = \underline{x}^d_k - \underline{x}^d_{k-1} \tag{6.31}$$

where ∇ is the backward difference operator. The variance of the first order differences, $\underline{\sigma}^2_{v_d}$, provide a measure of the total change in a specific state variable over the sampling interval t_k to t_{k+1}. The fraction of that change that can be explained by the deterministic elements of the model is then assumed, with the remainder of the variance attributed to modelling error. The variance of $\underline{w}_k^s$ is similarly estimated through a knowledge of the expected change in the stochastic states over a sampling interval. Typically, simulations are conducted to obtain settings which provide reasonable performance of the filter. In this study, the following initial

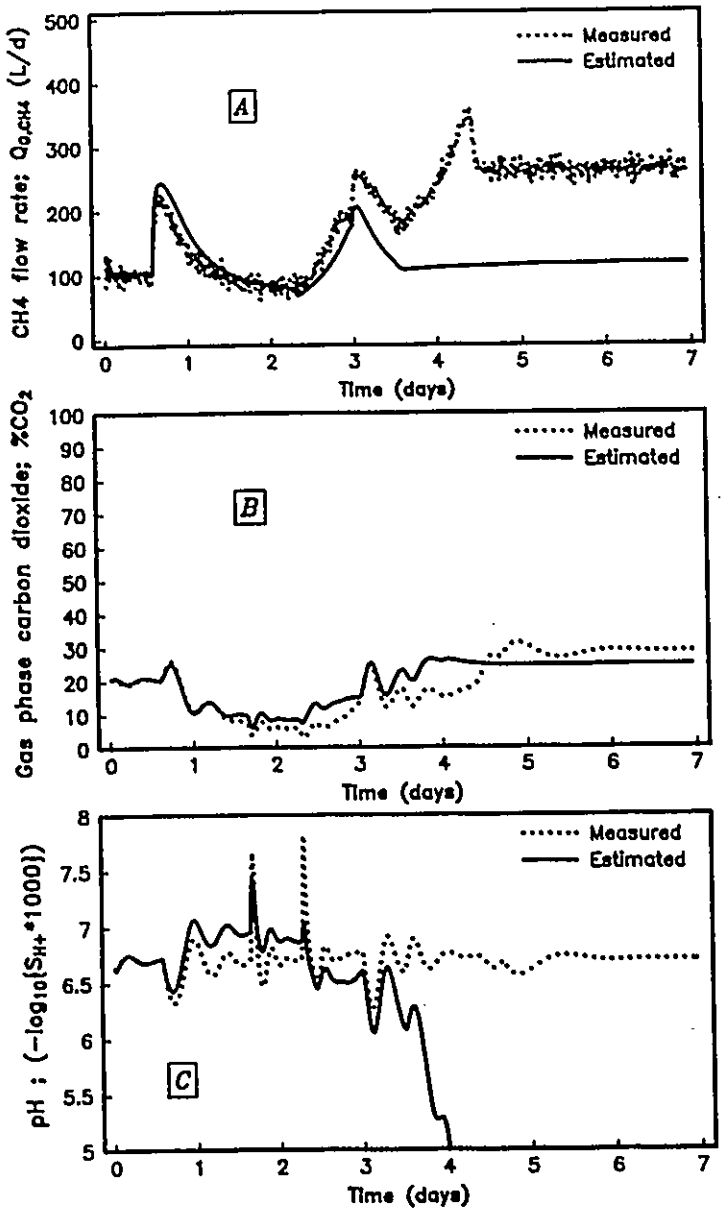

Figure 6.4: Open loop (model only) estimates of the variables 'measured' on-line in simulated state estimation run #1 - (A) $Q_{G,CH4}$; (B) $\%CO_2$; (C) pH.

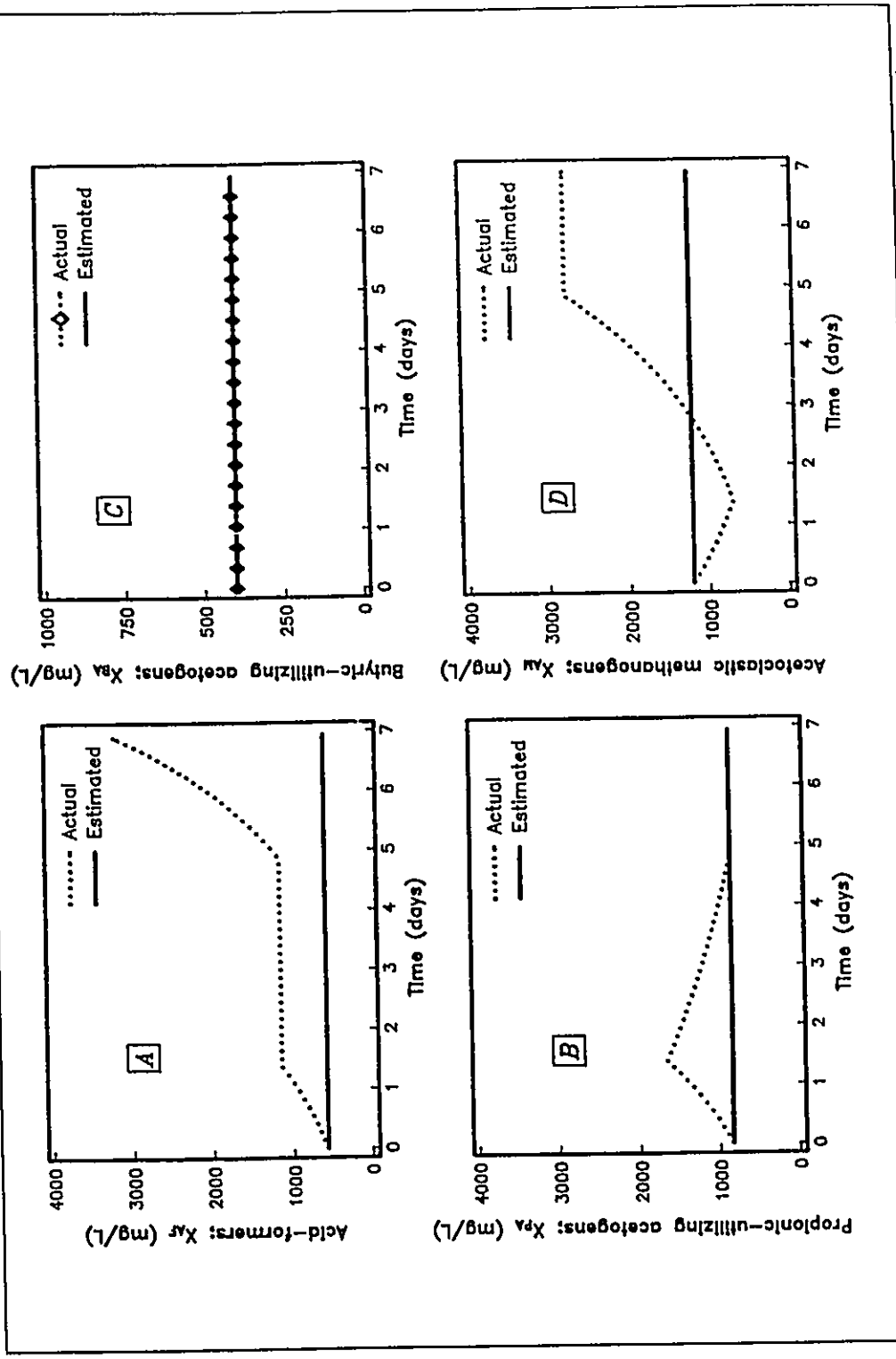

Figure 6.5: "Actual" bacteria concentrations compared to constant values assumed in model during simulated state estimation run #1 - (A) X_{AF}; (B) X_{PA}; (C) X_{BA}; (D) X_{AM}.

settings were used:

$$\underline{R}_w = Diag\ (\ 10.\ 30.\ 1.\ 30.\ 5.\ 5.\ 0.\ 0.001\ 100.\ 100.\ 100.\ 100.\ 0.\ 0.\ )$$

and,

$$\underline{P}_0 = Diag\ (\ 1.\ 1.\ 1.\ 1.\ 0.1\ 0.001\ 0\ 1.0\text{x}10^{-5}\ 100.\ 100.\ 100.\ 100.\ 0.001\ 0.01\ )$$

where $\underline{P}_0$ is the state covariance matrix $\underline{P}_{k|k}$ at k = 0, with magnitudes of the diagonal elements chosen to reflect the initial uncertainty in the state estimates. The diagonal elements in $\underline{R}_w$ corresponding to η_{AF}, and f_P were set to zero with the corresponding diagonal elements in $\underline{P}_0$ set to non-zero values. This was to represent the fact that these states were expected to be constant over time, with initially unknown values.

With the exception of the states X_{BA}, η_{AF}, and f_P, the initial conditions of all of the states in the extended Kalman filter were set equal to the initial conditions in the actual simulated process. The following initial conditions were used for the three remaining states:

$$X_{BA} = 600\ \text{mg/L}$$

$$\eta_{AF} = 0.4$$

$$f_P = 0.5$$

The results from simulated state estimation run #2 are shown in Figures 6.6 to 6.9. Figures 6.6 and 6.7 show that the biases between the measured and the estimated outputs were significantly reduced in comparison to the open-loop simulation. Some discrepancy between measured and estimated output values exists for $S_{COD,I}$ before day 2 of the simulation, and for $S_{B,I}$ between day 3 and day 4. Figures 6.8 and 6.9 indicate that a number of stochastic states were very poorly estimated. Figure 6.8 shows that although the estimates of X_{AF} and X_{AM} followed the trends of the actual values reasonably well, significant biases existed in the estimates of X_{PA} and X_{BA}. Figure 6.9 shows that the estimated value of η_{AF} converged on the actual value by the end of the simulation while the estimated value of f_P was extremely poor. Subsequent simulations with adjustments in the settings of $\underline{R}_w$ and $\underline{P}_0$ did not improve the estimates.

Some indication of the reason for the poor estimates in the simulated extended Kalman filter run can be found by examining the correlation coefficient matrix for the estimated stochastic states. The elements of the correlation coefficient matrix are given by

$$r_{ij} = \frac{p_{ij}}{\sqrt{p_{ii}\, p_{jj}}} \tag{6.32}$$

where, p_{ij} are the off-diagonal elements of the variance-covariance matrix, and p_{ii} and p_{jj} are the diagonal elements of $\underline{P}$. High correlations between parameters as reflected in the off-diagonal elements of the correlation matrix indicate that too many parameters are being estimated. If two parameters are highly correlated, one should be fixed at a constant value while the other parameter is estimated. The correlation coefficient matrix in Table 6.9 was calculated for the estimated stochastic states at the end of the simulated state estimation run. A high correlation was found between X_{BA} and f_P.

Table 6.9: Correlation coefficient matrix for estimated stochastic states

	X_{AF}	X_{PA}	X_{BA}	X_{AM}	η_{AF}	f_P
X_{AF}	1.00					
X_{PA}	-0.032	1.00				
X_{BA}	-0.027	-0.039	1.00			
X_{AM}	-0.0077	-0.16	-0.0002	1.00		
η_{AF}	0.15	-0.11	0.17	-0.0032	1.00	
f_P	0.0061	0.020	-0.86	-0.0011	0.047	1.00

(c) Simulated state estimation run #3

A subsequent simulated state estimation run was attempted in which X_{BA} was set to a constant value while all of the other stochastic states estimated in the previous run were again estimated. The results from this run are shown in Figures 6.10 to 6.13. Figures 6.10

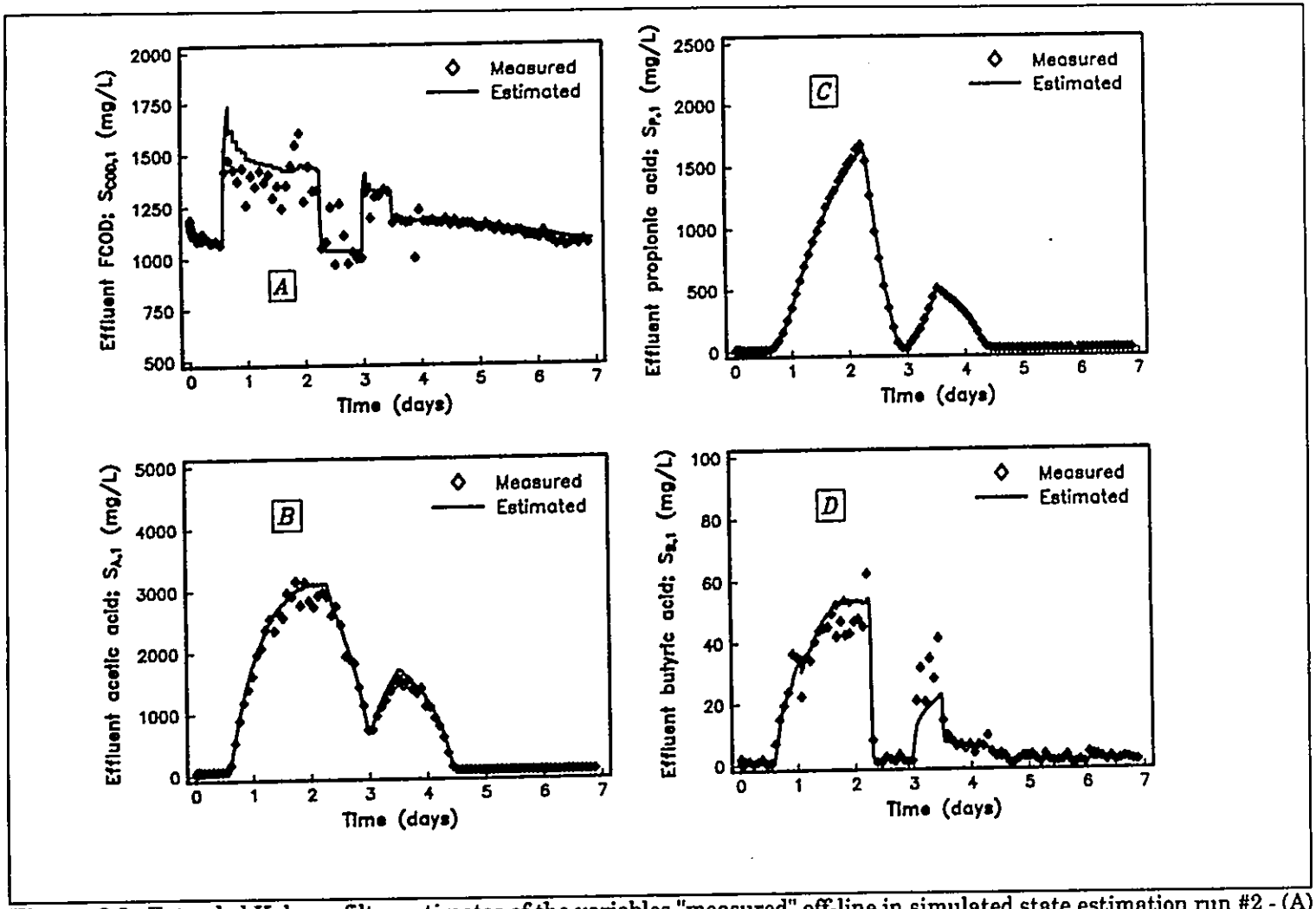

Figure 6.6: Extended Kalman filter estimates of the variables "measured" off-line in simulated state estimation run #2 - (A) $S_{COD,1}$; (B) $S_{A,1}$; (C) $S_{P,1}$; (D) $S_{B,1}$.

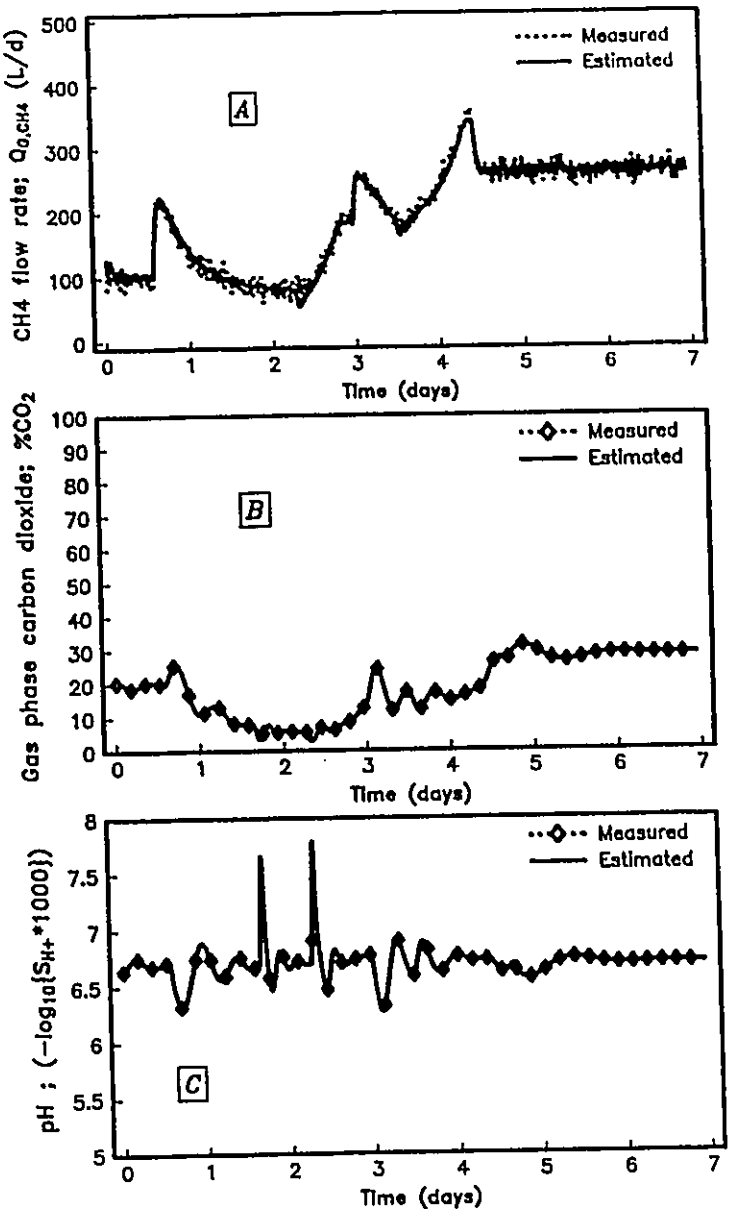

Figure 6.7: Extended Kalman filter estimates of the variables "measured" on-line in simulated state estimation run #2 - (A) $Q_{G,CH4}$; (B) $\%CO_2$; (C) pH.

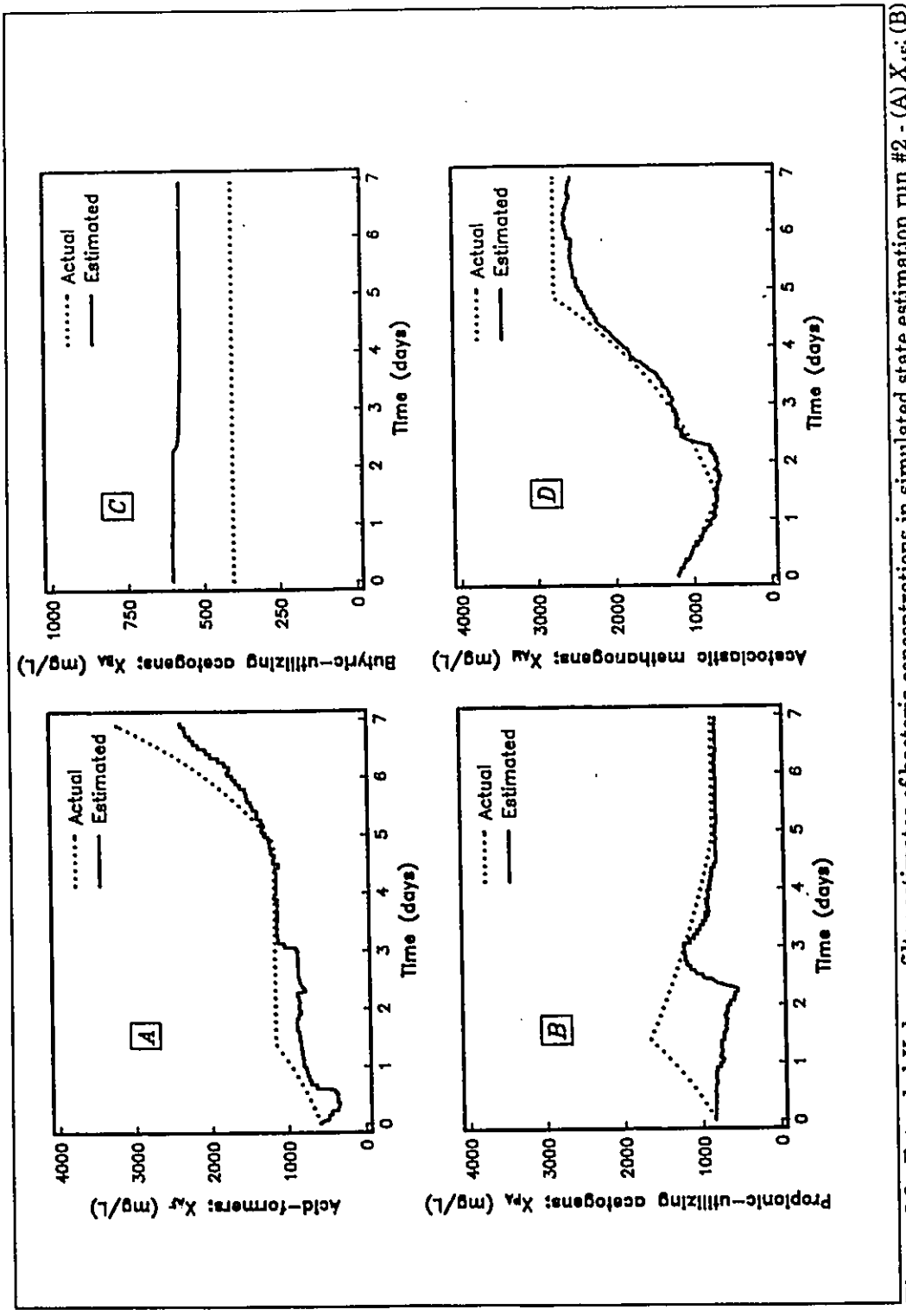

Figure 6.8: Extended Kalman filter estimates of bacteria concentrations in simulated state estimation run #2 - (A) X_{AF}; (B) X_{PA}; (C) X_{BA}; (D) X_{AM}.

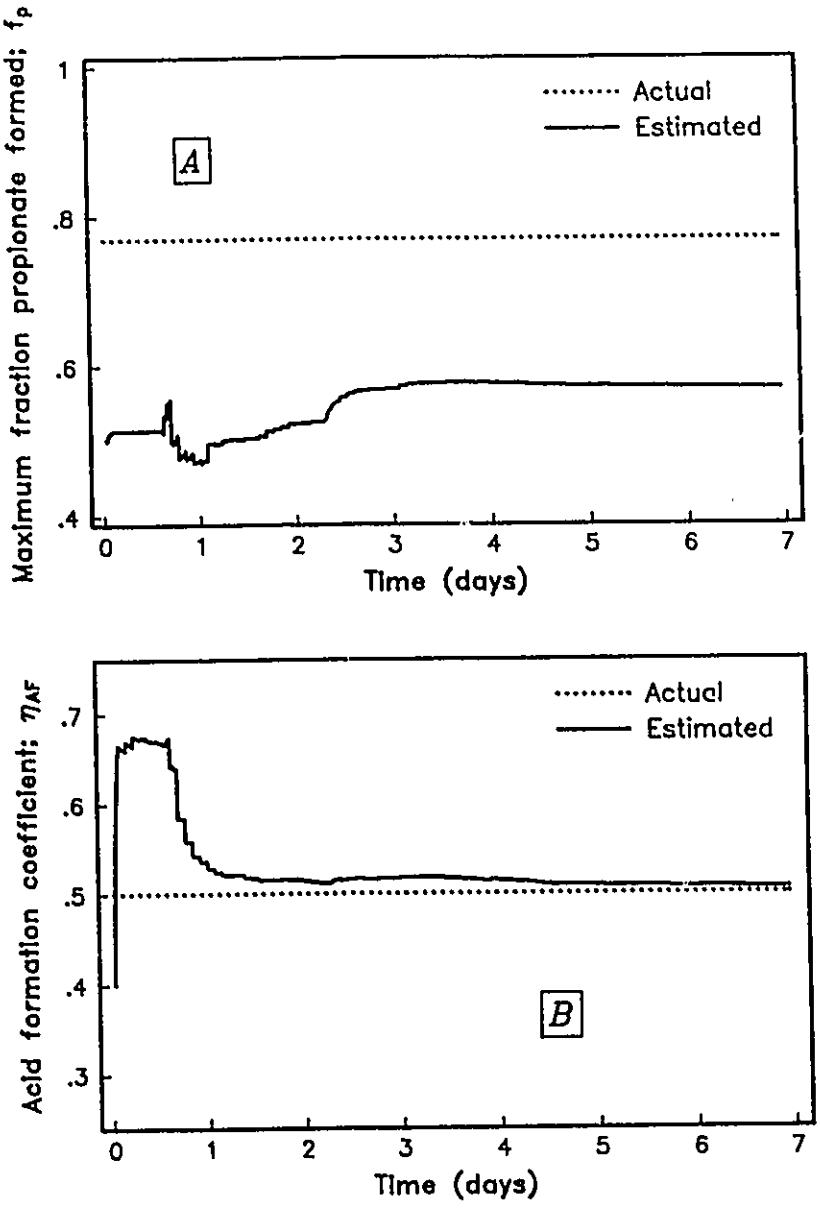

Figure 6.9: Simulated state estimation run #2 results showing extended Kalman filter estimates of (A) f_p, and (B) η_{AF}.

and 6.11 show that there was little bias between measured and estimated process outputs. Figures 6.12 and 6.13 show that the stochastic state estimates were significantly improved. Subsequent simulations with increased values in $\underline{P}_0$ for X_{PA} and f_P did not improve the slow initial convergence of these states. This behaviour may have been caused by a low sensitivity of the model predictions to errors in these states in the region of operation represented by the initial period of the simulation.

The correlation coefficient matrix calculated at the end of the second simulated state estimation run is shown in Table 6.10. In this run, there were no high correlations between the estimated stochastic states. The determinant of the subset of the variance-covariance matrix corresponding to the estimated stochastic states ($\underline{P}^s$) provides a measure of the total variance of the state estimates. Since the determinant of $\underline{P}^s$ is proportional to the volume of the approximate joint confidence regions of the stochastic state estimates (Box and Lucas, 1959), the value of $|\underline{P}^s|$ would be expected to decrease as the quality of information for state estimation increased. The logarithm of the determinant of $\underline{P}^s$ is plotted in Figure 6.14. It can be seen that the determinant of $\underline{P}^s$ increased until the beginning of the first influent substrate pulse near 0.5 days, where there was a sudden large decrease. Another smaller decrease is noticeable at the beginning of the second influent substrate pulse at 3 days. These changes indicate an increase in the amount of information on the stochastic state values due to the dynamic changes occurring in the process at these times. It can also be seen that the determinant of $\underline{P}^s$ increases between sampling times for the off-line laboratory data (2 hours) and decreases each time new laboratory results are obtained. This again indicates an increase in the amount of information as provided by the increase in the number of measurements at these points.

6.4 SUMMARY OF DYNAMIC MODEL CALIBRATION METHODOLOGY

An extended Kalman filter state estimation algorithm was chosen to estimate both

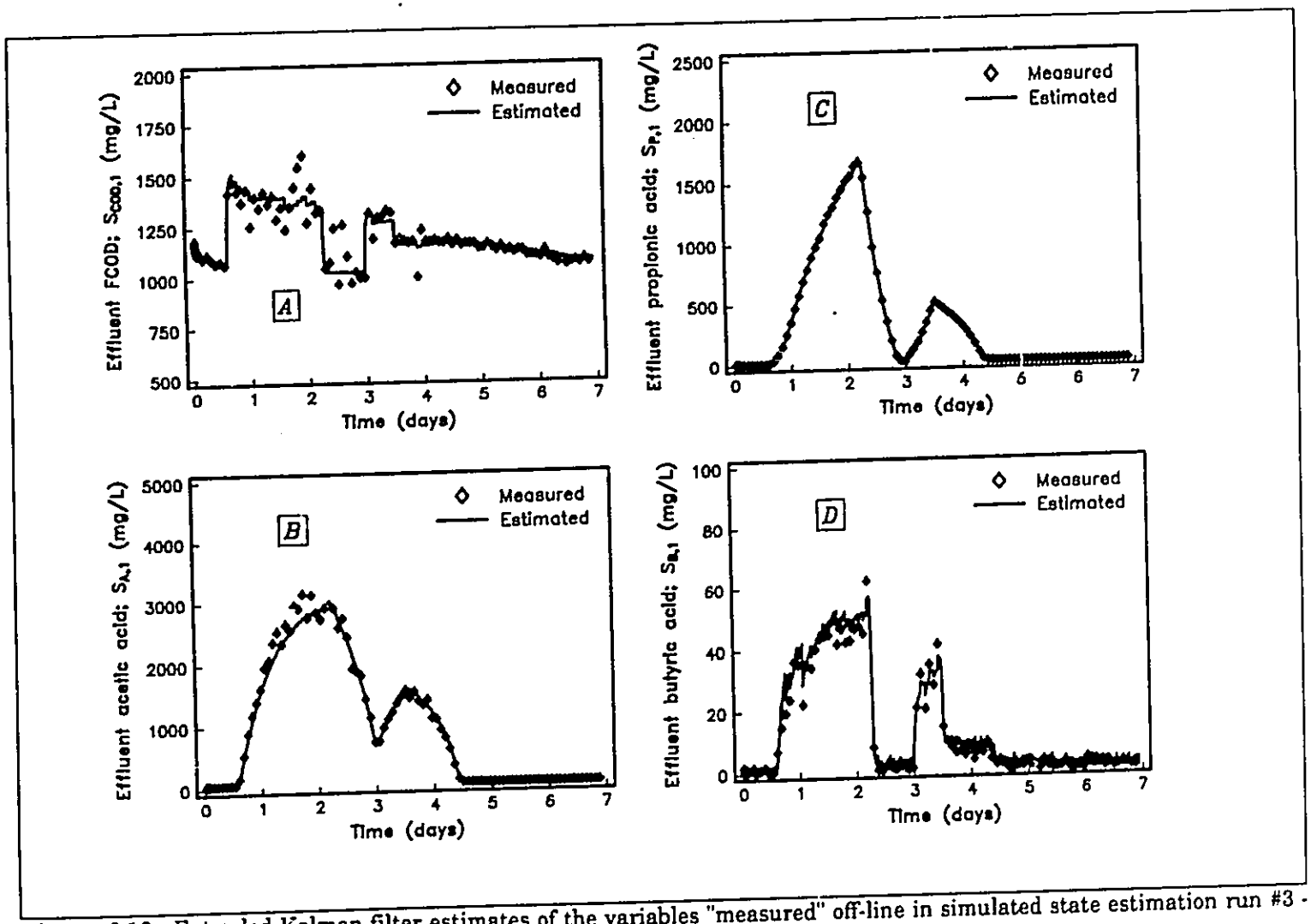

Figure 6.10: Extended Kalman filter estimates of the variables "measured" off-line in simulated state estimation run #3 - (A) $S_{COD,1}$; (B) $S_{A,1}$; (C) $S_{P,1}$; (D) $S_{B,1}$.

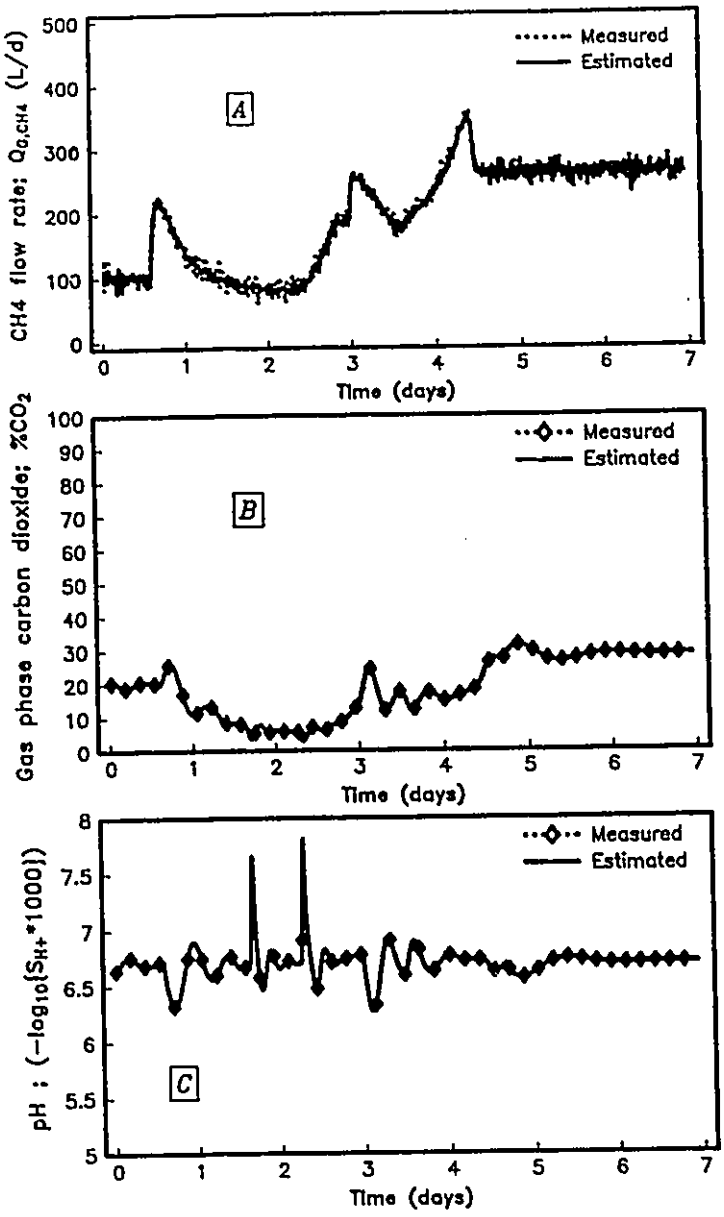

Figure 6.11: Extended Kalman filter estimates of the variables "measured" on-line in simulated state estimation run #3 - (A) $Q_{G,CH4}$; (B) $\%CO_2$; (C) pH.

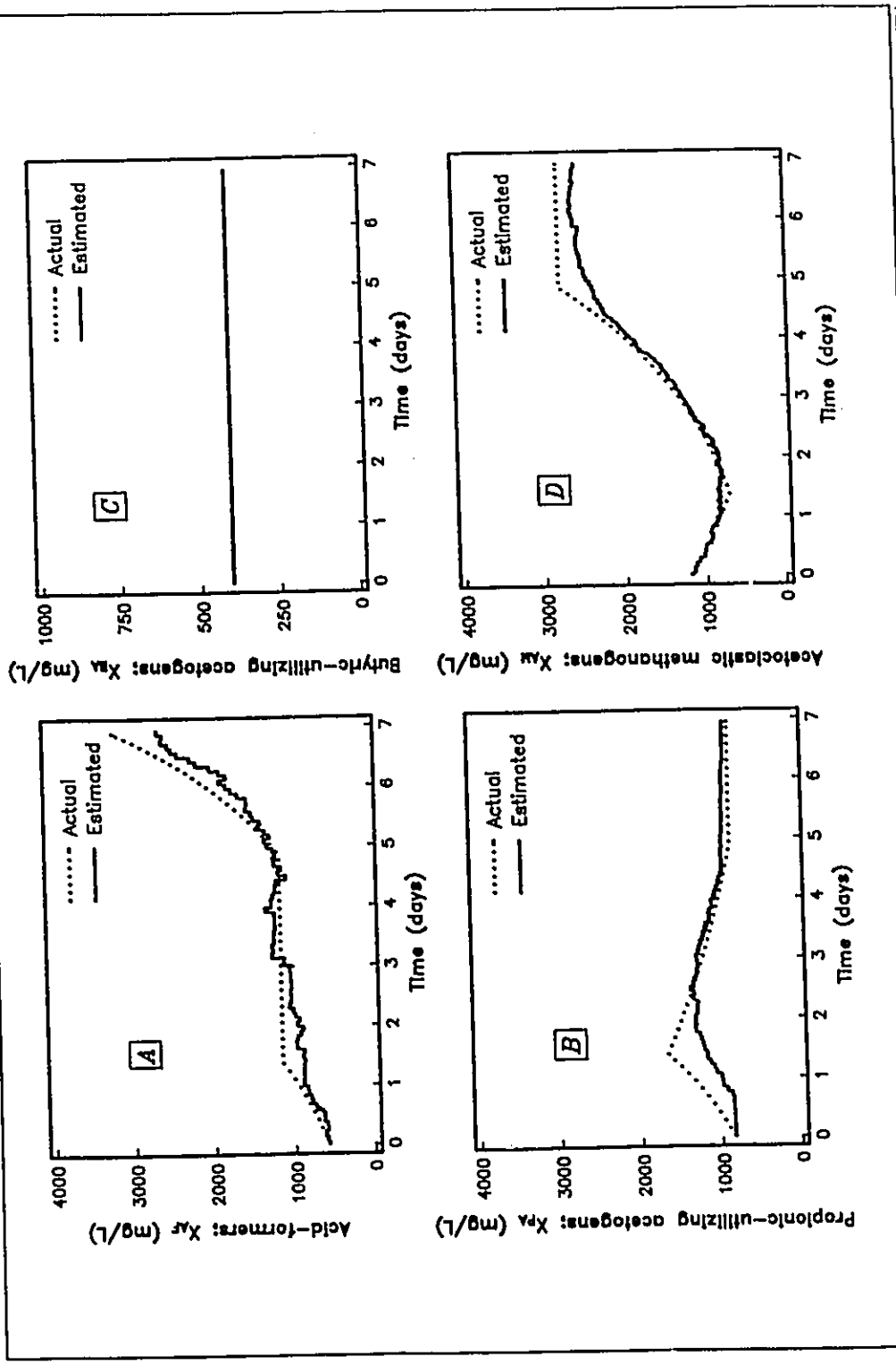

Figure 6.12: Extended Kalman filter estimates of bacteria concentrations in simulated state estimation run #3 - (A) X_{AF}; (B) X_{PA}; (C) X_{BA}; (D) X_{AM}.

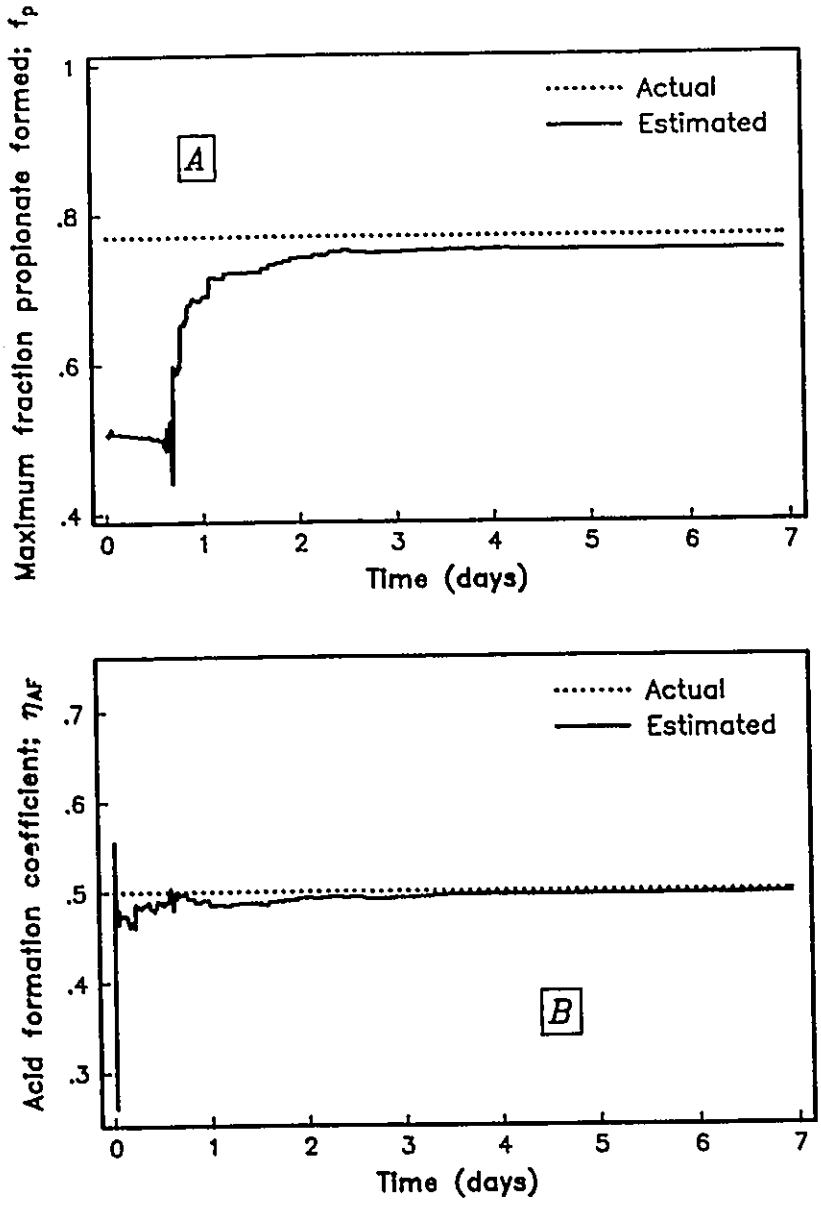

Figure 6.13: Simulated state estimation run #3 results showing extended Kalman filter estimates of (A) f_p, and (B) η_{AF}.

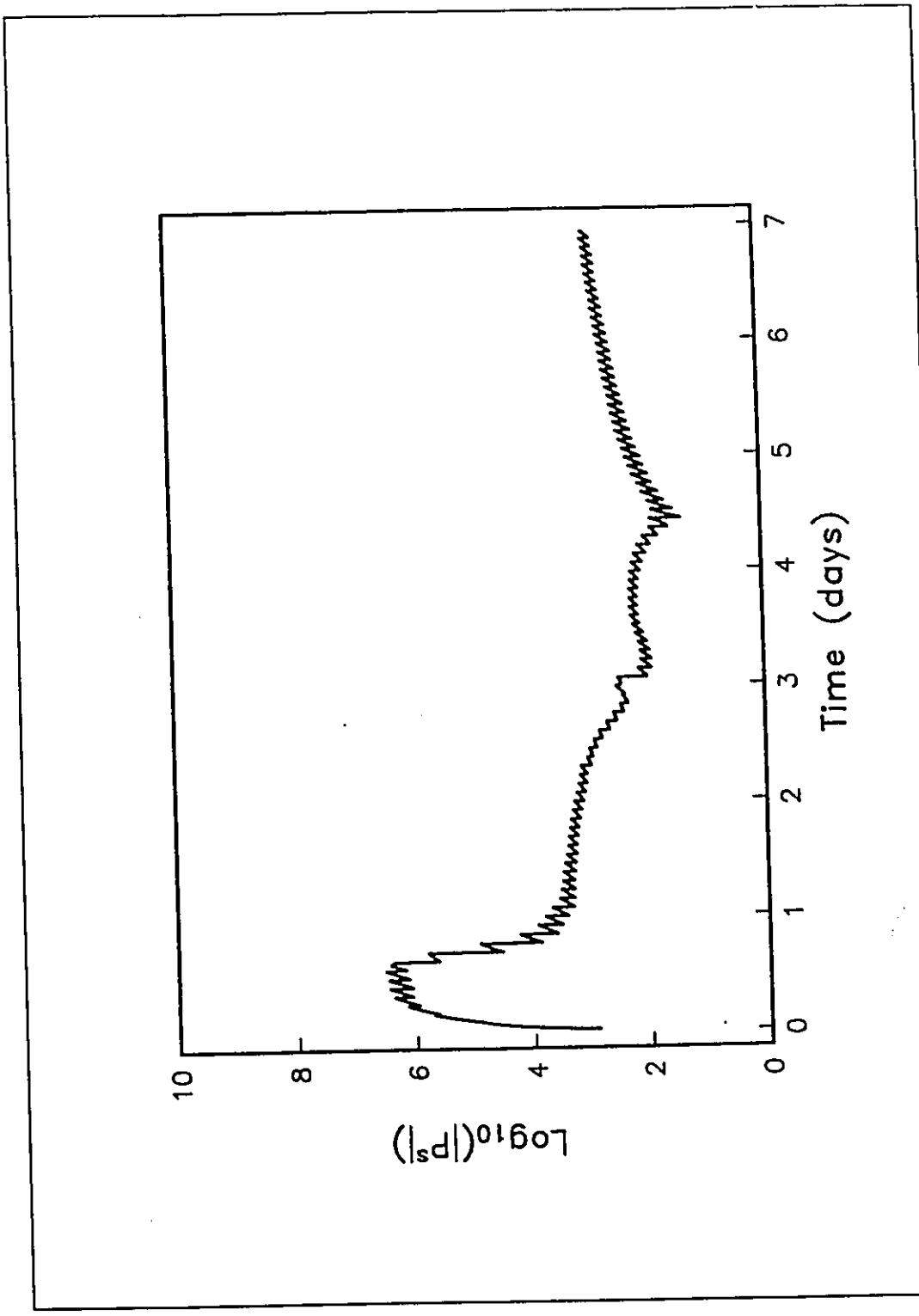

Figure 6.14: The determinant of $\underline{P}'$ during simulated state estimation run #3.

Table 6.10: Correlation coefficient matrix for estimated stochastic states in second simulated state estimation run

	X_{AF}	X_{PA}	X_{AM}	η_{AF}	f_P
X_{AF}	1.00				
X_{PA}	-0.032	1.00			
X_{AM}	-0.052	-0.13	1.00		
η_{AF}	0.051	-0.042	-0.013	1.00	
f_P	-0.0058	0.046	-0.0044	-0.093	1.00

unmeasured time-variable states and time-invariant parameters in the dynamic anaerobic process model specified in Chapter 5. Due to the large number of unmeasured states and unknown parameter values in the model, a model sensitivity analysis was conducted to determine which subset of the states and parameters should be estimated as stochastic states by the extended Kalman filter.

An important finding of the sensitivity analysis is that there is a wide variation in the sensitivity of the model predictions to changes in any specific stochastic or parameter state over different regions of process operation. As a result, the ability to estimate a stochastic state or parameter will depend on the region of process operation. An additional application of a sensitivity analysis could thus be to select an appropriate set of operating data or a suitable set of experimental conditions to generate data for model calibration.

Based on the sensitivity analysis, the estimation of an initial parameter subset consisting of X_{AF}, X_{PA}, X_{BA}, X_{AM}, η_{AF}, and f_P was tested in a simulated state estimation run. After finding that poor stochastic state estimates resulted from a high correlation between X_{BA} and f_P, a second run was conducted in which X_{BA} was set to its constant actual value. The results showed that the remaining states could be estimated reasonably well.

Correct formulation of the extended Kalman filter algorithm is important to make it useful in a real process environment. The extended Kalman filter corrections to the predicted

state vector ($\underline{\hat{x}}(t_{k+1}|t_k)$) are based on the magnitude of model error, as represented by $\underline{R}_w$, relative to the magnitude of the output measurement error, as represented by $\underline{R}_v$. The settings for $\underline{R}_w$ and $\underline{R}_v$ must therefore be based as much as possible on actual process knowledge. The proper selection of the stochastic states to be estimated by the extended Kalman filter is important to eliminate model biases. If an adequate knowledge of the actual physical system is used to select the disturbance states and parameters, their estimation by the Kalman filter can be a realistic representation of the actual behaviour of these states. However, the variation of the stochastic states as estimated by the filter will also account for unknown disturbances and modelling inadequacies such as an inappropriate model structure and errors in the values of constant model parameters. Such model inadequacies may cause errors in the stochastic state estimates. If unrealistic behaviour in the stochastic state estimates can be recognized during model identification, it can be used to reveal the model inadequacies and lead to improvements in the model (Beck, 1989).

CHAPTER 7

DYNAMIC MODEL STATE AND PARAMETER ESTIMATION

In this chapter, the estimation of the unmeasured time-variable states and the unknown values of time-invariant parameters of the dynamic model specified in Chapter 5 are summarized. The extended Kalman filter algorithm was used for estimation as outlined in Chapter 6. Measured process outputs during the dynamic experiments on the anaerobic fluidized bed pilot plant were used in this state estimation study. Possible model improvements were identified and tested after an examination of the state estimation results.

7.1 STATE AND PARAMETER ESTIMATION RESULTS

Because the acetic acid run, propionic acid run, and the first glucose run were implemented in sequence, the state and parameter estimation was conducted on the entire data set. The results from each section of this experimental period are illustrated separately.

All $S_{COD,I}$ measurements were corrected according to Equations (5.32) and (5.33).

7.1.1 Acetic Acid Run

Table 7.1 lists the state initial conditions, and the settings for the diagonal elements of $\underline{R}_w$, and $\underline{P}_0$ for the acetic acid run. The settings for $\underline{R}_v$ were based on the actual process output measurement error as listed in Chapter 6.

The results of the acetic acid state estimation run are plotted in Figures 7.1 to 7.4. In Figure 7.1, the updated state estimate (x_{A1A}) is plotted with the corresponding measured

Table 7 1: Initial conditions for acetic acid state estimation run

State ($\underline{x}$)	Initial conditions ($\underline{x}_0$)	Diagonal elements $\underline{R}_\omega$	Diagonal elements $\underline{P}_0$
$S_{G,I}$	300 mg/L	1.0	0.0
$S_{P,I}$	5 mg/L	10.0	1.0
$S_{B,I}$	2 mg/L	0.10	1.00
$S_{A,I}$	30 mg/L	10.00	0.001
$S_{Z,I}$	18 mmole/L	5.00	0.10
$S_{IC,I}$	25 mmole/L	5.00	0.001
$S_{I,I}$	760 mg/L	0.0	0.0
P_{pCO2}	0.20 atm	0.001	0.00001
X_{AF}	85 mg/L	1.0	0.0
X_{PA}	1250 mg/L	100.0	100.0
X_{BA}	400 mg/L	0.0	0.0
X_{AM}	1900 mg/L	1000.0	100.0
η_{AF}	0.80	0.0	0.0001
$K_{I,AM}$	1000 mg/L	0.0	0.0
K_{AF}	300 mg/L	0.0	0.0
K_{PA}	130 mg/L	0.0	0.0
K_{BA}	10 mg/L	0.0	0.0
K_{AM}	75 mg/L	0.0	0.0
$K_{I,PA}$	500 mg/L	0.0	0.0
$K_{I,BA}$	1000 mg/L	0.0	0.0
$K_{I,GA}$	250 mg/L	0.0	0.0
f_P	0.75	0.0	0.0001
K_{GP}	1000 mg/L	0.0	0.0

value (y_k) for $S_{A,I}$, $S_{P,I}$, and $S_{B,I}$. In Figures 7.1 and 7.2 respectively, plots of $S_{COD,I}$ and $Q_{G,CH4}$ show actual measured values with the corresponding filtered value ($h(\underline{x}_{k|k}, \underline{u}_k, t_k)$). The smooth tracking of the states and measurements observed through most of the run shows that the extended Kalman filter provides excellent tracking of the measured states.

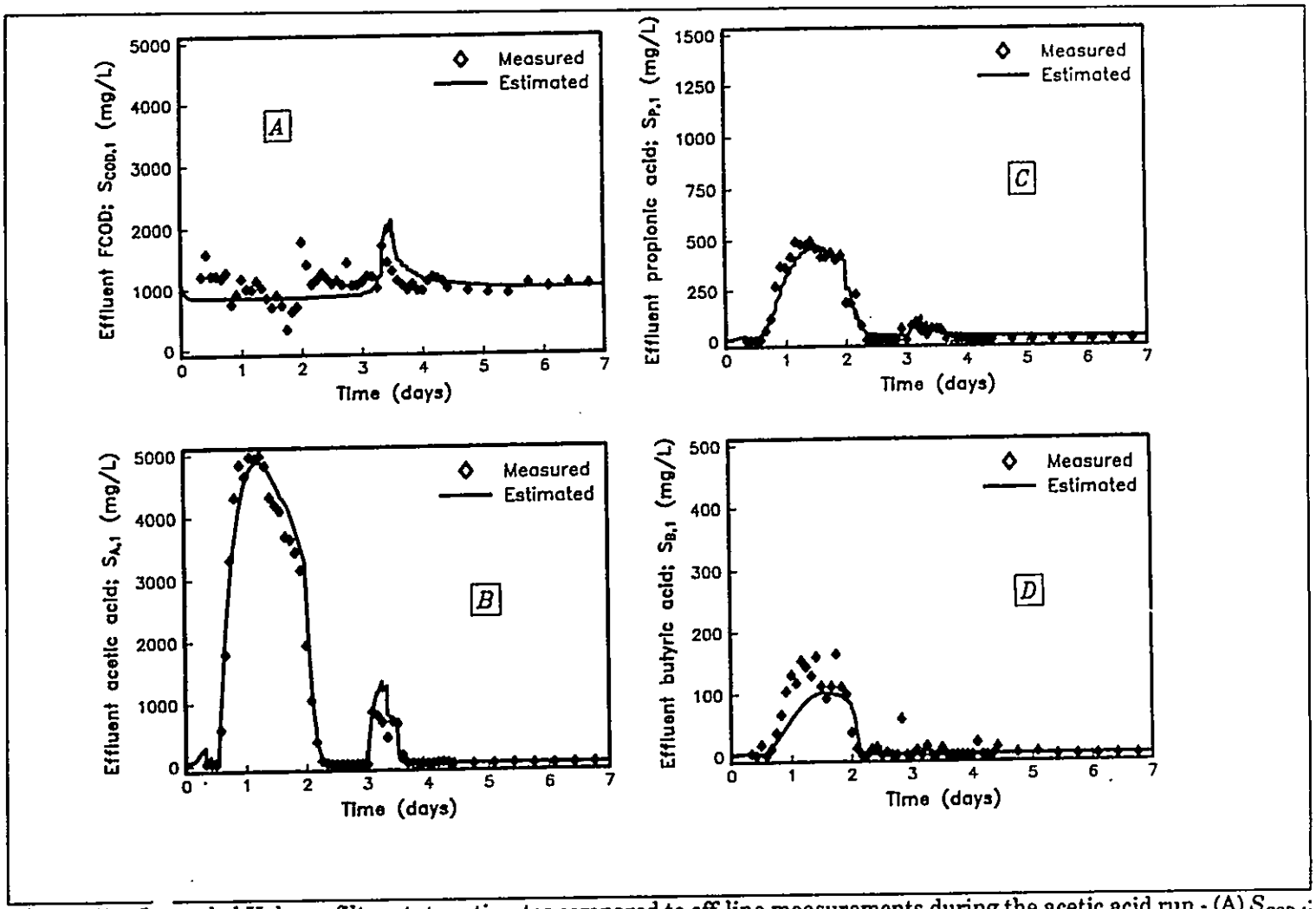

Figure 7.1: Extended Kalman filter state estimates compared to off-line measurements during the acetic acid run - (A) $S_{COD,1}$; (B) $S_{A,1}$; (C) $S_{P,1}$; (D) $S_{B,1}$.

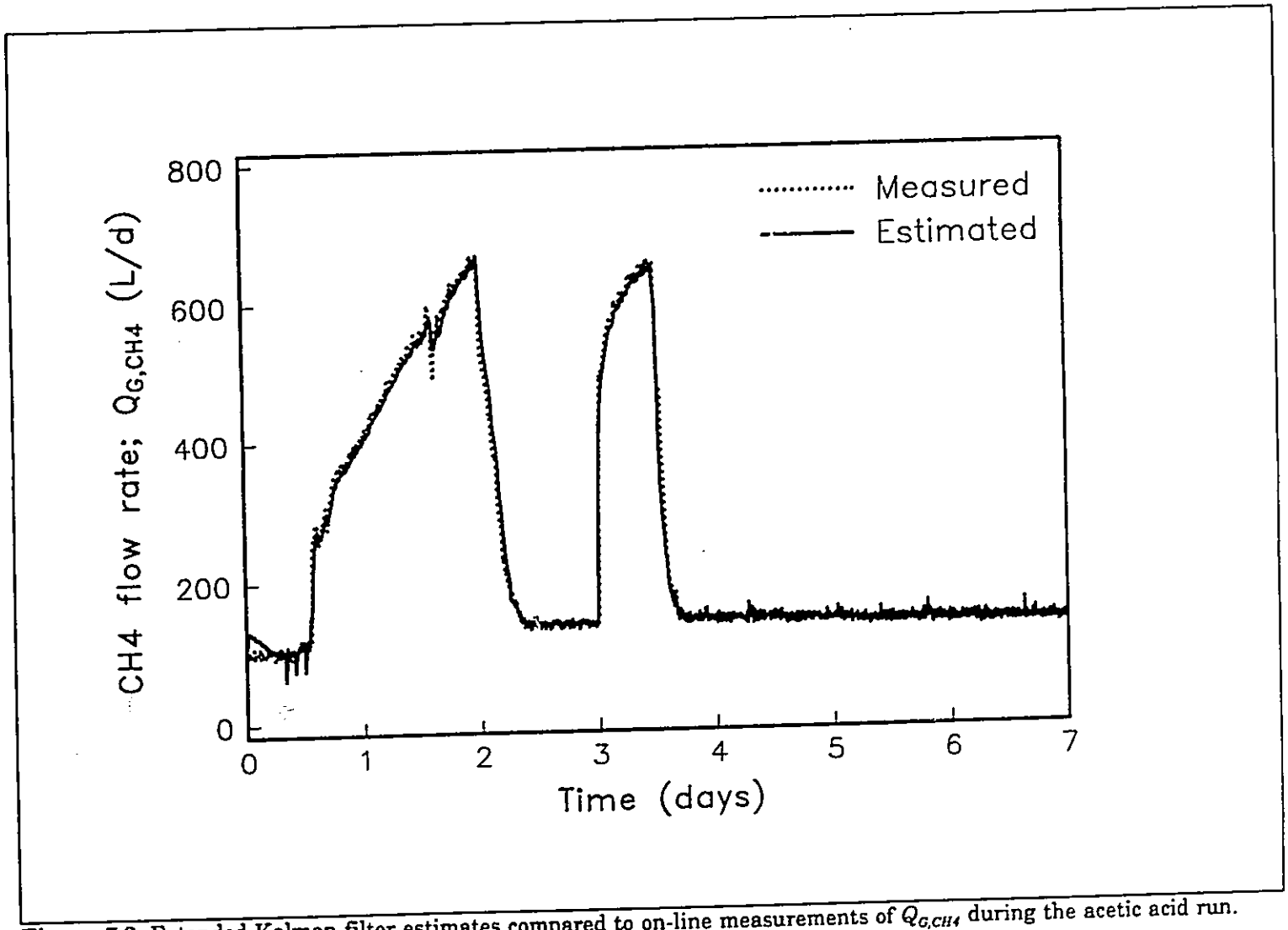

Figure 7.2: Extended Kalman filter estimates compared to on-line measurements of $Q_{G,CH4}$ during the acetic acid run.

The changes in the stochastic states required to achieve the performance observed in tracking the measured states are shown in Figure 7.3. The increased capacity of the process to degrade the influent acetic acid is reflected in increases in the estimated acetoclastic methanogen concentration during the influent pulses of acetic acid. With the exception of rapid variations between day 2 and day 4, the estimates of the acid-former concentration (X_{AF}) and the propionic acid utilizing acetogens (X_{PA}) were relatively constant during the run. The change in the mean level of X_{AF} between the beginning and the end of the run was probably due to a poor initial condition. The parameter states (f_P and η_{AF}) were relatively constant throughout the run (Figure 7.4).

It should be emphasized that the stochastic state estimates are only representative of true values of the stochastic states if the deterministic structure of the model, the value of all constant parameters in the model, and the value of all input variables are correct. A number of examples of changes in stochastic states to accommodate possible model errors can be found in this run. The rapid decrease in X_{AM} at the end of the first acetic acid pulse appears to be unrealistic. However, the effect of changes in X_{AM} in the model is to change the acetoclastic methanogen activity as represented by the product $\mu_{AM}X_{AM}$. Therefore, if the model structure does not change μ_{AM} rapidly enough, this can be accommodated through changes in X_{AM}. Another possible cause for such a rapid decrease in X_{AM} is an error in the value of $S_{A,0}$. If the actual acetic acid pulse ended before the value of $S_{A,0}$ was decreased in the model, the state estimator would attempt to track the decreasing methane flow rate ($Q_{G,CH4}$) by decreasing X_{AM}. However, the increasing mean level in X_{AM} during the acetic acid run would be consistent with a higher growth rate due to increased levels in substrate concentration. Another example can be seen in the rapid changes in the estimated values of X_{AF} and X_{PA} between days 2 and 4. The increase in the estimated value of $S_{COD,I}$ (Figure 7.1) between day 3 and day 4 appeared to occur as the result of a rapid decrease in the estimated value of X_{AF} (Figure 7.3). This transient corresponds to the start of the second acetic acid pulse. The decrease in the values

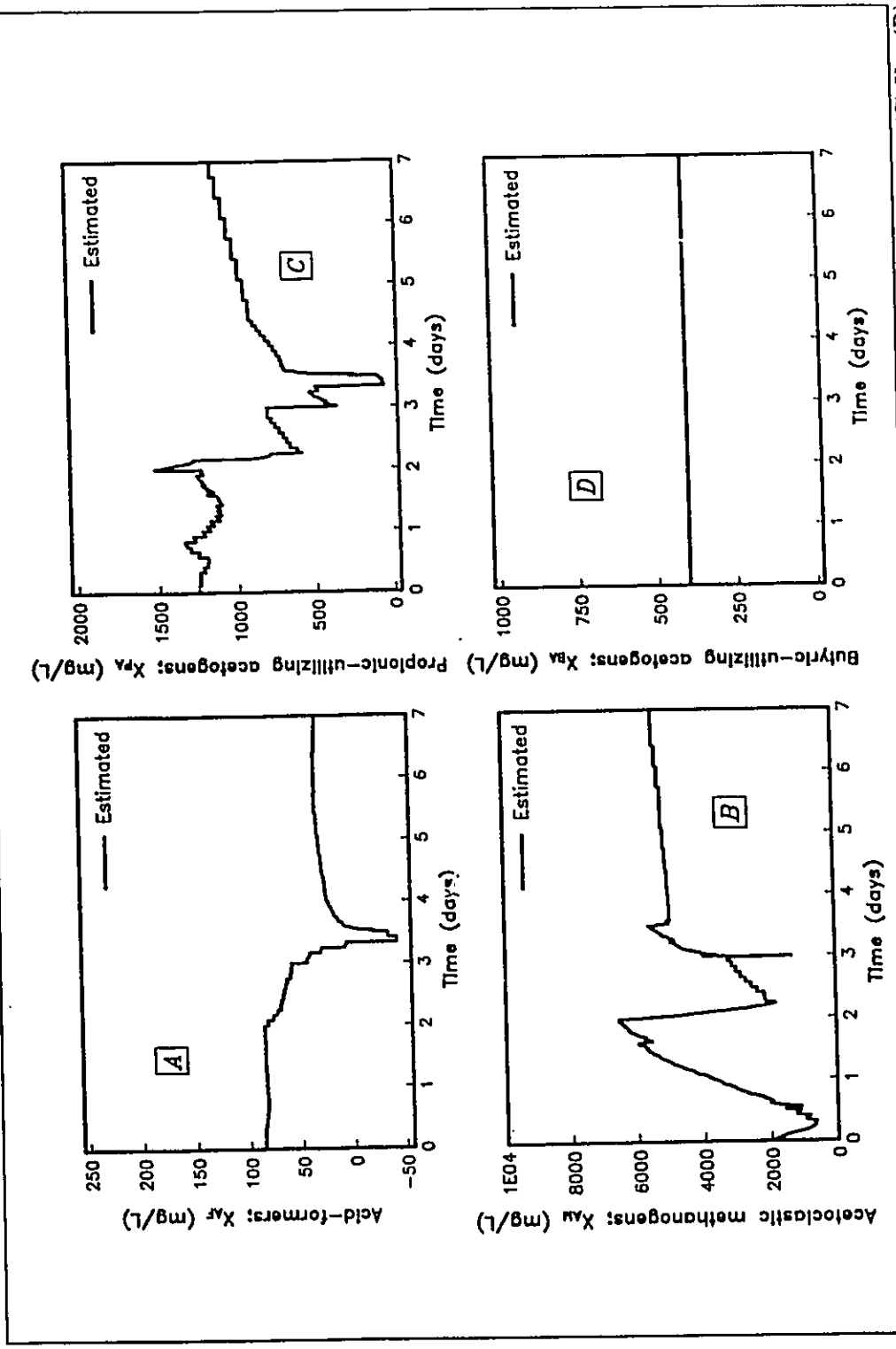

Figure 7.3: Extended Kalman filter estimates of stochastic states during the acetic acid run - (A) X_{AF}; (B) X_{AM}; (C) X_{PA}; (D) X_{BA}.

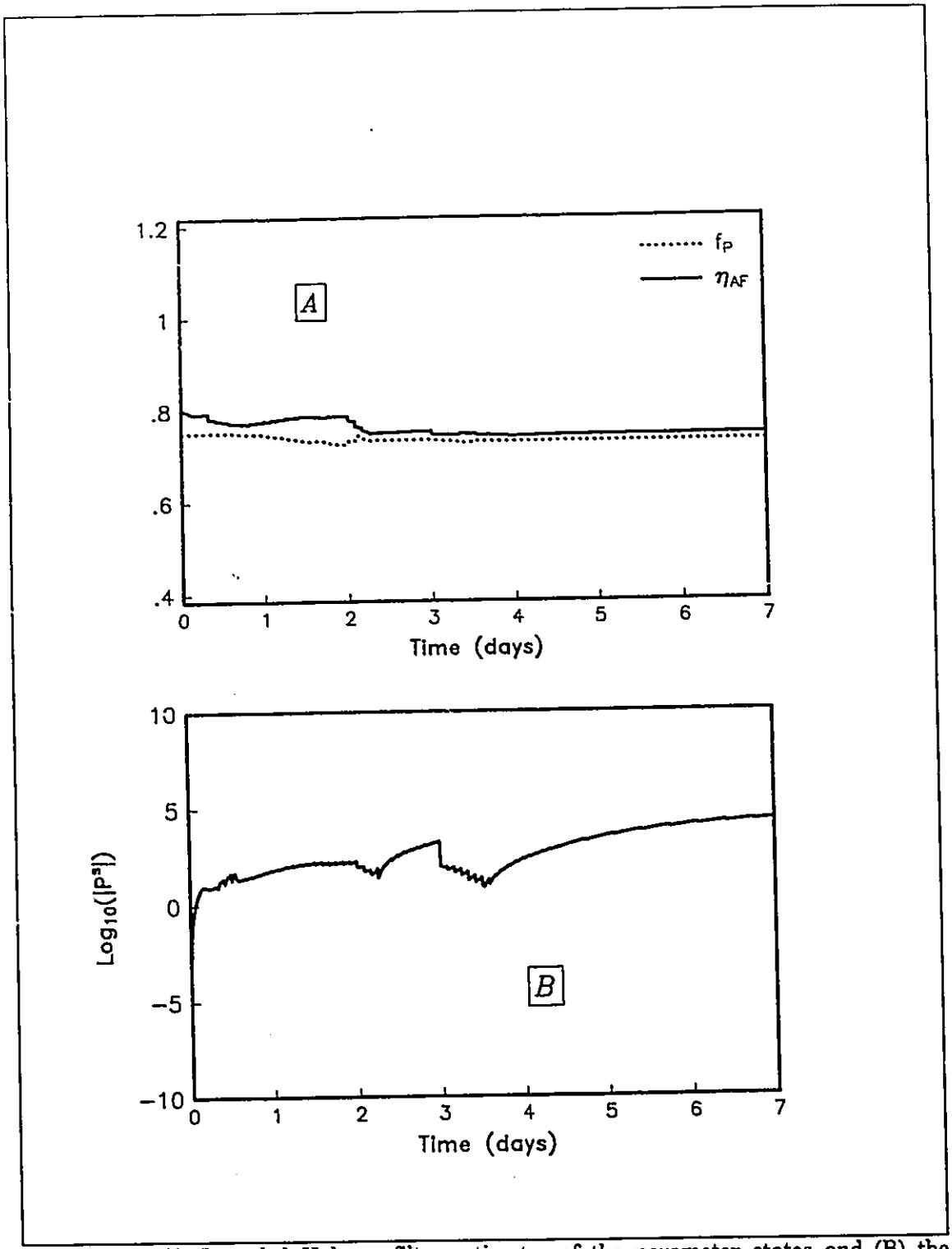

Figure 7.4: (A) Extended Kalman filter estimates of the parameter states and (B) the determinant of the variance-covariance matrix for the stochastic and parameter states ($|\underline{P}^a|$) during the acetic acid run.

of X_{AF} and X_{PA} at this time may have been due to an effort by the state estimator to decrease the production rate of acetic acid to accommodate the overestimated value of $S_{A,I}$.

The logarithm of the determinant of $\underline{P}^+$ calculated during the acetic acid run is plotted in Figure 7.4. As was observed in the simulated state estimation runs discussed in Chapter 6, the value of the determinant appears to decrease when the process undergoes a large transient, reflecting the increased amount of information provided for state estimation when the process is perturbed.

Table 7.2 shows the correlation coefficient matrix for the estimated stochastic states and parameters as calculated at day 7 of the run. There are no large correlations between the states or parameters indicating that the state estimation problem was not overspecified.

Table 7.2: Correlation coefficient matrix for estimated stochastic states at the end of the acetic acid run

	X_{AF}	X_{PA}	X_{AM}	η_{AF}	f_P
X_{AF}	1.00				
X_{PA}	-0.051	1.00			
X_{AM}	-0.027	-0.015	1.00		
η_{AF}	-0.027	-0.016	-0.0085	1.00	
f_P	0.0026	-0.0039	-0.0023	0.11	1.00

7.1.2 Propionic Acid Run

State and parameter estimation for the propionic acid run was conducted as a continuation of the acetic acid run. The results from the propionic acid portion of the run are plotted in Figures 7.5 to 7.8. Figures 7.5 and 7.6 indicate that the extended Kalman filter tracked the measurements reasonably well throughout the run, although $S_{A,I}$ appeared to be somewhat overestimated by the model between sample times. This reflects a bias in the estimate of $S_{A,I}$ which would become increasingly significant if the sampling interval was

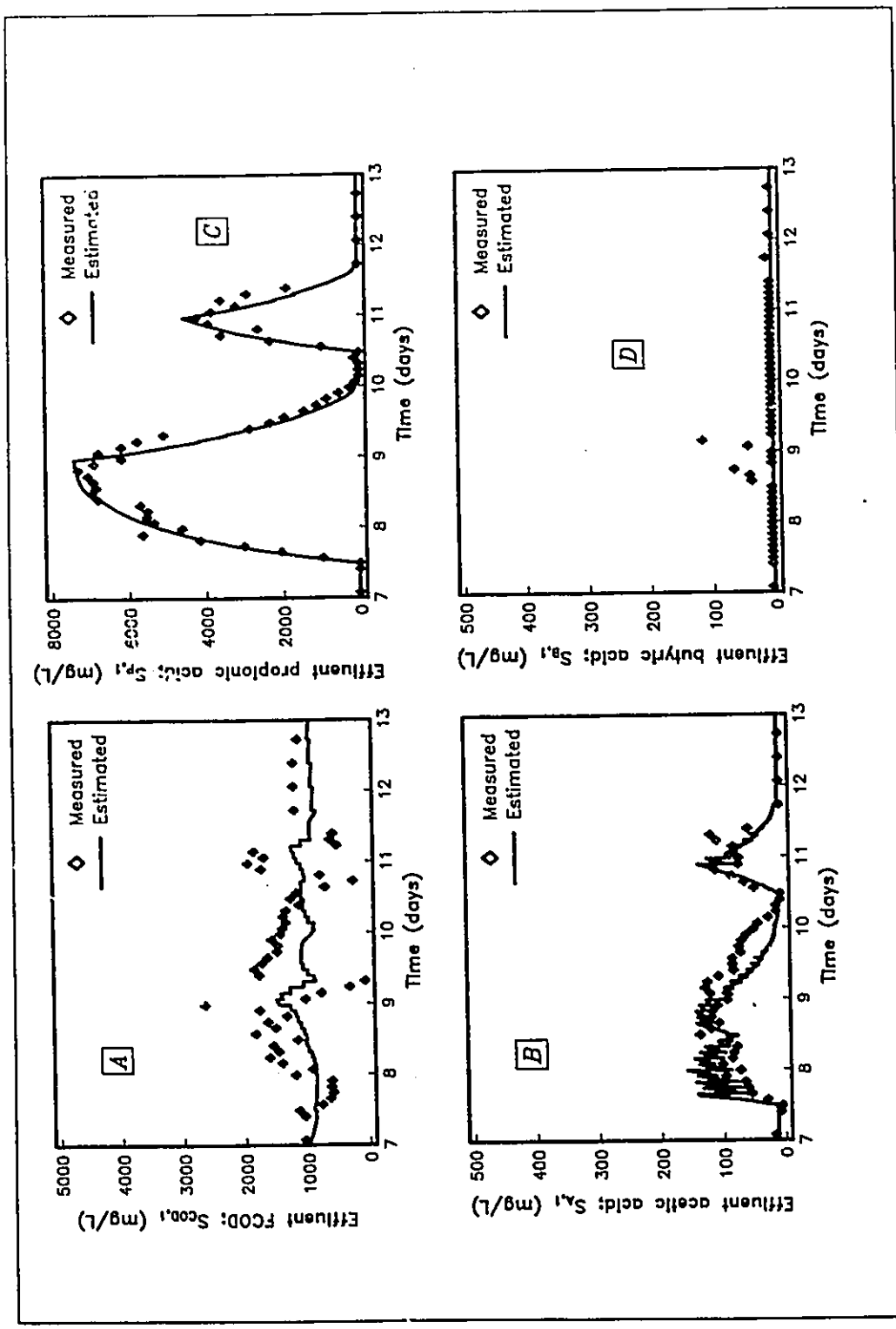

Figure 7.5: Extended Kalman filter state estimates compared to off-line measurements during the propionic acid run - (A) $S_{COD,1}$; (B) $S_{A,1}$; (C) $S_{P,1}$; (D) $S_{B,1}$.

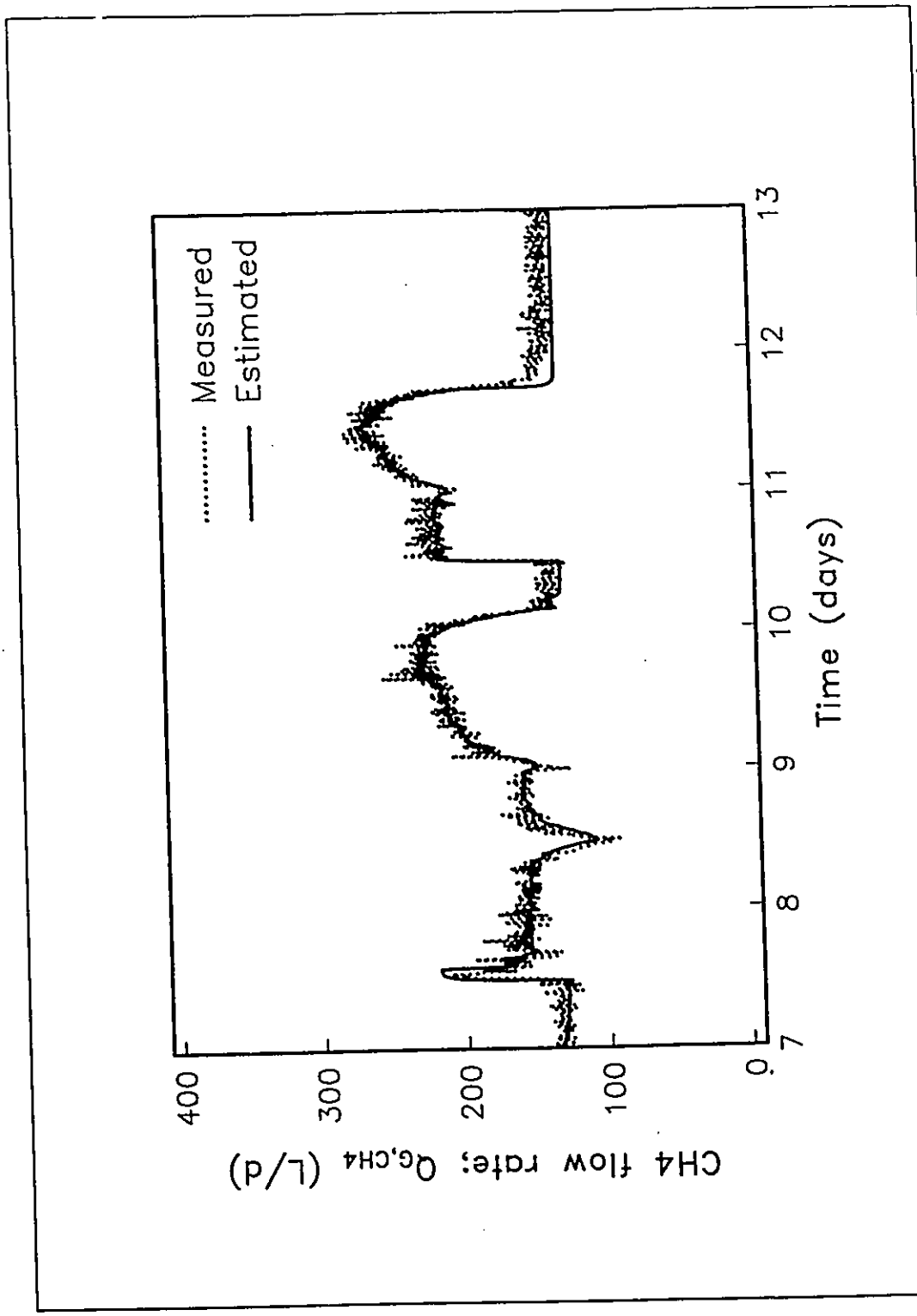

Figure 7.6: Extended Kalman filter estimates compared to on-line measurements of $Q_{G,CH4}$ during the propionic acid run.

increased.

Figure 7.7 shows the variations in the stochastic states estimated by the extended Kalman filter. The estimates of X_{AF} fluctuated around a constant mean level throughout the run. The estimated value of X_{AM} continued to increase over this portion of the run, as would be expected due to the increased substrate concentrations in the system. The rapid decrease in X_{PA} at the beginning of the first pulse may indicate that the propionate-utilizing bacteria were substrate inhibited. However, the behaviour of the X_{PA} estimate may also indicate that a poor initial condition was used for this state. The step in the propionic acid concentration in this portion of the experiment was the first time in the experiment that there was sufficient information in the data for the estimator to determine this.

Figure 7.8 shows that estimated parameters f_P and η_{AF} were constant throughout the run. The determinant of $\underline{P}^*$ decreased sharply at the start of the first propionic acid pulse, reflecting the increase in information for state estimation. The correlation coefficient matrix calculated on day 14 (Table 7.3) showed no high correlations between stochastic states and parameters.

Table 7.3: Correlation coefficient matrix for estimated stochastic states at the end of the propionic acid run

	X_{AF}	X_{PA}	X_{AM}	η_{AF}	f_P
X_{AF}	1.00				
X_{PA}	-0.035	1.00			
X_{AM}	-0.0016	-0.0063	1.00		
η_{AF}	0.024	-0.0067	-0.0026	1.00	
f_P	0.0026	-0.00058	-0.00028	0.11	1.00

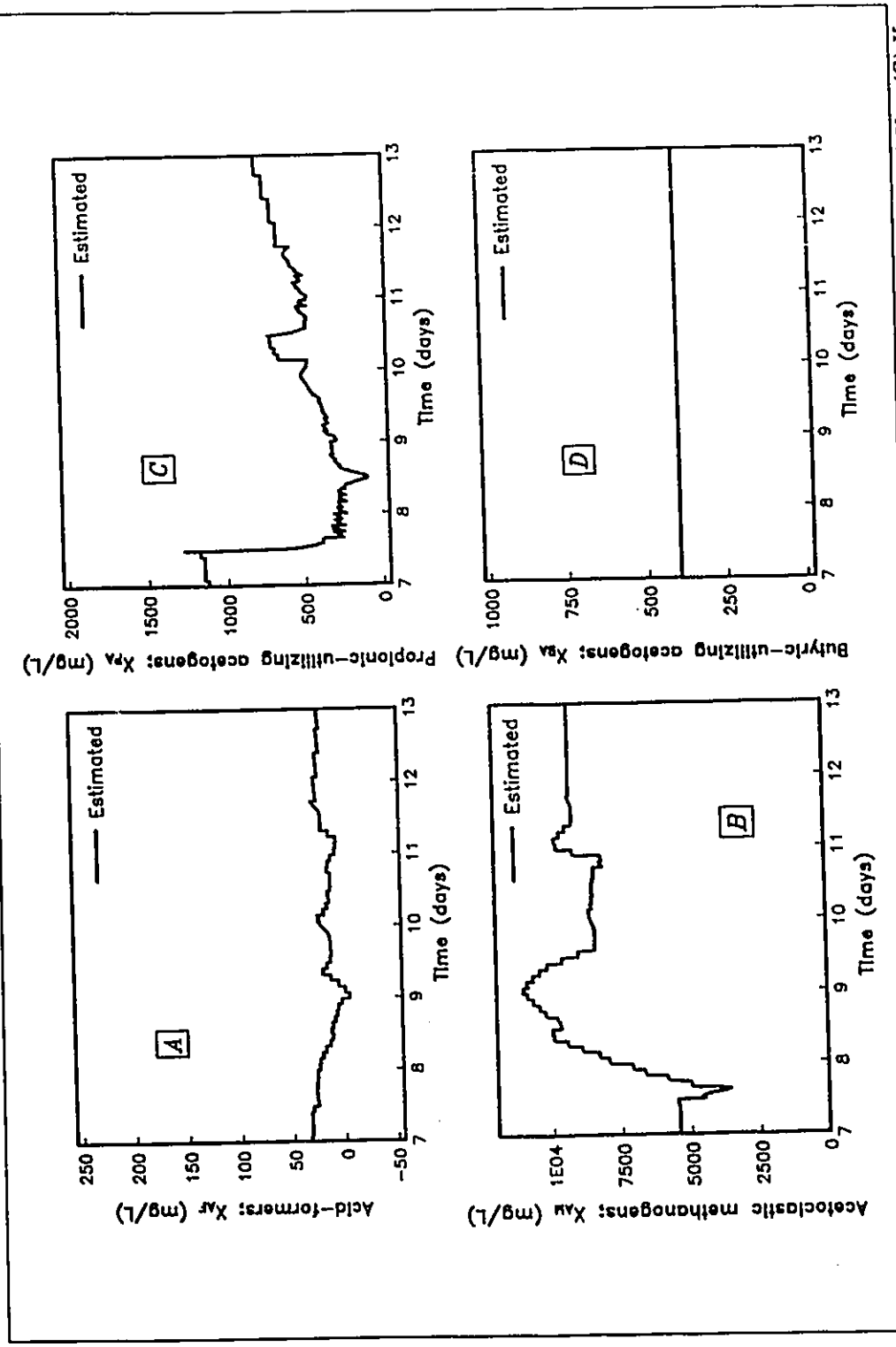

Figure 7.7: Extended Kalman filter estimates of stochastic states during the propionic acid run - (A) X_{AF}; (B) X_{AM}; (C) X_{PA}; (D) X_{BA}.

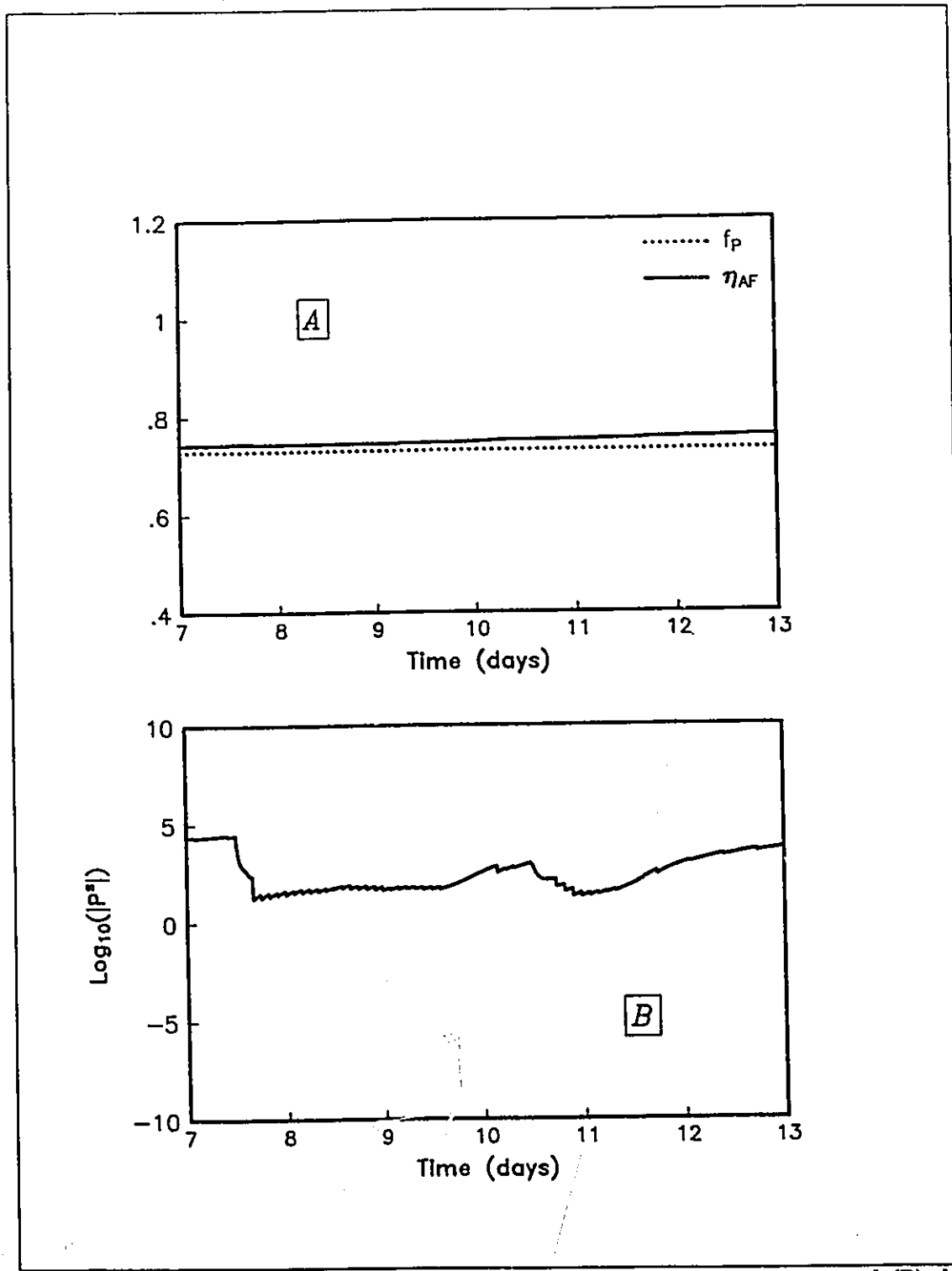

Figure 7.8: (A) Extended Kalman filter estimates of the parameter states and (B) the determinant of the variance-covariance matrix for the stochastic and parameter states ($|\underline{P}^a|$) during the propionic acid run.

7.1.3 Glucose Run #2

State and parameter estimation for glucose run #2 was conducted as a continuation of the propionic acid run. However, at the start of the first glucose pulse, the state covariance matrix was modified as follows to allow the state estimator to adapt quickly to the change in process conditions:

$$P_{12,12} = 10*P_{12,12};$$

$$P_{9,9} = 10*P_{9,9}.$$

To allow for the increased magnitude in the variation of the acid-former concentration (X_{AF}) expected during the pulse addition of glucose to the feed, the $\underline{R}_w$ matrix was modified as follows:

$$R_{w\,9,9} = 100*R_{w\,9,9}$$

The state and parameter estimation results for the glucose portion of the run are shown in Figures 7.9 to 7.12. $S_{COD,I}$ appears to be tracked reasonably well throughout the run. $S_{A,I}$ and $S_{P,I}$ appear to be underestimated between days 17 and 22. Both $S_{A,I}$ and $S_{II,I}$ are underestimated around day 30. A possible reason for the underestimation of the volatile acids is that volatile acids produced by the acid-former organisms in the suspended phase of the reactor were less readily available to acetogenic and methanogenic organisms in the fixed film phase of the reactor. This could be caused by mass transfer limitations in the system. However, the analysis presented in Chapter 5 indicated that mass transfer limitations to volatile acid consumption should not be a significant factor.

Figure 7.11 shows the large changes required in the stochastic states at the beginning of the glucose pulses. X_{AF} required a tenfold increase at the beginning of each influent glucose pulse. As discussed in Chapter 4, a rapid growth in suspended solids which may have been partially comprised of acid-former bacteria was observed during this period of experimentation. However, the change in the estimate of X_{AF} was too rapid to be completely explained by actual acid-former growth. Another possible reason for this major adjustment in the model is that

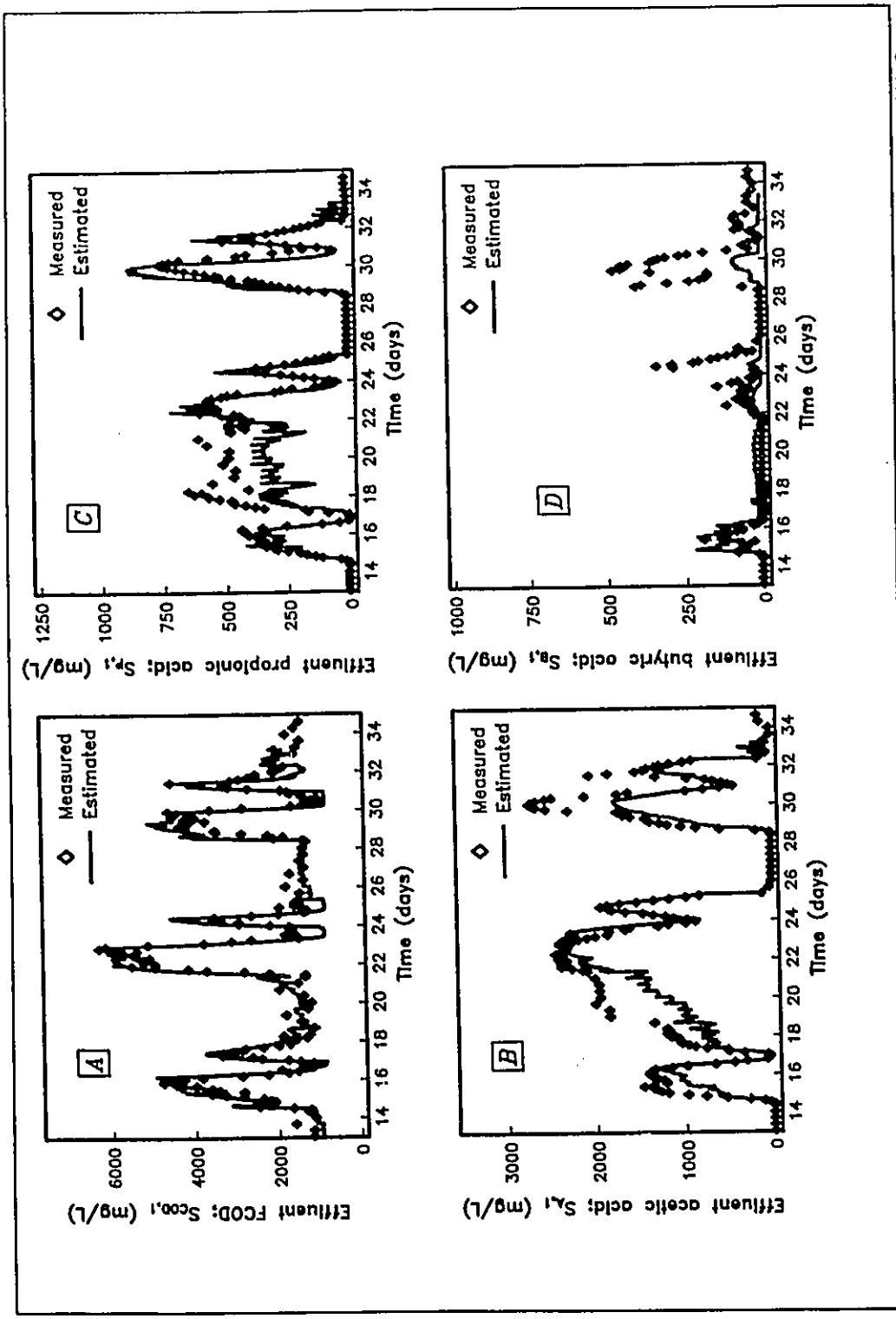

Figure 7.9: Extended Kalman filter state estimates compared to off-line measurements during glucose run #2 - (A) $S_{COD,I}$; (B) $S_{A,I}$; (C) $S_{P,I}$; (D) $S_{B,I}$.

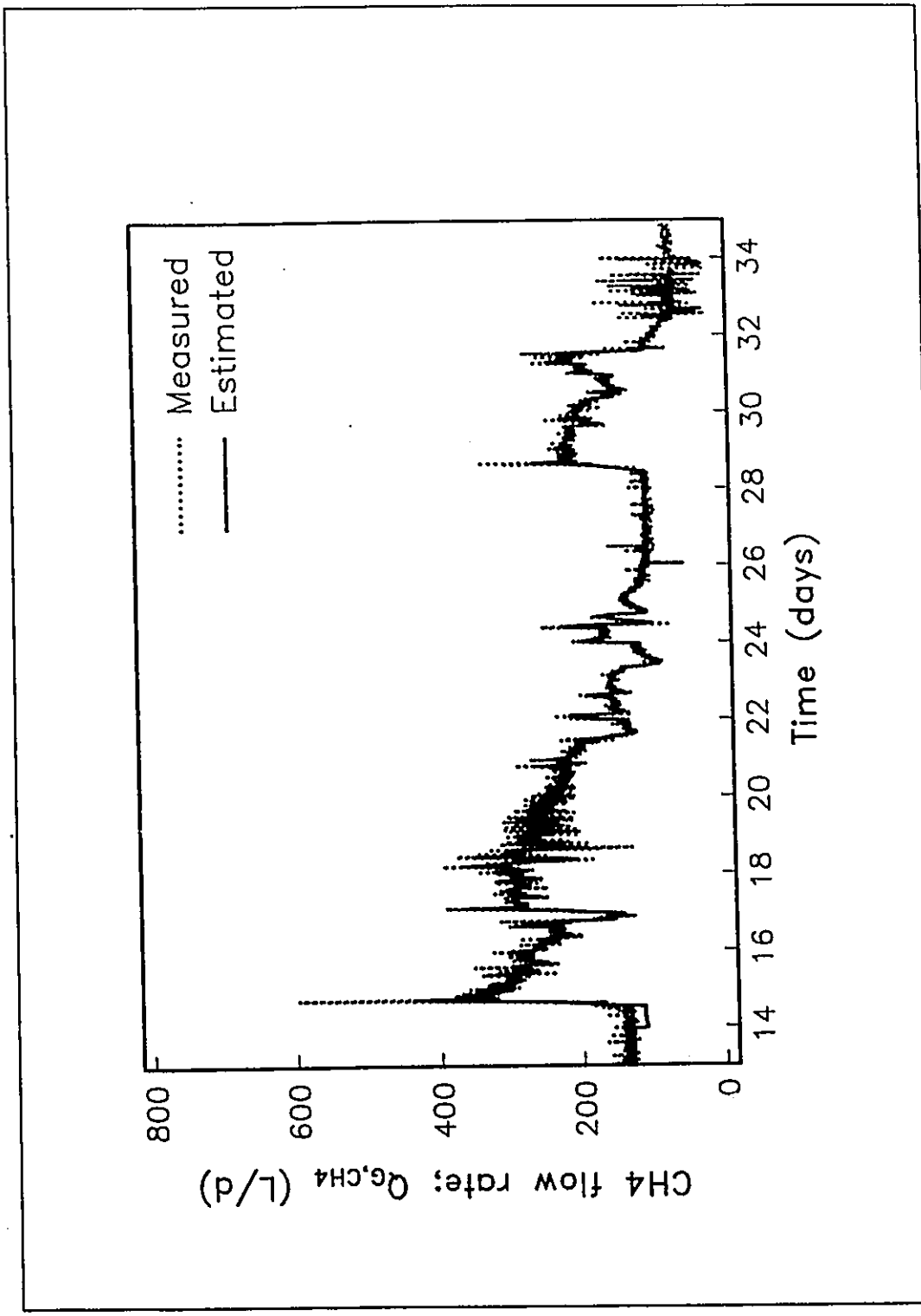

Figure 7.10: Extended Kalman filter estimates compared to on-line measurements of $Q_{G,CH4}$ during glucose run #2.

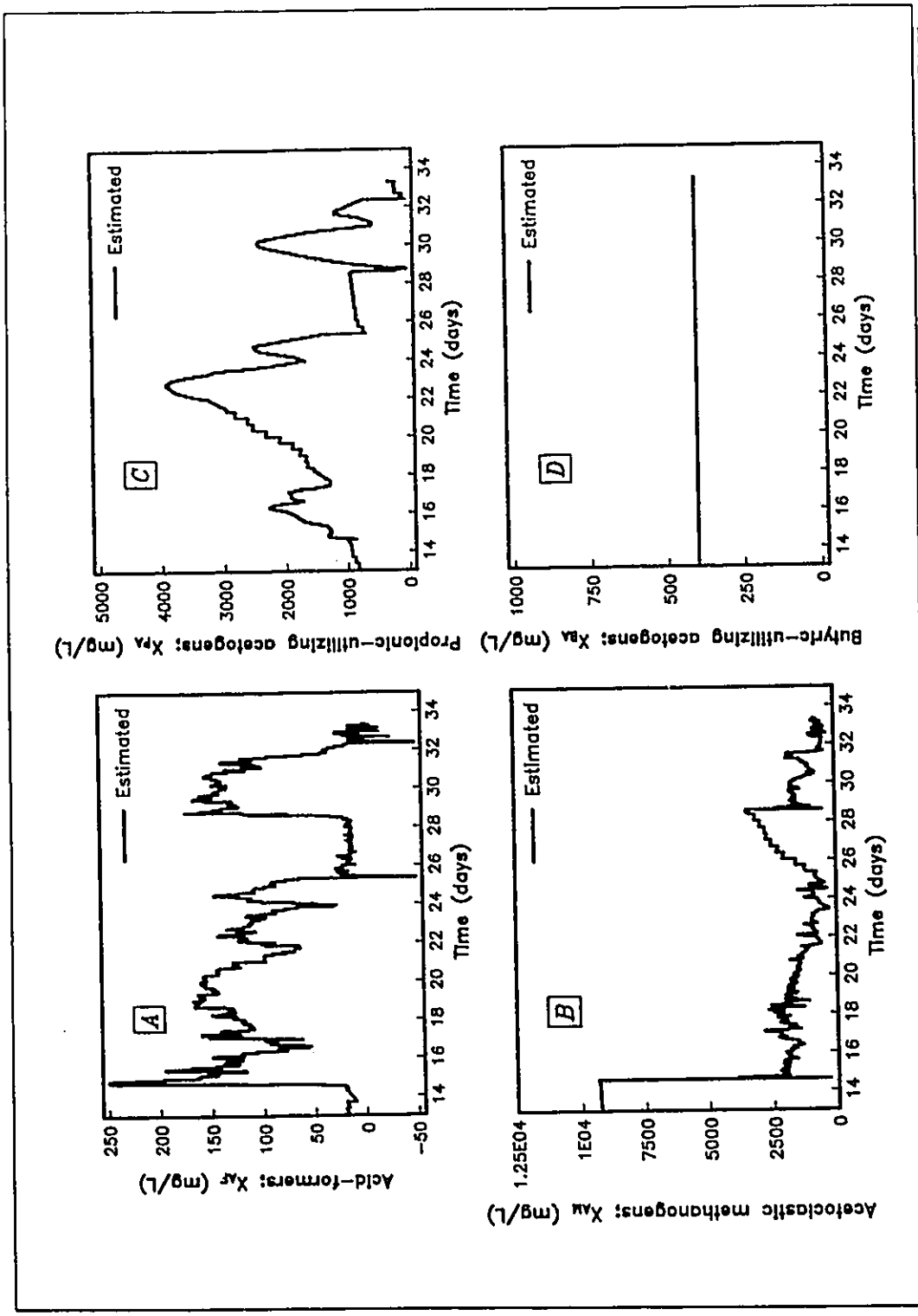

Figure 7.11: Extended Kalman filter estimates of stochastic states during glucose run #2 - (A) X_{AF}; (B) X_{AM}; (C) X_{PA}; (D) X_{BA}.

the substrates in the baseline stillage feed were less readily biodegradable than glucose. A major change in the kinetics would be required for the model to predict the acid-former substrate degradation when the glucose pulses were introduced to the system. The extended Kalman filter also estimated a large decrease in X_{AM} at the start of the glucose pulses near day 15. However, this adjustment may also have been made to accommodate the change in the kinetics of the acid-formers. It is also impossible to determine if the estimated variations in X_{PA} and f_P (Figure 7.12) are realistic without first investigating the possible model inadequacies. The underestimation of $S_{B,I}$ near day 30 was probably caused by the increase in f_P.

The fact that there were no major increases in the value of the determinant of $\underline{P}^*$ (Figure 7.12) indicates that variations in the stochastic states and parameters were not due to ill-conditioning of the state estimation problem. The result of an ill-conditioned state estimation problem is that large changes in the unmeasured state variables (such as the stochastic states and parameters) can occur without significantly affecting the estimated values of the measured states. The correlation coefficient matrix is shown in Table 7.4. The slight negative correlation apparent between X_{AF} and X_{AM} indicates that some degree of variation in one of these states may have been due to changes in the other state.

Table 7.4: Correlation coefficient matrix for estimated stochastic states at the end of glucose run #2

	X_{AF}	X_{PA}	X_{AM}	η_{AF}	f_P
X_{AF}	1.00				
X_{PA}	-0.11	1.00			
X_{AM}	-0.34	-0.022	1.00		
η_{AF}	0.00042	-0.00092	-0.00018	1.00	
f_P	0.00002	0.00077	-0.00016	0.28	1.00

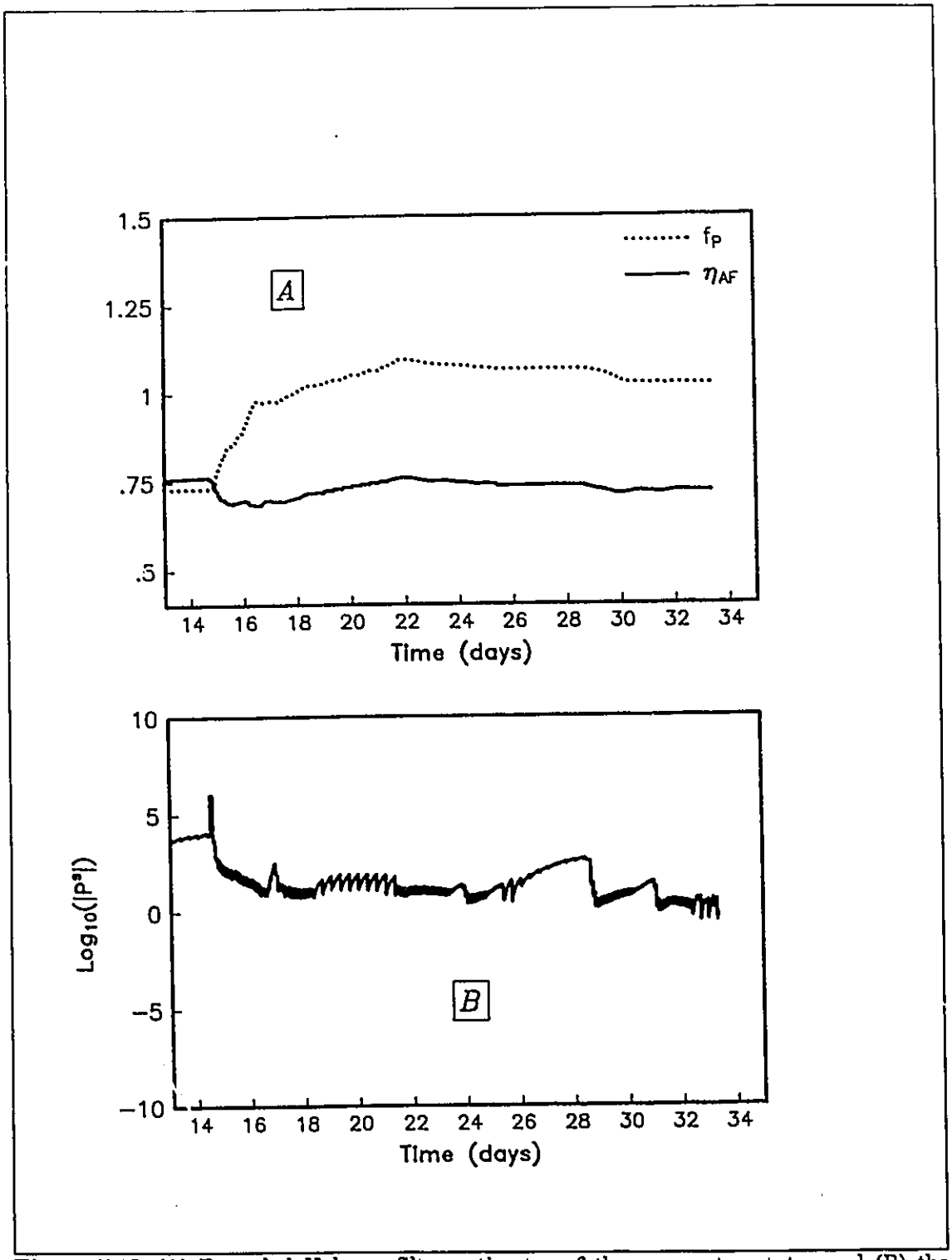

Figure 7.12: (A) Extended Kalman filter estimates of the parameter states and (B) the determinant of the variance-covariance matrix for the stochastic and parameter states ($|\underline{P}^*|$) during glucose run #2.

7.1.4 Butyric Acid Run

Table 7.5 lists the state initial conditions, and the settings for the diagonal elements of $\underline{R}_v$ and $\underline{P}_o$ for the butyric acid run. State and parameter estimation results during the butyric acid run are summarized in Figures 7.13 to 7.16. In this run, the parameter state η_{AP} was replaced with the stochastic state X_{BA} in the subset of estimated stochastic and parameter states.

The deterministic model portion of the Kalman filter would not predict any variation in $S_{COD,I}$ during a pulse in butyric acid substrate. However, a large amount of random noise is apparent in the $S_{COD,I}$ measurements during the experiment (Figure 7.13). The fact that the state estimator did not completely filter the variations in $S_{COD,I}$ indicates that the measurement variance was not set sufficiently high in $\underline{R}_v$. The estimated variations in X_{AP} (Figure 7.14) may therefore have resulted from the tracking of the random noise in $S_{COD,I}$. Throughout the run, the model does not appear to be adapting quickly enough to estimate the trends in $S_{A,I}$, $S_{P,I}$, and $S_{B,I}$ (Figure 7.13). Until day 4 of the run, the estimates of X_{AM} appear to essentially be following the trends in $Q_{G,CH4}$ (Figure 7.15). After day 4, the large variations in X_{AM} and the increase of several orders of magnitude in the value of the determinant of $\underline{P}^+$ (Figure 7.16) indicate that the state estimation problem may be ill-conditioned. The estimated value of f_P also changed rapidly during this period. The decrease in the estimated value of X_{BA} between day 2 and 3 of the run could be explained by substrate inhibition of the butyrate-utilizing bacteria. Because substrate inhibition was not included in the deterministic model, some of the variations in the estimates of X_{BA}, X_{PA}, and X_{AM} may have been due to this inadequacy in the model structure. There were no high correlations between stochastic states and parameters at the end of the butyric acid run (Table 7.6).

Table 7.5: Initial conditions for butyric acid state estimation run

State ($\underline{x}$)	Initial conditions ($\underline{x}_0$)	Diagonal elements $\underline{R}_w$	Diagonal elements $\underline{P}_0$
$S_{G,1}$	300 mg/L	1.0	0.0
$S_{P,1}$	5 mg/L	10.0	1.0
$S_{B,1}$	2 mg/L	0.10	1.00
$S_{A,1}$	30 mg/L	10.00	0.001
$S_{Z,1}$	18 mmole/L	5.00	0.10
$S_{IC,1}$	25 mmole/L	5.00	0.001
$S_{I,1}$	760 mg/L	0.0	0.0
P_{pCO2}	0.20 atm	0.001	0.00001
X_{AF}	15 mg/L	1.0	0.0
X_{PA}	40 mg/L	100.0	100.0
X_{BA}	400 mg/L	100.0	100.0
X_{AM}	1000 mg/L	100.0	100.0
η_{AF}	0.80	0.0	0.0
$K_{I,AM}$	1000 mg/L	0.0	0.0
K_{AF}	300 mg/L	0.0	0.0
K_{PA}	130 mg/L	0.0	0.0
K_{BA}	10 mg/L	0.0	0.0
K_{AM}	75 mg/L	0.0	0.0
$K_{I,PA}$	500 mg/L	0.0	0.0
$K_{I,BA}$	1000 mg/L	0.0	0.0
$K_{I,GA}$	250 mg/L	0.0	0.0
f_P	0.75	0.0	0.0001
K_{GP}	1000 mg/L	0.0	0.0

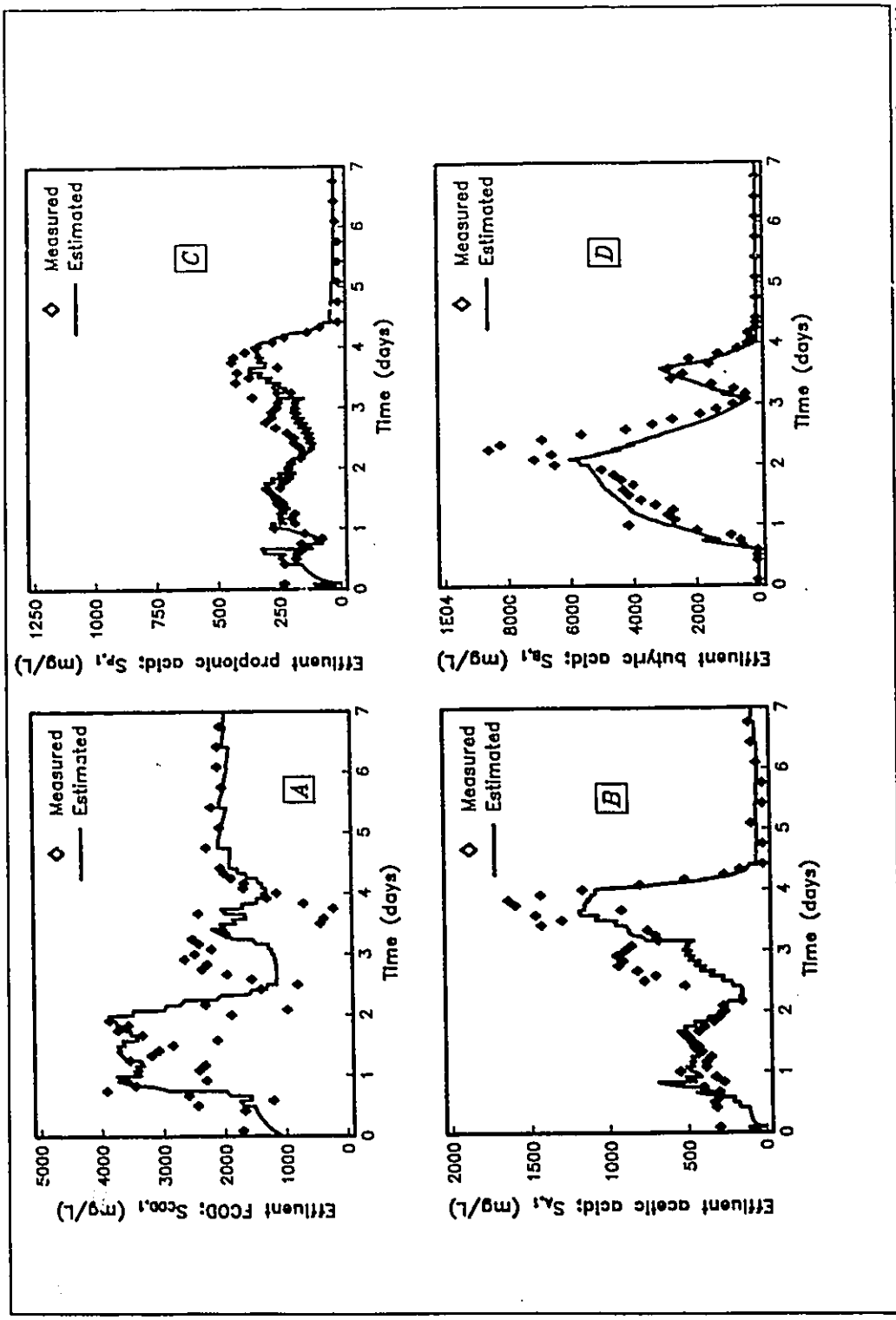

Figure 7.13: Extended Kalman filter state estimates compared to off-line measurements during the butyric acid run - (A) $S_{COD,1}$; (B) $S_{A,1}$; (C) $S_{P,1}$; (D) $S_{B,1}$.

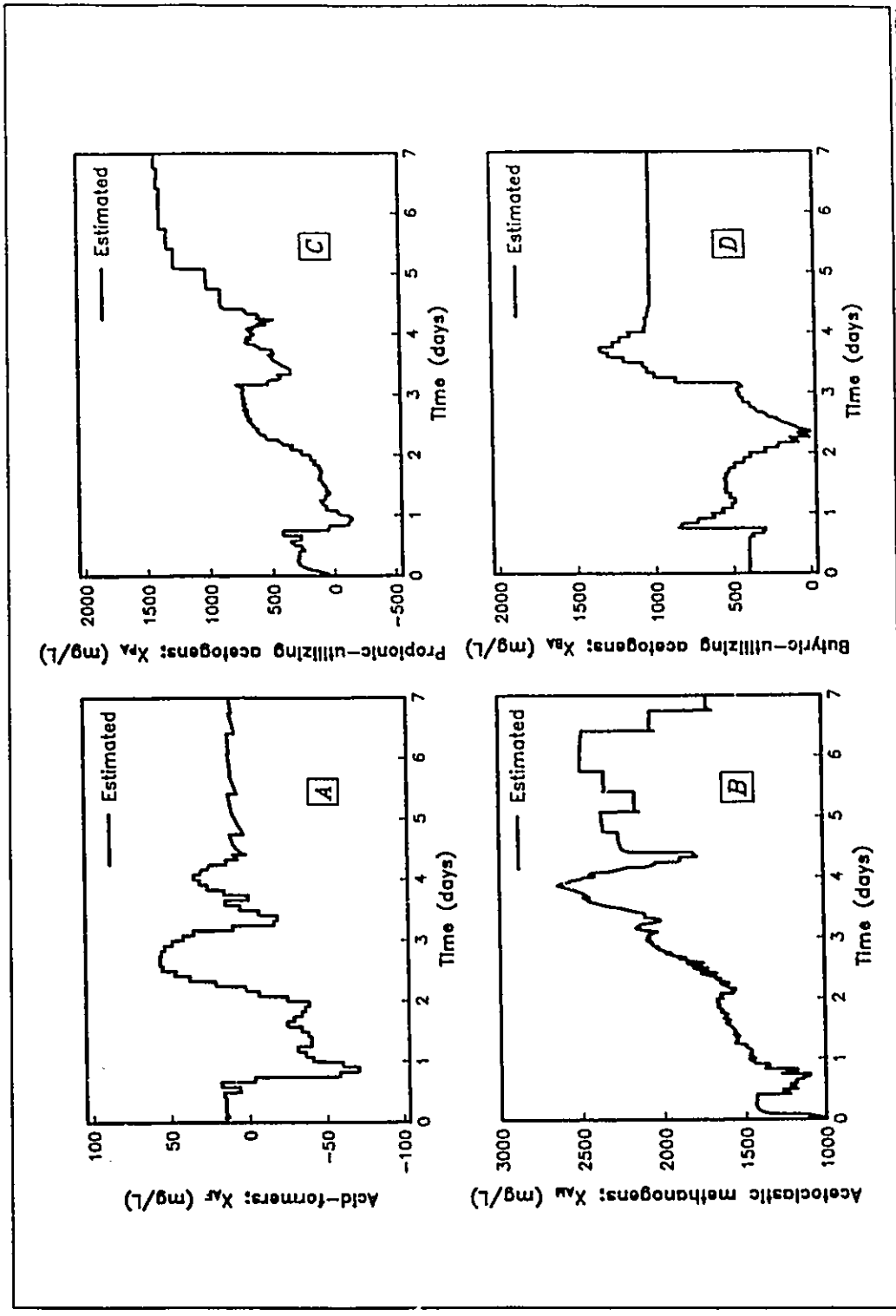

Figure 7.14: Extended Kalman filter estimates of stochastic states during the butyric acid run - (A) X_{AF}; (B) X_{AM}; (C) X_{PA}; (D) X_{BA}.

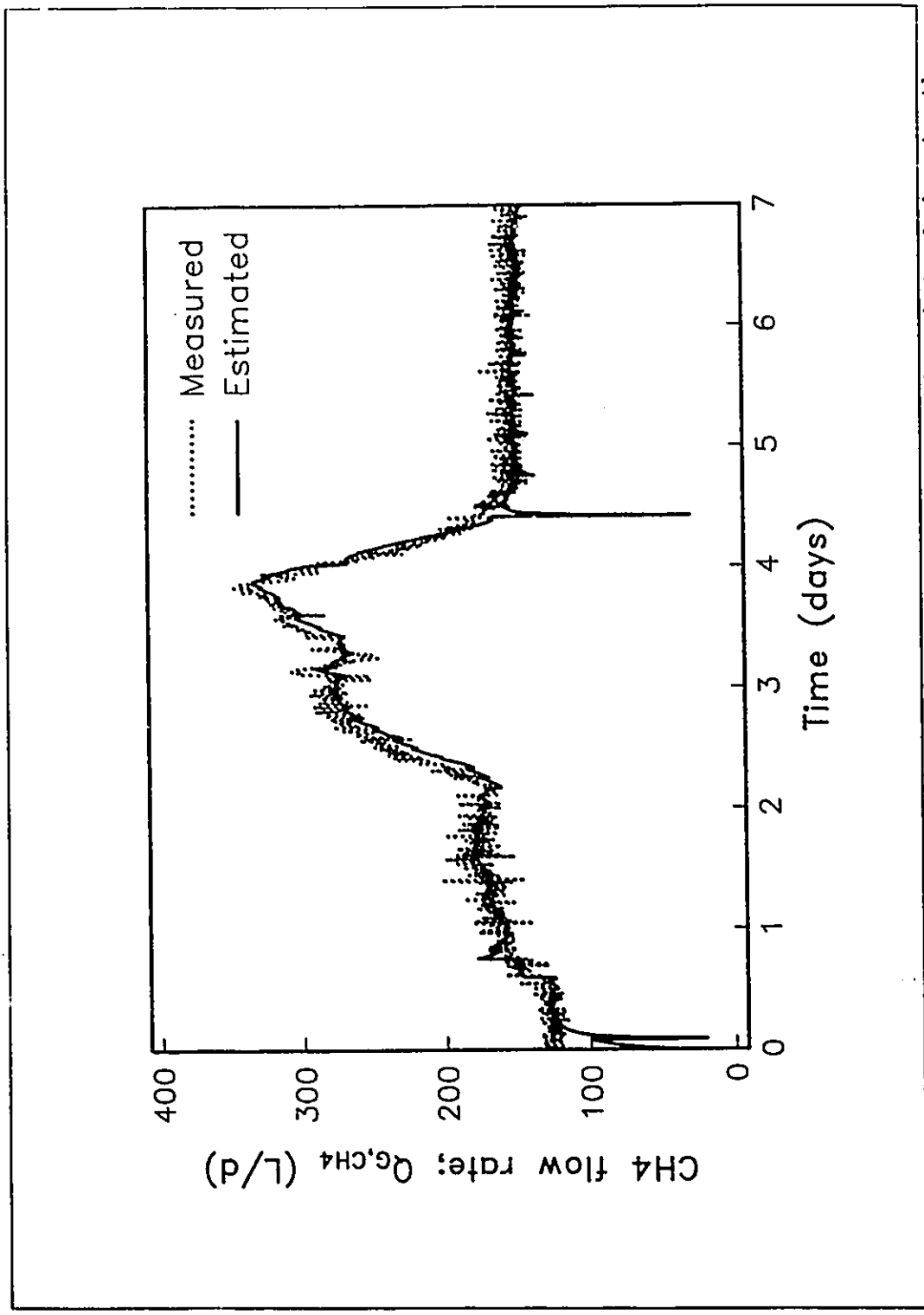

Figure 7.15: Extended Kalman filter estimates compared to on-line measurements of $Q_{G,CH4}$ during the butyric acid run.

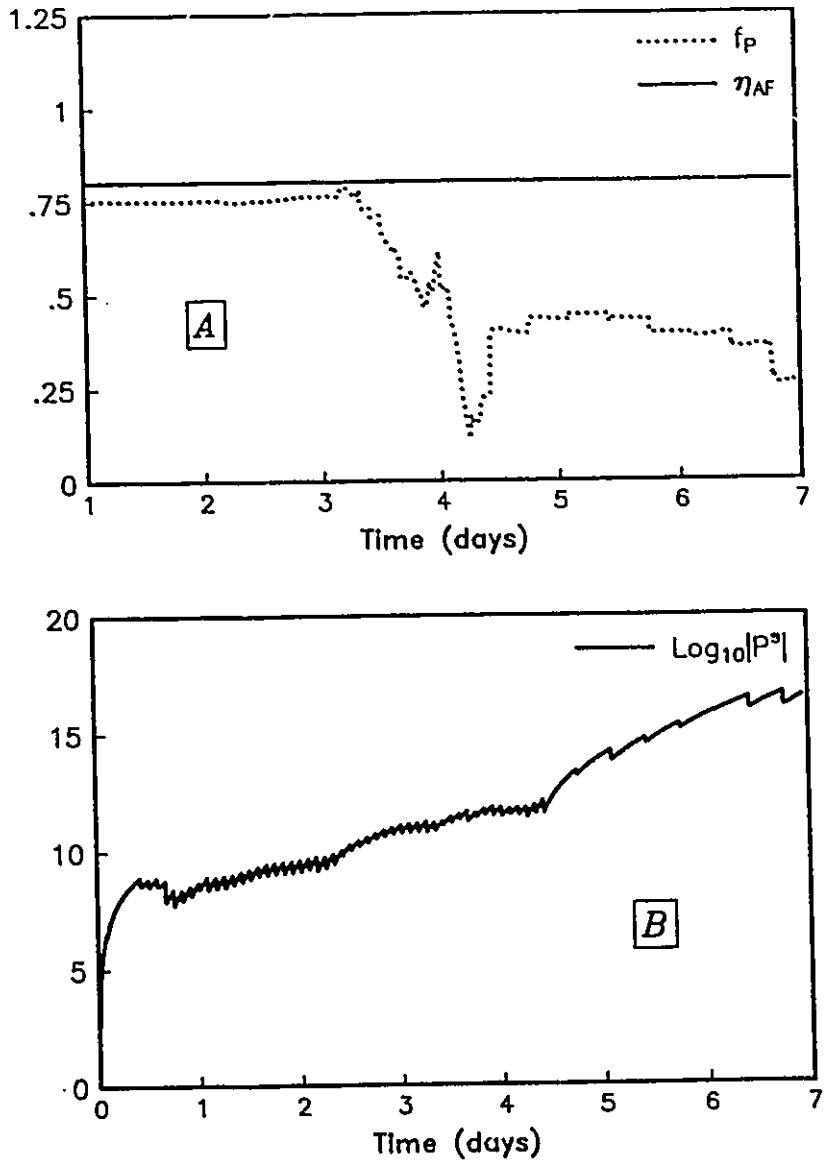

Figure 7.16: (A) Extended Kalman filter estimates of the parameter states and (B) the determinant of the variance-covariance matrix for the stochastic and parameter states ($|\underline{P}^*|$) during the butyric acid run.

Table 7.6: Correlation coefficient matrix for estimated stochastic states at the end of the butyric acid run

	X_{AF}	X_{PA}	X_{BA}	X_{AM}	f_P
X_{AF}	1.00				
X_{PA}	-0.052	1.00			
X_{BA}	-0.0016	-0.0088	1.00		
X_{AM}	-0.10	-0.13	-0.0020	1.00	
f_P	0.025	0.18	-0.049	0.036	1.00

7.1.5 Glucose Run #3

State and parameter estimation results for glucose run #3 are shown in Figures 7.17 to 7.20. The results plotted in Figure 7.17 indicate that the extended Kalman filter did not track $S_{COD,I}$, $S_{A,I}$, and $S_{P,I}$ very well, while estimates of $S_{B,I}$ were reasonable. The state estimates of $S_{COD,I}$ and X_{AF} (Figure 7.17) reinforce the hypothesis that different kinetics are required to model the degradation of different wastewater constituents in the feed. X_{AF} was increased by the state estimator at the start of a pulse (at times 0.5 days, 3 days, 6.5 days, and 9 days) to eliminate positive biases between the estimated and actual values of $S_{COD,I}$. X_{AF} was decreased by the state estimator at lower loading periods to eliminate a negative bias between estimated and actual values of $S_{COD,I}$. These results indicate that acid-former substrates in the stillage feed may have been less readily degradable than glucose. This factor may have been much more significant in this run than in glucose run #2. The measured values of $S_{COD,I}$ were much higher during baseline loading periods than in glucose run #2. A shipment of distillery wastewater feed was received before the butyric acid run (Table 3.2). These data indicate that this feed may have contained a lower concentration of readily degradable components than the distillery wastewater feed used during glucose run #2.

State estimates involving the acetogenic and methanogenic stages of the model may

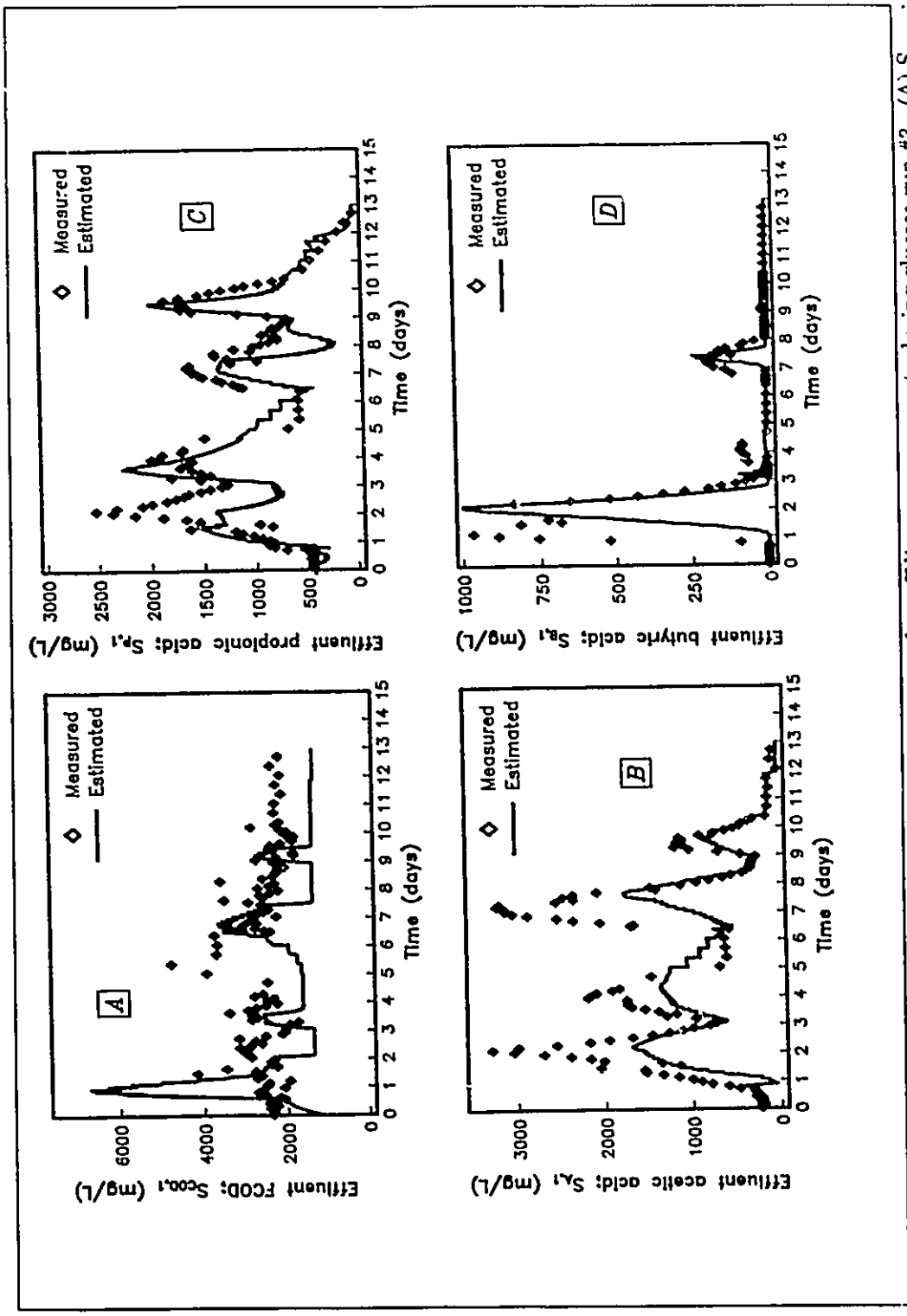

Figure 7.17: Extended Kalman filter state estimates compared to off-line measurements during glucose run #3 - (A) $S_{COD,1}$; (B) $S_{A,1}$; (C) $S_{P,1}$; (D) $S_{B,1}$.

also have been affected by the poor model performance at the acid-forming stage. For example, if the model underestimates the degradation rate of acid-former substrates, the production rate of acetic acid, propionic acid, and hydrogen will also be underestimated. This results in low estimates of $S_{A,I}$, $S_{P,I}$ and $Q_{G,CH4}$. In response, the state estimator reduces X_{AM} and X_{PA} to reduce the degradation rate of acetic acid and propionic acid to increase $S_{A,I}$ and $S_{P,I}$ while a low estimate of $Q_{G,CH4}$ tends to increase X_{AM} and X_{PA}. However, $Q_{G,CH4}$ (Figure 7.18) is measured at 10 minute intervals while $S_{A,I}$ and $S_{P,I}$ are measured at 2 hour intervals and the variance of the $Q_{G,CH4}$ measurements are lower than the variance of the $S_{A,I}$ and $S_{P,I}$ measurements at high concentrations (Table 6.7). Therefore, the $Q_{G,CH4}$ appeared to have the more significant effect on the stochastic state estimates. X_{AM} and X_{PA} estimates appeared to increase at the beginning of each glucose pulse in this experiment. Changes in the estimated values of η_{AF} and f_P (Figure 7.20) may also have been due to inadequacies in the acid-former kinetics. In summary, because of the sequential nature of the reactions in the process, any inadequacy in one portion of the model structure can have profound effects throughout the model.

7.2 DISCUSSION OF STATE AND PARAMETER ESTIMATION RESULTS: RECOMMENDATIONS FOR MODEL MODIFICATIONS

The previous section indicated that the extended Kalman filter state estimator could provide reasonable estimates of the measurements $S_{COD,I}$, $S_{A,I}$, $S_{P,I}$, $S_{B,I}$, and $Q_{G,CH4}$ during most of the dynamic experiments on the anaerobic fluidized bed pilot plant. However, the time-variable behaviour of the stochastic states (X_{AF}, X_{PA}, X_{BA}, and X_{AM}) indicated a number of model modifications which could be made. These changes could improve the open loop performance of the model and result in more realistic estimates of stochastic states and parameters by the state estimator. The following is a list of recommended model modifications to investigate.

1) The increase in X_{AM} during the acetic acid and propionic acid run indicated the inadequacy of the assumption of constant bacterial concentrations in a fluidized bed

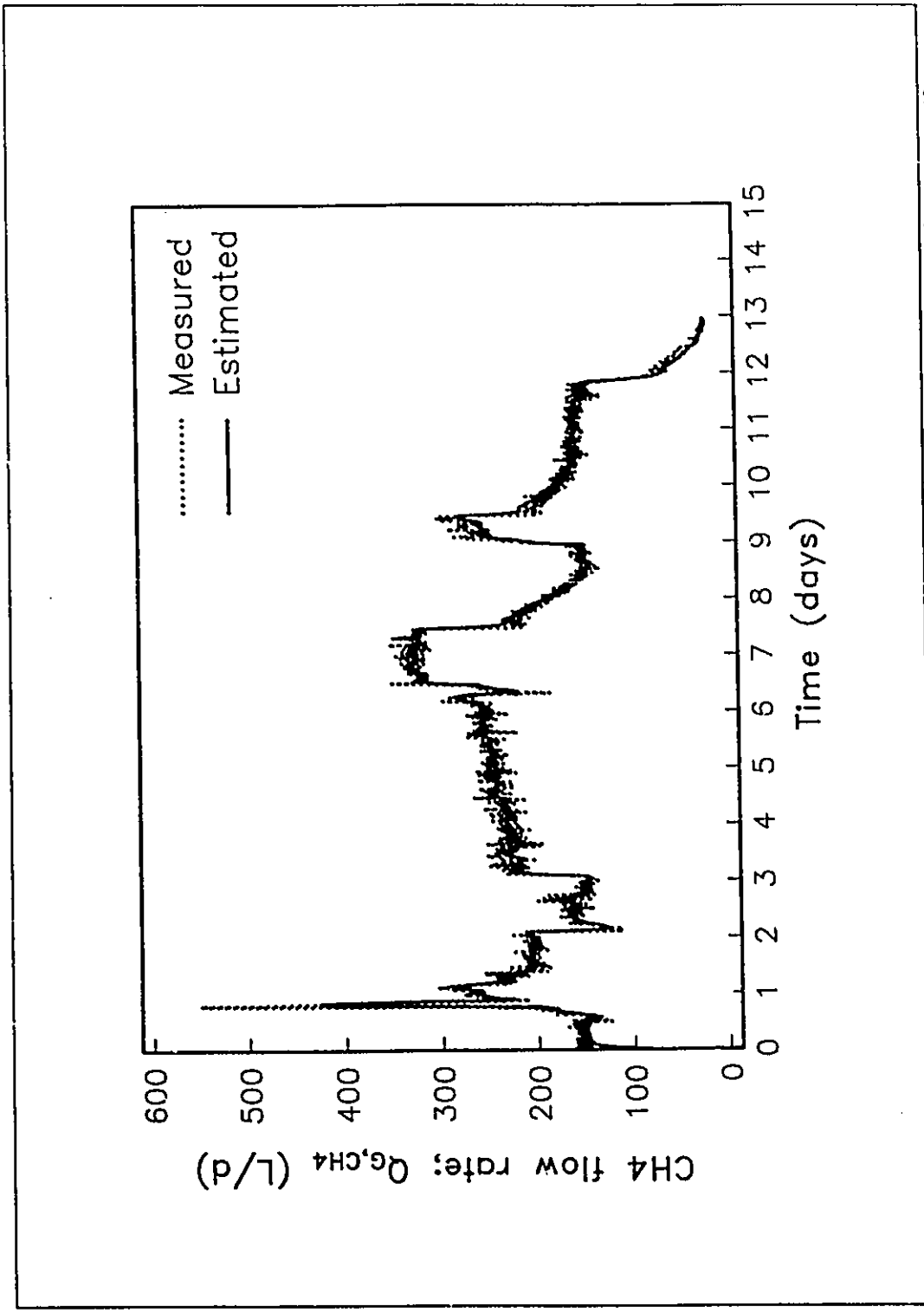

Figure 7.18: Extended Kalman filter estimates compared to on-line measurements of $Q_{G,CH4}$ during glucose run #3.

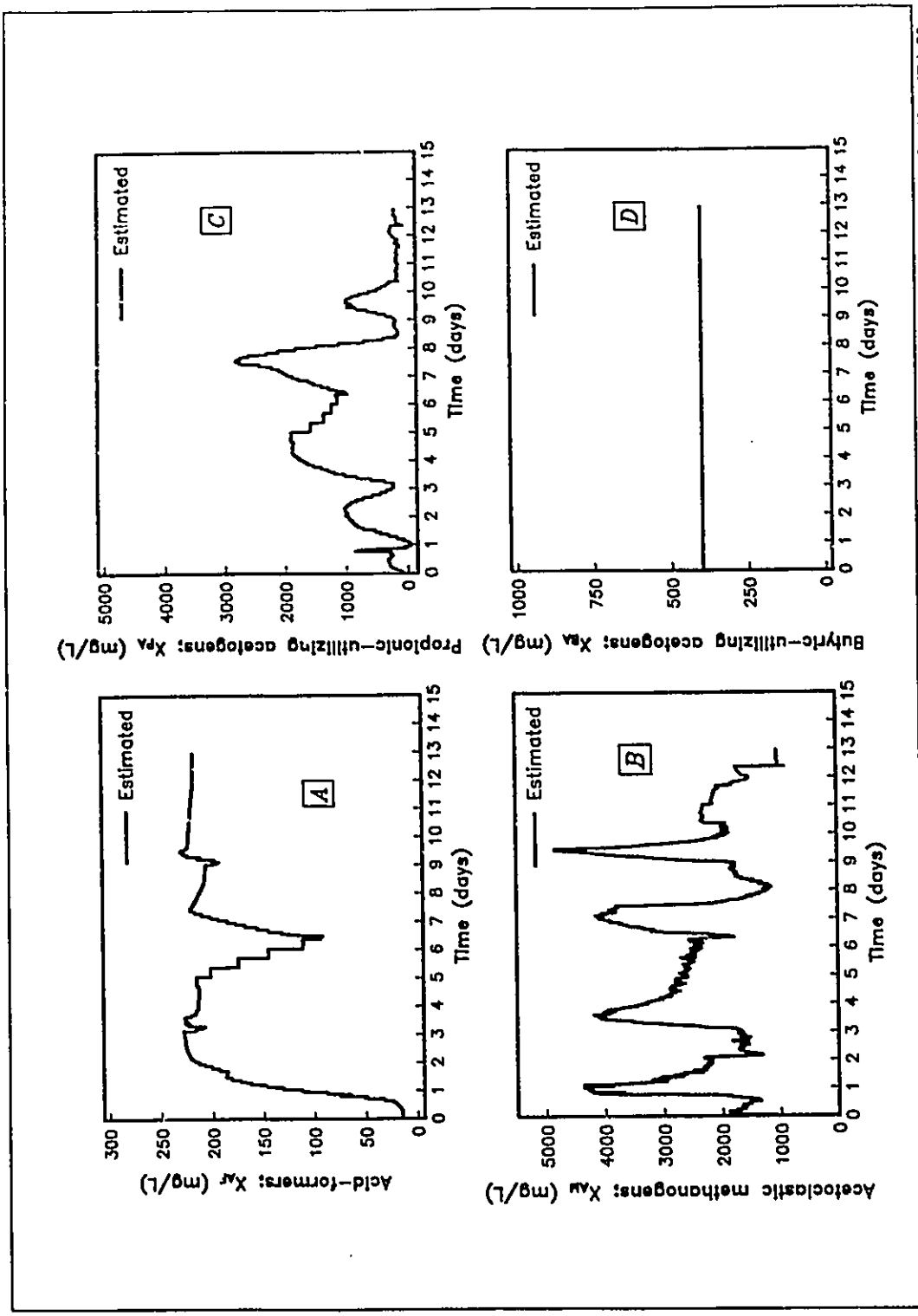

Figure 7.19: Extended Kalman filter estimates of stochastic states during glucose run #3 - (A) X_{Ar}; (B) X_{Am}; (C) X_{Pa}; (D) X_{Ba}.

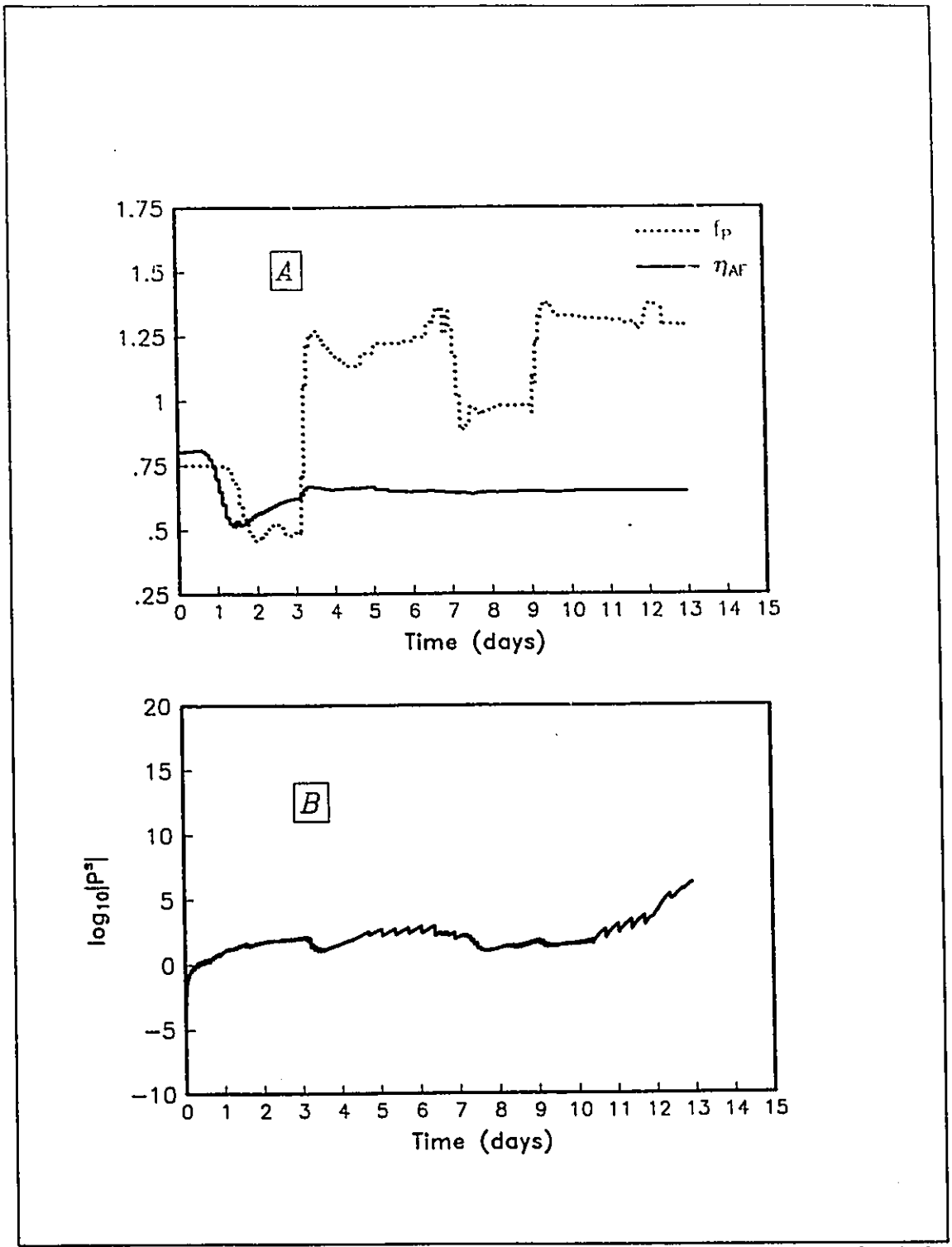

Figure 7.20: (A) Extended Kalman filter estimates of the parameter states and (B) the determinant of the variance-covariance matrix for the stochastic and parameter states ($|\underline{P}^*|$) during glucose run #3.

Table 7.7: Initial conditions for the glucose state estimation run #3

State ($\underline{x}$)	Initial conditions ($\underline{x}_0$)	Diagonal elements $\underline{R}_w$	Diagonal elements $\underline{P}_0$
$S_{G,I}$	300 mg/L	1.0	0.0
$S_{P,I}$	500 mg/L	10.0	1.0
$S_{B,I}$	2 mg/L	0.10	1.00
$S_{A,I}$	250 mg/L	10.00	0.001
$S_{Z,I}$	18 mmole/L	5.00	0.10
$S_{IC,I}$	25 mmole/L	5.00	0.001
$S_{I,I}$	760 mg/L	0.0	0.0
P_{pCO2}	0.20 atm	0.001	0.00001
X_{AF}	14 mg/L	1.0	0.0
X_{PA}	40 mg/L	100.0	100.0
X_{BA}	400 mg/L	0.0	0.0
X_{AM}	1100 mg/L	1000.0	100.0
η_{AF}	0.80	0.0	0.0001
$K_{I,AM}$	1000 mg/L	0.0	0.0
K_{AF}	300 mg/L	0.0	0.0
K_{PA}	130 mg/L	0.0	0.0
K_{BA}	10 mg/L	0.0	0.0
K_{AM}	75 mg/L	0.0	0.0
$K_{I,PA}$	500 mg/L	0.0	0.0
$K_{I,BA}$	1000 mg/L	0.0	0.0
$K_{I,GA}$	250 mg/L	0.0	0.0
f_P	0.75	0.0	0.0001
K_{GP}	1000 mg/L	0.0	0.0

Table 7.8: Correlation coefficient matrix for estimated stochastic states at the end of the glucose run #3

	X_{AF}	X_{PA}	X_{AM}	η_{AF}	f_P
X_{AF}	1.00				
X_{PA}	0.0014	1.00			
X_{AM}	0.0016	-0.16	1.00		
η_{AF}	0.041	-0.0066	0.002	1.00	
f_P	0.088	0.0072	-0.030	0.10	1.00

reactor with a constant expanded bed height. The general bacterial mass balance (Equation 5.30) relating the bacterial concentrations to the respective growth rate expressions should be investigated. The difficulty in completion of the bacterial mass balances is that expressions for the loss rate, $B_{V,k}$, are required for each bacterial group. One approach for quantifying the loss rates is to run the extended Kalman filter with the bacterial concentrations as deterministic states and the $B_{V,k}$ terms as stochastic states. Model identification would then go through a further iteration by examining the time variable behaviour of the $B_{V,k}$ estimates. However, deterministic models for the bacterial concentrations would be difficult to verify because of the difficulties in measuring reactor and effluent concentrations of individual bacterial species. Also, the glucose runs indicated that bacterial growth can be expected to occur in the suspended phase of the reactor. Separate mass balance expressions would be required for the fixed film phase and the suspended phase for each bacterial species. Additional experimentation could provide more information for the formulation of bacterial mass balances. One possible experimental strategy would be to sample solids from both the suspended phase and the fixed film phase of the reactor throughout a dynamic disturbance. These solids could then be used to seed batch experiments which would be used to quantify the activities of the individual bacterial groups in

each phase of the reactor. For example, during a glucose experiment, individual batch tests could be conducted on the degradation rates of glucose, propionic acid, butyric acid and acetic acid using seed from both the suspended and the fixed film phases of the reactor.

2) The estimates of X_{AM} during the acetic acid run indicated that the present Monod kinetic equation in the model for μ_{AM} may not adequately represent the acetic acid degradation kinetics. The variations in X_{AM} were more rapid than would be expected from a growth or wash-out response alone. One possible explanation discussed is that the state estimates were changing to accommodate errors in the model for μ_{AM}. Some researchers have suggested that simple Monod kinetics are not suitable for modelling the short term dynamics of bacterial growth and substrate degradation (Daigger and Grady, 1982). Alternate kinetic models should be postulated and tested.

3) The estimates of X_{PA} during the propionic acid run and X_{BA} during the butyric acid run indicated that substrate inhibition expressions for μ_{PA} and μ_{BA} should be investigated. Labib *et al.*(1988) developed a kinetic expression for butyrate degradation which could be included in this model.

4) The estimates of X_{AF} during the glucose runs indicated that the acid-former substrate in the feed may need to be partitioned into different fractions and the kinetics of each fraction individually included in the model. This is similar to the approach used in the International Association on Water Pollution Research and Control (IAWPRC) activated sludge model (Grady, 1989). Such a detailed characterization of the reactor feed would be of particular importance when applying the model to a wastewater treatment process at a large industrial plant in which a large number of wastewater generating processes exist. In this application, the feed to the wastewater treatment process could consist of a combination of wastewater streams, each of which may have different predominant components exhibiting independent variations and widely

differing removal kinetics.

The general trend in the estimated acetoclastic methanogen concentration during the acetic acid, propionic acid, and glucose experimental period indicated that a simple lumped parameter bacterial mass balance for this group of organisms may be reasonable. The following equation was tested in the model:

$$\frac{dX_{AM}}{dt} = \mu_{AM}X_{AM} - \frac{1}{\theta_{c,AM}}X_{AM} \qquad (7.1)$$

where, $\theta_{c,AM}$ = acetoclastic methanogen retention time (d)

The modified model was used to simulate the acetic acid, propionic acid and glucose run #2 experimental period. Table 7.9 lists the state initial conditions and modified constants for the new model. All other state initial conditions were as listed in Table 7.1. All other model constants were unchanged from the values listed in Tables 5.8 and 5.9. The values of $\mu_{max,AM}$, $\theta_{c,AM}$ and K_{AM} were adjusted to give the best visual fit of the $S_{A,I}$ and $Q_{G,CH4}$ response during the acetic acid and propionic acid portions of the run. At the start of the glucose run, $\mu_{max,AM}$ was reduced to 0.15 d^{-1}, $\theta_{c,AM}$ was reduced to 8 days and X_{AF} was increased to 160 mg/L. The results of the open loop simulations with the modified model are plotted in Figures 7.21 to 7.23.

The simulation results show that the modified model was able to provide reasonable predictions throughout this experimental period. The addition of the mass balance for the acetoclastic methanogens resulted in improved model performance during the glucose portion of the experimental period as compared to the form of the model tested in a fixed parameter simulation in Chapter 5. This model was better able to track the gradual changes in process response that occurred during the glucose run. The model provided excellent predictions of the system response during the acetic acid run and the propionic acid run. Although dynamic models of the anaerobic process have been published which are much more detailed than the

model presented here, no other study to date has demonstrated such accurate model predictions of the detailed dynamic response over such a long period of time. However, the adjustments required in $\mu_{max,AM}$, $\theta_{c,AM}$ and X_{AF} indicate that model inadequacies still exist. As recommended previously in this section, further experimental work coupled with additional modelling studies are required to identify and rectify these inadequacies.

Table 7.9: State initial conditions and modified constants for modified anaerobic dynamic model

Symbol	Value
$\mu_{max,AM}$	0.8 d^{-1}
$\theta_{c,AM}$	25 d
K_{AM}	300 mg/L
X_{AF}	26 mg/L
X_{PA}	1000 mg/L
X_{IIA}	250 mg/L
X_{AM}	1100 mg/L

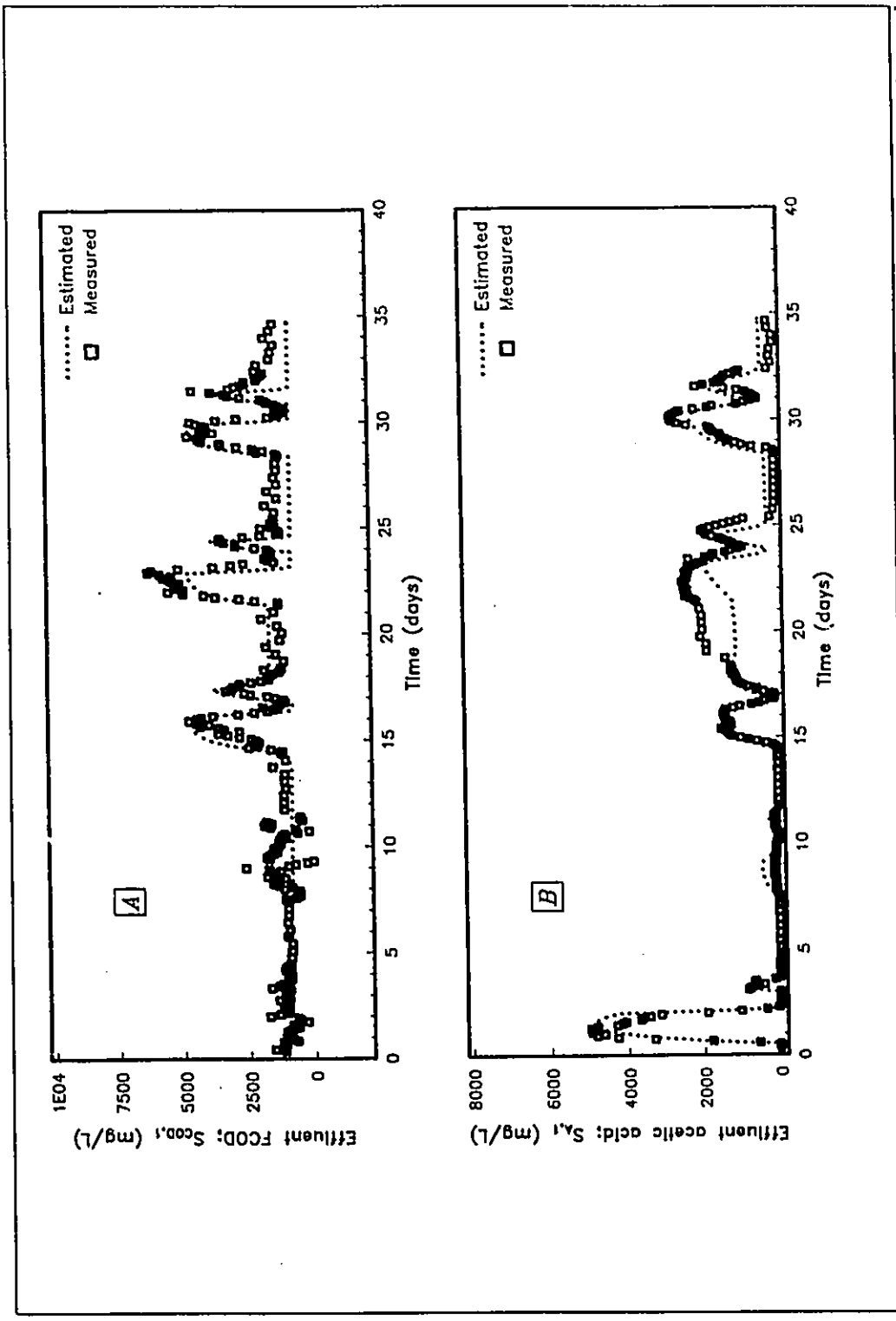

Figure 7.21: Open-loop (model only) simulation of the acetic acid run, propionic acid run and glucose run #2 experimental period - (A) $S_{COD,i}$; (B) $S_{A,i}$.

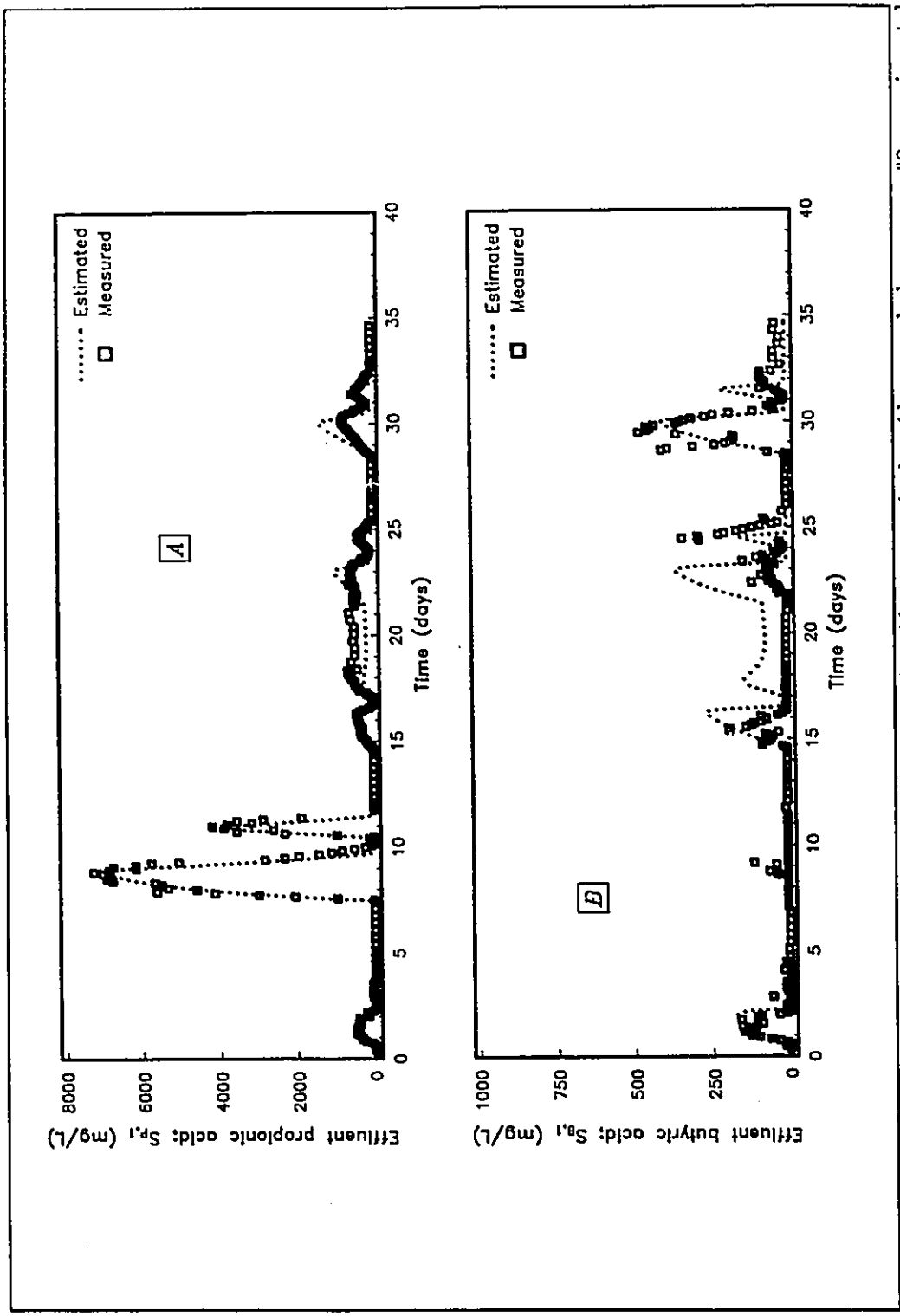

Figure 7.22: Open-loop (model only) simulation of the acetic acid run, propionic acid run and glucose run #2 experimental period - (A) $S_{P,i}$; (B) $S_{B,i}$.

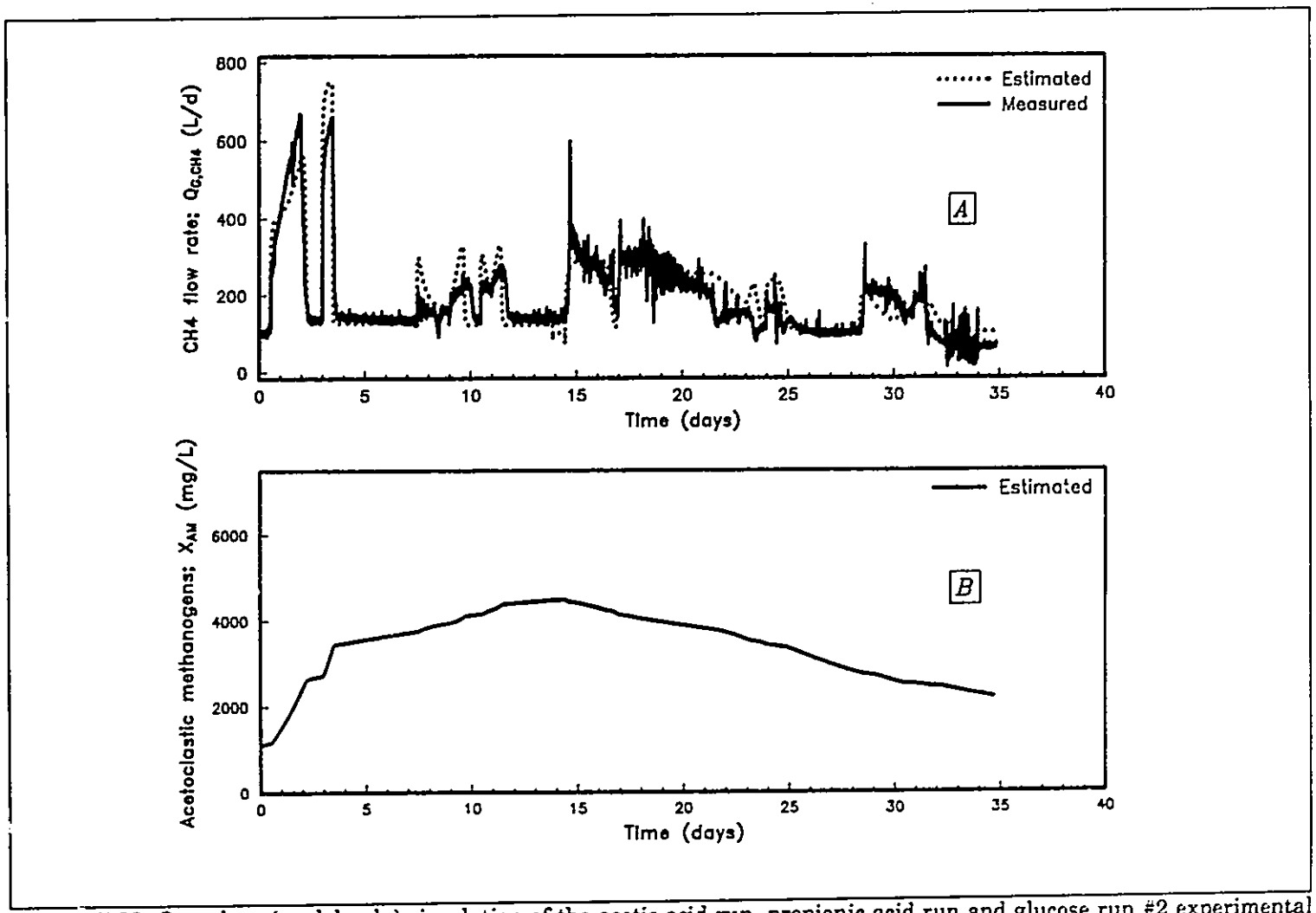

Figure 7.23: Open-loop (model only) simulation of the acetic acid run, propionic acid run and glucose run #2 experimental period - (A) $Q_{G,CH4}$; (B) X_{AM}.

CHAPTER 8

ENGINEERING SIGNIFICANCE

This chapter discusses the environmental and economic significance of a process upset to a high rate anaerobic treatment system. Potential impacts are based on the experimental observations in this study. The availability of process control options and the practicality of implementing certain options are also discussed. The impact of loading equalization is illustrated through a simulation.

8.1 DYNAMIC PERFORMANCE OF HIGH RATE ANAEROBIC WASTEWATER TREATMENT PROCESSES

There are a number of potential economic and environmental impacts of the dynamic response characteristics of high rate anaerobic wastewater treatment processes. Table 8.1 summarizes the increased effluent COD loading and caustic consumption observed during dynamic experiments and provides an estimate of the potential methane production represented by COD losses in the effluent of the process. The obvious environmental impact of increased effluent COD loading from a treatment system during dynamic operation is that the assimilative capacity of a receiving stream may be exceeded if the treatment process discharges directly to the stream. If an anaerobic process discharges to an aerobic polishing step such as an activated sludge process, the increased loading to the polishing step could lead to process upsets which would ultimately lead to increased loading to the receiving stream. Increased effluent COD could also result in increased fines or surcharges, or increased aeration

Table 8.1: Summary of effluent loading and caustic consumption observed during dynamic experiments

Experiment	Effluent FCOD ($kg/m^3 \cdot d$)	NaOH consumed (kg/m^3 wastewater) [b]	Potential lost CH_4 (m^3 CH_4/m^3 wastewater) [c]
Baseline	2.0 [a]	0.21	0.0
Acetic acid run	2.6	1.8	0.13
Propionic acid run	6.8	1.8	1.1
Glucose run #2	5.4	1.4	0.77
Butyric acid run	8.5	1.0	1.3
Glucose run #3	6.8	1.6	1.1

Notes:

[a] Assumes baseline FCOD loading equal to 8.0 $kg/m^3 \cdot d$ and 75% FCOD removal efficiency - Expressed on a per unit reactor volume (77 L) basis

[b] From dynamic experiment results - Expressed as mass per unit volume of wastewater treated

[c] ((Baseline effluent FCOD load - Effluent FCOD load) * 0.35 m^3 CH_4/kg $COD_{removed}$) × 0.077 m^3 (reactor volume) ÷ 0.120 m^3/d (feed flowrate)

and sludge disposal costs in a downstream polishing step, although the magnitude of this effect would be site-specific. Increased chemical costs for pH control and a loss in potential methane production when the process cannot respond quickly enough to degrade the higher level of COD entering the system represent the most significant costs of an organic overload. Increased chemical consumption for pH control results from higher effluent volatile acid concentrations and increased carbon dioxide production.

Table 8.2 assigns potential costs to the experimental observations of this study. In this study, chemical consumption for pH control represented the most significant potential cost of an organic overload. Further site-specific considerations such as the alkalinity concentrations in the raw wastewater, and whether or not the biogas is utilized to offset the cost of other

Table 8.2: Potential costs of organic overload based on pilot plant dynamic experiments

Experiment	NaOH Cost [a] ($/m^3 wastewater)	Lost CH_4 Value [b] ($/m^3 wastewater)
Baseline	0.11	0.0
Acetic acid run	0.95	0.02
Propionic acid run	0.95	0.16
Glucose run #2	0.74	0.11
Butyric acid run	0.53	0.19
Glucose run #3	0.85	0.16

[a] Based on $CDN 530 /dry tonne NaOH

[b] Based on:

Natural gas cost = $CDN 0.15/$m^3$
Natural gas heating value = 37,300 kJ/m^3
Methane heating value = 35,800 kJ/m^3
Lost CH_4 value = Potential Lost CH_4 (Table 8.1) * 0.15 * 35,800/37,300

forms of energy will affect the true cost of a process upset. However, this analysis indicates that stable operation of an anaerobic treatment process may have an economic as well as an environmental benefit.

8.2 CONTROL OF HIGH RATE ANAEROBIC TREATMENT PROCESSES

Control strategies will minimize the economic and environmental impact of dynamic increases in process organic loading if the organic removal rate is maximized and chemical addition for pH control is minimized. Increased organic removal rates will contribute to reducing chemical consumption for pH control, although the increased carbon dioxide produced during loading increases may require additional neutralization.

Chemical consumption for pH control will be minimized by removing the compounds that reduce the pH such as volatile acids and carbon dioxide. This can be achieved by

maintaining stable operation to minimize volatile acid accumulation and by removing dissolved CO_2 (Andrews, 1989). A reduction in the pH control setpoint could also reduce chemical consumption. However, as the setpoint is moved closer to the minimum of the optimal pH range, the pH controller must reduce the variance of the pH about the setpoint. Although not addressed in this study, options for optimizing pH control should be investigated.

Once pH and temperature are maintained within the proper range for anaerobic treatment, there are few control options available for maximizing organic removal. In the absence of practical constraints, the obvious option is to control the loading to the system.

To investigate the possible impact of loading control, simulations were conducted using the modified anaerobic dynamic model described in Chapter 7. In one case, the simulated reactor was subjected to a 1.5 day COD loading rate increment similar in magnitude to the pulses used in this study. In another case, the same incremental mass of COD was spread over 4.5 days (Figure 8.1 (A)). In both cases, the COD loading rate increment was comprised of equal COD equivalents of acetic acid and propionic acid. This is representative of an application in which the raw wastewater undergoes a preacidification step. As shown in Chapter 7, the performance of the modified dynamic model in predicting the process response to influent pulses of acetic and propionic acid is excellent. The HRT was maintained at 12 hours throughout both simulations. All other parameter values, constant values and state initial conditions were as listed for the modified model open loop simulations described in Chapter 7.

The results of both cases are plotted over a 7 day simulation period in Figures 8.1 and 8.2. It can be seen that the effluent acetic, propionic and butyric acid concentrations (Figure 8.1 (B),(C),and (D), respectively) are dramatically reduced and the methane production rate (Figure 8.2(A)) is dramatically increased during the 4.5 day pulse. An overall COD balance on soluble and gaseous components in the system over the 7 day simulation period for both cases (Table 8.3) indicates the magnitude of the improvement in performance during the

4.5 day pulse. The reason for the improvement appears to be reduced inhibition of methanogenesis because of lower propionic acid concentrations and a longer period to allow for methanogen growth (Figure 8.2(B)).

In full scale application, the addition of large volumes of tankage for equalization may not be economically viable. However, the required equalization volume could be minimized if the wastewater streams causing the largest variations in loading rate are equalized prior to addition to the combined wastewater feed to the process. The control strategy would involve the controlled addition rate of the segregated stream, depending on the available equalization volume and the performance of the process. The addition rate would be increased with improved process performance and decreased available equalization volume. A suitable dynamic model of the anaerobic treatment process can be used to size the equalization capacity required for a given set of dynamic loading conditions.

A loading control strategy utilizing equalization will require some measure of process performance for feedback. Although hydrogen had previously been recommended as an indicator of overall process performance (Mosey, 1983), subsequent studies including this research have indicated that the hydrogen response cannot be interpreted in isolation of other process state variables. This study has indicated that the response of a process to dynamic disturbances is highly dependent on the relative active concentrations of the organisms present in the process, and that these relative active concentrations can change rapidly. Therefore, monitoring of system performance for feedback process control must utilize more than a single variable as a measure of performance.

The type and degree of control action to eliminate an upset may also depend on the disturbance causing the upset. For example, increased organic loading of a preacidified wastewater consisting predominantly of acetic acid may not require the same degree of equalization as increased propionic acid loading. The process appears able to increase its capacity to degrade increased loadings of acetic acid much more readily than propionic acid.

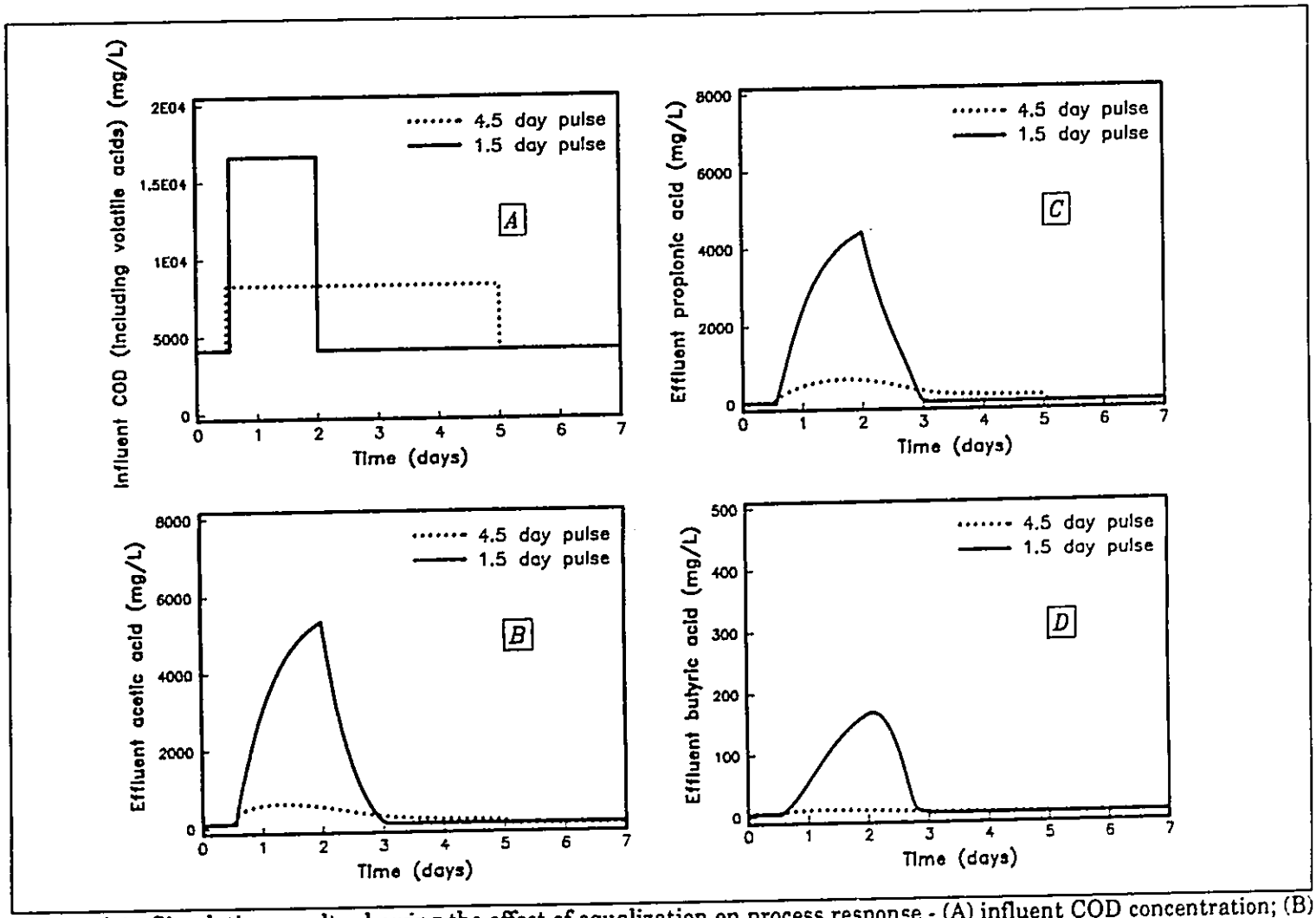

Figure 8.1: Simulation results showing the effect of equalization on process response - (A) influent COD concentration; (B) effluent acetic acid concentration; (C) effluent propionic acid concentration; (D) effluent butyric acid concentration.

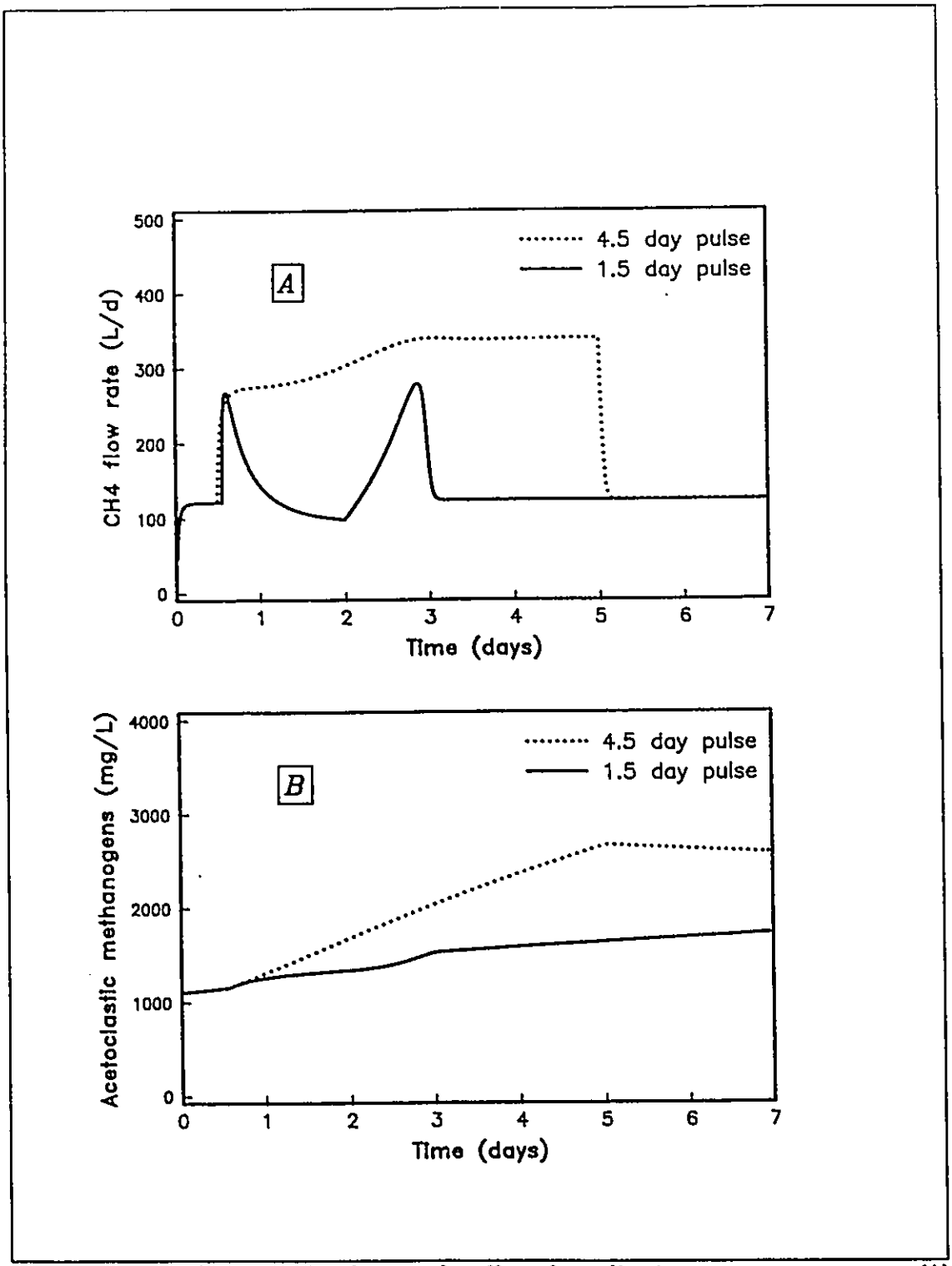

Figure 8.2: Simulation results showing the effect of equalization on process response - (A) methane production rate; (B) acetoclastic methanogen concentration.

Table 8.3: Oxygen demand balance for loading control simulations		
Parameter	Mass COD (kg/(m^3 of reactor volume))	
	1.5 day pulse	4.5 day pulse
Input COD	94	94
Effluent Acetic Acid	15	2.5
Effluent Propionic Acid	19	2.3
Effluent Butyric Acid	1	0.1
Effluent COD (less acid)	15	15
Biogas Methane	39	70

In addition, increased propionic acid concentrations inhibit acetoclastic methanogenesis. Equalization could allow the process a longer period for methanogen growth resulting in very little upset in the process effluent quality in the case of a dynamic disturbance in the influent acetic acid loading. Equalization may not improve the response to a dynamic increase in propionic acid loading because the process cannot adapt within a reasonable period of time to increase its capacity to degrade propionic acid. The best control in this case could be no control, so as to minimize the amount of time that elevated levels of propionic acid would inhibit methanogenesis.

A dynamic model could be utilized by a plant operator to decide on the type and degree of control action suitable for a given input disturbance. However, as shown in this research, model parameters will require frequent updating for the model to be a realistic representation of the actual process. An extended Kalman filter can be utilized to estimate the appropriate states and parameters in the dynamic model. Available on-line measurements of gas production rates and composition, and intermittent off-line measurements of the states such as volatile acid and COD concentrations are required to allow estimation of the stochastic states and parameters in the model. If unmeasured stochastic states in the model are not estimated, the predictions of the states required for control will develop time-dependent biases

from the actual state values. Improving the open loop performance of the dynamic model will allow the measurement interval of off-line states to be increased. This study found a number of potential model improvements to investigate.

CHAPTER 9

SUMMARY AND CONCLUSIONS

The overall goal of this research was to develop an improved understanding of the dynamic behaviour necessary to define monitoring and control requirements of high rate anaerobic treatment processes. As part of this effort, it was proposed to formulate a dynamic mathematical model of the process which could have subsequent application to improving operation and control. Although a number of comprehensive dynamic models have been proposed for anaerobic treatment processes by previous researchers, there are a limited number of studies in which these models have been calibrated and tested using actual process data. In addition, there are few data sets available which sufficiently characterize both the short term and long term dynamic response of an anaerobic process to be useful for model structure evaluation. Calibration difficulties caused by the large number of parameters in anaerobic process models and the possible time-variable nature of these parameters have not previously been addressed. The key steps involved in this research effort were:

i) to gather a data set on the response of a high rate anaerobic reactor which would be useful for dynamic model selection, calibration and verification;

ii) to compile a dynamic model describing the observed process responses;

iii) to explore the requirements for calibrating a dynamic model when faced with a high level of uncertainty in the model structure;

iv) to utilize the dynamic model and the data set to determine critical areas for further research on operation and control of anaerobic treatment systems.

Dynamic experimentation was conducted on a 77 L pilot scale anaerobic fluidized bed reactor. The experiments were designed to perturb the various reaction steps in the anaerobic degradation process. This was achieved by introducing feed pulses of glucose, propionic acid, butyric acid and acetic acid substrates into the system. The response of a number of conventional monitoring parameters were recorded in addition to trace concentrations of gas phase hydrogen. A dynamic model was formulated based on a four-bacterial population structure and the experimental results from the pilot plant. Model calibration involved the use of the extended Kalman filter non-linear state estimator which allowed simultaneous estimation of the model parameters and the time-variable disturbances affecting the model. Due to the large number of parameters and possible stochastic states in the model, a sensitivity analysis was required to select the most important subset of parameters and stochastic states for estimation. The observability of the estimated states and parameters was tested using a simulated data set.

The conclusions based on observation and analysis of the experimental results, and the formulation and testing of a dynamic mathematical model of the process, are presented below.

1) The gas phase hydrogen concentration did not respond during volatile acid pulse experiments and the response was inconsistent during glucose pulse experiments. The observations of the hydrogen response indicated that the gas phase hydrogen concentration alone has limited utility as a monitoring variable. Interpretation of the hydrogen response requires a knowledge of the changes in the relative activity of the various organisms producing or consuming hydrogen. In addition, the lack of a consistent correlation between the accumulation of volatile acids and the gas phase hydrogen concentration indicates that inhibition of propionate and butyrate degradation by hydrogen is not the most important factor affecting the response of volatile acid intermediates during organic overloads.

2) Acetoclastic methanogenesis was not significantly inhibited by elevated concentrations

of acetic acid during dynamic experimentation. For this reason, a substrate inhibition term in the kinetic expression for acetoclastic methanogenesis was not included in the dynamic model. This is in contrast to a number of previously published dynamic models of the anaerobic process.

3) High acetic acid concentrations resulted in increases in reactor concentrations of propionic and butyric acids. These results demonstrated the significance of acetate inhibition on the net degradation rates of propionate and butyrate in a continuous-flow, high rate anaerobic system. There was not sufficient information from the experiments to determine whether acetate more significantly affected the production rates or the degradation rates of propionate and butyrate.

4) The rate of acetic acid to methane conversion increased relatively rapidly in response to influent pulses of acetic acid. The conversion rate of butyric and propionic acid did not increase during pulse addition of these substrates.

5) Dynamic increases in the influent concentrations of highly biodegradable carbohydrate substrates such as glucose can cause a rapid increase in effluent suspended solids in a high rate anaerobic reactor. Material balances on the fluidized bed process during glucose pulse experiments indicated that an increase in suspended solids could be attributed to the growth of acid-former organisms.

6) A process upset caused by an organic overload can have significant economic as well as environmental costs. The most significant costs are due to the increased chemical costs for pH control and the loss in potential methane production.

7) A four-bacterial population dynamic model of the anaerobic process was used to predict the process response to a three week glucose pulse experiment. It was found that although the model could predict the dynamic process response reasonably well over time periods up to five days, the model predictions eventually deviated significantly from the actual process response. The major reason for this behaviour was the lack

of suitable mechanistic models for the time-variable behaviour of bacterial concentrations in the process.

8) An extended Kalman filter allowed the anaerobic process model to combine both mechanistic and stochastic models for the process states. The bacterial concentration states were described entirely by stochastic models and were recursively estimated based on the measured input-output behaviour of the process. The combined mechanistic-stochastic model was shown to track the measured effluent concentrations of COD, acetic acid, propionic acid and butyric acid, and the measured methane production rate. However, in some cases the tracking of the measurements could only be achieved through unrealistic adjustments in the bacterial concentration states.

9) A fixed parameter simulation using the four-bacterial population model without the extended Kalman filter was found to provide excellent predictions of the process response during the acetic acid, propionic acid, and glucose experimental period when a simple lumped parameter mechanistic material balance for the acetoclastic methanogens was included in the model. However, a major adjustment in model parameters was required at one point in the simulation. This indicated that further model improvements are required.

10) An important finding of the sensitivity analysis was that there is a wide variation in the sensitivity of the model predictions to changes in any specific stochastic or parameter state over different regions of process operation. As a result, the ability to estimate a stochastic state or parameter will depend on the region of process operation. An additional application of a sensitivity analysis could thus be to select an appropriate set of operating data or a suitable set of experimental conditions to generate data for model calibration.

CHAPTER 10

RECOMMENDATIONS

1) Models for the dynamics of bacterial concentrations in high rate anaerobic reactors must be improved to improve the performance of process models. Advances in methods for characterizing relative concentrations of organism species may be required to verify these models. However, one possible approach could use an extended Kalman filter to provide estimates of specific factors affecting the bacteria concentrations or activities while appropriate sample collection and off-line activity determinations using appropriate substrate consumption batch experiments could provide an estimate of the relative organism species concentrations.

2) In future modelling studies, acid-former substrates in the reactor feed should be partitioned into different fractions and the kinetics of each fraction individually included in the model. This is similar to the approach used in the International Association on Water Pollution Research and Control (IAWPRC) activated sludge model. This would be of particular importance in industrial treatment applications, where wastewaters could be comprised of a wide variety of substrates each exhibiting widely different removal kinetics.

3) Substrate inhibition expressions should be included in the kinetics for acetogenic degradation of butyrate and propionate in future models.

4) Any high rate anaerobic process application in which large dynamic increases in highly biodegradable carbohydrate substrates are expected should consider the growth in suspended solids expected and if necessary provide for separation of these solids from

the reactor liquid phase.

5) Methods for minimizing the cost of pH control should be explored. This study indicated that reducing dynamic organic overloads through equalization may contribute to a reduction in pH control chemical consumption. Methods of reducing the liquid phase dissolved carbon dioxide concentration and pH controller optimization should also be investigated.

6) Segregation of wastewater streams causing the largest dynamic loading changes should be considered when designing high rate anaerobic treatment systems. The dynamic changes in flow or concentration in these streams can then be equalized before addition to the main wastewater stream thereby minimizing the equalization volume required.

7) As dynamic model performance is improved, the use of a dynamic model coupled with a Kalman filter state estimation routine should be investigated for providing information on which to base suitable control actions to specific process disturbances.

8) This study only addressed the dynamic behaviour of a high rate anaerobic treatment process in response to inputs of organic, biodegradable substrates. Further study is required to characterize and model the response of anaerobic processes to toxic inputs such as chlorinated organic compounds and heavy metals. This is particularly important in industrial applications such as in the pulp and paper and petrochemical sectors.

REFERENCES

Andrews, J.F. (1969). Dynamic model of the anaerobic digestion process. *J. Sanit. Engng Div. Proc. ASCE*, 95 (SA1), 95-116.

Andrews, J.F., and Graef, S.P. (1971). Dynamic modeling and simulation of the anaerobic digestion process. *Anaerobic biological treatment processes*. Advances in Chemistry Series, R.F. Gould (Ed)., 105, American Chemical Society, New York, 126-162.

Andrews, J.F. (1989). Dynamics, stability and control of the anaerobic digestion process. *Dynamic Modeling and Expert Systems in Wastewater Engineering*. G.G. Patry and D. Chapman (Ed)., Lewis, Chelsea, MI, 83-127.

Astrom, K.J. and Wittenmark, B. (1984). *Computer Controlled Systems Theory and Design*. Prentice-Hall, Englewood Cliffs, New Jersey.

Atherton, R.W., Schainker, R.B., and Ducot, E.R. (1975). On the statistical sensitivity analysis of models for chemical kinetics. *AICHE Journal*. 21, 441-448.

Atkinson, B. and Davies, I.J. (1974). The overall rate of substrate uptake (reaction) by microbial films. Part I.a. Biological rate equation. *Transactions, Institution of Chemical Engineers*. 52, 248-259.

Attal, A., Ehlinger, F., Audic, J.M., and Faup, G.M. (1988). pH inhibition mechanisms of acetogenic, acetoclastic and hydrogenotrophic populations. *Anaerobic Digestion 1988*. Proc. of the 5th International Symposium on Anaerobic Digestion, Bologna, Italy, 22-26 May, 71-77.

Barnes, D., Bliss, P.J., Grauer, B., and Robins, K. (1984). Pretreatment of high strength wastewater by an anaerobic fluidised bed process. Part II Response to Organic Load Transients. *Environ. Technol. Letters*. 6, 73-78.

Bastin, G. and Dochain, D. (1986). On-line estimation of microbial specific growth rates. *Automatica*, 22, 705-709.

Beck, M.B. (1989). System Identification and Control. *Dynamic Modeling and Expert Systems in Wastewater Engineering*. G.G. Patry and D. Chapman (Ed)., Lewis, Chelsea, MI, 261-323.

Beck, M.B. (1981). Operational estimation and prediction of nitrification dynamics in the activated sludge process. *Wat. Res.*, 15, 1313-1330.

Beck, M.B., and Young, P.C. (1976). Systematic identification of DO-BOD model structure. *J. Environ. Eng.*, ASCE, 102 (EE5), 902-907.

Boone, D.R., and Bryant, M.P. (1980). Propionate-degrading bacterium, *Syntrophobacter wolinii* sp.nov.gen.nov., from methanogenic ecosystems. *Appl. Env. Microbiol.*, 40, 626-632.

Box, G.E.P. and Lucas, H.L. (1959). Design of experiments in non-linear situations. *Biometrika*, 46, 77-90.

Bryant, M.P., Wolin, E.A., Wolin, M.J., and Wolfe, R.S. (1967). *Methanobacillus omelianskii*, a symbiotic association of two species of bacteria. *Arch. Microbiol.*, 59, 20-31.

Carr A.D., and O'Donnell, R.C. (1977). The dynamic behaviour of an anaerobic digester. *Prog. Wat. Tech.*, 9, 727-738.

Chalon, A., Bastin, G., and Installé, M. (1982). Identification of a biomethanization process: A case study. *6th IFAC Symposium on Identification on System Parameter Estimation.* Washington, June 7-11.

Chung, K-T. (1976). Inhibitory Effects of H_2 on Growth of *Clostridium cellobioparum*. *Appl. Env. Microbiol.*, 31, 342-348.

Costello, D.J., Greenfield, P.F., Lee, P.L. (1991a). Dynamic modelling of a single stage high-rate anaerobic reactor-I. Model derivation. *Wat. Res.*, 25, 847-858.

Costello, D.J., Greenfield, P.F., Lee, P.L. (1991b). Dynamic modelling of a single stage high-rate anaerobic reactor-I. Model verification. *Wat. Res.*, 25, 847-858.

Daigger, G.T. and Grady, C.P.L. (1982). The Dynamics of Microbial Growth on Soluble Substrates: A Unifying Theory. *Wat. Res.*, 16, 365-382.

Denac, M., Griffin, K., Lee, P.L., and Greenfield, P.F. (1988a). Selection of controlled variables for a high rate anaerobic reactor. *Environ. Technol. Letters*, 9, 1029-1040.

Denac, M., Miguel, A. and Dunn, I.J. (1988b). Modeling dynamic experiments on the anaerobic degradation of molasses wastewater. *Biotechnol. Bioengng.*, 31, 1-10.

Dochain, D., Perrier, M., and Pauss, A. (1991). Adaptive control of the hydrogen concentration in anaerobic digestion. *Ind. Eng. Chem. Res.*, 30, 129-136.

Dochain, D. and Bastin, G. (1985). Stable adaptive controllers for waste treatment by anaerobic digesters. *Environ. Technol. Letters*, 6, 584-593.

Eng, S.C., Fernandes, X.A. and Paskins, A.R. (1986). Biochemical effects of administering shock loads of sucrose to a laboratory-scale anaerobic (UASB) effluent treatment plant. *Wat. Res.*, 20, 789-794.

Fukuzaki, S., Nishio, N., Shobayashi,M. and Nagai, S. (1990). Inhibition of the fermentation of propionate to methane by hydrogen, acetate, and propionate. *Appl. Env. Microbiol.*, 56, 719-723.

Furumai, H., Kuba, T., Imai, T., and Kusuda, T. (1991). Transient responses of wastewater treatment and biomass development in a methanogenic fluidized bed. *Wat. Sci. Tech.*, 23, 1327-1336.

Gear, C.W. (1971). *Numerical Initial Value Problems in Ordinary Differential Equations.* Prentice-Hall, Englewood Cliffs, New Jersey.

Grady, C.P.L. and Lim, H.C. (1980). *Biological Wastewater Treatment: Theory and Applications*, Marcel Dekker, New York.

Grady, C.P.L (1989). Dynamic modeling of suspended growth biological wastewater treatment processes. *Dynamic Modeling and Expert Systems in Wastewater Engineering*, G.G. Patry and D. Chapman (Ed)., Lewis, Chelsea, MI, 1-38.

Grauer, R.B. (1986). Performance of an Anaerobic Fluidized Bed Digester Under Steady-State and Shock Loading Conditions. Ph.D. dissertation, University of New South Wales, Australia.

Guiot, S.R. and van den Berg, L. (1984). Dynamic performance of an anaerobic reacter combining an upflow sludge blanket and a filter for the treatment of sugar waste. *Proc. 39th Ind. Waste Conf.*, Purdue University, 705-717.

Hall, E.R. (1985). Non-intrusive estimation of active volume in anaerobic reactors. *Water Poll. Res. J. Canada*, 20, 44-54.

Harper, S.R., and Pohland, F.G. (1986). Recent developments in hydrogen management during anaerobic biological wastewater treatment. *Biotechnol. Bioengng.*, 28, 585-602.

Henry, M. and Varaldo, C. (1988). Anaerobic digestion treatment of chemical industry wastewaters at the Cuise-Lamonte (Oise) plant of Societe Francais Hoechst. *Anaerobic Digestion 1988*, Proc. of the 5th International Symposium on Anaerobic Digestion, Bologna, Italy, 22-26 May, 479-486.

Henze, M. and Harremoes, P. (1983). Anaerobic treatment of wastewater in fixed film reactors - A literature review. *Wat. Sci. Tech.*, 15, 1-101.

Heyes, R.H. and Hall, R.J. (1983). Kinetics of two subgroups of propionate-using organisms in anaerobic digestion. *Appl. Env. Microbiol.*, 46, 710-715.

Hickey, R.F., Wu, W.-M., Veiga, M.C. and Jones, R. (1991). Start-up, operation, monitoring and control of high-rate anaerobic treatment systems. *Wat. Sci. Tech.*, 24, 207-255.

Hickey, R.F. and Switzenbaum, M.S. (1991). The response and utility of hydrogen and carbon monoxide as process indicators of anaerobic digesters subject to organic and toxic overloads. *Research Journal WPCF*, 63, 129-140.

Hill, D.T. and Barth, C.L. (1977). A dynamic model for simulation of animal waste digestion. *J. Wat. Pollut. Control Fed.*, 10, 2129-2143.

Hilton, M.G. and Archer, D.B. (1988). Anaerobic Digestion of Sulfate-Rich Molasses Wastewater: Inhibition of Hydrogen Sulfide Production. *Biotechnol. Bioengng.*, 31, 885-888.

Hilton, B.L., and Oleszkiewicz, J.A. (1988). Sulfide-induced inhibition of anaerobic digestion. *J. Environ. Eng.*, ASCE, 114, 1377-1391.

Holmberg, U. and Olsson, G. (1985). Simultaneous on-line estimation of oxygen transfer rate and respiration rate. *Proc. 1st IFAC Symposium on Modelling and Control of Biotechnological Processes*, Noordwijkerhout, The Netherlands, 11-13 Dec., 205-209.

Hoover, S.R. and Porges, N. (1952). Assimilation of dairy wastes by activated sludge - II - The equations of synthesis and rate of oxygen utilization. *Sewage and Industrial Wastes*, 24, 306-312.

Ide, S. (1988). Dynamics, Stability, and Control of Anaerobic Packed Bed Processes. Ph.D. thesis, Rice University, Houston, Texas.

Iza, J., Colleran, E., Paris, J.M. and Wu, W.-M. (1991). International workshop on anaerobic treatment technology for municipal and industrial wastewaters: summary paper. *Wat. Sci. Tech.*, 24, 1-16.

Jazwinski, A.H. (1970). *Stochastic Processes and Filtering Theory*, Academic Press, New York.

Jones, R.M., Hall, E.R. and Murphy, K.L. (1988). On-line estimation of process variables for operation and control in high rate anaerobic wastewater treatment. *Poster Papers*, 5th International Symposium on Anaerobic Digestion, Bologna, Italy, 22-26 May, 191-194.

Jones, R.M. and Hall, E.R. (1989). Assessment of dynamic models for a high rate anaerobic treatment process. *Environ. Technol. Letters*, 10, 551-566.

Jones, R.M., MacGregor, J.F. and Murphy, K.L. (1989). State estimation in wastewater engineering: Application to an anaerobic process. *Environmental Monitoring and Assessment*, 12, 271-282.

Kalman, R.E. (1960). A new approach to linear filtering and prediction problems. *Trans. ASME, J. Basic Eng.*, Series 82D, 35-45.

Kaspar, H.F. and Wuhrmann, K. (1978). Kinetic parameters and relative turnovers of some important catabolic reactions in digesting sludge. *Appl. Env. Microbiol.*, 36, 1-7.

Kennedy, K.J., Muzar, M., and Copp, G.H. (1985). Stability and performance of mesophilic anaerobic fixed-film reactors during organic overloading. *Biotechnol. Bioengng.*, 27, 86-93.

Kissel, J.C. (1986). Modeling mass transfer in biological wastewater treatment processes. *Wat. Sci. Tech.*, 18, 35-45.

Kozub, D.J. and MacGregor, J.F. (1992). State estimation and control for semi-batch polymerization reactors. *Chem. Eng. Science*, 47, 1047-1062.

Labib, F., Ferguson, J.F. and Benjamin, M.M. (1988). The response of a butyrate-fed fluidized bed reactor to transient loadings. *Proc. 43rd Ind. Waste Conf.*, Purdue University, 363-370.

Leis, J.R. and Kramer, M.A. (1988). The simultaneous solution and sensitivity analysis of systems described by ordinary differential equations. *ACM Transactions on Mathematical Software*, 14, 45-60.

Lettinga, G. and Hulshoff Pol, L.W. (1991). UASB-process design for various types of wastewaters. *Wat. Sci. Tech.*, 24, 87-107.

Levenspiel, O. (1972). *Chemical Reaction Engineering*, 2nd Edition, John Wiley & Sons, New York.

Luong, J.H.T. (1987). Generalization of monod kinetics for analysis of growth data with substrate inhibition. *Biotechnol. Bioengng.*, 29, 242-248.

Mawson, A.J., Earle, R.L., Larsen, V.F. (1991). Degradation of acetic and propionic acids in the methane fermentation. *Wat. Res.*, 25, 1549-1554.

McCarty, P.L. and Mosey, F.E. (1991). Modelling of anaerobic digestion processes (a discussion of concepts). *Wat. Sci. Tech.*, 24, 17-33.

McCarty, P.L. (1964). Anaerobic waste treatment fundamentals. *Public Works*, September, 107-112.

McInerney, M.J., Bryant, M.P., Hespell, R.B., and Costerton, J.W. (1981). *Syntrophomonas wolfei* gen. nov. sp. nov., an anaerobic, syntrophic, fatty acid-oxidizing bacterium. *Appl. Env. Microbiol.*, 41, 1029-1039.

McInerney, M.J., Bryant, M.P., and Stafford,D.A. (1979). Metabolic stages and energetics of mircobial anaerobic digestion. *Anaerobic Digestion*, Proc. of the 1st International Symposium of Anaerobic Digestion, University College, Cardiff, Wales, 91-98.

Mitchell and Gauthier Associates Inc. (1987). *Advanced Continuous Simulation Language*. Mitchell and Gauthier, Concord, Mass.

Moletta, R., Verrier, D. and Albagnac, G. (1986). Dynamic modelling of anaerobic digestion. *Wat. Res.*, 20, 427-434.

Mosey, F.E. (1983). Mathematical modelling of the anaerobic digestion process: regulatory mechanisms for the formation of short-chain volatile acids from glucose. *Wat. Sci. Tech.*, 15, 209-232.

Mosey, F.E. and Fernandes, X.A. (1989). Patterns of hydrogen in biogas from the anaerobic digestion of milk sugars. *Wat. Sci. Technol.*, 21, 187-196.

Mueller, J.A. and Mancini, J.L. (1975). Anaerobic filter - kinetics and application. *Proc. 30th Ind. Waste Conf.*, Purdue University, 423-427.

Parkin, G.F. and Owen, W.F. (1986). Fundamentals of anaerobic digestion of wastewater sludges. *J. Environ. Eng.*, ASCE, 112 (EE5), 867-920.

Pauss, A., Andre, G., Perrier, M., and Guiot, S.R. (1990a). Liquid-to-gas mass transfer in anaerobic processes: Inevitable transfer limitations of methane and hydrogen in the biomethanation process. *Appl. Env. Microbiol.*, 56, 1636-1644.

Pauss, A., Rozzi, A., Ledrut M.-J., Naveau, H. and Nyns, E.-J. (1990b). Bicarbonate determination in complex acid-base solutions by a back-titration method. *Environmental Technology*, 11, 469-476.

Pavlostathis, S.G. and Giraldo-Gomez, E. (1991). Kinetics of anaerobic treatment. *Wat. Sci. Tech.*, 24, 35-59.

Price, E.J. (1985). The microbiology of anaerobic digestion. *Biotechnology, Applications and Research*, P.N. Cheremisinoff and R.P. Oullette (Ed). Technomic Publishing, Lancaster, Pennsylvania, 52-59.

Renard, P., Dochain, D., Bastin, G., Naveau, H., and Nyns, E.-J. (1988). Adaptive control of anaerobic digestion processes - a pilot scale application. *Biotechnol. Bioengng.*, 31, 287-294.

Rintala, J. and Vuoriranta, P. (1988). Anaerobic-aerobic treatment of thermomechanical pulping effluents. *Tappi Journal*, 71, 201-207.

Rittmann, B.E. and McCarty, P.L. (1981). Substrate flux into biofilms of any thickness. *J. Environ. Eng.*, ASCE, 107 (EE4), 831-849.

Rozzi, A. (1984). Modelling and control of anaerobic digestion processes. *Trans Inst M C*, 6 (3), 153-159.

Rozzi, A., Di Pinto, A.C. and Brunetti, A. (1985a). Anaerobic process control by bicarbonate monitoring. *Environ. Technol. Letters*, 6, 594-601.

Rozzi, A., Merlini, S., Passino, R. (1985b). Development of a four population model of the anaerobic degradation of carbohydrates. *Environ. Technol. Letters*, 6, 610-619.

Saslawsky, J., Liziard, Y., and Chave, E. (1988). Anaerobic treatment of evaporator condendates in a sulfite pulp mill. *Anaerobic Digestion 1988*, Proc. of the 5th International Symposium on Anaerobic Digestion, Bologna, Italy, 22-26 May, 499-505.

Schlott, D.A., Charbonneau, S.G., Greiner, J.A., Green, R.E., Quane, D.E. and Robertson, W.M. (1988). Design, construction, and start-up of an anaerobic treatment system for pharmaceutical wastewater. *Proc. 43rd Ind. Waste Conf.*, Purdue University, 651-660.

Smith, D.P. and McCarty, P.L. (1990). Factors governing methane fluctuations following shock loading of digesters. *Research Journal WPCF*, 62, 58-64.

Souza, M.E., Fuzaro, G., and Polegato, A.R. (1991). Thermophilic anaerobic digestion of vinasse in pilot plant UASB reactor. In: *Paper Preprints: Sixth International Symposium on Anaerobic Digestion*, Sao Paulo, Brazil, 12-16 May, 191-200.

Standard Methods for the Examination of Water and Wastewater (1985). 16th Ed., Am. Public Health Assoc., Washington, D.C.

Steiner, E.C., Blau, G.E. and Agin, G.L. (1986). *Introductory Guide to SIMUSOLV*. Dow Chemical Company, Midland, Michigan.

Stephanopoulos, G. and San, K.-Y. (1984). Studies on on-line bioreactor identification. I. Theory. *Biotechnol. Bioengng.* 26, 1176-1188.

Stover, E.L., Gonzalez, R., and Gomathinayagam, G. (1985). Shock load capabilities of anaerobic systems treating high strength wastewaters. *Proc. 40th Ind. Waste Conf.*, Purdue University.

Totzke, D. (1990). Commercial systems. Course notes: *Anaerobic Treatment of High Strength Wastes*, University of Wisconsin-Milwaukee, 3-4 Dec.

Trace Analytical (1985). *RGD2 Reduction Gas Detector Operating Manual.* Trace Analytical, Menlo Park, California.

Van den Berg, L., Patel, G.B., Clark, D.S., Lentz, C.P. (1976). Factors affecting rate of methane formation from acetic acid by enriched methanogenic cultures. *Can. J. Microbiol.*, 22, 1312-1319.

Wang, Y-T, Suidan, M.T. and Rittman, B.E. (1986). Kinetics of methanogens in an expanded-bed reactor. *J. Environ. Eng.*, ASCE, 112 (EE1), 155-170.

Weiland, P. and Rozzi, A. (1991). The start-up, operation and monitoring of high-rate anaerobic treatment systems: Discusser's report. *Wat. Sci. Tech.*, 24, 257-277.

Weng, C. and Jeris, J.S. (1976). Biochemical mechanisms in the methane fermentation of glutamic and oleic acids. *Wat. Res.*, 10, 9-18.

Wheatley, A.D., Johnson, K.A., and Winstanley, C.I. (1988). The reliability of anaerobic digestion for the treatment of food processing effluents. *Anaerobic Digestion 1988*, Proc. of the 5th International Symposium on Anerobic Digestion, Bologna, Italy, 22-26 May, 135-146.

Williamson, K. and McCarty, D.L. (1976). A model of substrate utilization by bacterial films. *J. Wat. Pollut. Control Fed.*, 48, 9-24.

Zeikus, J.G. (1979). Microbial populations in digesters. *Anaerobic Digestion.* Proc. 1st International Symposium on Anaerobic Digestion, University College, Cardiff, Wales, 61-87.

APPENDIX A

SAMPLE PREPARATION AND ANALYSIS

Chemical Oxygen Demand (COD)

Samples were acidified to a pH less than 4.0 with concentrated H_2SO_4. Analysis was by the closed reflux, colorimetric method (*Standard Methods*, 1985).

Filtered Chemical Oxygen Demand (FCOD)

Samples were acidified to a pH less than 4.0 with H_2SO_4 and filtered using a Whatman GF/A glass fibre filter. Analysis was by the closed reflux, colorimetric method (*Standard Methods*, 1985).

Five Day Biochemical Oxygen Demand (BOD_5)

Analysis was according to Standard Methods (1985).

Filtered Five Day Biochemical Oxygen Demand ($FBOD_5$)

Samples were filtered with Whatman GF/A glass fibre filter. Analysis was according to Standard Methods (1985).

Total Organic Carbon (TOC)

Samples were centrifuged and then filtered with a 0.45 µm membrane filter. The sample pH was adjusted to less than 4.0 with H_2SO_4. Analysis was conducted using a Dohrmann total organic carbon analyser.

Total Kjeldahl Nitrogen (TKN)

Samples were acidified to a pH less than 4.0 with H_2SO_4. Analysis was conducted according to Standard Methods (1985).

Filtered Total Kjeldahl Nitrogen (FTKN)

Samples centrifuged and then filtered through a 0.45 µm membrane filter, and acidified to a pH less then 4.0 with H_2SO_4. Analysis was conducted according to Standard Methods (1985).

Ammonia Nitrogen (NH_4-N)

Samples centrifuged and filtered through a 0.45 µm membrane filter. The sample pH was adjusted to 5.0 with H_2SO_4 or NaOH. Analysis was conducted using a Technicon Autoanalyzer (*Standard Methods*, 1985).

Total Phosphorus (TP)

Sample pH was adjusted to less than 4.0 with H_2SO_4. Analysis was conducted using a Technicon Autoanalyzer (*Standard Methods*, 1985).

Filtered Total Phosphorus (FTP)

Samples were centrifuged and filtered through a 0.45 µm membrane filter. Sample pH was adjusted to less than 4.0 with H_2SO_4. Analysis was conducted using a Technicon Autoanalyzer (*Standard Methods*, 1985).

Volatile Acids

Samples were centrifuged with $CdCl_2$ and filtered through a 0.45 µm membrane filter. Analysis was conducted by gas chromatography.

Total Volatile Solids (Reactor Solids Profiles)

Samples of the reactor sand medium were removed from various locations in the reactor. The sample volume as measured in a graduated cylinder was recorded. Each sample was dried at 103 °C and then weighed. After ignition in a 550 °C muffle furnace, the sample was weighed

again. Total volatile solids concentration at that point in the reactor was determined as the difference between the dried sample weight and the ignited sample weight divided by the sample volume.

APPENDIX B

DETERMINATION OF PARAMETERS USED IN MASS TRANSFER CALCULATIONS

1. Porosity of the fluidized bed, ε_f

The porosity of the settled bed is given by the following equation:

$$\varepsilon_S = \frac{V_{V,S}}{V_{T,S}} \tag{B.1}$$

where, ε_S = porosity of the settled bed
= 0.5 (assumed);
$V_{V,S}$ = void volume of the settled bed (m^3)
$V_{T,S}$ = total volume of the settled bed (m^3)

The total volume, $V_{T,S}$ is calculated as follows:

$$\begin{aligned} V_{T,S} &= h_S A_S \\ &= (1.85\ m)(0.0177\ m^2) \\ &= 0.0327\ m^3 \end{aligned} \tag{B.2}$$

where, h_S = the height of the settled bed (m)
A_S = the cross-sectional area of the bed (m^2)

Therefore, from Equation B.1,

$$\begin{aligned} V_{V,S} &= \varepsilon_S V_{T,S} \\ &= (0.5)(0.0327\ m^3) \\ &= 0.1635\ m^3 \end{aligned}$$

The volume occupied by the media particles, V_P is

$$V_P = V_{T,S} - V_{V,S} \tag{B.3}$$

The total volume of the fluidized bed, $V_{T,f}$ is

$$V_{T,f} = h_f A_S = (2.65\ m)(0.0177\ m^2) = 0.047\ m^3 \quad \text{(B.4)}$$

where, h_f = the fluidized bed height (m)

The void volume in the fluidized bed, $V_{V,f}$ is

$$V_{V,f} = V_{T,f} - V_P = 0.047\ m^3 - 0.01635\ m^3 = 0.03065\ m^3 \quad \text{(B.5)}$$

Finally, the porosity of the fluidized bed, ε_f, is

$$\varepsilon_f = \frac{V_{V,f}}{V_{T,f}} = \frac{(0.03065\ m^3)}{(0.047\ m^3)} = 0.65 \quad \text{(B.6)}$$

2. Number of media particles, N

An estimate of the volume of 1 media particle is

$$V_{P,p} = \frac{1}{6}\pi(dp_{10})^3 = \frac{1}{6}\pi(120\times10^{-6}\ m)^3 = 9.05\times10^{-9}\ m^3 \quad \text{(B.7)}$$

Therefore, the number of media particles is,

$$N = \frac{V_P}{V_{P,p}} = \frac{0.01635\ m^3}{9.05\times10^{-13}\ m^3} = 1.8\times10^{10} \quad \text{(B.8)}$$

3. Total surface area of the biofilm, a_s

$$a_s = N\pi(dp_{10} + L_f)^2 \qquad (B.9)$$
$$= 1.6 \times 10^3 \ m^2$$

4. Total volume of the biofilm, V_f

$$V_f = N\frac{1}{6}\pi((dp_{10} + L_f)^3 - (dp_{10})^3)$$
$$= 0.03 \ m^2$$

APPENDIX C

DATA FROM DYNAMIC EXPERIMENTS

Data has been stored in ASCII format on 3.5", double-sided, high density floppy disks. The name, description of contents and column layout of each data file are listed below.

C.1 DESCRIPTION OF FILE CONTENTS

1) File: G1_IN.DAT

   Input data for the preliminary experiment (glucose run #1).

2) File: G1_OUT.DAT

   Output data from the preliminary experiment (glucose run #1).

3) File: APG_IN.DAT

   Input data from the acetic acid, propionic acid and glucose run #2 experimental period.

4) File: APG_OUT.DAT

   Output data from the acetic acid, propionic acid and glucose run #2 experimental period.

5) File: B_IN.DAT

   Input data from the butyric acid experiment.

6) File: B_OUT.DAT

   Output data from the butyric acid experiment.

7) File: G3_IN.DAT

   Input data from glucose run #3.

8) File: G3_OUT.DAT

   Output data from glucose run #3.

C.2 FILE COLUMN LAYOUT

The layout of the *_IN.DAT files is listed below.

Column #	Description
1	Time (days)
2	Influent flowrate (L/d)
3	Influent total COD concentration (less COD equivalent of measured influent volatile acids) (mg/L)
4	Influent filtered COD concentration (less COD equivalent of measured influent volatile acids) (mg/L)
5	Influent acetic acid concentration (mg/L)
6	Influent propionic acid concentration (mg/L)
7	Influent butyric acid concentration (mg/L)
8	Concentration of sodium hydroxide added for pH control (mmole/L)
9	Sodium hydroxide addition pump time-on per five minute control cycle.

The layout of the *_OUT.DAT files is listed below.

Column #	Description
1	Time (d)
2	Effluent acetic acid concentration (mg/L)
3	Effluent propionic acid concentration (mg/L)
4	Effluent butyric acid concentration (mg/L)
5	Concentration of hydrogen in the biogas (ppm)
6	Carbon dioxide gas flowrate (L/d)
7	Methane gas flowrate (L/d)
8	Effluent pH
9	Effluent total COD concentration (less COD equivalent of measured volatile acids) (mg/L)
10	Effluent filtered COD concentration (less COD equivalent of measured volatile acids) (mg/L)
11	Reactor temperature (°C)

APPENDIX D

PILOT PLANT DAILY OPERATING DATA

The file DAILY.WK1 has been stored as a LOTUS 1-2-3 (Release 2) worksheet on a 3.5", doubled sided, high density floppy disk. The layout of the worksheet is listed below.

Column	Description
A	Day
B	Date (day/month/year)
C	Diluted stillage feed pH
D	Diluted stillage feed acetic acid concentration (mg/L)
E	Diluted stillage feed propionic acid concentration (mg/L)
F	Diluted stillage feed butyric acid concentration (mg/L)
G	Diluted stillage feed total COD concentration (mg/L)
H	Diluted stillage feed filtered COD concentration (mg/L)
I	Diluted stillage feed flowrate (L/d)
J	Anaerobic reactor gas production rate (L/d)
K	Anaerobic reactor effluent pH
L	Anaerobic reactor temperature (°F)
M	Anaerobic reactor biogas % methane content
N	Anaerobic reactor effluent acetic acid concentration (mg/L)
O	Anaerobic reactor effluent propionic acid concentration (mg/L)
P	Anaerobic reactor effluent butyric acid concentration (mg/L)
Q	Anaerobic reactor effluent total COD concentration (mg/L)
R	Anaerobic reactor effluent filtered COD concentration (mg/L)